AIR JET VORTEX GENERATORS FOR WIND TURBINES

by

ANDREW G. OLIVER

Thesis submitted as part of the requirements for the degree of
Doctor of Philosophy

Centre for Aeronautics
School of Mechanical Engineering and Aeronautics
City University, London

DECEMBER 1997

TABLE OF CONTENTS

LIST OF FIGURES

LIST OF TABLES

ACKNOWLEDGEMENTS

I would like to thank the European Union for funding the project which was the basis for the work contained in this thesis.

I would like to acknowledge the work of Professor H.H. Pearcey on air jet vortex generators, without which this thesis would not have been possible.

I am indebted to Professor L.R. Wootton, and Mr. David Sykes whose invaluable knowledge and experience has helped and inspired me.

Thanks are due to Mr. Mike Smith, Mr. Chris Barber and Mr. Martin Young for their assistance in the design and manufacture of the wind tunnel model.

I would also like to express my gratitude to Mr. David Milborrow and Mr. Josep Prats, for the invaluable meetings, phone calls and faxes which have furthered my understanding of wind turbines and have helped to focus my thoughts.

Finally, I would like to thank all the dedicated professionals, too numerous to mention, in the field of wind energy, whose encouragement and advice has been a source of strength throughout my post-graduate study.

DECLARATION

'I grant powers to the university librarian to allow this thesis to be copied in whole or in part without further reference to me. This permission only covers single copies made for study purposes, subject to normal conditions of acknowledgement.'

ABSTRACT

Air jet vortex generators are a boundary layer control device and as such can effect a significant delay to the stall of an aerofoil. They can also reattach a separated flow, as long as the angle of attack is less than the air jets 'on' stall angle.

A wind tunnel model was built and tested and then modified to incorporate air jets. The air jets increased $C_{L\ max}$ by 55% and reduced the drag throughout the incidence range, α, for the chosen blowing pressure of 1 p.s.i. (6900Pa). By varying the air supply so that the jets operate between 'off' and fully 'on' a whole family of aerofoil L/D characteristics could be derived.

The blade set of a 150 kW stall regulated wind turbine was then modified with air jet vortex generators and tested at full scale. This was done primarily to increase its energy yield by reducing energy loss in the region of the power curve 'knee', but also to allow a degree of power regulation in high wind speeds. The air supply in this demonstration was supplied by a fan mounted on, and rotating with, the rotor.

Full-scale trials demonstrated that air jets can indeed be used to straighten the power curve prior to rated wind speed. This important result means that a stall regulated machine can be made to behave in the same way as a pitch controlled machine without having to pitch the blades.

Of the two air jet configurations tested in the wind tunnel, the second had an improved L/D characteristic and required less mass flow, even though the physical change was minor. This indicates that further optimisation of air jets may be achieved.

Further wind tunnel testing showed that it should be possible to eliminate the fan used in the full scale trials and use one of two 'passive' blowing techniques. It was shown that the air jets can be supplied by air at atmospheric pressure due to the suction on the upper surface of the aerofoil which is sufficient to pull air through the jet exits and create vortices.

However, to achieve an optimised air jet configuration and to investigate the possibilities of using passive blowing, air jet vortex generators will need to be modelled numerically, so that this innovative concept can be brought to market quickly.

NOTATION

a	Axial inflow induction factor
a′	Tangential inflow induction factor
A	Swept area of rotor (m^2)
AR	Aspect ratio of rectangular air jet
c	Chord length of aerofoil or blade (m)
C_C	Chordwise force coefficient of aerofoil or blade
C_D	Drag coefficient of aerofoil or blade
C_L	Lift coefficient of aerofoil or blade
C_N	Normal force coefficient of aerofoil or blade
C_P	Power coefficient or pressure coefficient
g	Acceleration due to gravity (m/s^2)
h	Height of fluid in manometer (m)
H	Total pressure (N/m^2)
J & K	Numerical constants
L	Length of air jet slot (m)
L/D	Lift to drag ratio
$\dot{m}$	Mass flow rate (kg/m^3)
p	Static pressure (N/m^2)
p_b	Gauge blowing pressure (N/m^2)
p_{plenum}	Absolute blowing pressure (N/m^2)
P	Power (kW)
q	Dynamic pressure (N/m^2)
Q	Torque of rotor (Nm)
r	Radial distance along blade (m)
R	Radius of the wind turbine rotor (m)
Re	Reynolds number
U	Wind speed at wind turbine hub height or tunnel speed (m/s)
V	Velocity (m/s)
VR	Velocity ratio - Air jet velocity/ local velocity into which jet is issuing
W	Width of air jet slot (m)
x	Distance along the chord measured from leading edge (m)

Greek

α	Angle of attack of aerofoil or blade (°)
β	Blade setting angle (°)
η	Drive train efficiency
θ	Air jet skew angle (°)
λ	Tip speed ratio
ρ	Density - of air unless followed by subscript (kg/m^3)
ϕ	Air jet pitch angle or relative flow angle (°)
Ω	Angular velocity of wind turbine rotor (rad/s)

Abbreviations

ajvg	Air jet vortex generator
vvg	Vane vortex generator
ADC	Analogue to digital conversion
DAS	Data acquisition system

Subscripts

∞	Freestream condition
a	Atmospheric
av.	Annual average
exit	At the jet exit
jet	Of or pertaining to the air jet
man	Of manometer fluid
r	Rotational
t.e.	Trailing edge
down	Downstream location in tunnel contraction
up	Upstream location in tunnel contraction
max.	Maximum
min.	Minimum
elec	Electrical power
shaft	Shaft power
zero	Zero load loss
1	Close behind aerofoil
2	Far downstream behind aerofoil

NB A separate notation is provided for the appendices. Notation used in the power prediction program can be found at the start of the program listing, Appendix 3.

1. INTRODUCTION

1.1 Wind energy

One of the biggest threats to the survival of mankind is his own pollution of the environment. With global warming now recognised as fact, the Rio Earth summit was convened in 1992 at which many governments promised to return CO_2 emissions to those of 1990 levels by the year 2000. With the burning of fossil fuels being the primary cause of rising levels of CO_2 and other 'greenhouse' gases and the nuclear catastrophe at Chernobyl still fresh in our minds, the interest in renewable and in particular, sustainable, forms of energy has blossomed.

Wind energy, created by uneven solar heating of the atmosphere, is both renewable and sustainable. There will always be wind and as a resource it is vastly greater than mankind's energy needs are ever likely to be. Its energy has long been harnessed by man but the modern wind energy industry, that is for generation of electricity, is really only about 20 years old. In that time it has come from being risibly un-economic, to arguably being as competitive as coal and nuclear power for regions with high average wind speed.

For wind energy to make a significant contribution to our energy requirements in the 21st. century, assuming that economics and not environmental considerations will be the predominant factor, the cost of energy from the wind must continue to be reduced. Only then will it become commercially viable to erect wind turbines at sites of lower average wind speeds which are, by their nature, more abundant and accessible. This would inevitably allow wind energy to flourish in less mountainous regions, where perhaps the environmental impact is not as great.

The average wind speed at which economic generation of electricity from the wind is possible varies widely throughout Europe due to the price that the generators receive from the utilities (e.g. in Germany the price of electricity is nearly double that which it is in the U.K. making wind energy a more viable proposition in the former for an identical site). We may, however, use a simple example to show that even a small reduction in the average wind speed at which wind energy can be economically generated significantly increases the land mass where wind energy becomes viable.

Figure 1, is a map showing regions of equivalent wind speed of the, then twelve, member states of the European Union (Troen et al, 1989). The majority of wind farms in these countries are in the two darkest of the shaded wind speed bands. This represents approximately 25% of the total land mass. If the average wind speed for the economic generation of wind energy could be reduced by 1m/s then the middle band, representing a further 23%, becomes available. Of course the average wind speed also depends on the local topography and so wind development cannot be ruled out in northern Italy at a good site, just as it cannot be ruled in in Scotland at a bad one. On average though, we could expect approximately a 23% increase in the 'good' sites where it is possible to generate electricity from the wind economically.

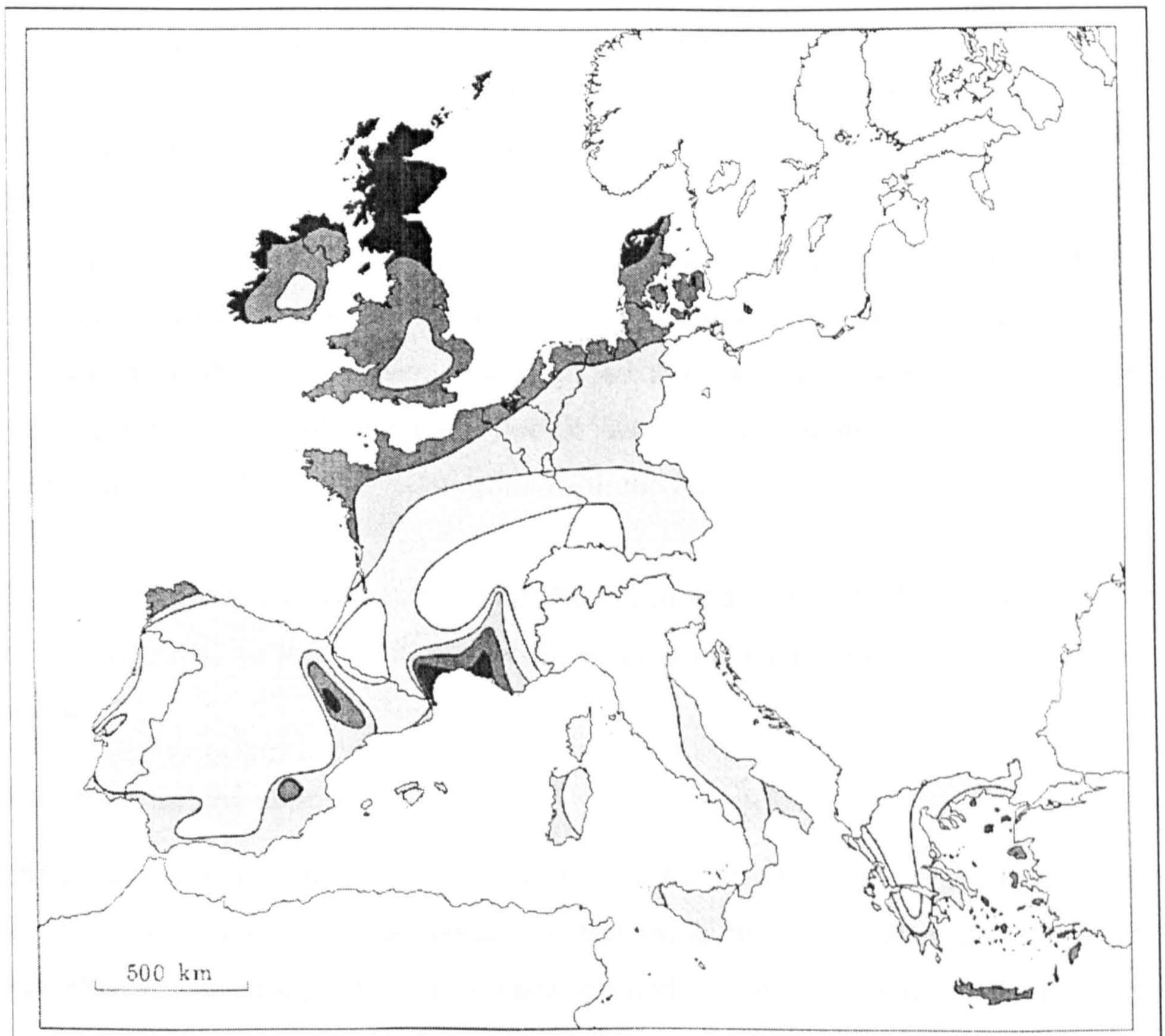

Wind resources[1] at 50 metres above ground level for five different topographic conditions

	Sheltered terrain[2]		Open plain[3]		At a sea coast[4]		Open sea[5]		Hills and ridges[6]	
	$m\,s^{-1}$	Wm^{-2}	$m\,s^{-1}$	Wm^{-2}	$m\,s^{-1}$	Wm^{-2}	$m\,s^{-1}$	Wm^{-2}	$m\,s^{-1}$	Wm^{-2}
	> 6.0	> 250	> 7.5	> 500	> 8.5	> 700	> 9.0	> 800	> 11.5	> 1800
	5.0-6.0	150-250	6.5-7.5	300-500	7.0-8.5	400-700	8.0-9.0	600-800	10.0-11.5	1200-1800
	4.5-5.0	100-150	5.5-6.5	200-300	6.0-7.0	250-400	7.0-8.0	400-600	8.5-10.0	700-1200
	3.5-4.5	50-100	4.5-5.5	100-200	5.0-6.0	150-250	5.5-7.0	200-400	7.0-8.5	400-700
	< 3.5	< 50	< 4.5	< 100	< 5.0	< 150	< 5.5	< 200	< 7.0	< 400

Figure 1 Wind resource map of Europe (Troen et al, 1989)

The cost of energy from the wind, at a given site, is represented by the ratio of the annual cost of producing this energy to the annual energy production. To reduce the cost of wind energy then, and neglecting factors over which we have no control such as loan interest rate, there are three principal ways in which the unit cost of wind energy may be reduced:

1. By increasing the energy capture of individual wind turbines.
2. By reducing the cost of individual wind turbines.
3. By reducing the planning and construction costs of a wind farm.

The first category above may be divided into three sub-headings:

i. Value engineering of turbines currently available.
ii. New concepts to replace the current commercially successful designs.
iii. Larger Mega-Watt scale machines.

This thesis describes how an existing machine was modified with Air Jet Vortex Generators with the aim of increasing energy capture and, as such, falls into the first category above. However, it is intended that 'air jets' will eventually become the basis for a completely new design with much greater potential than the conversion described herein (Category 1 (ii) above).

By increasing the energy capture and thus reducing the cost of energy, this work aims, indirectly, to lead wind power development to sites of lower average wind speed.

1.2 Wind turbine control

Energy available in the wind is proportional to the cube of the wind speed. Hence, for the same wind turbine design, if the wind speed is doubled, the energy available increases eight-fold. In theory, a wind turbine's generator could be rated at the power it would produce at its maximum operational wind speed. However, there are two main reasons why this is not done and a wind turbine's maximum power output is usually limited at around 12m/s compared with a typical shut down wind speed of around 24m/s.

These reasons are:

1. Generator cost and size both increase with the rated power output and higher wind speeds are rare. There is therefore is a trade off between the cost of the generator and nacelle housing and the value of the extra energy produced.

2. Electrical generators are more efficient when operating near their rated power. Since lower wind speeds are more abundant, a higher efficiency can be attained by capping the wind turbines power output.

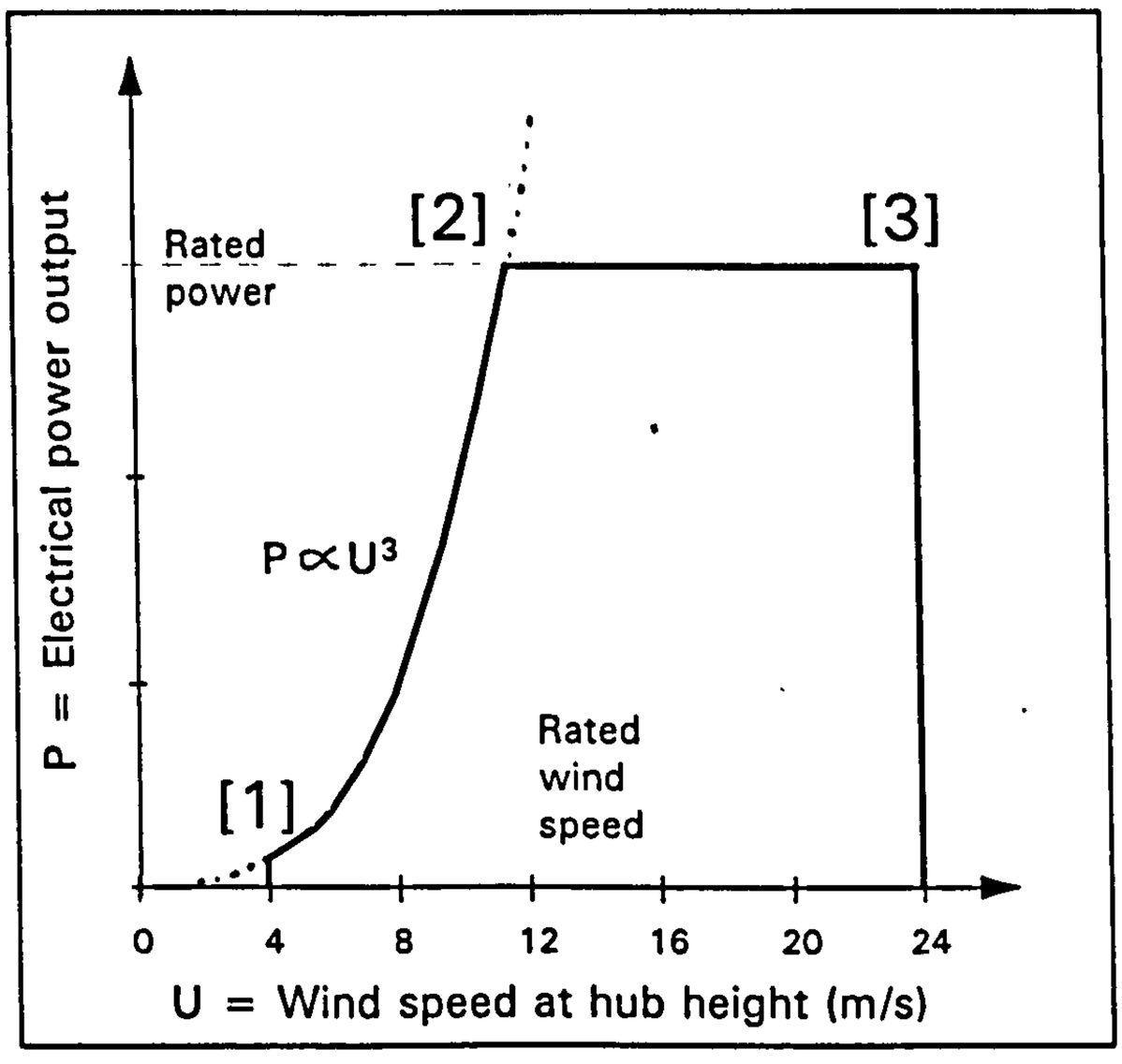

For a wind turbine it is therefore desirable to have two operating regimes, as shown. The first is to maximise the energy yield between 'cut-in' [1] and 'rated' power [2]. The second is to try and follow rated as closely as possible between [2] and [3], the 'cut-out' wind speed. The latter part of this strategy is referred to as 'power regulation' from this point forward.

Figure 2 Ideal power curve of a wind turbine

To understand why air jets were used in the way that they were, it is first necessary to know about the wind turbine control types currently in use.

1.2.1 Stall regulation.

Stall regulation is the method applied to a wind turbine which has a constant rotational speed (with a fixed gear ratio to the constant frequency of the electricity grid) and fixed pitch blades. The main disadvantage of this control method is that the progressive stall of blade from root to tip leads to a rounding of the power curve (see Figure 3 below). Stall machines do not therefore closely follow the ideal strategy outlined above.

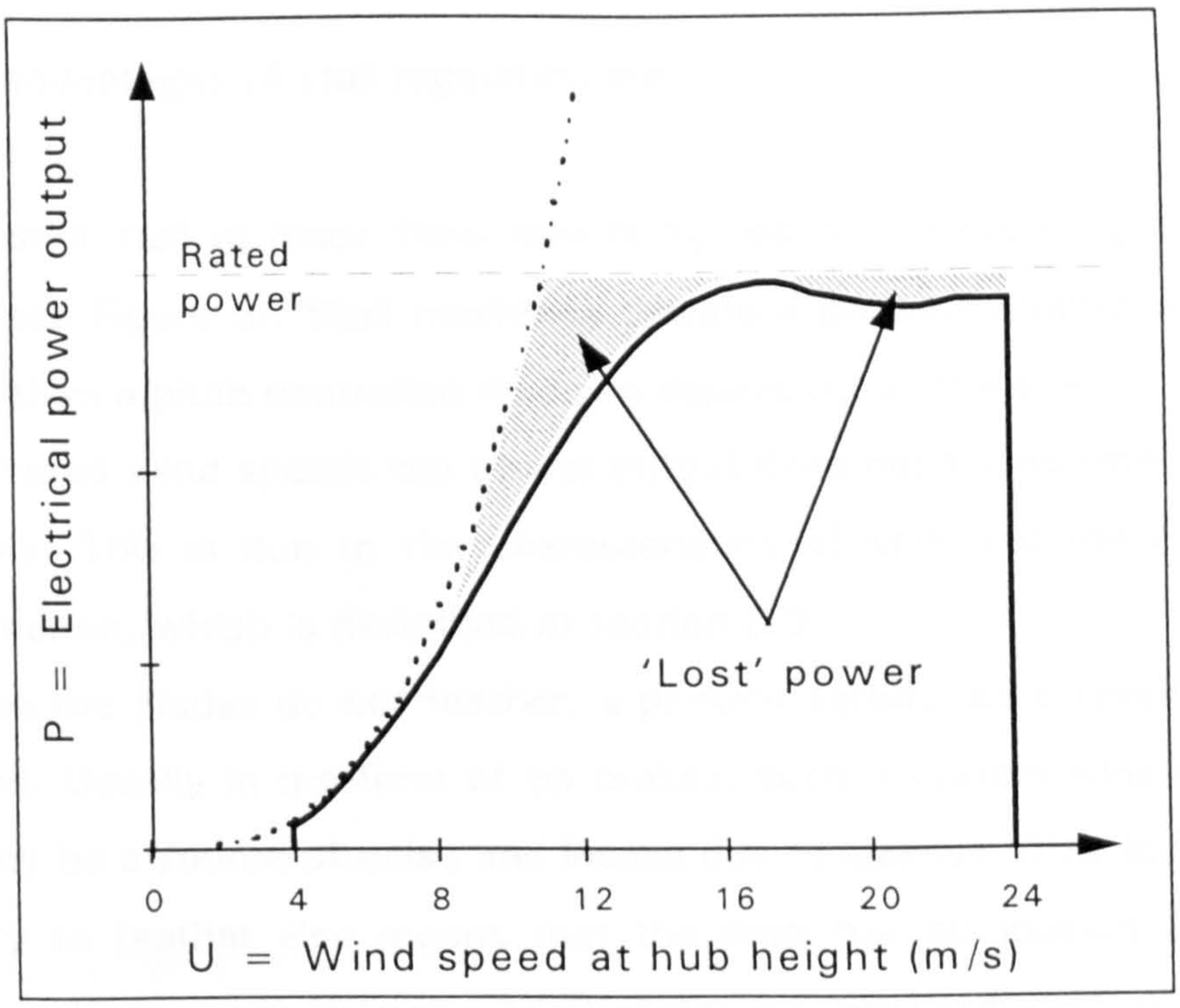

Figure 3 Typical stall regulated power curve

Stall regulation works because as the wind speed, U, increases, the angle of attack on any given spanwise section of blade will increase, as shown in Figure 4. As the wind speed continues to increase the blade begins to stall (from the root outwards). This reduces rotor lift and increases rotor drag, thus limiting blade torque and hence power output. The regulation of the power curve is achieved only by the variation of twist and profile along the blade, although a small amount of 'tuning' can be achieved by altering the blade setting angle, β at installation.

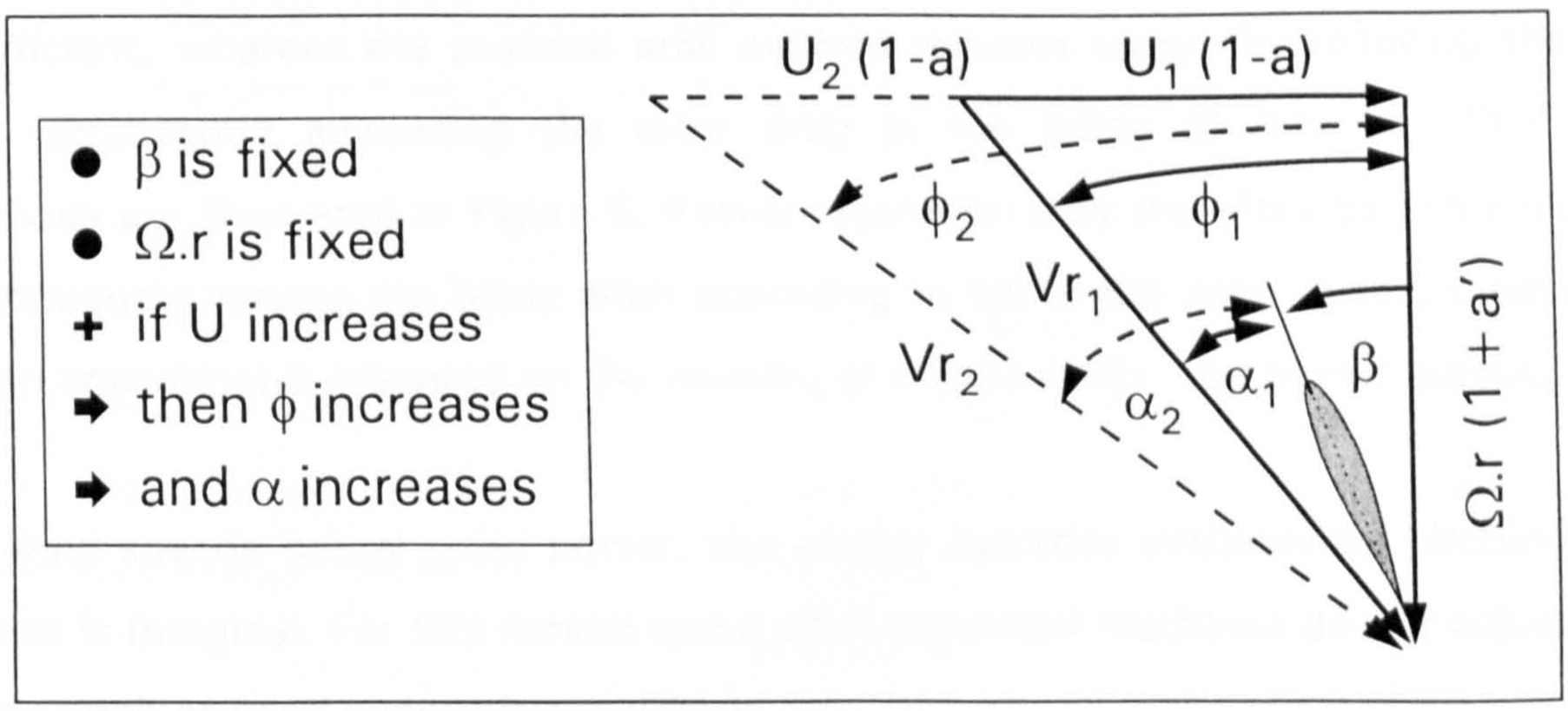

Figure 4 The mechanics of stall regulation

The principle advantage of this control method is its simplicity as there are no power control mechanisms, pitch bearings or assemblies. This leads to savings in weight, complexity, capital and maintenance costs.

The main disadvantages of stall regulation are:

- Progressive stall of blade from root to tip leads to a rounding of the power curve (see Figure 3). Stall machines therefore produce around 5 - 10% less energy than a pitch controlled machine depending on the site.
- Above rated wind speeds the power output does not follow rated power very precisely. This is due to the characteristics of stall and the dynamic stall phenomenon, which is described in section 6.9.
- Because the blades do not feather, a primary aerodynamic braking system is required. Usually in the form of tip brakes, such a system adds extra weight and may be a source of noise and losses due to leakage of air at the join.
- Inability to feather also means that the drag (thrust) loading on stationary blades in high winds is large. Additionally, an 'assisted start' is not possible as the blades are at almost 90° to the relative wind direction on start-up.

1.2.2 Pitch regulation

Pitch regulation is the method whereby the blades may be turned (pitched), principally for power regulation. At higher than rated wind speeds, power is regulated by pitching the blades either positively (feathering) or negatively (assisted stall). Referring back to Figure 4, an increase in blade pitch, β will result in a reduction in the blade angle of attack, α and vice-versa. The feathering method therefore reduces blade torque by moving the blade operating point to a lower lift coefficient, whereas the assisted stall method reduces torque by reducing the lift and significantly increasing the rotor drag in the plane of rotation. The two methods are illustrated in Figure 5. Power regulation may therefore be achieved by continuously varying the blade pitch according to either the wind speed, measured by an anemometer mounted on the nacelle, or more usually, the power output.

At wind speeds below rated power, the energy increase available by pitching the blades is marginal. For this reason some pitch regulated machines do not adjust the blade pitch at wind speeds below rated.

Generally the blades are pitched together but on some machines this is done individually. A pitch regulated machine may be of variable rotational speed (section 1.2.3) although more usually the rotational speed is fixed.

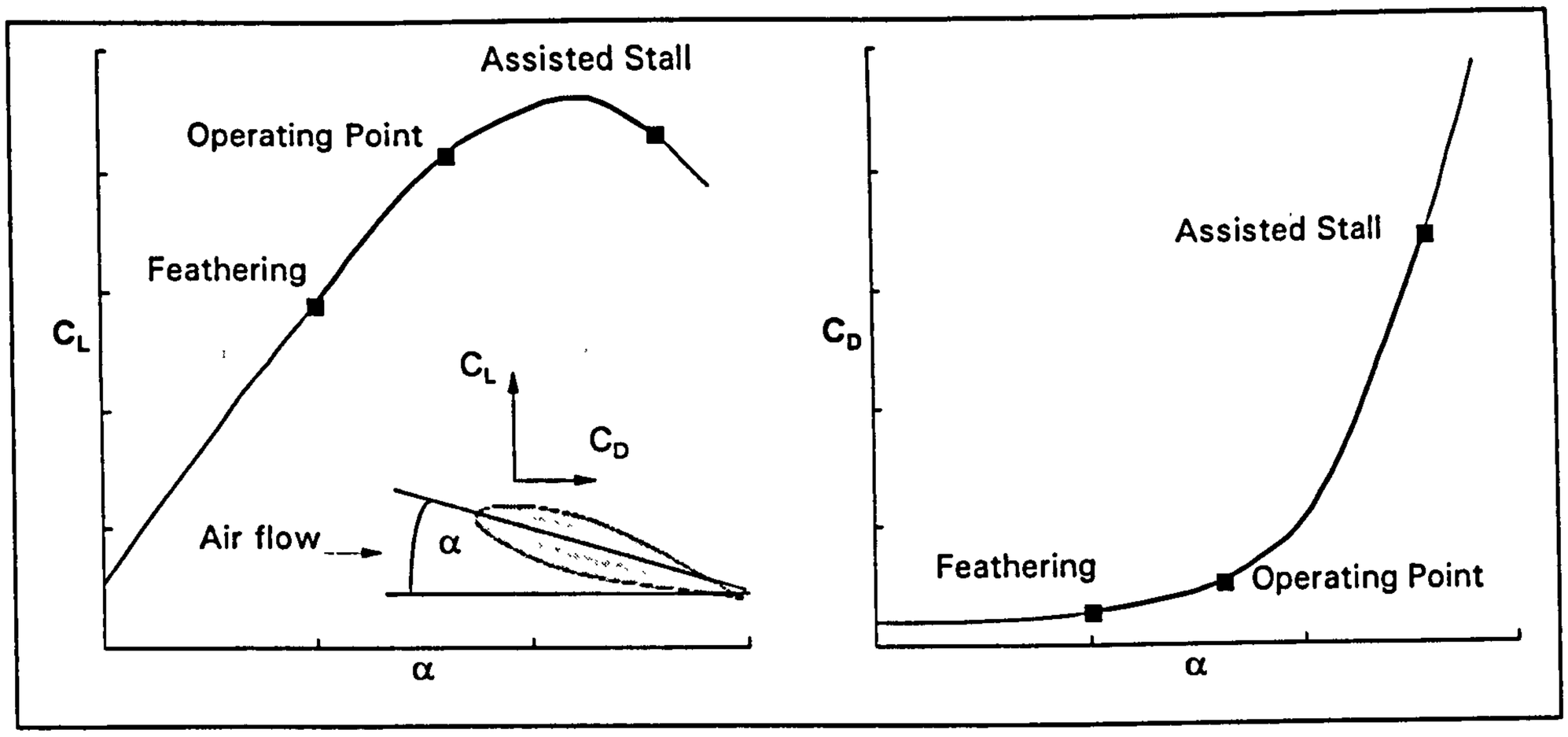

Figure 5 The two methods of reducing torque by pitching the blades

The advantages of pitch regulation over stall regulation are:

- Better power regulation.
- Higher energy yield (no 'knee' in power curve).
- Low drag loads when blades are stationary since blades are fully feathered.
- Assisted start is possible. As the blades are at full feather on start-up they are aligned such that the blade lift vector is in the plane of rotation.
- Built-in braking since blade fail-safe position is at full feather.
- Loads are reducing with wind speed (only feathering method).

The disadvantages are of course; the additional cost and weight of the pitch control mechanism and the extra complexity which reduces reliability.

1.2.3 Variable speed

It is important to note that although power regulation can theoretically be achieved with a variable speed strategy, in practice the blade is regulated by stall unless a pitch mechanism is added. The Variable Speed concept does have other advantages though and these are described below.

From an energy capture point of view, variable speed strategy is very promising for sites of low to moderate wind speeds because it allows increased energy yield at below rated wind speeds. In this part of the power curve it is required that the power coefficient should be maximised for any given wind speed, since power produced is equal to:

$$P = \tfrac{1}{2}\,\rho.\,U^3.\,A.\,C_p \qquad \text{.....(1 - 1)}$$

The governing variable for achieving optimum power coefficient is the Tip Speed Ratio, λ , the ratio of the blade tip speed to the wind speed (Ω.R/U). Every wind turbine has only one tip speed ratio, λ_{max} at which optimum energy extraction takes place and this is specific to the aerodynamic properties of the machine in question. Figure 6 shows a typical variation of C_p with λ.

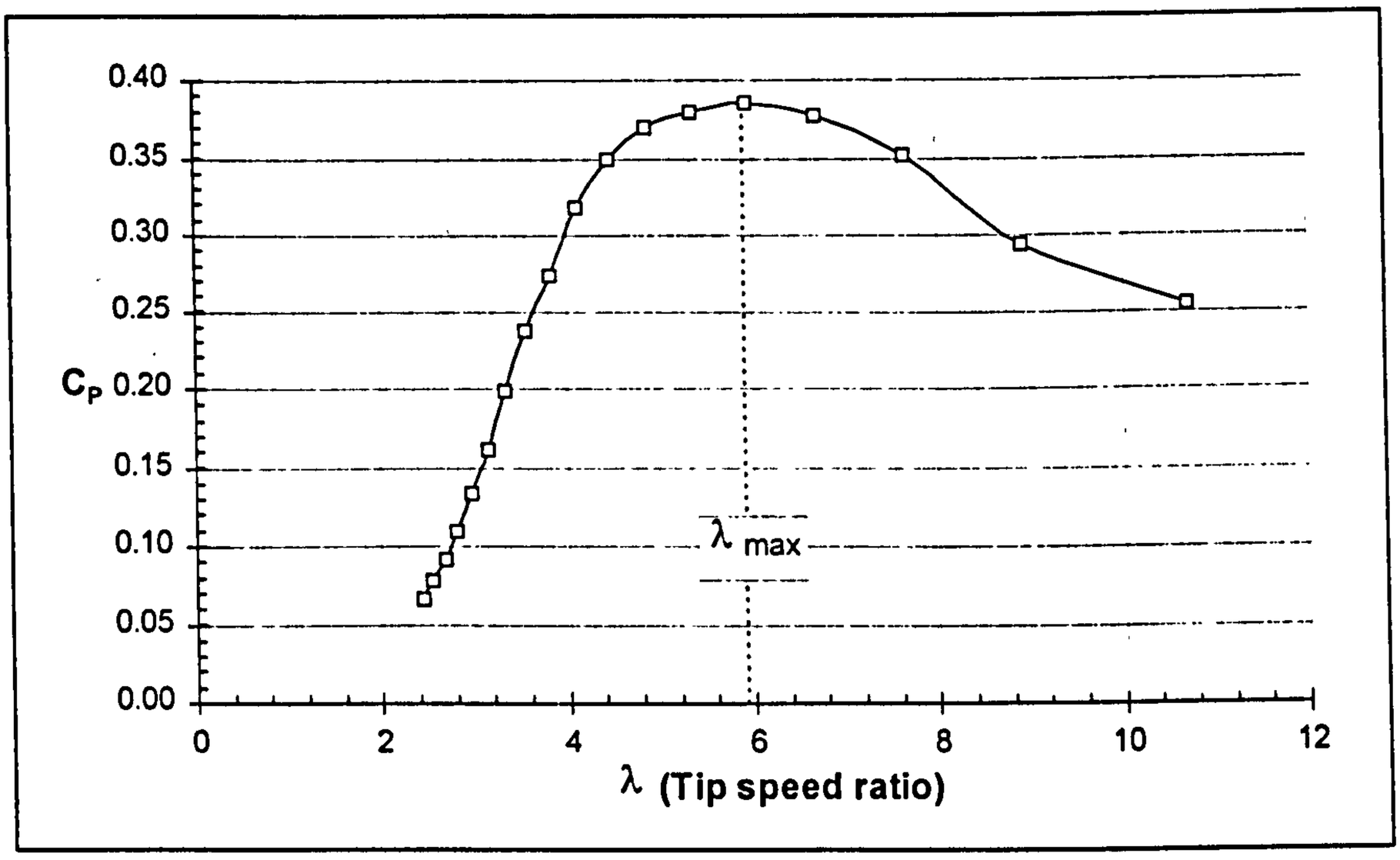

Figure 6 Example variation of power coefficient, Cp with λ.

The ideal strategy then, is to keep λ constant at λ_{max} so that the machine is always operating at the top of the Cp - λ curve. As the wind speed increases, the tip speed must be increased proportionally.

The fact that the rotor rotates more slowly than that of a fixed speed machine at lower wind speeds is also advantageous. This is because aerodynamic noise is a positive function of tip speed. Therefore any aerodynamic noise produced at lower wind speeds by a Variable Speed machine will be better masked by the background noise, which increases with wind speed.

The major disadvantage of Variable Speed technology is the problem in producing constant frequency AC from a drive shaft of varying rotational speed and whether the extra energy produced merits the complexity involved. Currently, Variable Speed technology is expensive and as such only a handful of manufacturers employ variable speed for the large scale production of electricity. However, as power electronics continue to develop, costs will reduce.

1.3 Objectives of the work

Summarising section 1.2, it can be said that Stall Regulation is cheaper and simpler than Pitch Regulation but that the energy capture is lower. Ideally then, one would like to retain the simplicity of having fixed pitch blades (stall regulated machine) but to regulate the power as effectively as a pitch controlled machine.

The objective of this work was to demonstrate that by modifying a wind turbine blade with air jet vortex generators (ajvg's), its aerodynamic characteristics could be continuously altered without having to pitch it.

Success would enable a fixed-pitch wind turbine fitted with the modified blades to emulate a pitch regulated machine. Consequently, the modified wind turbine would have a relatively simple form of power regulation and improved energy capture over stall regulated machines, yet still retain the benefit of having the relatively low manufacturing, operation and maintenance costs that are associated with fixed pitch machines. This will reduce the cost of energy, ultimately leading to wind farm development at sites of lower mean wind speed.

1.4 Technical approach and expected achievements

Air jet vortex generators, more fully described in section 2.1, are a form of boundary layer control and as such can delay the stall of an aerofoil, thereby increasing its maximum lift and hence Lift to Drag ratio.

The Lift to Drag ratio (L/D) is considered to be an important factor governing the performance of a wind turbine as it is an indication of driving torque at any given blade radius, $Q = L.\sin \phi - D.\cos \phi$, where ϕ is the angle of the relative wind incident on the blade (relative flow angle).

For a constant speed (Ω), fixed pitch (β) wind turbine (stall regulated), increasing wind speed implies increasing ϕ, and hence angle of attack, α (Figure 4). For power to be maximised over the rising part of the power curve (Figure 2) it is therefore desirable to maintain a high lift to drag ratio (torque) over as wide a range of alpha as possible since power is directly proportional to torque, $P = \Omega.Q$. In the rising part of the power curve, the air jets will therefore be operated with maximum blowing (maximum lift to drag ratio). This will delay the stall of the blade, increasing its aerodynamic efficiency and power production.

Once at rated power, the effect of reducing blade angle of attack may be achieved by supplying less air to the jets to achieve a lower lift to drag ratio and hence lower torque. Rated power will lie somewhere between the air jets 'fully on' (maximum blowing) and jets 'off'. Having determined several power curves with intermediary air flow rates, power regulation may be achieved by blowing at the correct flow rate. Figure 7 shows qualitatively the strategy outlined above and the expected modification to the power curve of a stall regulated machine.

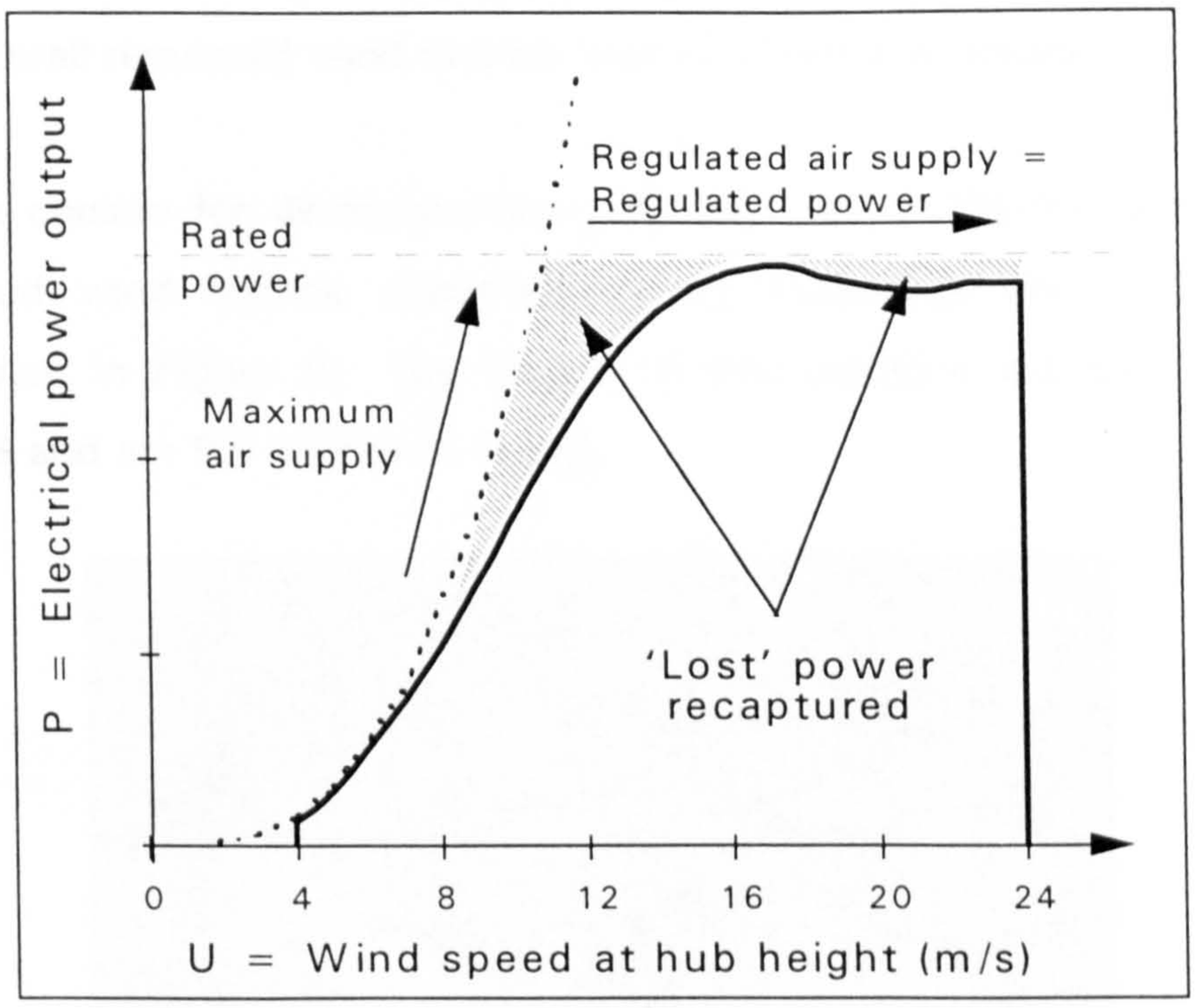

Figure 7 Expected benefits of using air jet vortex generators

The effect of 'switching on' or 'switching off' ajvg's and reducing or increasing the air flow, has been found to be instantaneous and so such a control mechanism should adjust to changes in wind speed (or measured torque or power) quickly and simply. Pitch regulation, being a mechanical system, cannot always respond quickly enough to changes in wind speed. Machines fitted with ajvg's would therefore be more suited to sites in complex terrain, for example, where the fast changes of the inflow direction (dynamic yaw) and the appreciable vertical velocity component change the point of operation very abruptly.

1.5 Work described in this thesis

This thesis is a result of work carried out for the European Union under their JOULE 2 programme. The project was entitled, 'Optimising the performance and control of wind turbines'.

In this first application, the main goal was to confirm that air jets could eliminate the 'knee' in the rising part of the power curve. The secondary objective was to demonstrate the potential for power regulation rather than determine the precise control strategy.

As a pilot study, it was necessary to demonstrate that air jets could achieve the objectives as cost effectively as possible. This ruled out the design, manufacture and testing of a completely new blade incorporating air jets. Instead, an existing blade from a stall regulated wind turbine was modified and tested.

The machine chosen for demonstration purposes was a 150kW, 20m. diameter, stall regulated wind turbine manufactured by Ecotecnia Scc. Ltd. (Ecotecnia 20/150, shown in Figure 8). The blades of this machine are supplied by L.M. Glasfiber A/S and are 9.7 metres in length.

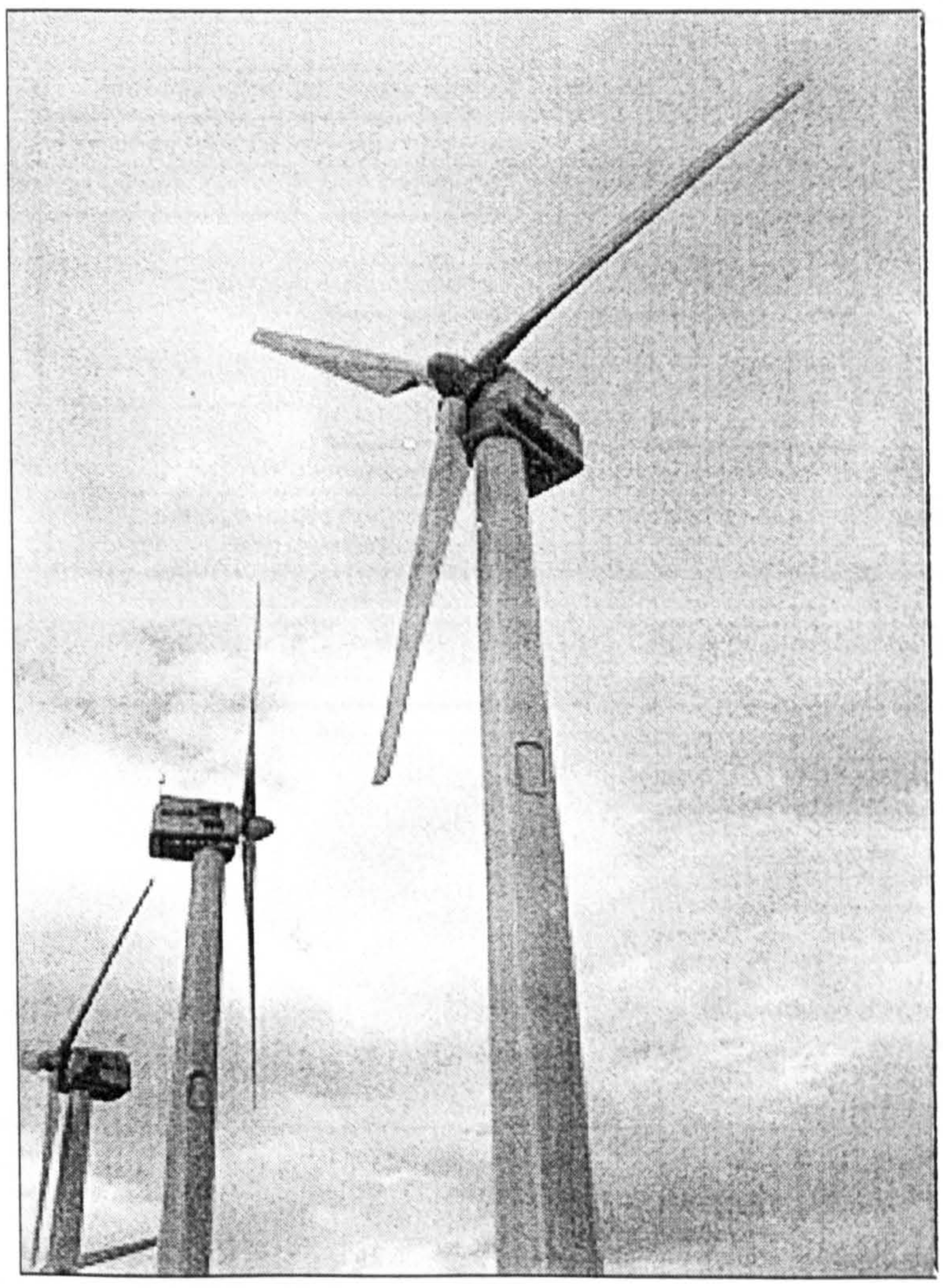

Figure 8 Ecotecnia 20/150 wind turbine.

In order to achieve the objectives a work programme was devised which consisted of three inter-related modules. These were:

1. Wind tunnel testing of air jet vortex generators (ajvg's).
2. Application of results to the full scale design of a modified blade set.
3. Full scale testing of the modified blade set.

Figure 9 shows a flow chart highlighting the individual project tasks undertaken and their relationship with one another. Although presented in a linear fashion, it should be noted that the project was iterative in its approach and that several of the tasks were inter-dependent.

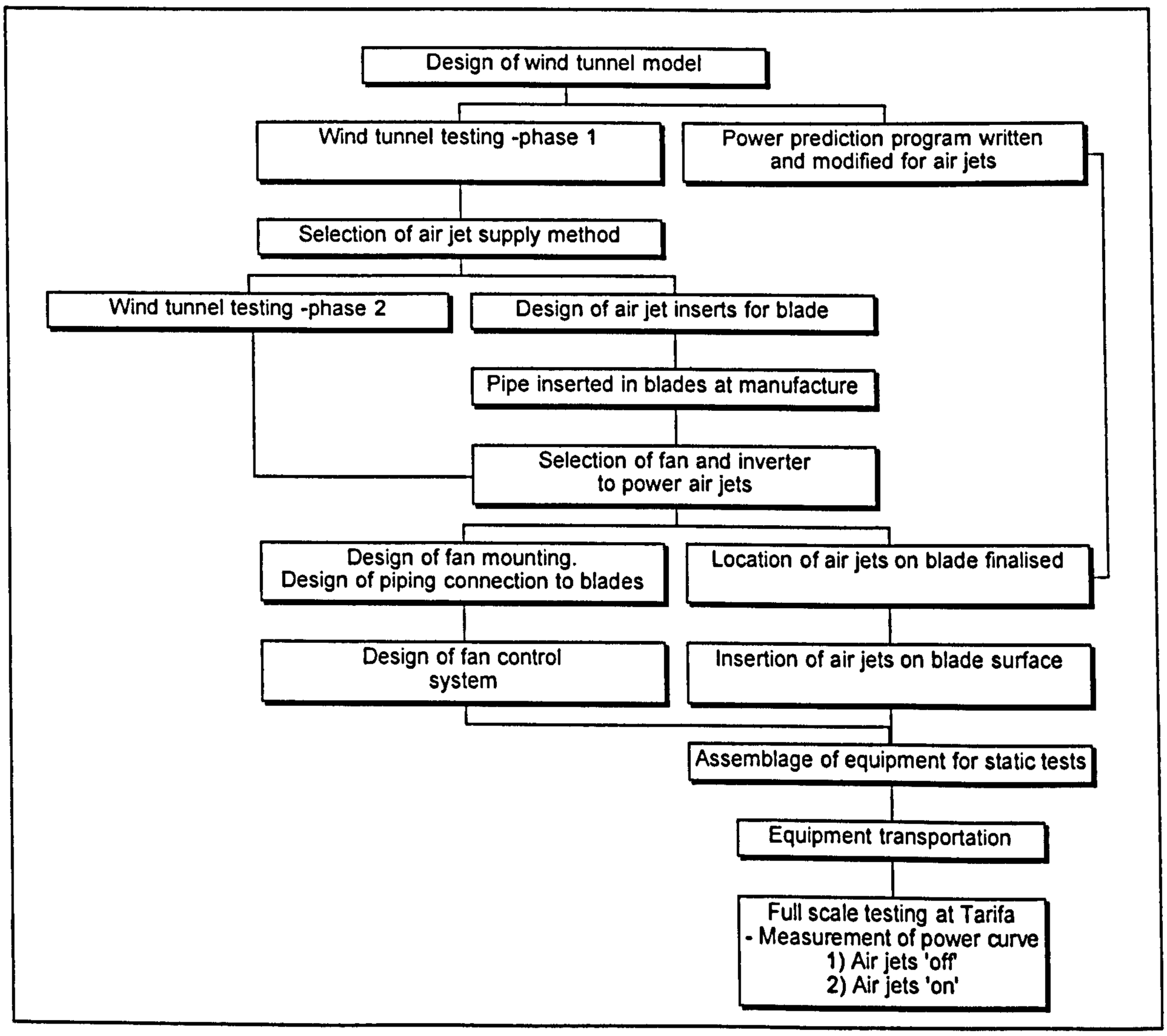

Figure 9 Project tasks

All of the above (The European Contract) are described in detail in Chapter's 3 to 9 of this thesis.

In addition to this, Chapter 10 describes wind tunnel testing that was carried out after the project had finished which showed that Air Jet Vortex Generators do not require an active power supply (the inherent thought up to now).

1.6 Work not undertaken solely by the author

This thesis is the result of a project and for it to be coherent it is necessary to describe the project in full. In the instances where the author was not directly involved it is stated clearly.

1.7 Contract management

The author was responsible for the co-ordination and technical leadership of the project, including budget management, planning and administration. More detail is given in Appendix 1.

2. THEORY

2.1 Air jet vortex generators

The use of vortex generators is a technique which essentially re-energises the boundary layer, reduces its growth in the adverse pressure gradient and delays separation. A helical vortex with high streamwise momentum, its core situated at approximately boundary layer height, will transfer momentum from the free stream to slower moving air near the surface of the aerofoil. This has the effect of increasing skin friction, reducing boundary layer growth in the adverse gradient and delaying flow reversal and separation (Pearcey, 1961).

The mixing with and replacement of retarded fluid particles continues in the chordwise direction as long as the vortices can impose this helical motion. Figure 10 shows the mechanism by which a vortex forms around a pitched and skewed rectangular jet of air.

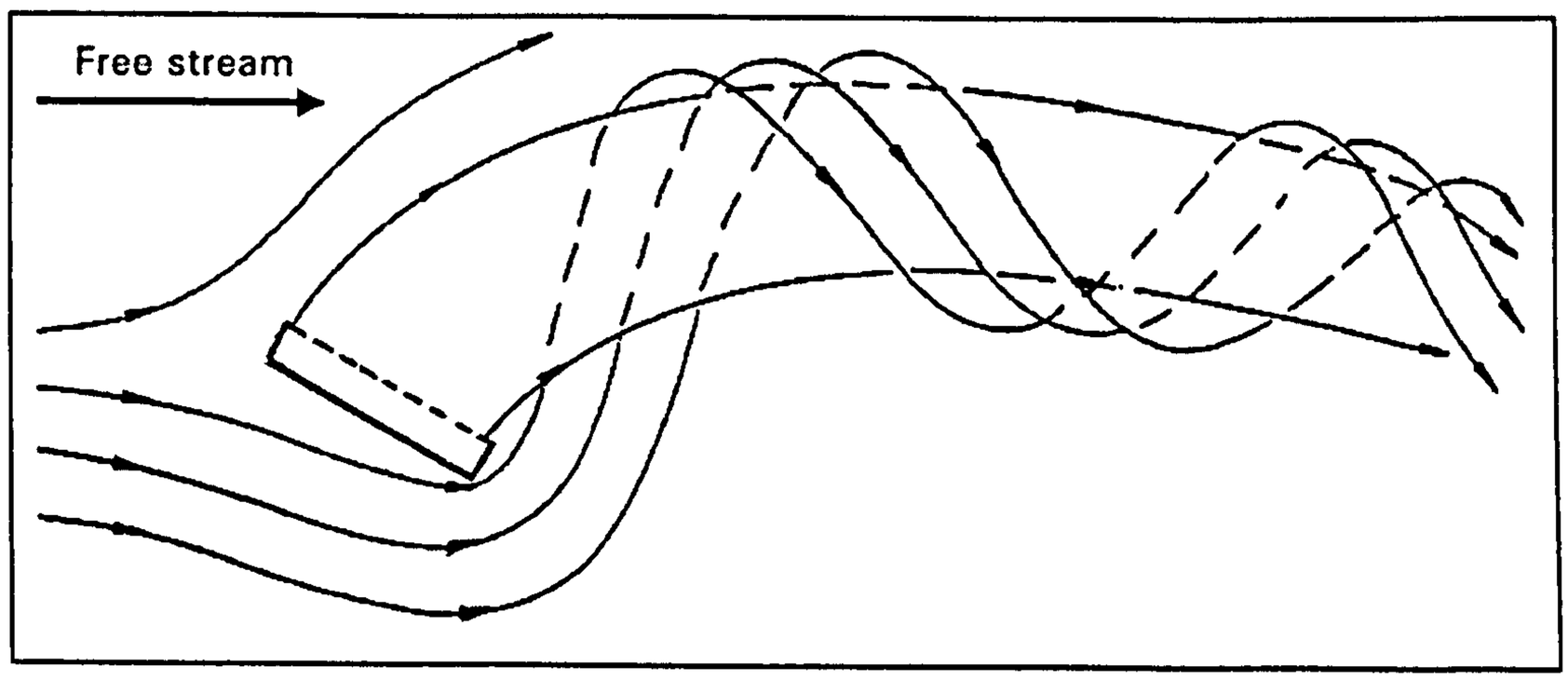

Figure 10 Vortex formation around a jet of air (Rao, 1988)

2.2 Review of previous work (1) - Air jet vortex generators

Air jets were conceived by Wallis (1952), who used spanwise rows of round air jets issuing normal to the surface in the control of low speed turbulent separation. Later, he introduced a spanwise component of flow by inclining the jets across the main flow. This had the effect of producing a single strong vortex as opposed to two weaker counter-rotating vortices. From these results he concluded that a row of inclined air jets were closely analogous to a row of vane vortex generators (Wallis, 1956). The literature history then shows that although other authors investigated air jets around this time, principally in the control of shock-induced separation, the subject was not investigated further until the mid 1980's.

A set of experiments on the vorticity produced by a single air jet by Freestone (1985), concluded that by giving the jet of air a downstream component of velocity (skew: see section 2.3.5) as well as a spanwise component (pitch: see section 2.3.4), stronger vortices are formed. He also noted that by fairing the jet exit the vorticity increased. It has been reported correctly elsewhere that the rectangular jet used produced greater vorticity than circular jets. However it was *not* concluded that rectangular jets were better than circular jets, and rightly so, because the experiments did not compare like with like. In Freestones tests the rounder jet had a much larger exit area and was pitched at a different angle.

Rao (1988), investigates the effects of air jets on a half wing in the control of shock induced separation. A useful insight into the development of the vortex was gleaned when a jet of coloured dye was ejected into a flow of water. The test revealed that the vortex core is, as previously thought, the jet itself (Figure 10). This is one of the main flow features which distinguishes a vortex produced by a vane, which has a low velocity core, to that produced by an air jet. Compton and Johnston (1991), confirmed this finding on a flat wall in an adverse pressure gradient with a single jet pitched at 45° and suggested that an optimum skew angle lies somewhere between 45° and 90°.

An important result of Compton and Johnston (1991) was to show that the vortex strength is a function of the velocity ratio, VR, the ratio of jet exit velocity, V_{jet} to the local flow velocity at the jet exit, V_{exit}. This was confirmed computationally by Henry et al (1994).

The first notable parametric study of air jet vortex generators is undertaken by Selby et al, (1992) who conducted experiments on a rearward facing ramp. Tests were performed for various skew and pitch angles, sizes of jet, and flow rates. The effectiveness of the various configurations was based on their ability to control flow separation from the ramp. Skew was first held constant at 90° whilst pitch was changed (15°, 25°, 45° and 90°), of which the 25° pitch proved to be the best, although the optimum angle could lie either side of this. After this the pitch was fixed at 15° and then 45° whilst the skew was varied. The best results (in terms of pressure recovery and reattachment line location) were obtained for skew angles of 60° and 90° respectively. Strangely it appears that skew was not varied at the best pitch angle of 25°.

Innes, (1995), installed an array of rectangular air jet vortex generators on a two-dimensional, three-element high-lift system. His choice of pitch and skew were 45° and 60° respectively. He concluded that, "The improvements (increased lift over whole alpha range and substantial increase in $C_{Lmax.}$) are much greater than those typically associated with vane vortex generators and cannot simply be associated with the suppression of boundary layer separation." Detailed shear layer investigations revealed that the jets penetrated through and interacted with the complex shear layers above the high lift system.

Computational evaluation of air jet vortex generators on a flat plate by Zhang (1993), confirmed that a counter-rotating system (section 2.3.1) of vortices does indeed produce stronger vortices in the near field close to the jet exits but that these tend to leave the surface earlier than vortices produced by a co-rotating system. He did not find any significant difference between circular and rectangular jets of equal exit area in the vortex strength produced, although the aspect ratio (section 2.3.6) of these jets was very low at 2.5. He went on to suggest that a 'narrow slot' rather than a rectangular jet may produce a stronger vortex.

More recent computational work by Henry and Pearcey (1994) drew much of the previous experimental work together. On the premise that increasing skin friction is a good measure of vortex strength since it implies a thinning boundary layer, the effects of exit velocity, pitch and skew on vortex strength were calculated and shown to be in agreement with the previous experimental data of Johnston and Nishi (1990) and Compton and Johnston (1991). An optimum pitch and skew of 30° and 60° respectively were suggested and these values, coincidentally, are those that were chosen for this study early in 1994. Skin friction (vortex strength) was shown to be little affected by the slot geometry, although Compton and Johnston's (1991) finding that the vortex strength is a strong function of the velocity ratio, VR, was confirmed.

2.3 AJVG considerations and design

When designing a system of vortex generators there are many variables to be considered such as spacing, pitch of jet, skew of jet, etc. A great many ajvg configurations are therefore possible. Previous research into ajvg's has yet to describe a set of hard and fast rules for their design, unlike vanes (Pearcey, 1961). In the following section each variable is described in turn and the choice made for the current work is reasoned. As two different configurations have been employed the precise configurations are re-iterated in the appropriate section of results.

2.3.1 Co- or counter-rotating vortices?

Experimental work carried out on vanes has shown that a higher C_{Lmax} may be obtained by using Counter-rotating pairs, provided they are correctly located in relation to the position of separation. However, such vortices tend to move together and leave the surface, under the influence of their image vortices. This renders their chordwise location difficult with respect to delaying separation (Pearcey, 1961). This has also been found to be true of vortices generated by air jet (Zhang, 1993).

For a wind turbine blade, whose stall characteristics are notoriously difficult to predict, (partly because of the three dimensional nature of the flow), it makes sense to choose Co-rotating vortices which, while sacrificing some vortex strength, tend to remain close to the surface for an extensive chordwise distance. Their effectiveness is therefore relatively insensitive to the choice of position with respect to the point of separation. The figure below shows how a vane generated Counter-rotating pair of vortices have moved closer together and away from the surface under their own induced velocities.

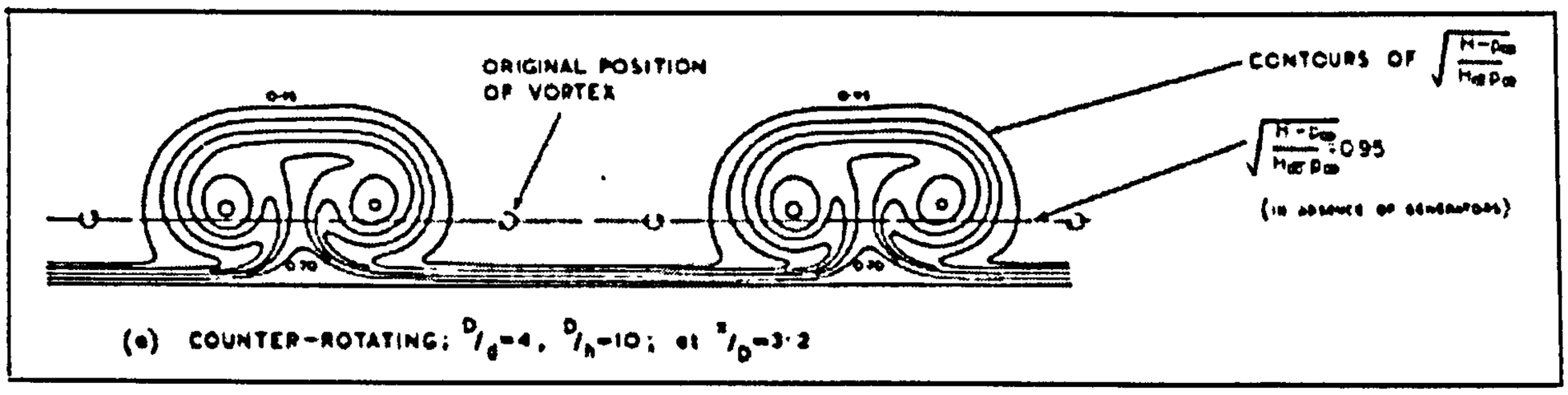

Figure 11 Counter-rotating vane vortex pair (Pearcey, 1961)

Also, Pearcey (1961) says that Co-rotating vane vortex generators are relatively insensitive to local flow direction, thereby implying that Counter-rotating systems are not. Additionally, Counter-rotating pairs of air jet vortex generators have not yet been investigated with an element of cross-flow velocity, as occurs on a wind turbine. Figure 12 illustrates how Co-rotating jets of air emanating from the surface of a wind turbine blade create longitudinal vortices which trail over the blade in the chordwise direction when viewed from the leading edge.

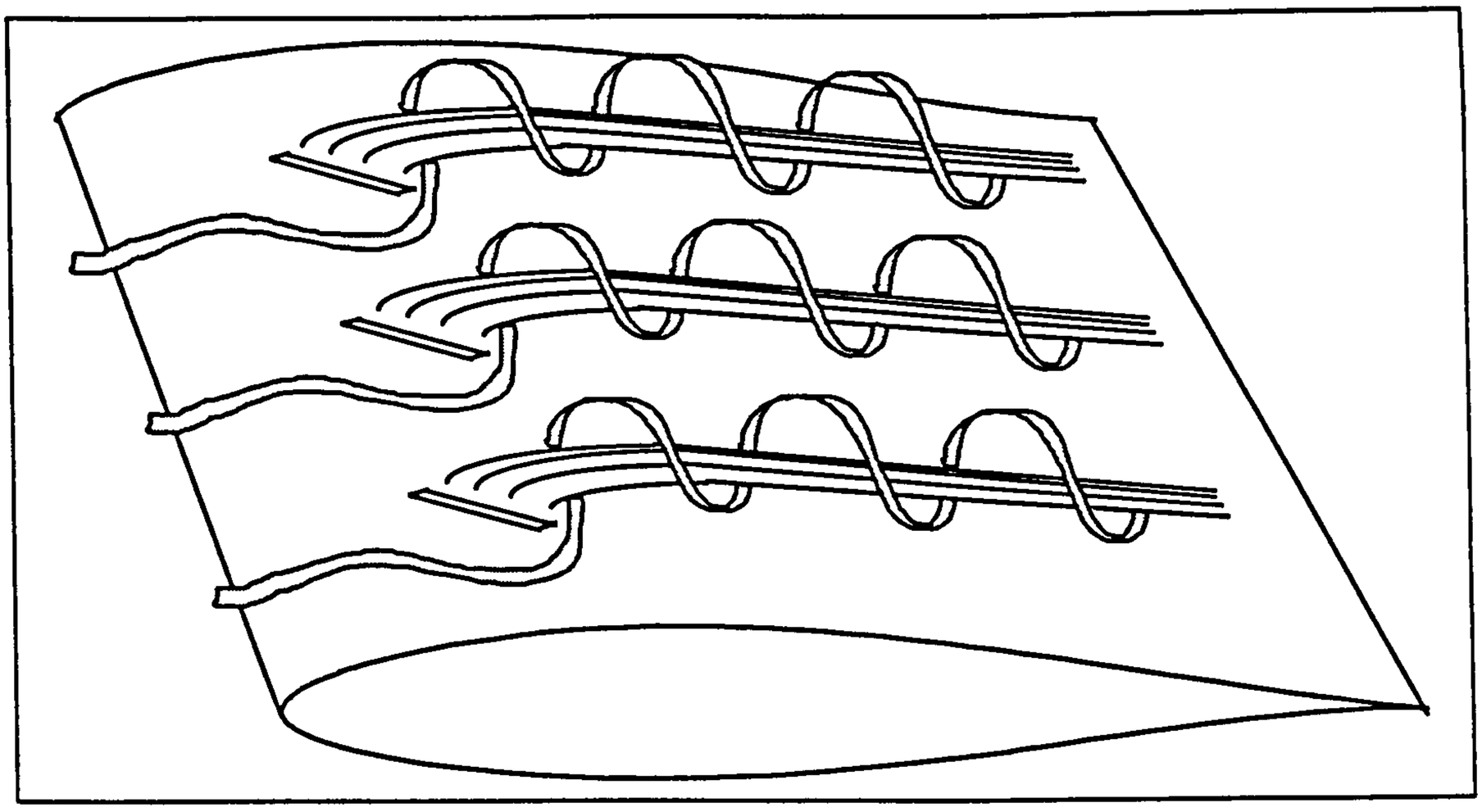

Figure 12 Co-rotating vortices trailing over 'blade'.

2.3.2 Chordwise location.

The chordwise location of air jets is not very well understood at present. However, the inherent thought is that they need to be set far enough forward that they are in flow with a high local velocity. In this way a greater jet exit velocity is obtained due to the higher pressure difference between plenum and surface, for a given plenum pressure. Conversely, they must be far enough back that the generated vortices retain their strength where separation is likely to occur, although this is not as critical for co-rotating systems, as was discussed above.

A further consideration could be the boundary layer thickness, which is dependent on a number of factors, including Reynolds number. Henry and Pearcey (1994), showed that jets with a greater mass flow rate (jet velocity) produce vortices that penetrate farther into the main flow and that the resulting vortex is situated farther from the surface. Minimising the mass flow in the full scale application means that the vortex will be generated relatively closer to the surface and so it makes sense to generate the vortex in a thinner boundary layer, i.e. closer to the leading edge than trailing edge. Computation of the aerofoil pressure distributions with the Williams code (Williams, 1984) were made (sections 2.6 and 4.1). These showed that the peak suction of the NACA 63_2-217 (the profile of the wind tunnel model) is very close to the leading edge at incidences greater than where the lift curve begins to de-linearise, i.e. where improved performance is required. It was therefore decided to locate the jets just behind the peak suction at 10% chord, in the strong adverse pressure gradient.

2.3.3 Blowing pressure.

This is the pressure in the plenum chamber of the model or blade which is driving the jets. The greater the blowing pressure, the greater the jet velocity, up to a point, and hence strength of the induced vortex.

In the experimental arrangement, the blowing pressure could be measured directly with a mercury manometer and so was easily repeatable from one experiment to the next. Mass flow supplied could be calculated but could not be measured directly. Thus when comparing two different air jet systems, in addition to the aerodynamic characteristics, it was the mass flow requirements that were compared at a constant blowing pressure and not vice versa. Of course for a given system of vortex generators the mass flow is mainly a function of blowing pressure supplied. It was discovered, though, that it is also a weak function of angle of attack (upper surface pressure at jet exit).

2.3.4 Pitch

In previous work pitch has variously been referred to with the symbols, α, ϕ, and θ. Here pitch is denoted by ϕ and is the angle at which the jet of air exits the local aerofoil surface (measured relative to the local surface in the chord direction). Its optimum appears to be a function of skew and vice versa.

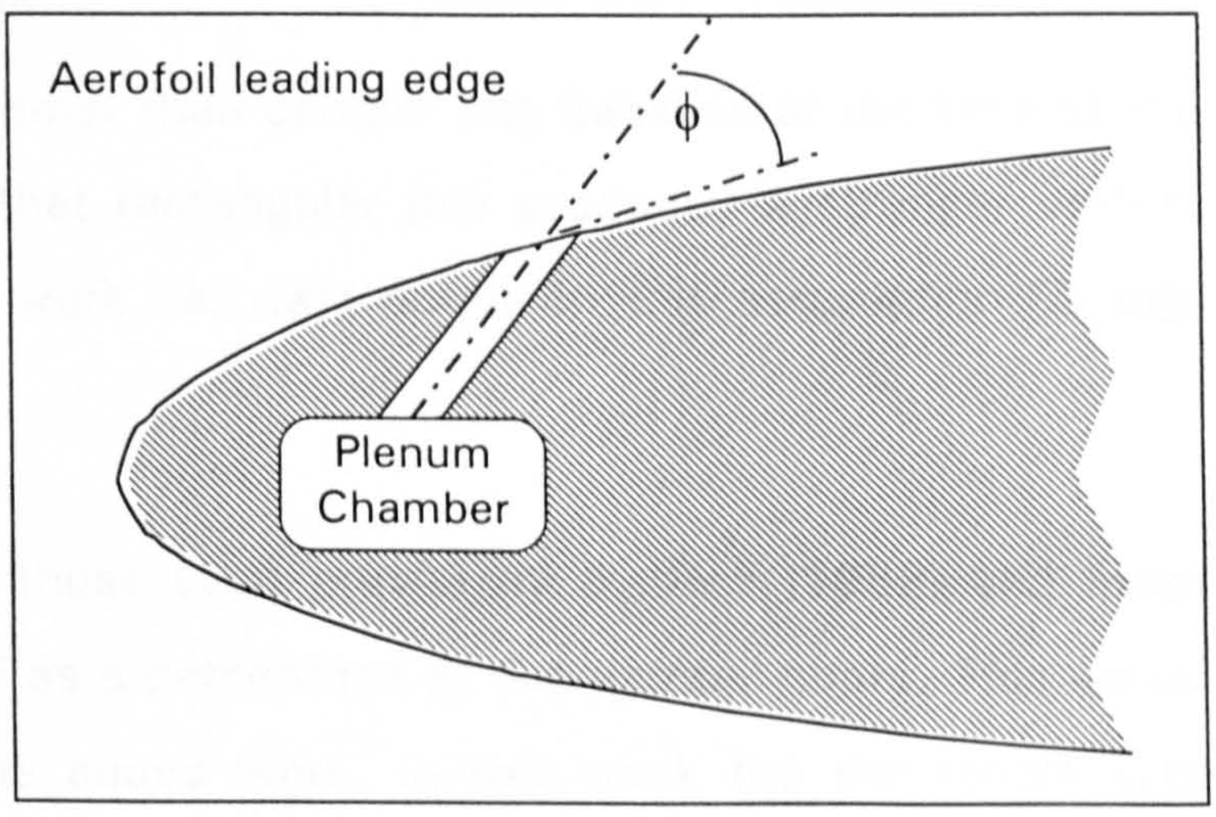

Figure 13 Illustration of jet pitch angle

Most previous work has been with a pitch of 45°, but the parametric study by Selby et al (1992) showed that pitches of 15°, 25° and 45° could all be effective when combined with the right skew angle. A pitch in the middle of this range of $\phi = 30°$ was chosen for this study.

2.3.5 Skew.

Skew, θ, (previously referred to as β, θ, ϕ) is the angle that the air jet makes with the free stream and is illustrated in Figure 14, opposite. Compton and Johnston (1991) said that an optimum skew may be in the region $45° < \theta < 90$. In this study a skew of 60° was used.

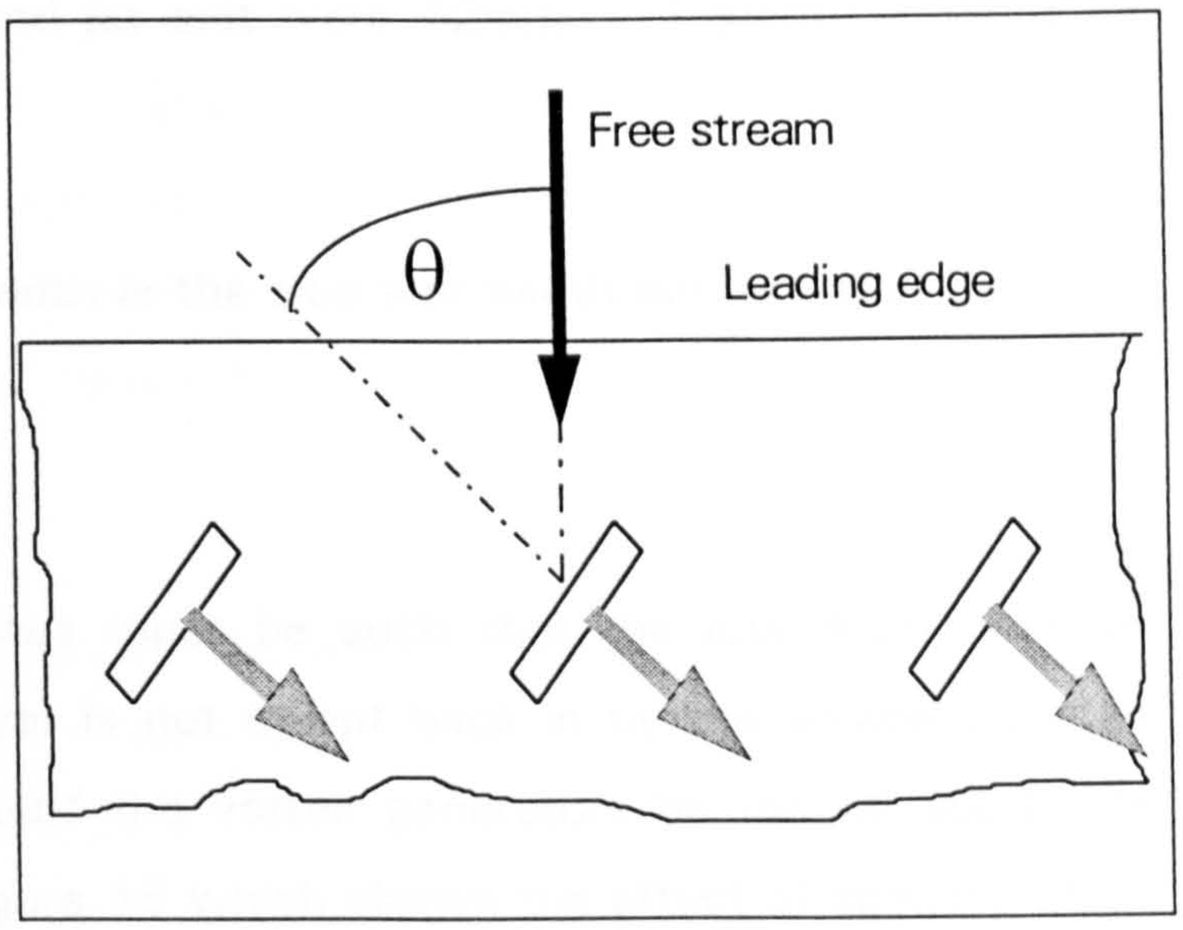

Figure 14 Illustration of skew angle

The selected combination of pitch, $\phi = 30°$ and skew, $\theta = 60°$ was later proposed by Henry and Pearcey (1994) as an optimum.

2.3.6 Air jet type and dimensions.

Rectangular jets were selected rather than circular jets because at the time of the system design it was thought that rectangular jets produced a stronger vortex. However, recent computational work has cast doubt on this assumption (Zhang, 1993).

To keep the system similar to those used previously by Rao (1988) and Innes (1995) the slot length was fixed as a percentage of the aerofoil chord. This varied between 2.5% and 4.2% in the above work. In this work the slot length was originally 16mm. or 3.2% of the aerofoil chord.

With slot length fixed as a function of aerofoil chord, it was considered that, for a given jet velocity (vortex strength), the mass flow requirement could be minimised by adopting a small slot width. In previous work the slot aspect ratio (ratio of slot length to width) has varied from 2.5 to 8. The larger aspect ratio was therefore selected giving the jet exit size as 16mm. x 2mm. Subsequent computational work (Henry & Pearcey, 1994) suggests that vortex strength is little affected by slot geometry, so this does seem to be a reasonable approach to reducing the mass flow requirement.

A second jet size was also tested, the reasons for which are explained in section 5.4. The dimensions of this second jet exit were 12mm. x 1.5mm., keeping the aspect ratio constant at 8.

It should be noted that the slot width is the true slot width and not that projected onto the aerofoil surface.

2.3.7 Spacing.

The spacing of co-rotating vortices must be such that the low momentum air swept out from the boundary layer is not swept back in by the adjacent vortex. Neither, for obvious reasons, should the vortex generators be too far apart. The damping effect is illustrated in Figure 15 which shows the effect of spacing, D, on co-rotating *vane* vortex generators of height, h (Pearcey, 1961). Innes (1995) used a spacing of approximately four times the length of the jet exits, L and a similar spacing of 3.75 x L , was adopted for this study.

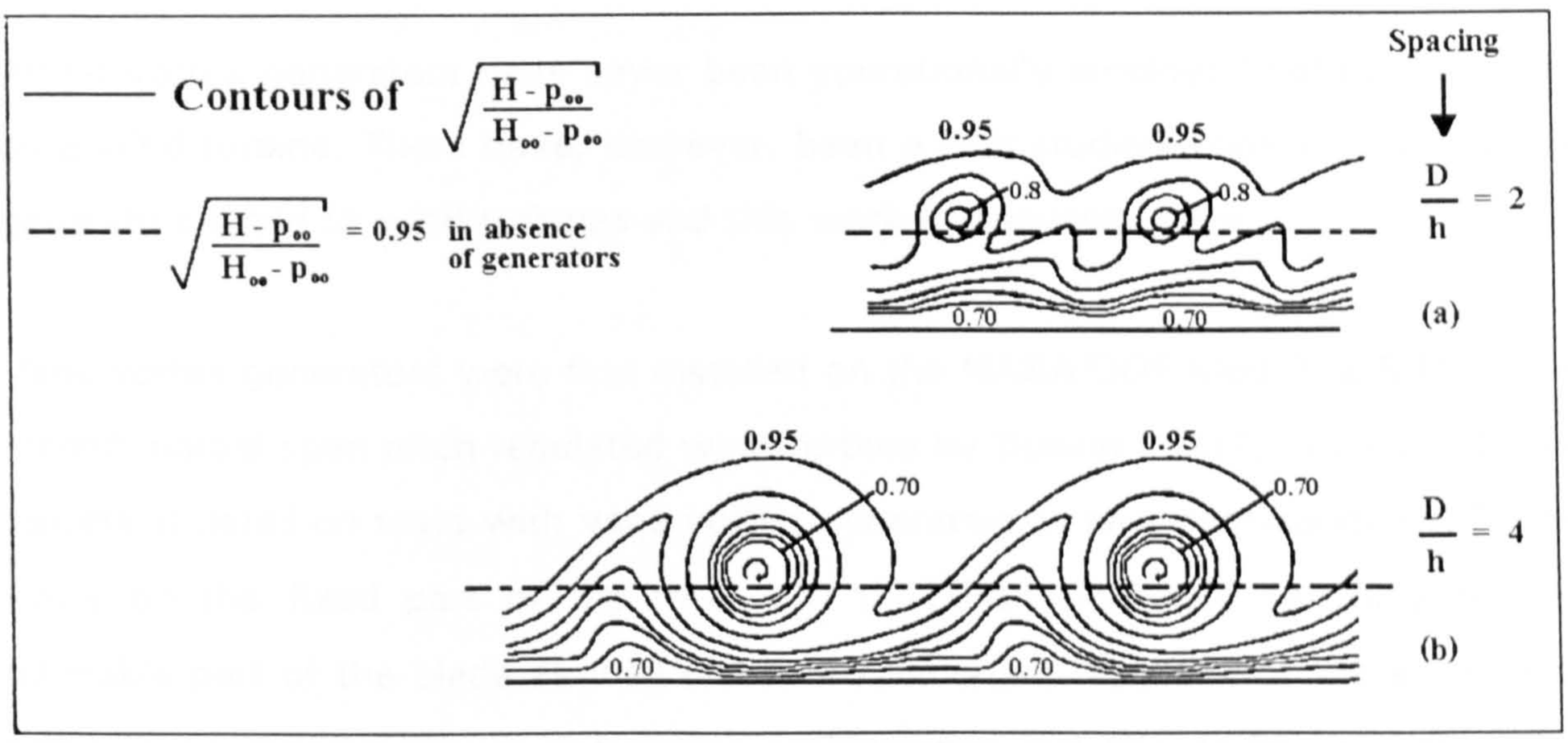

Figure 15 Effect of spacing on co-rotating vane v.g's (Pearcey, 1961).

2.4 Advantages of ajvg's over vvg's for a wind turbine application

Vane vortex generators have been used extensively as a method of boundary layer control, for many high speed aircraft. However, at low angles of attack, α, the total drag with vanes is greater than that of the unmodified aerofoil. Retracting the vanes at low angles of attack is an option but this means a rotor weight penalty which, for a wind turbine, is undesirable.

With air jet vortex generators, the drag penalty is not as severe because the jets of air impart momentum to the flow. This acts to counter the effects of the parasitic drag caused by the irregularity of the jet exit on the aerofoil surface. Furthermore ajvg's also have the advantage over vvg's in that they can reattach a separated flow by penetrating the region of separation to generate vortices in the outer flow. Vanes cannot because there is no flow over them to generate vortices when the aerofoil is stalled.

For a wind turbine application, though, the greatest advantage that ajvg's hold over vvg's is their controllability. A configuration of vvg's cannot be physically altered to yield more than one aerofoil Lift/Drag characteristic. By controlling the air supplied to ajvg's on the other hand, a whole family of Lift/Drag characteristics are obtainable. It was on this premise that ajvg's could be used as a form of power regulation for wind turbines.

2.5 Review of previous work (2) - VVG's applied to wind turbines

Air jet vortex generators have never been operationally employed before, let alone on a wind turbine. There have, however, been a few studies made of vane vortex generators fitted to wind turbines and this work is discussed here.

Vane vortex generators were first installed on the NASA/DOE Mod-2, 2.5 MW two bladed, partial-span pitch regulated wind turbine by Boeing (1982). Sullivan (1984) reports in detail on tests with vane vortex generators in two configurations. Firstly vvg's on the fixed part of the rotor (20 to 70% span) and secondly on the pitchable part of the blade as well (70 to 100% span). The aim of the study was primarily to improve power conversion performance but also to improve the drive train stability. The vvg's were arranged in a counter-rotating system and three sizes of vortex generator were employed, with the largest vanes being used for the larger chords at the blade root and smallest vanes at the tip.

One criterion used to asses the effectiveness of the vvg's was the wind speed at which the turbine reached rated power (rated wind speed). With no vvg's this value exceeded 16m/s. Vvg's on 70% of the span reduced this to 13.8m/s and 100% vvg's reduced it further still to 13.5m/s. The measured power curves are reproduced in Figure 16.

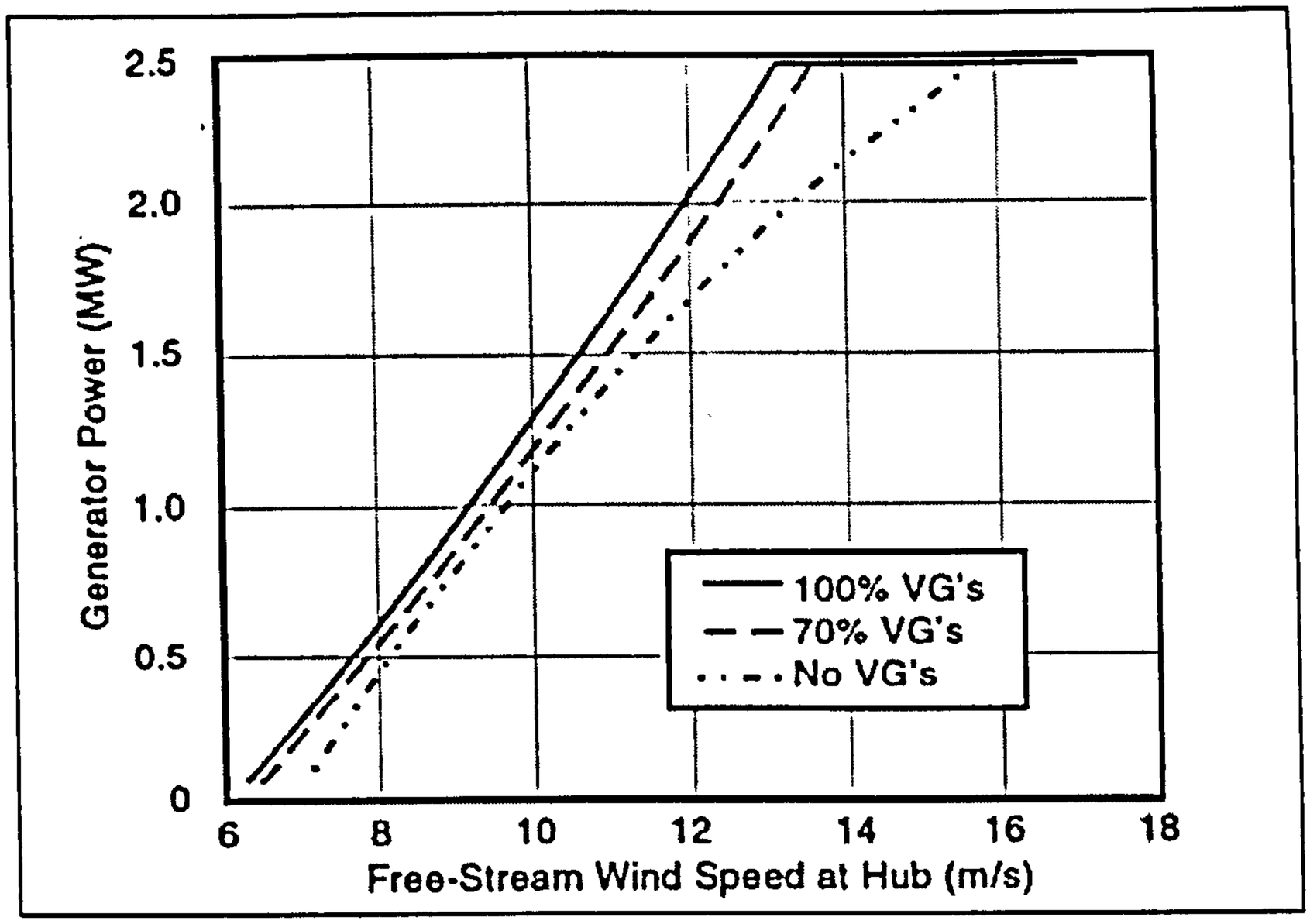

Figure 16 Power curves of the Mod-2 with and without vvg's (Sullivan, 1984)

For an average wind speed of 6.4m/s (10m. height), and a Weibull distribution (shape parameter, k, not given) Sullivan calculates 11% and 20% increases for the two vvg cases. One suspects, however, that this margin of increase was due more to the poor original power curve, as it was tailing off long before rated power. He concluded that these gains were at little or no cost in increased dynamic loads. Indeed he speculated that both blade and tower fatigue life would improve with the introduction of vvg's because peak steady loads were reduced. Later pressure measurements on this turbine by Nyland (1987) at 65% blade span confirmed that the vvg's were delaying separation. This work, however, was principally to measure pressure distributions on a rotating blade and compare them with those obtained in the steady state conditions of a wind tunnel.

Following on from this work, Corrigan and Savino (1985) investigated whether vvg's could improve the performance of intermediate sizes of wind turbines; specifically the NASA Mod-0, 100kW, 39 metre diameter machine. Full scale wind tunnel tests were conducted on a tip section (outer 7.31m.) through a full 360°. A counter-rotating system of vvg's was fitted to the outer 5.85m. of the tip, corresponding to the outer 30% of the blade. Five different sizes of vane were used over this distance, a 'trip strip' was installed and the vvg's were situated at 10% blade chord. Analysis of the wind tunnel results showed that the net force in the plane of rotation would be increased by 30% upon installation of vvg's at full scale. It was therefore concluded that vvg's did have some potential for improving

the power conversion performance of this turbine. This conclusion was upheld by subsequent field tests with increased rotor power measured for wind speeds above 6m/s and a 30% maximum increase in power.

Also in light of the success with the Mod-2, Garrad (1985) undertook wind tunnel tests and a theoretical study on behalf of James Howden and Co. to see if vortex generators could enhance the energy capture of their HWP 330. These tests again consisted of a counter-rotating system of vvg's. Various runs were completed, with vanes located at 30%, 40%, 45% and 50% chord with two different vane spacings and sizes. The larger vvg's located at 30% chord with the denser spacing proved to yield the largest increase in C_{Lmax}. Further tests were then carried out with the vvg's moving progressively forward from 20% to 10% to 6.7% chord and the maximum lift coefficient increased further still. The two foremost locations increasing C_{Lmax} from 1.30 on the unmodified GAW (1) section to 1.58. Garrad concluded that there was also a small drag penalty at low incidence.

The theoretical part of this study consisted of using a power prediction code to estimate the percentage increase in annual energy yield expected by modifying the blade with vortex generators. Garrad concluded that even quite large changes in C_{Lmax} of this pitch regulated machine would produce only small increases in energy yield of around 1%. This contrasted markedly with the findings of Sullivan (1984) who measured a 20% increase. Garrad goes on to present a previously published power curve of the Mod-2 alongside that used as the reference power curve by Sullivan. The latter was considerably poorer and Garrad suggests that either the blades were cleaned when the vortex generators were applied or that the vvg's corrected the power curve back to what it should be in its clean blade state. He adds that the NACA 230xx profile of the Mod-2 was later replaced by the GAW(1) because it was found to be susceptible to dirt.

These findings (maximum of 1% increase in energy yield), do not detract from using air jet vortex generators on a stall regulated wind turbine because of the 'knee' in its power curve described in section 1.2.1 and also the desire to regulate the power at above rated wind speeds.

Gyatt (1986) applies a counter-rotating system to the Carter 25 kW, stall regulated machine basing its design on the one used by Sullivan (1984). Field tests were conducted with vvg's on the inboard, outboard and complete blade. Leading edge roughness was employed on the outboard part of the blade to determine how vvg's may or may not overcome it. The study concluded that vvg's did improve the energy capture for sites above 13 m.p.h. (5.8m/s) average wind speed (at 10m. height assuming a Raleigh distribution). This was due to a slightly degraded performance at low wind speeds. Almost all of the benefit (5kW improvement in the best case) was due to vvg's on the outer half of the blade, probably because the inner half was almost certainly well above the stall angle of the blade with vanes. At 18 m.p.h. (8.0m/s) he calculates an 8.3% increase in energy yield.

Gyatt's modified and unmodified energy yields have both been recalculated to within +0.3% using his Weibull parameters and assumption of 1/7th power law for the earth's boundary layer by reading power straight from the graphs presented. However, it was discovered that the quoted increase of 8.3% is calculated on the basis that all of the 5kW power increase, over and above rated power, could be obtained in real life operation. This is doubtful because the modified power curve risks damage to the generator, particularly in a sustained period of high wind speeds. As the Carter is a stall regulated machine, then either a new generator of higher rated power would have to be installed or the blade setting angle would need to be reduced, both of which would almost certainly preclude any advantage gained by using vanes. Nevertheless, an important finding of this work was that vvg's can, to some extent, alleviate the effects of leading edge roughness such as would be caused by insect and dirt accumulation.

The literature survey showed that only one attempt to numerically model vvg's on a wind turbine has so far been attempted, (Afjeh et al, 1990). Their work numerically modelled the original tests carried out by Sullivan (1984) on the Mod-2. An excellent prediction of power was obtained for the case with 100% vortex generators, but the code over-predicted power for the case with no vvg's. This result lends weight to the argument put forward by Garrad (1985) that the blades of the Mod-2 may have been dirty when the tests were carried out.

Timmer and van Rooy (1994) combine wind tunnel tests with a performance prediction program to estimate the effect of vortex generators located on the inner 55% and 65% of the blades of a theoretical 600kW stall regulated machine. An impressive increase in C_{Lmax} of 40% delaying the stall angle from 8° to 18° was recorded. Full details of the configuration used are not given but these results were for vvg's located at 20% chord at a Reynolds number of 1 million on a 21% thick aerofoil designed in-house at the Delft University. The paper concluded that the application of vvg's would significantly improve the power output for 'the medium wind speeds' and would lead to a reduction of the rated wind speed (Figure 17). Although a cautionary note is added that the results obtained by the performance program rely in part on the adopted three-dimensional aerofoil performance. This is discussed in sections 6.6 and 6.7.3 of this thesis which describe the Himmelskamp effect and the extrapolation of lift and drag data into deep stall respectively.

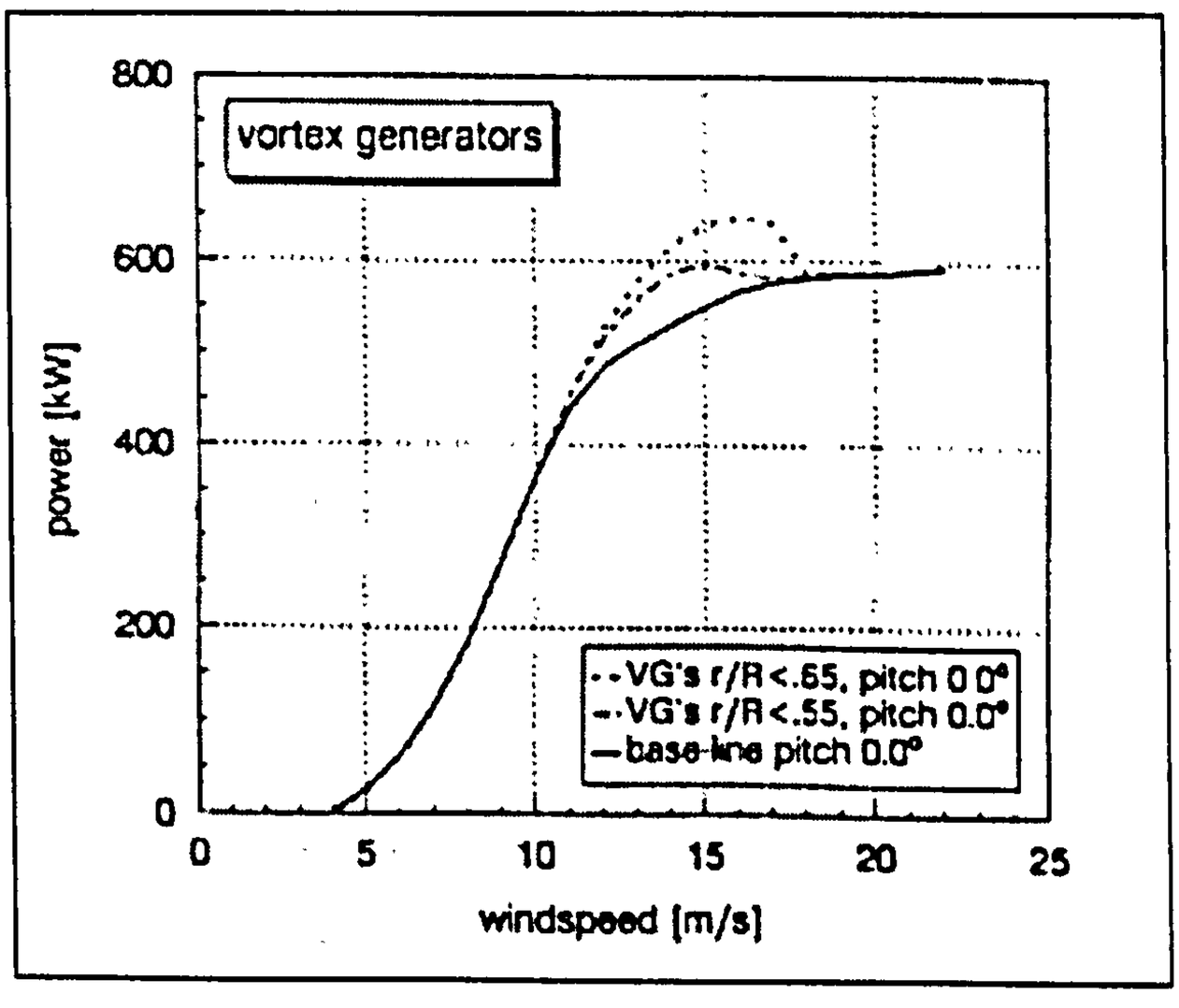

Figure 17 **Calculated power curves for rotor with vvg's (Timmer et al, 1994)**

Experimental wind tunnel investigations by Wetzel and Farokhi (1995) were carried out on the NREL S807 aerofoil, which is used principally on the inboard sections of stall regulated wind turbines, at Reynolds numbers of 0.5, 1.0 and 1.5 million. This research differs from the previous work in that rather than using vane vortex generators, 'Wishbone' vortex generators were employed, so called because their appearance resembles the wishbone of a chicken. Their advantage is that they have been shown to give increases in lift similar to traditional vvg's but with 'far less drag' (cited references). However, the results appear to contradict this with an

increase of 48% on C_{Dmin} at Re = 1.0 * 10^6 . (e.g. compare Corrigan and Savino (1985), above, who measured an increase of only 6% at α =5° , Re = 1.5 * 10^6 with traditional vvg's). The authors attribute this to using wishbone vortex generators which extended outside of the boundary layer too far. C_{Lmax} was found to increase upon application of the vg's by 15% at the same Reynolds number.

Applying the Wishbone generators to the inner 60% of the blades of an imaginary 80kW stall regulated wind turbine, it was predicted that although the vortex generators had generally degraded the power coefficient, there was a narrow band of tip speed ratios (4< λ <6) for which the performance would be improved. This would result in an overall increase in *predicted* energy yield for sites with a mean wind speed of 5.5m/s (hub height) or greater, rising to a maximum of about 4%.

Finally, Øye (1995) and Antoniou et al (1996) describe the application of counter-rotating vane vortex generators to the Elkraft 1000kW (rated power = 1100kW), stall regulated, Mega-Watt scale demonstration turbine. In this application the vvg's were used to correct the power curve of the prototype to the design calculations. Originally at a blade setting angle of -1.0° the power curve above 9m/s had a reduced slope and rated power was never reached (Figure 18; compare 'Meas. -1.0, no VG' to 'Design'). The pitch was changed to +0.5° and although this improved performance significantly, the resultant energy capture was still below the design goal by some 6% for a mean wind speed of 7m/s. It was suspected that the cause of the reduced performance was early flow separation from the very thick sections of blade that had been used at the root for structural reasons (24% to 40% t/c at corresponding r/R of 45% and 25%). Application of vvg's at the original blade setting angle of -1.0° increased the energy production to within 1% of the design goal and the resultant power curve is also shown in Figure 18 ('Meas. -1.0, with VG').

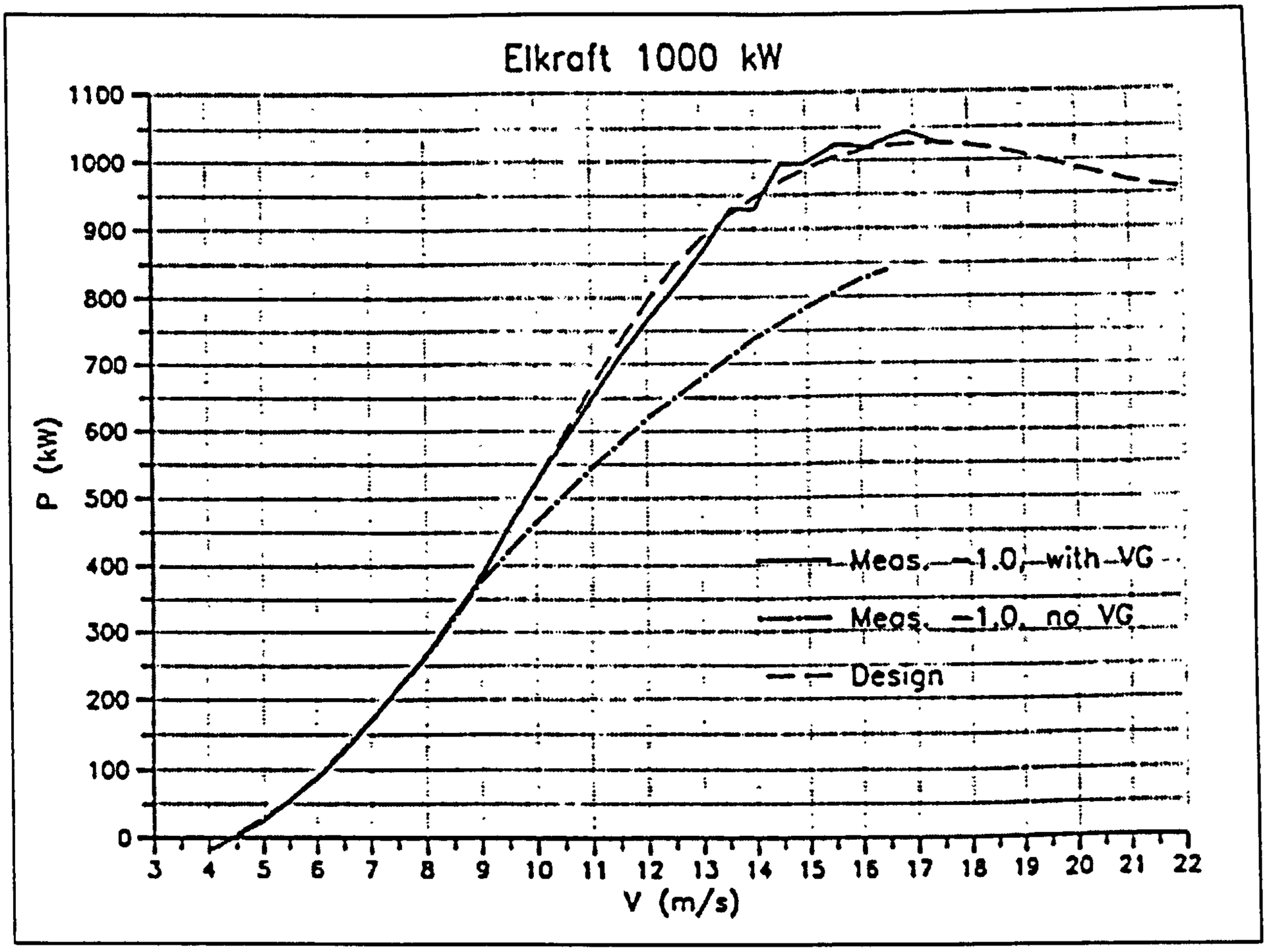

Figure 18 **Measured power curves with and without vvg's (Øye, 1995)**

2.5.1 Summary of literature review

Previous work undertaken with vane vortex generators for wind turbines has been exclusively with counter-rotating vvg's. This is somewhat surprising, considering that the effectiveness of co-rotating vvg's is much less sensitive to their chordwise location than that of counter-rotating vvg's. The former were chosen for this study (Section 2.3.1).

Vvg's are ideal when applied to a pitch regulated wind turbine because the maximum power output can be limited by blade pitch. They can therefore be applied to 100% of the blade. Any increase in annual energy yield is mean wind speed dependent and there will be a mean wind speed where the net effect on energy capture of installing vanes is zero. This is because the power is degraded at lower wind speeds due to increased drag with vvg's at low angles of attack.

There appears to be some confusion as to the amount of extra energy that could be expected by applying vvg's to a pitch regulated machine. In the example given by Sullivan (1984), the vortex generators were probably being used to correct the power curve back to the design condition, i.e. clean blades, and so the quoted

increase in energy yield of 20% is thought to be highly optimistic. If the pitch regulated machine is well designed and suited to the average wind speed of the site, then Garrad's (1985) estimate of 1% is probably much nearer the mark, particularly for efficient modern wind turbines.

Rather than only considering energy increase we should also consider vortex generators (vvg's and ajvg's) as having the ability to save energy as the blades become dirty. Both Gyatt (1986) (stall regulated machine) and unwittingly, Sullivan, showed that these boundary layer control devices compensate for the effects of dirt. Over the period of a year the difference in energy capture between a standard pitch regulated machine and one modified with vvg's operated side by side would therefore be expected to be greater than the figure of 1% quoted by Garrad. When it is also considered that the blades may not have to be washed as frequently the application of vvg's to pitch regulated machines appears to be a very attractive proposition. In any case, even a 1% increase is worth having when it is such a cheap and simple procedure to fit vanes to a blade. This is probably not the case for ajvg's which are rather more complex to install and would probably achieve a similar result (pitch regulated machine only).

For stall regulated machines, one has to be much more careful when installing vvg's that the peak power still remains close to rated as there is now no control mechanism to limit it. Although a figure of 8.3% was reported by Gyatt (1986), it was shown that this is unlikely to be achieved in operation. In fact one could go so far as to say that if the stall regulated machine is well designed, there is unlikely to be any benefit of using vvg's as a retro-fitted component. The exception being the example given by Øye (1995) and Antoniou et al (1996) where vvg's were used to correct the power curve of a prototype machine to the design curve.

The advantage of using air jets is that this feature is, theoretically, not a problem since the power can be regulated by altering the air supply. If Gyatt's improvement of the power curve was limited to rated power, then the figure would drop from 8.3% to 2.6%. This may be a good first approximation to the potential for air jets to improve the energy yield of a stall regulated machine. In short, vane vortex generators should be used for pitch regulated wind turbines and air jet vortex generators should be used for stall regulated wind turbines.

The example given by Øye (1995) and Antoniou et al (1996) is perhaps the most promising of all. They thought that the poor power curve of the prototype was due to the very thick sections (up to 40%) that were used. It may therefore be possible to design even thicker blade roots, knowing that either vvg's or ajvg's will prevent early separation. This would allow much larger blades to be manufactured leading to machines of larger rated power and the associated economies of scale.

The increased lift provided by vortex generators may also allow blades which are more slender to be designed. This would lead to a lighter rotor and, for stall regulated machines, lower peak loads when the blades are parked in high winds.

The studies where a power prediction code has been used to estimate increased energy yield due to vortex generators, including this thesis, must be treated with some caution as the authors themselves acknowledge. Much is yet to be understood about the way in which vortex generators modify the lift and drag curves in deep stall and how the performance of vortex generators is affected by three-dimensional effects. (Since these effects are produced by separation on the blade and vortex generators delay separation).

2.6 Williams code

The Williams code models the incompressible flow around a two-dimensional aerofoil up to stall using the Viscous-Inviscid Interaction approach (Williams, 1984). Characteristics such as pressure distribution, wake pressures, boundary layer thickness etc. are calculated. It is simple to use in that it requires only a few inputs such as the aerofoil co-ordinates (read from an external file), Reynolds number, Mach number etc. The user specifies either fixed or free transition and prescribes a sequence of angles of attack for which the characteristics are to be calculated.

Its use in the project was primarily to gain an insight into the pressure distribution of the NACA aerofoil in order to locate the air jet vortex generators and to determine a suitable transition strip for the model. A brief guide to using the code and its inputs can be found in Appendix 2.

3. EXPERIMENTAL TECHNIQUES

3.1 Wind tunnel

The wind tunnel testing was carried out in City University's T2 wind tunnel which is of the closed circuit type. The working section is vented to atmosphere at the rear and its dimensions are 0.81m. * 1.12m. with a length of 1.68m. The tunnel has a Reynolds number capability of 3.1 million per metre of model (The speed range is 0 - 45m/s).

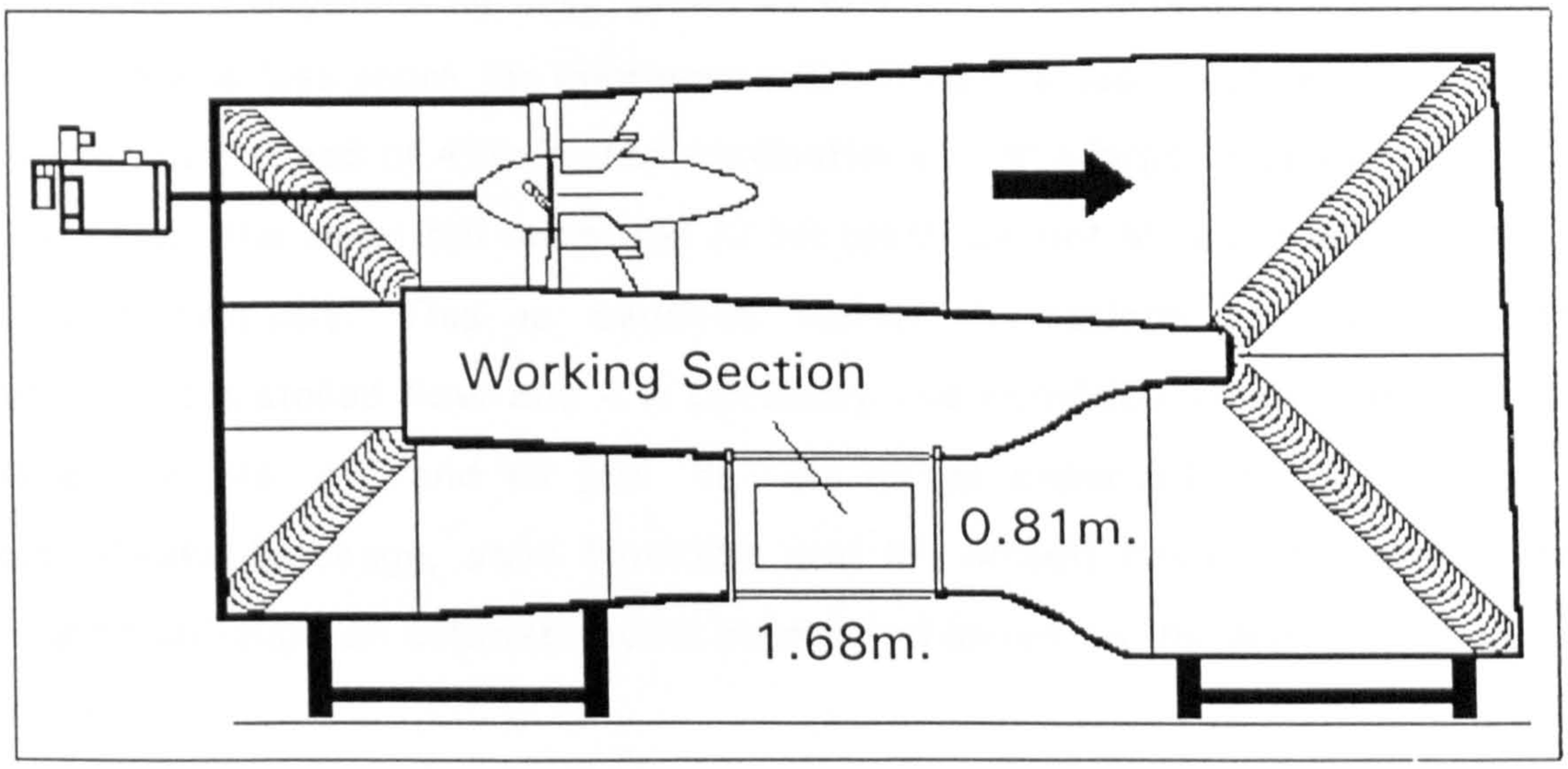

Figure 19 Illustration of the wind tunnel

3.2 Profile type, dimensions and test conditions

The profile of the wind tunnel model was the NACA 63_2-2xx which is the same as the blades of the test machine. Appendix 3 describes this profile in more detail and the derivation of its co-ordinates.

Initially it was not known whether air jets would be located over the whole blade or just part of the blade in the spanwise sense. However, the spanwise blade radius on which to base the model had to be chosen as this would determine the model thickness. It was decided that the wind tunnel model should be based on a section roughly 80% along the span of the blade. Here the tip effects would be diminishing but a modification to the blade aerodynamic characteristics by air jets would be able to effect a significant change in the power curve at wind speeds around rated power. The spanwise radius of r/R = 0.806 was chosen as the manufacturers data lists the blade properties at this point without the need for interpolation.

At this radius the blade chord is 0.61m. and the thickness to chord ratio is 17.05%. The rotor speed of the test wind turbine is 51.1 r.p.m giving a rotational velocity of 43m/s and a Reynolds number of 1.8 million at this point on the blade, ignoring the effects of wind speed.

The model chord selected of 0.5m. represents a considerable blockage (14.5%) for the incidence range to be measured ($0° \leq \alpha \leq 19°$). However, it was felt essential that the Reynolds number should be kept as close as possible to that of the test machine because the performance of high lift devices generally tends to diminish with increasing Reynolds number. (Viscous effects become relatively less dominant and so there is less room for improvement). Thus the test Reynolds number was 1.4 million at a speed of 43m/s. The implications of this large blockage ratio is that the data from the clean foil tests and air jet tests are not absolute and can only be used comparatively. This is because tunnel corrections cannot be applied accurately to a stalled flow and it is precisely this condition where the differences between air jets 'off' and air jets 'on' are to be expected. Tunnel interference effects (Wake blockage, solid blockage and lift effect) have not therefore been calculated although an estimate could be derived based on the work of Maskell and Gould, etc.

3.3 Design of the wind tunnel model.

The aerofoil co-ordinates were input into a CNC milling machine to enable a profile template to be made. This was used to aid manufacture of the wooden model.

Due to the large number of air jet configurations possible, the model was manufactured to have a removable leading edge. Several leading edges were made which could have different air jet configurations manufactured into them or be left blank for the clean foil tests. Figure 20 shows the model with the leading edge removed. Air is injected into the plenum chamber and dispersed at a constant pressure by a baffle plate during air jet testing. Rubber 'O' ring seals prevented air leakage from the plenum. This forward plenum chamber was sufficient to allow air jets to be located between 6% and 30% chord. Although a rear plenum was also manufactured into the model (50% to 65% chord), it was not used.

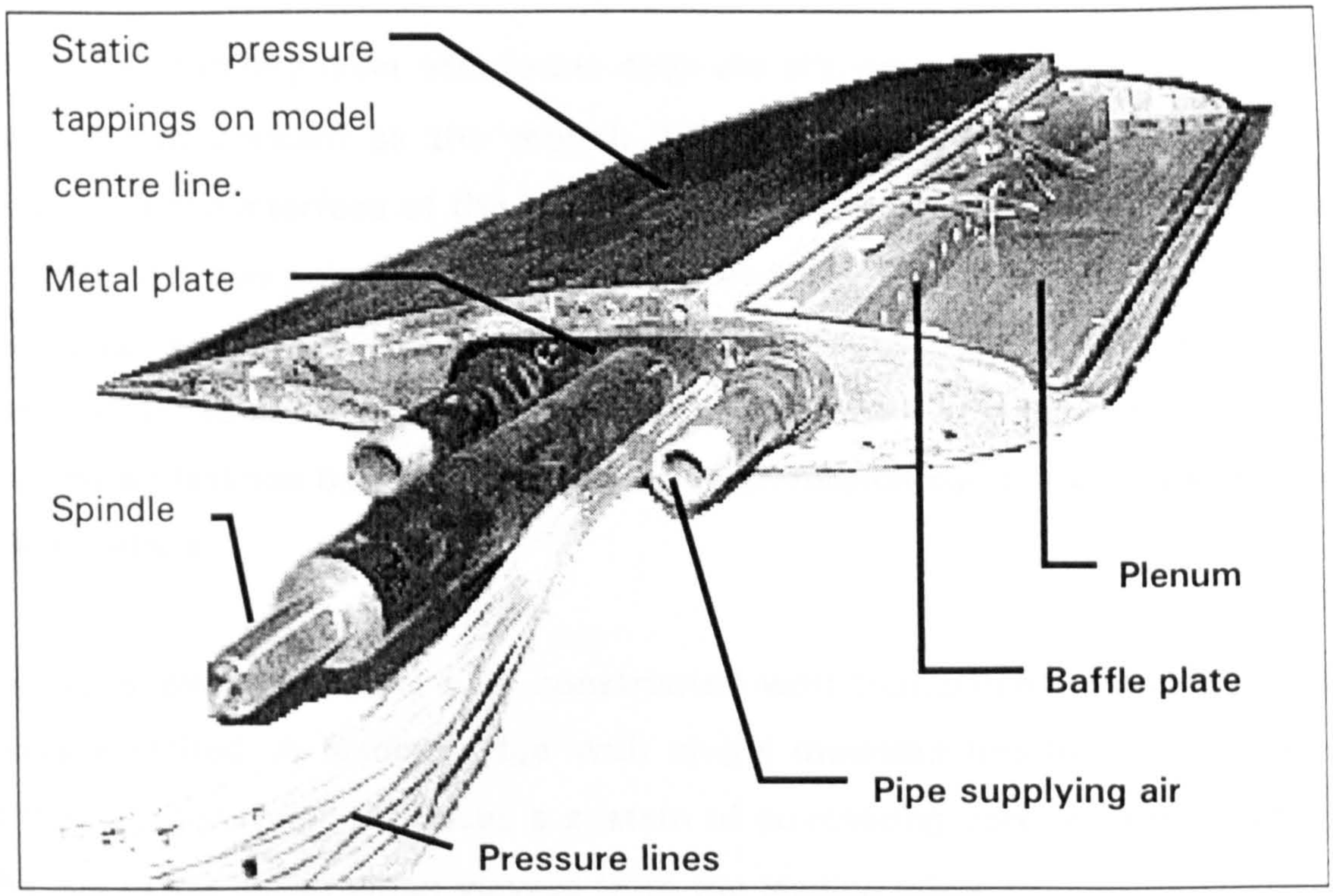

Figure 20 Internal construction of the wind tunnel model

A metal plate was sunk into each end of the model. Attached to each plate were the spindle, about which the model rotates, and the two pipes that supply air to the forward and aft plenum chambers. By housing the spindle in a metal plate the risk of it shearing and damaging the wooden model were reduced.

3.4 End plates and slot blowing for two dimensional testing.

End-plates were attached to the model to prevent spillage from the tunnel wall boundary layer. The total span of model between end plates was 741mm.

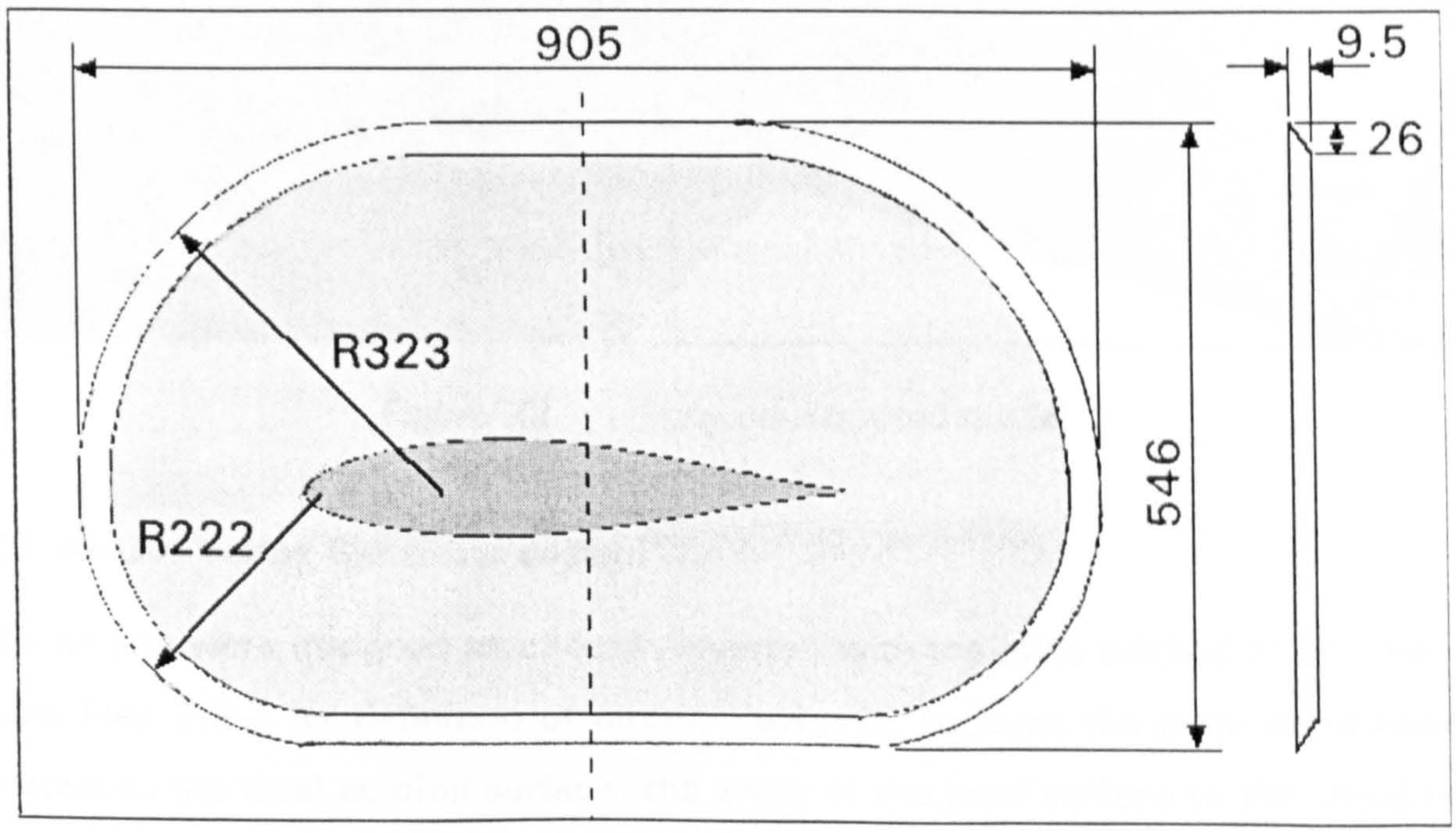

Figure 21 End plate dimensions

However, a boundary layer still forms over the end-plates because they are in the same pressure gradient as the model. This leads to eventual flow reversal and separation at the interface of the model and end-plate. To eliminate this feature the end-plates had two pairs of slots manufactured into them. By blowing air through these slots, set at 15° to the surface, better two-dimensional flow could be established up to and beyond stall (Innes, 1995). Rubber seals and silicon sealant prevented air leakage between upper and lower aerofoil surface at the endplate and model interface.

Figure 22 shows the model fully constructed with transparent end plates and slot blowers attached. A leading edge with ajvg's mounted has been installed. Note that this configuration produces a system of co-rotating vortices which will rotate in the clockwise sense when viewed from the leading edge.

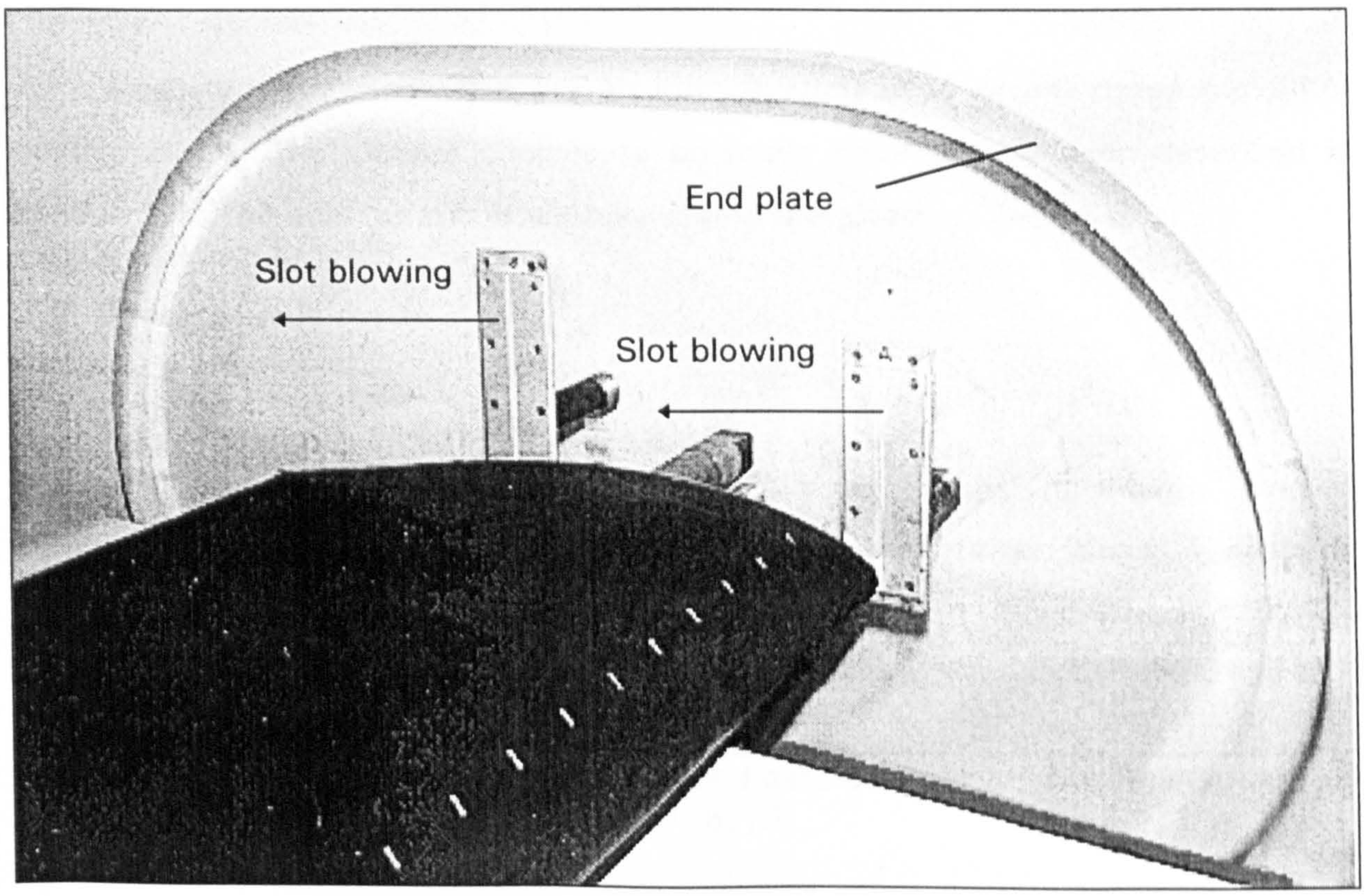

Figure 22 Fully constructed model

3.5 Air Jet Vortex Generator design.

The air jets were designed as circular 'inserts', with the exits pitched at 30° for all tests (see 2.3.4 for definition of pitch). However, because the pitch is measured relative to the local aerofoil surface, the angle of the local surface to the chord line had to be calculated before the leading edge was drilled. (This was achieved by using the 'Angle enquiry' feature on the drawing package, AutoCAD.)

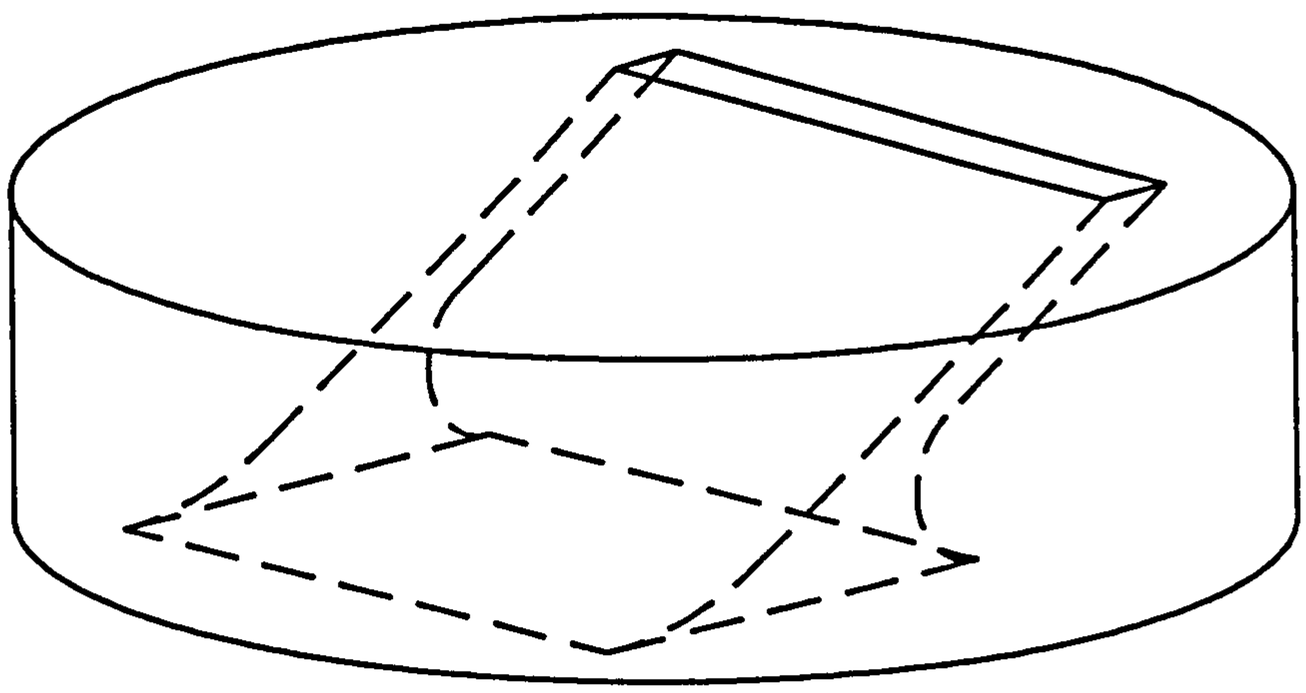

Figure 23 Depiction of an air jet 'insert'

The under-side of the ajvg 'inserts' were faired so that flow separation in the slots would be minimised. The 'inserts' were then glued into one of the aerofoil 'leading edges' at the correct skew angle and spacing before being filed flush with the surface.

As previously mentioned there are an infinite number of air jet vortex generator configurations. The various choices to be made have already been described in section 2.1. The configurations actually tested are given in Chapter 5.

3.6 Measurements made

3.6.1 Drag

The drag was determined using the B.M. Jones momentum integral method (1936), which assumes that in any given stream tube between planes 1 (close to the aerofoil) and 2 (far downstream), the total pressure, H, could be considered to remain constant. This is very nearly the case in practice, even in turbulent wakes.

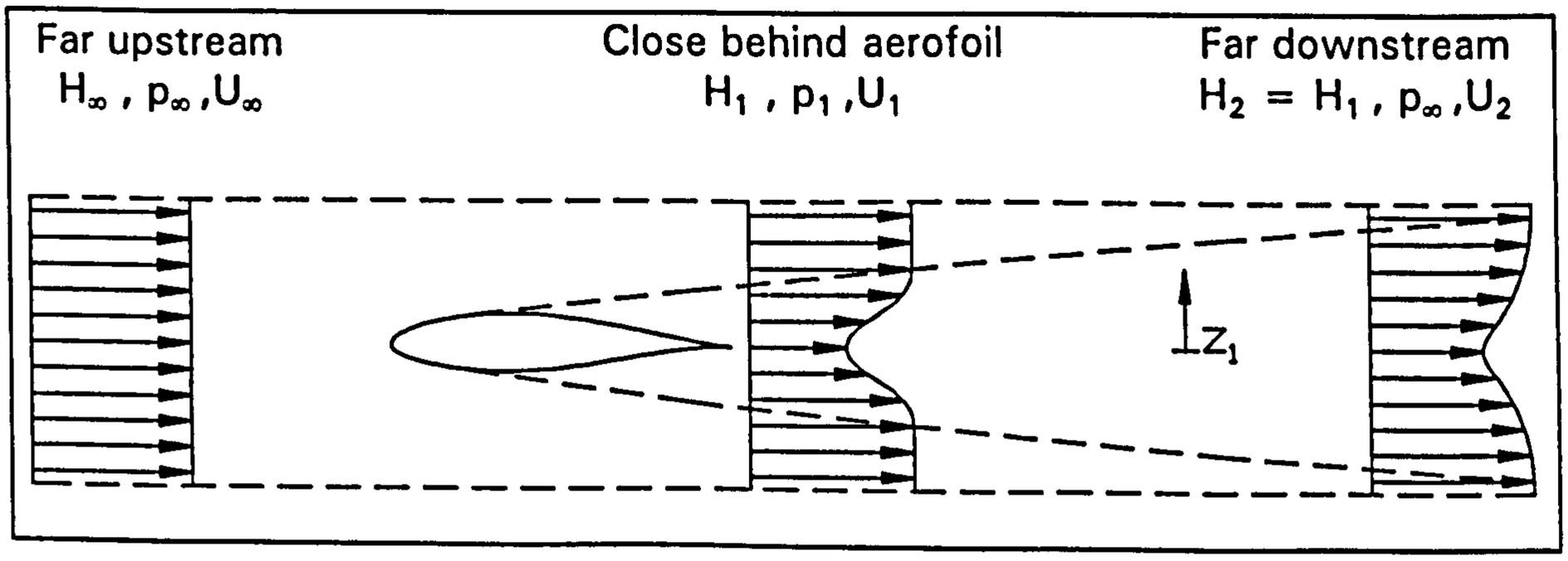

Figure 24 B.M. Jones wake model.

After the analysis is performed, equation 3-1 is arrived at, which allows the calculation of C_D by measurement of total pressure (H_1) and static pressure (p_1) close behind the aerofoil. (Houghton et al, 1960)

$$C_D = 2 \int \left\{ \sqrt{\frac{H_1 - p_1}{H_\infty - p_\infty}} \left[1 - \sqrt{\frac{H_1 - p_\infty}{H_\infty - p_\infty}} \right] \right\} d\left(\frac{z_1}{c}\right) \quad \text{..... (3 - 1)}$$

In order to measure total and static pressures behind the model, a wake rake was mounted at the centre span and one chord length down stream of the model. The rake was 240mm. wide and consisted of five static pressure probes spaced at 60mm. and 39 stagnation pressure probes. The latter being spaced at intervals of 5mm., except for the first six probes at either end which were spaced at intervals of 10mm.

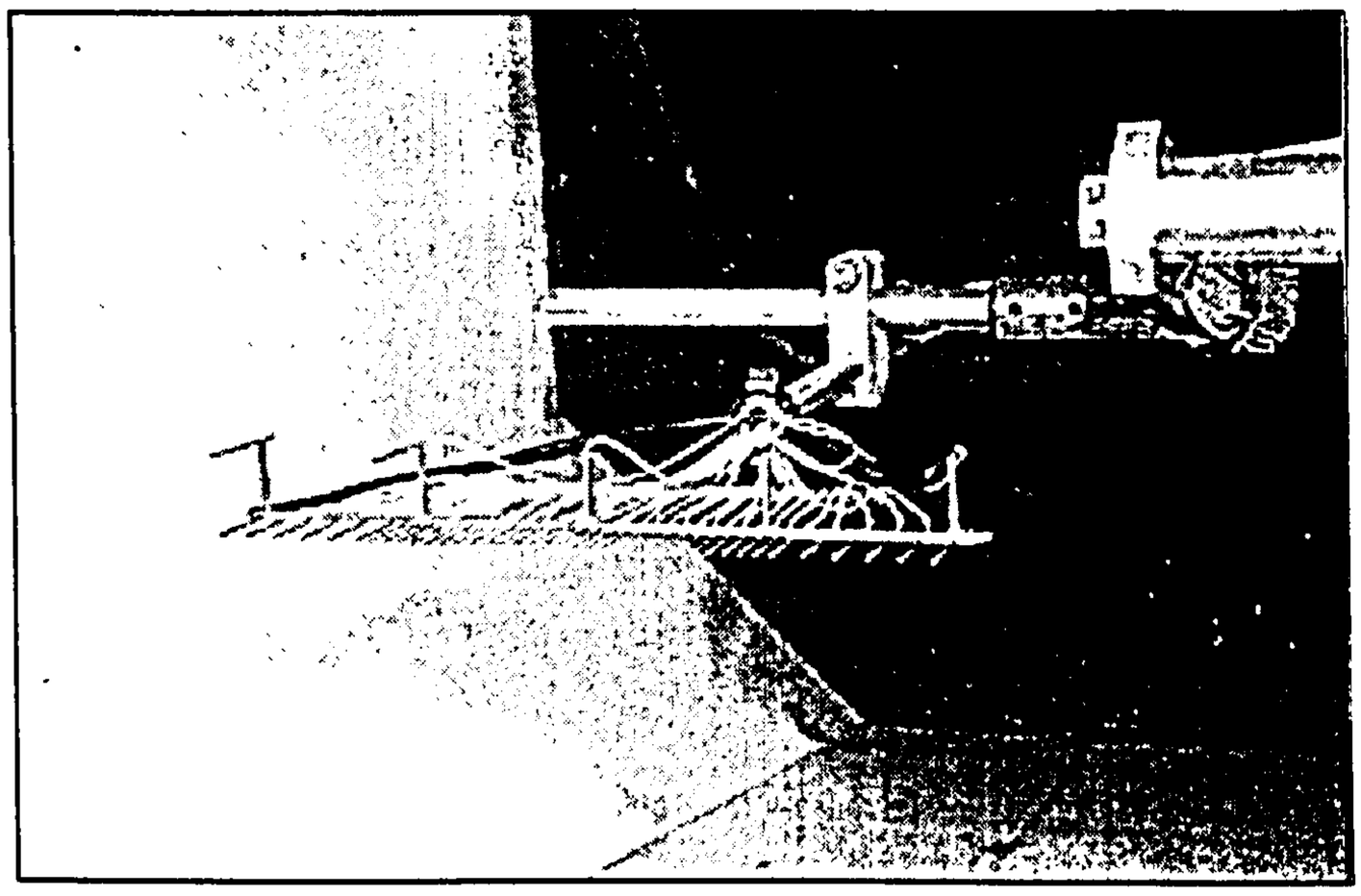

Figure 25 Wake rake

3.6.2 Normal force

As the end plate and slot blowing keep the flow two dimensional up to and beyond stall, normal force could be calculated by measuring surface pressure coefficients and integrating with respect to chord. As such, a balance was not required. Surface pressures were measured with a pressure transducer which was connected, via a scani-valve, to a total of 31 static pressure tappings on the model surface, the locations of which are given in Figure 26.

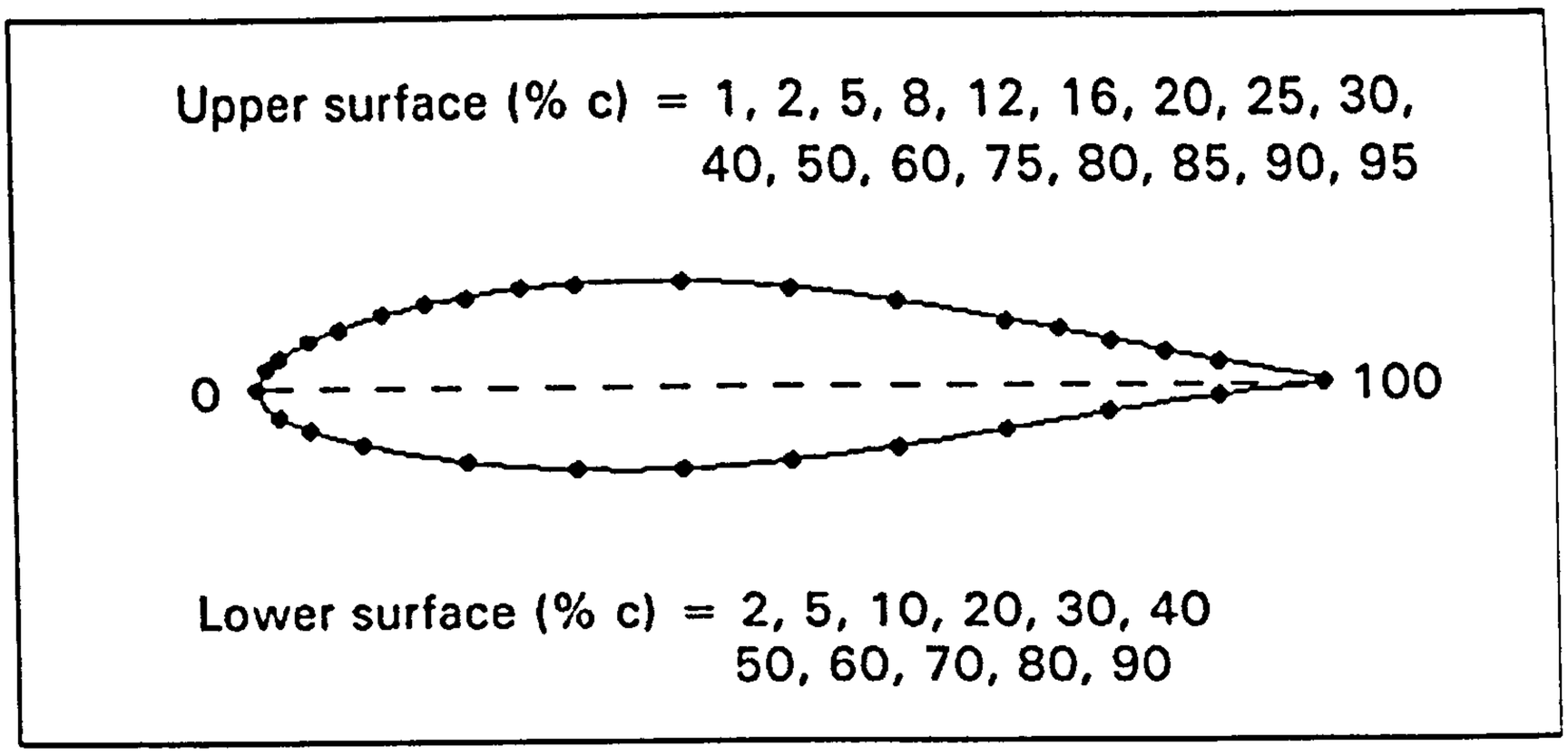

Figure 26 Location of static pressure tappings.

A procedure was developed (Innes, 1995) whereby an absolute calibration of the pressure transducers was not required, allowing the Cp's to be derived from transducer output voltages alone. This was achieved through manipulation of the standard equation:

$$Cp = (p - p_\infty) / \tfrac{1}{2}.\rho.U_\infty^2 \quad \text{..... (3 - 2)}$$

$$Cp = \{(p - p_a) - (p_\infty - p_a)\} / \tfrac{1}{2}.\rho.U_\infty^2 \quad \text{..... (3 - 3)}$$

Assuming $$\tfrac{1}{2}.\rho.U_\infty^2 = J.(p_{up} - p_{down}) \quad \text{..... (3 - 4)}$$

and $$p_{down} - p_\infty = K.(p_{up} - p_{down}) \quad \text{..... (3 - 5)}$$

where $(p_{up} - p_{down})$ is the static pressure drop along the tunnel contraction, p_∞ is the static pressure in the working section and J and K are constants. Rearranging gives:

$$Cp = \{(p - p_a) - (p_{down} - p_a)\} / \{J.(p_{up} - p_{down})\} + K/J \quad \text{..... (3 - 6)}$$

Regular calibration of the wind tunnel yields the constants J and K which are contained within the data acquisition software.

3.6.3 Lift

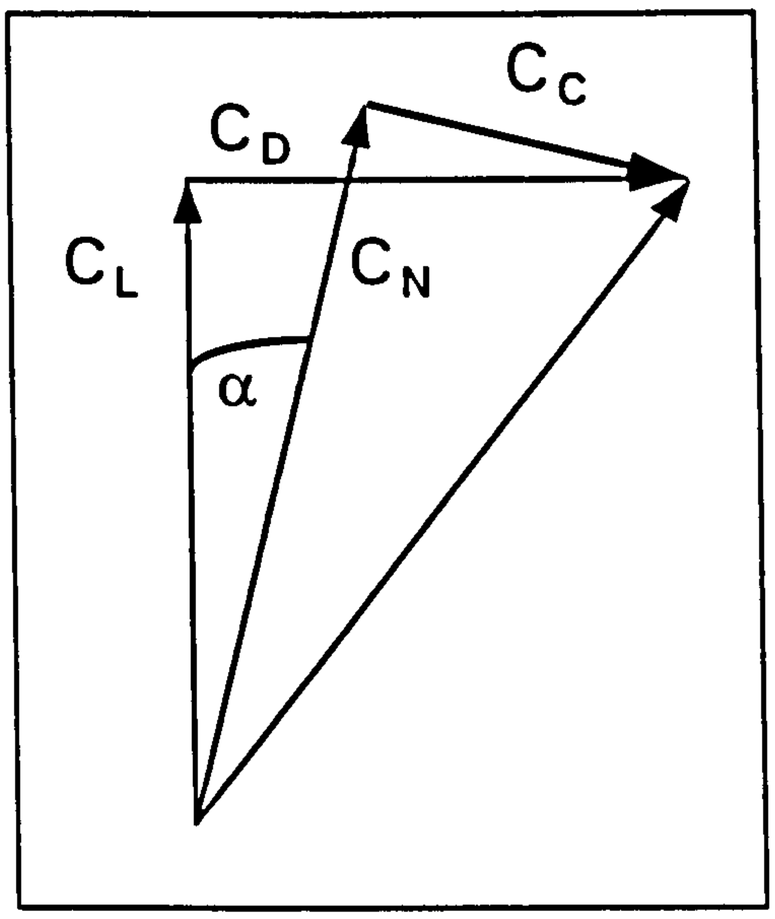

Figure 27 Vector diagram.

Lift coefficients were calculated from the drag and normal force using simple trigonometry.

$$C_L = C_N.\cos\alpha - C_C.\sin\alpha \quad \text{..... (3 - 7)}$$

$$C_D = C_N.\sin\alpha + C_C.\cos\alpha \quad \text{..... (3 - 8)}$$

Rearranging equation 3-8 for C_C and substituting in equation 3-7, yields:

$$C_L = C_N.\sec\alpha - C_D.\tan\alpha \quad \text{..... (3 - 9)}$$

3.6.4 Mass flow and blowing pressure supplied to ajvg's

To determine the relative performance and power consumption of different ajvg arrays the mass flow supplied to the air jets and pressure behind them had to be measured. The former was measured using an orifice plate already in place and the latter with 3 static pressure tappings located in the plenum chamber of the model. These readings were recorded manually, i.e. they were not an integral part of the Data Acquisition System, discussed in the following section.

Blowing pressure was the fixed variable, as this could be measured directly on a mercury manometer. Hence, the lift curves and mass flow required for two different air jet configurations would be compared at the same blowing pressure. The manometer's scale reads pounds per square inch and so for convenience tests were conducted at multiples of this unit rather than in the SI unit of Pascals.

3.7 Data Acquisition

The system used to record the aerofoil pressure distribution and wake pressure measurements was that constructed by Innes (1995), full details of which can be found in his thesis. Only the fundamental operation of the system is described here.

The Data Acquisition System (DAS) comprises a Personal Computer (PC), a Cambridge Electronic Design (CED) 1401 and two pressure transducer / scani-valve combinations which are connected to the rake and model pressure lines.

The CED 1401 is a multi-tasking system designed in such a way that when performing a task, it can be interrupted to perform a separate task before returning to the original task where it left off. It is ideal for data acquisition because it allows analogue to digital conversion of electronic signals (ADC).

In this application, the CED 1401 is controlled by the PC running the DAS software, written by Innes. The two in combination are used to step the scani-valve to the next port and then read and record the transducer output voltage until all ports have been scanned. The transducer output voltages are then written to disc in a 'raw' data file. The following table lists the characteristics of the two pressure transducers used.

Measurement	Surface pressure	Wake Pressure
Transducer	Druck PDCR22	Setra 237
Range	0 - 175mB (≈ 2.5 p.s.i.)	0 - 0.25 p.s.i. (≈ 17mB)
Amplification required?	Yes	No

3.8 Data processing

The DAS software carries out a great deal of the data reduction in that it converts the raw voltages to pressure coefficients (equation 3 - 6). This information is also written to disc as a 'semi-processed' file , along with the test conditions such as atmospheric pressure and angle of attack.

Post-experiment processing of the data included several spread-sheet 'macros' which were written to integrate the wake and surface pressure distributions and a short program to calculate mass flow.

3.9 Error assessment analysis

3.9.1 Aerofoil

The model profile was measured in order to determine the accuracy to which it had been manufactured. To do this the model was first mounted on a digital lathe being careful to ensure that the chord-line was parallel to the lathe surface. This allowed the required abscissa to be input, whereupon a digital measuring device ('Digitometer'), also mounted on the lathe, allowed the upper surface ordinate to be measured. The model was turned over and the procedure repeated to determine the lower surface ordinates.

The maximum positive and negative errors in total thickness were found to be +0.64 mm. (0.13% c) and -1.11 mm. (0.22%c) respectively. The surface finish was smooth and continuous with no discontinuities and as such these small deviations were not thought to be a significant source of pressure distribution error.

In the same way, the locations of the static pressure tappings were checked as these are difficult to position with a high degree of accuracy during manufacture. It is not essential to relate the differences between the required and actual locations of the static pressure tappings, as the pressure plots are integrated with respect to the actual positions.

3.9.2 Measurement of angle of attack

The perspex end-plate had the aerofoil chord-line scored along its length. The incidence of the model could therefore be set to 0° by alignment of this line with the tunnel centre-line. It is estimated that this could be repeated to within ± 0.11° by aligning the two lines to within 1mm. at the downstream end of the end-plate. A pointer is then attached to the spindle of the aerofoil outside the tunnel. This was used to measure aerofoil incidence to an accuracy of ± 0.06°. Adding these errors, it is expected that the total incidence error could not have exceeded ± 0.17°.

3.9.3 Pressure measurements

The resolution in the measurement of pressure coefficient has been determined to be in excess of Cp ± 0.0012.

4. WIND TUNNEL RESULTS (1) ~ CLEAN FOIL

4.1 Plain aerofoil, transition free

The aerofoil was initially tested with free transition and compared with Williams VII code predictions (section 2.6), at the same Reynolds number of 1.4 million, to ensure that the aerofoil was performing as it should. As the Williams code calculates for an aerofoil in free air (no wall boundaries) and the wind tunnel results are uncorrected, an exact match was not expected.

4.1.1 Comparison of lift curve with Williams code prediction

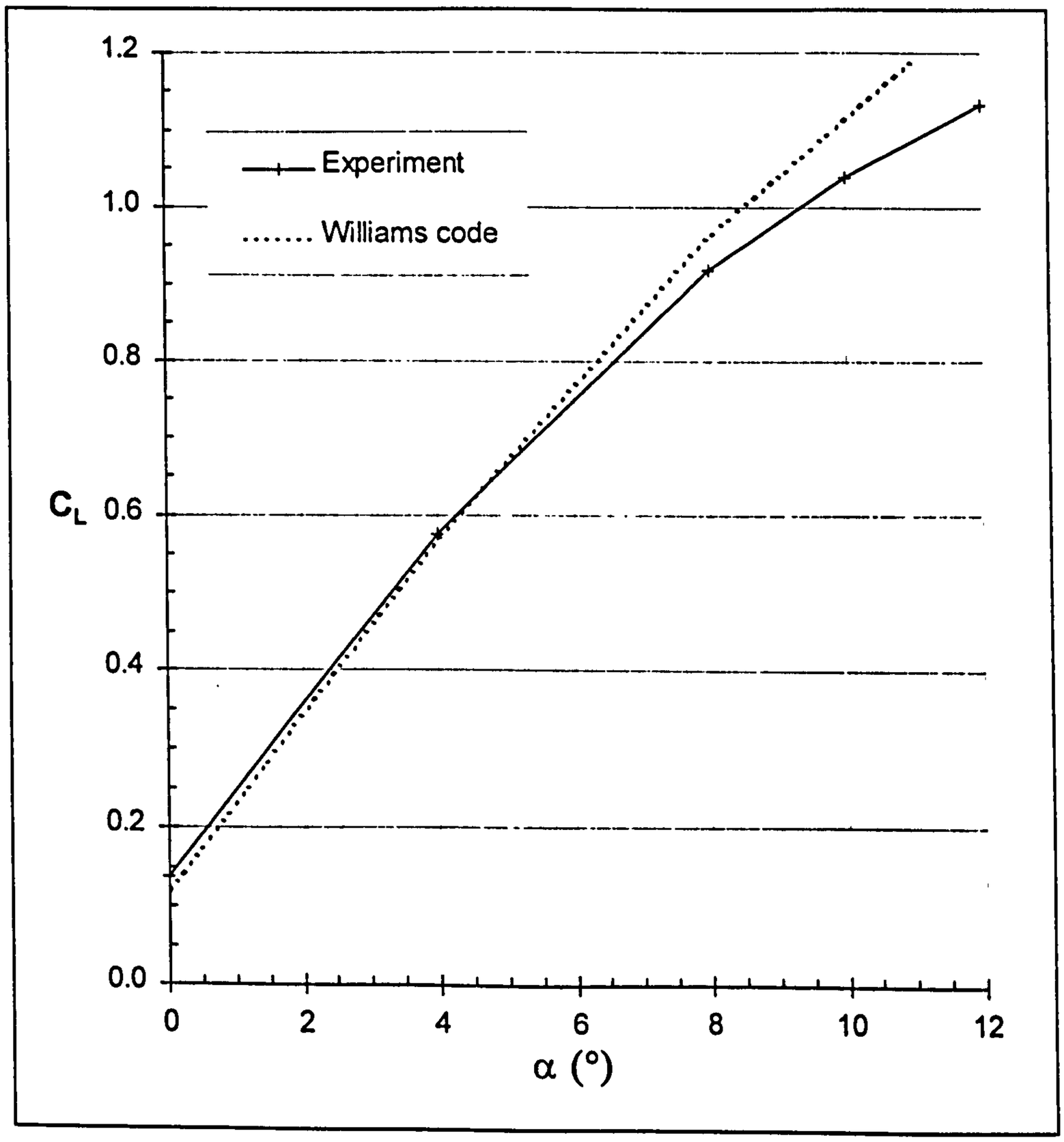

Figure 28 Predicted and experimental lift curves (Free transition)

Examination of the lift curve shows very good prediction at low angles of attack, up to about $\alpha = 5°$, with measured lift only slightly exceeding the predicted lift. At higher angles than this the prediction exceeds the measured data and continues to diverge. Above $\alpha = 12°$, the iteration procedure in the code breaks down and no more results are produced.

4.1.2 Comparison of pressure distributions with Williams code prediction

Figure 29, shows the measured and calculated pressure distributions for the aerofoil with free transition at one of these angles of attack ($\alpha = 8°$). Apart from the discrepancies in pressure recovery at the trailing edge and peak suction the overall shape of the pressure distribution is well predicted. The distribution of pressure at the trailing edge has been enlarged for clarity.

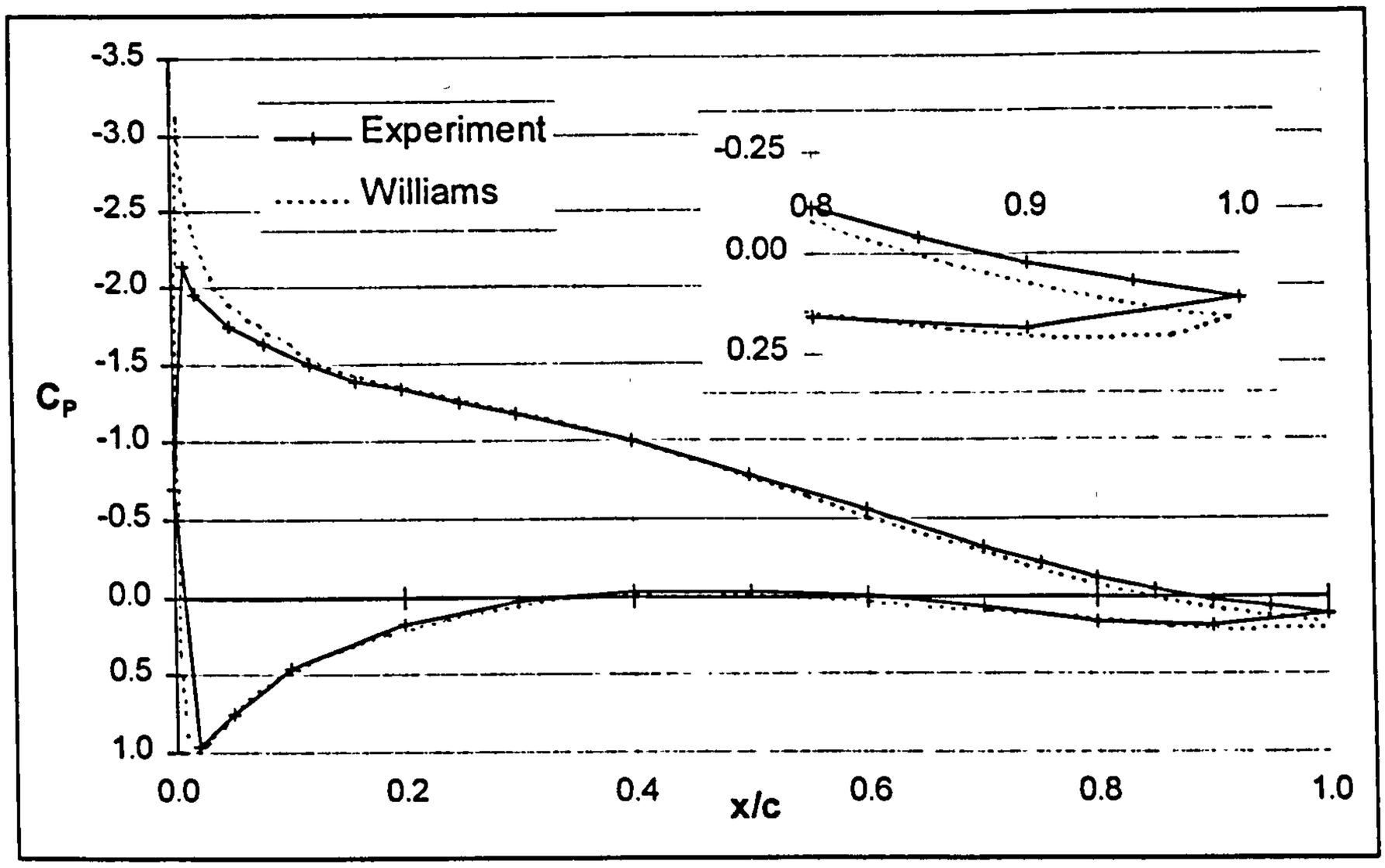

Figure 29 Predicted and experimental pressure distribution at $\alpha = 8°$

Inspection of the corresponding pressure distributions over the whole range of incidence showed that the code consistently over-estimated the pressure recovery and, at angles of attack greater than $\alpha = 4°$, the magnitude of the peak suction as well. These results suggest that the effect of viscosity on the overall circulation is being under-estimated by the program since the effect of boundary constraint and the lift effect would tend to produce an increase, not a reduction, in apparent loading on the aerofoil in the wind tunnel (Pankhurst et al, 1952).

4.1.3 Williams code failure

At angles of attack above 12° the code iteration procedure breaks down and predictions for higher angles of attack are not calculated. Similar problems were encountered by Hill et al, (1989), who found that the program '... cannot always deal with reattachment of laminar separation bubbles where pressure gradients are low, such as those which occur on the lower surface.' A fix to this problem, suggested by Williams the author of the program, was to prevent laminar separation from occurring by fixing transition at 50% on the lower surface. This allowed calculation of lift at higher angles of attack for two out of three aerofoils,

before the program again failed. Although this method was implemented, no results for angles of attack above $\alpha = 12°$ could be obtained for our aerofoil.

4.1.4 Comparison of drag curve with Williams code prediction

Prediction of the drag curve by the Williams code also gave close agreement with experiment for lower angles of attack (Figure 30). At angles of attack greater than $\alpha = 8°$, the slope of the drag curve again indicates that viscous effects are being under-estimated.

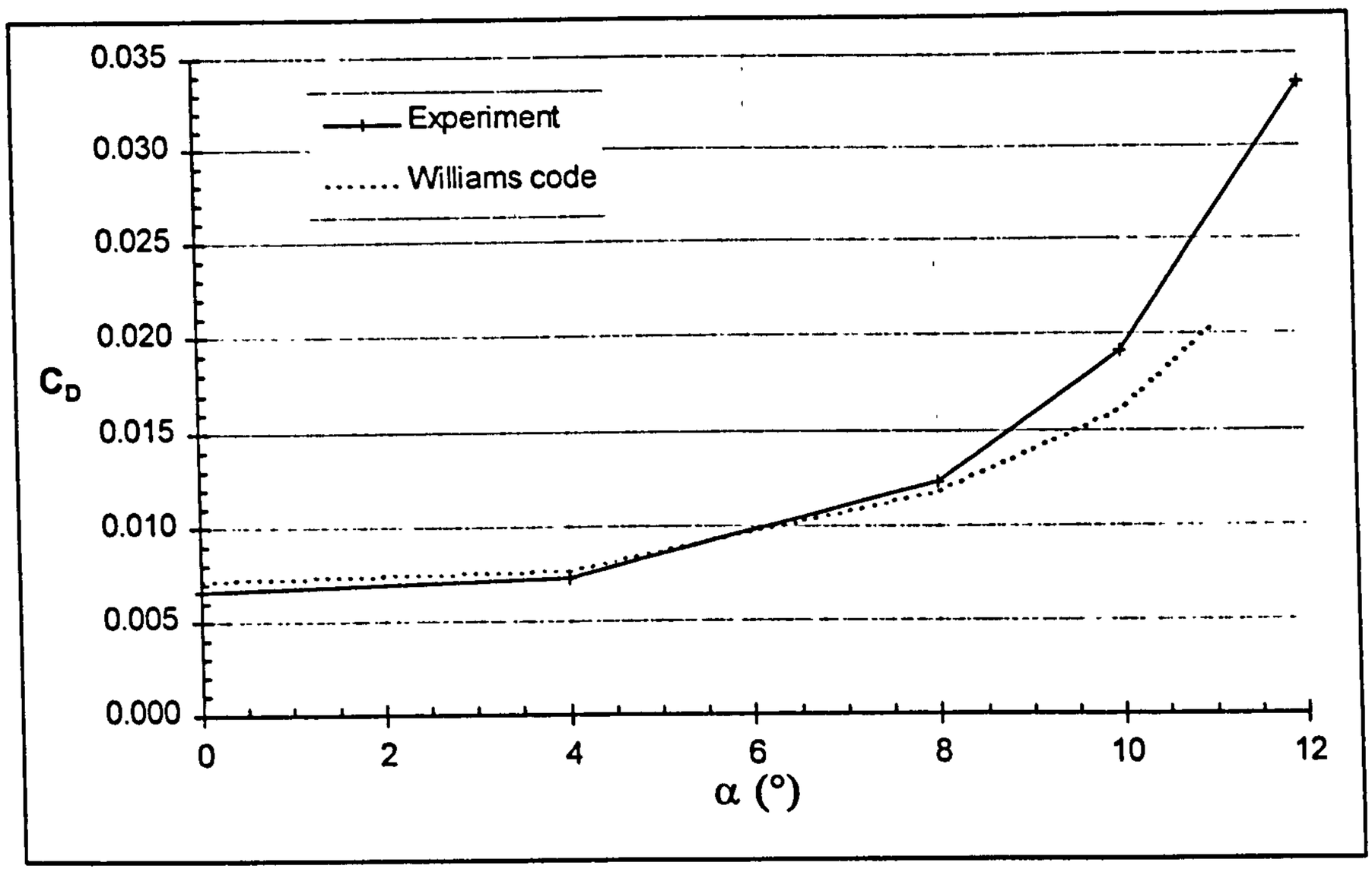

Figure 30 Predicted and experimental drag curves (Free transition)

In conclusion the lift and drag predictions appear to be good but it may be said that the code is underestimating the effects of viscosity. This becomes clearer as we move up the lift curve. Whereas the measured lift begins to move away from the linear inviscid slope, the prediction does not.

4.2 Transition fixing

The aerofoil was initially tested with free transition as described above. This is unlikely to occur on a wind turbine blade because small insects and dirt rapidly build up and, unlike aircraft, the blades (wings) are not cleaned regularly. Roughness elements of such a size coupled with the swirl and free stream turbulence in the wind approaching a blade would almost certainly provoke early transition to turbulent flow. With this in mind it was necessary to establish the aerodynamic characteristics of the aerofoil with transition between laminar and turbulent flow fixed. A brief study of transition fixing was therefore undertaken.

Having obtained good predictions of the lift and drag for the free transition case at angles of attack up to about $\alpha = 8°$, it seemed reasonable to use the Williams code to aid selection of a transition device. It was considered that a suitable transition strip could be found by varying the strip width and grain size until the low incidence drag range coincided with that calculated by the Williams code.

In order to simplify the tests it was decided to fix transition only on the upper surface, as this would be the dominating factor. The transition strip was located in the strong adverse pressure gradient at 6.5% chord, directly between the static pressure tappings at 5% and 8% chord so as not to block the holes.

The strips were created by coating thin double-sided sticky tape with carborundum powder and cutting to the desired chordwise width. Two different grain sizes were used. These were fine (0.2 mm) and medium (0.4mm). A total of seven grain and width combinations were tested for which the lift and drag were measured at the angles of attack 0° , 4° and 8°.

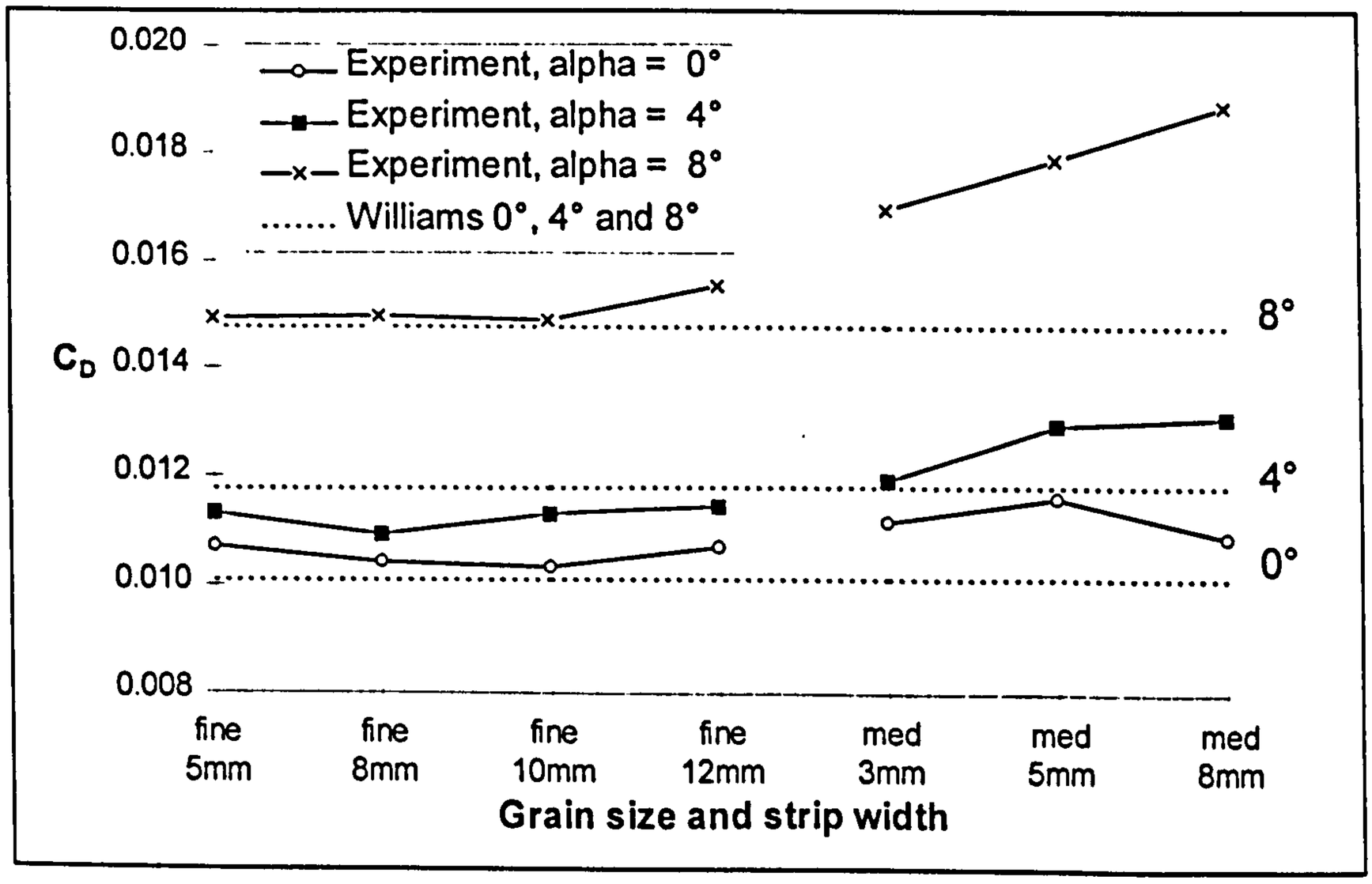

Figure 31 Variation of drag with different transition strips.

The above figure shows the variation of drag for each of the seven combinations of strip width and grain size tested. Each solid line represents the results for one angle of attack (0°, 4° or 8°) and each point on these lines represents the drag measured with one of the seven strips fitted. The dotted lines represent the Williams code predictions at the same angles of attack. It can be seen that the

larger grain size (med.) is clearly too severe, particularly at $\alpha = 8°$. For this larger grain size a small increment in the strip width moves the measured drag further from the predicted result in all cases, except when the strip width changes from 5mm. to 8mm. at 0°. The fine grained strips produced a much better fit to the predicted data. The 10mm. (0.2% c) fine grained strip was selected as this gave the closest fit overall, the other strips fitting badly at one or more angles of attack.

4.2.1 Comparison of lift and drag curves with Williams code predictions

The complete lift and drag characteristics of the profile were determined with this transition strip and the lift and drag curves obtained are shown in Figure 32. It is noted that the comparison of both curves with the Williams prediction are similar to those obtained for free transition, with the predicted lift and drag being higher and lower respectively than the measured values at angles of attack greater than $\alpha \approx 8°$. The program shows signs of failing at $\alpha = 11°$ with an obscure drag prediction and failed completely after this.

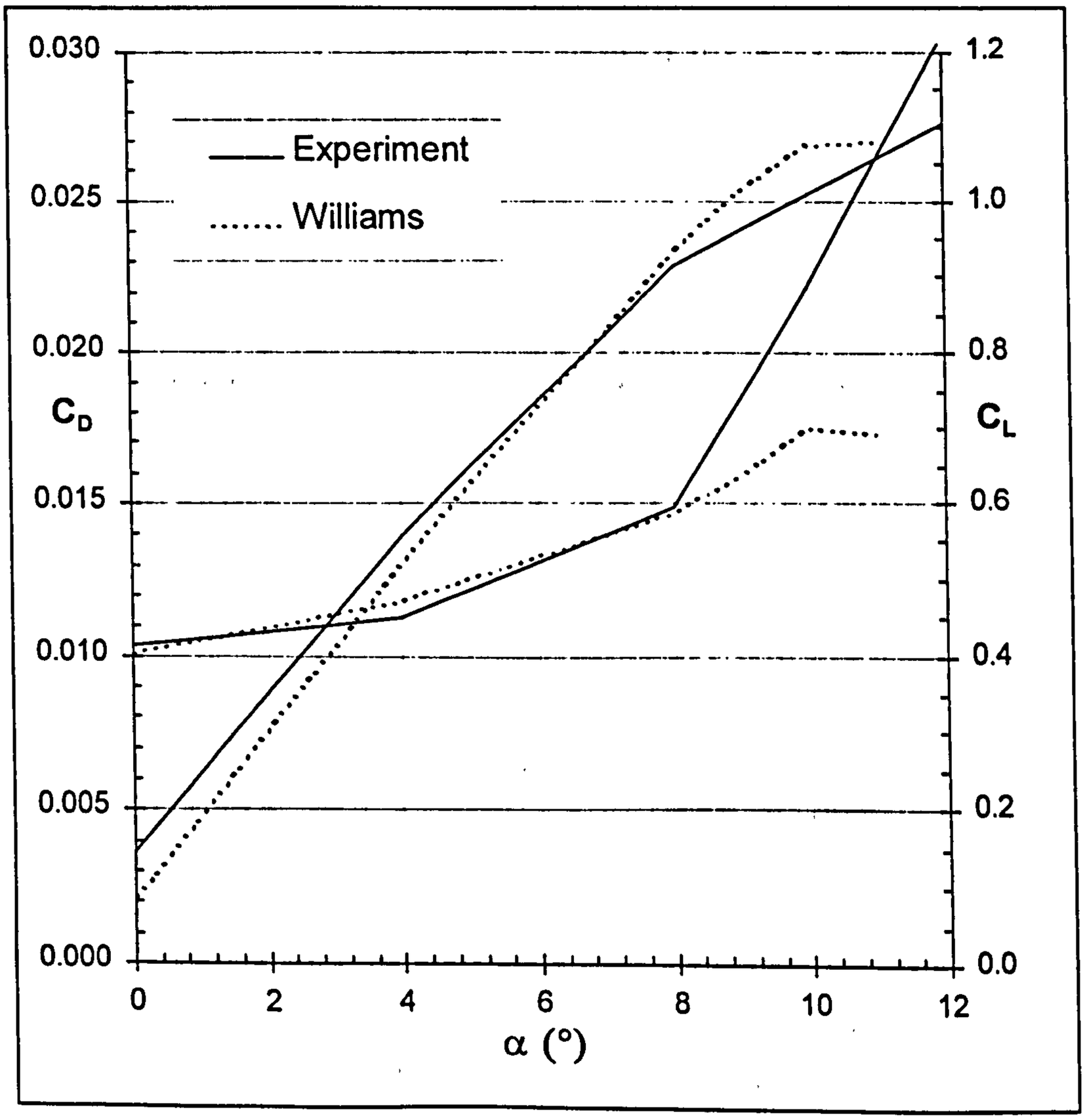

Figure 32 Predicted and experimental lift and drag curves (fixed transition)

5. WIND TUNNEL RESULTS (2) ~ FORCED BLOWING OF AJVG'S

5.1 Presentation of the results

This chapter presents the results from the first air jet testing phase. It deals only with those results which were used in the design of equipment for the full scale tests, i.e. air jets actively supplied with air. Results from the later wind tunnel tests where air jets were passively blown are presented in Chapter 10.

The results from two different air jet configurations are described in this chapter. The first configuration is dealt with briefly as this was not chosen for the full scale tests. There then follows a section describing why it was necessary to test a second configuration and the implications for the full scale design. Finally, the results from the second configuration are compared with those from the first and a more detailed analysis follows.

5.2 First air jet configuration tested

With the original profile characteristics established for both transition free and fixed cases, the leading edge was removed and replaced by one containing the first air jet configuration to be tested. Details of this configuration are given in Table 1. For a full explanation of these parameters and the selected values, the reader is referred back to section 2.3.

Parameter	First Configuration
Vortex system	Co-rotating
Chord-wise location of jets, x/c	0.10
Blowing pressures, P_b	1.0 p.s.i. & 2.0 p.s.i.
Pitch of air jet, ϕ	30°
Skew of air jet, θ	60°
Dimension of jet (L x W)	16mm. x 2mm.
Aspect ratio of jet (L / W)	8
Spacing of air jets	60mm. (3.75 x L)
Number of jets on model	12

Table 1 Details of first air jet configuration

5.2.1 Modified lift curve

The first configuration was tested at two different nominal blowing pressures, 1.0p.s.i. (≈ 6.9 kPa) and 2.0p.s.i. (≈ 13.8 kPa). The ability of air jets to delay the stall is clearly illustrated in Figure 33, below, with the lower and higher blowing pressures increasing C_L at $\alpha = 19°$ from 1.17 to 1.71 (46%) and 1.84 (58%) respectively. The improvement is also noticeable in the linear region of the lift curve indicating that the vortices are reducing boundary layer growth on the upper surface. The vortices are effectively reducing the amount of de-cambering caused by boundary layer growth.

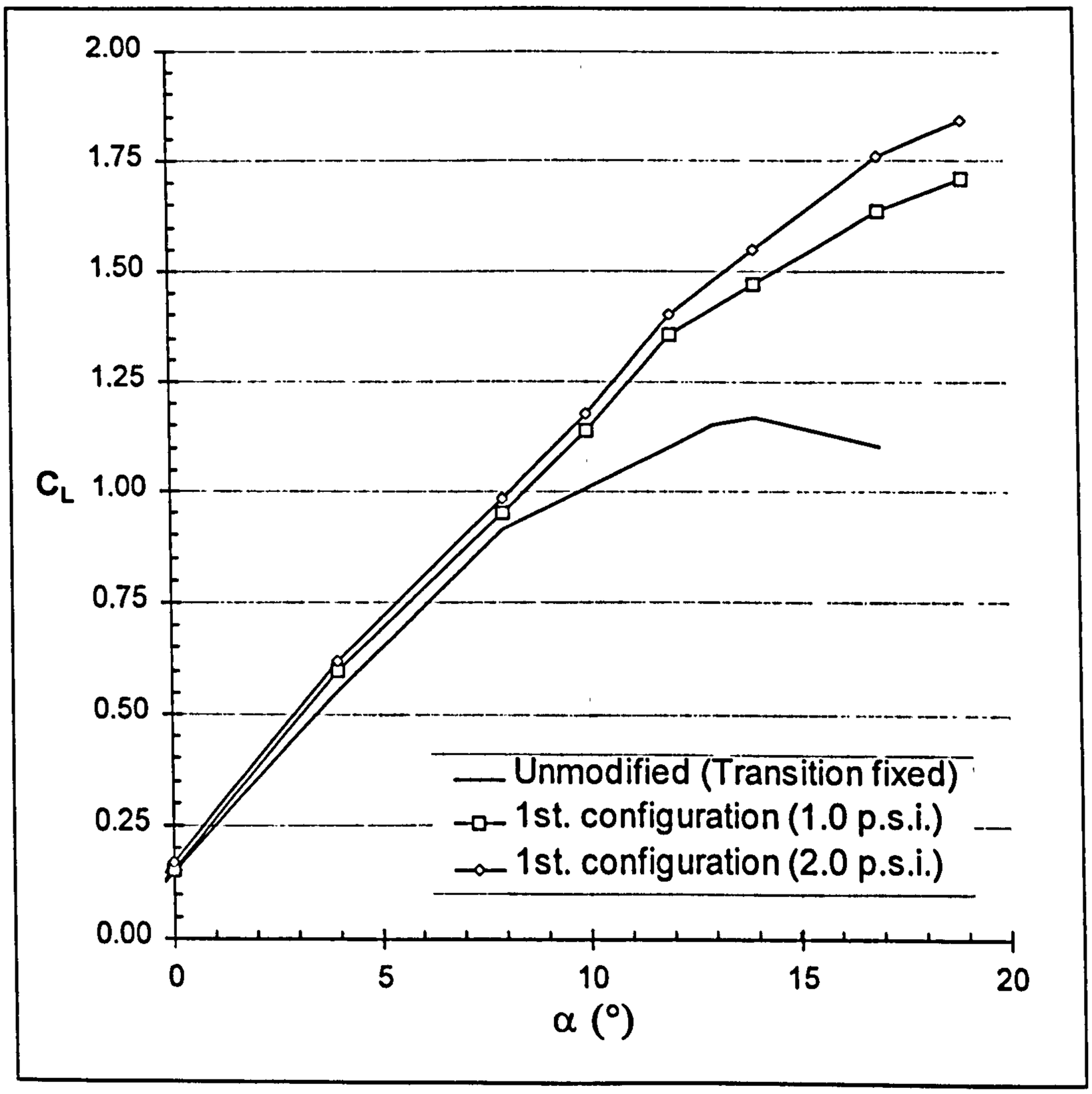

Figure 33 Lift curve modified by air jets (1st. configuration)

No further lift data (drag dependent) were measured for angles of attack above $\alpha = 19°$, even though the aerofoil with ajvg's is not yet fully stalled. The reasons for this were threefold. First, the blockage ratio was now becoming excessively large; second, two tunnel runs would have been required to capture the whole wake and third it was considered unsafe for the rake to be employed because a loss of air jet air supply would suddenly place it in a very turbulent flow regime.

Nevertheless, the rake was removed and normal force measurements alone were used to determine the approximate jets 'on' stall angle (section 5.5.3).

5.2.2 Modified drag curve

The corresponding drag curves are given in Figure 34 and show that although both blowing pressures delay the rise in drag post stall, the lower blowing pressure has increased drag for angles of attack below $\alpha = 10°$. The higher blowing pressure, however, has reduced drag. This result suggests that two opposing effects are being introduced by the air jets. Firstly that air jets do have a small drag penalty associated with them. Secondly, that this may be overcome, or reduced by increasing the blowing pressure.

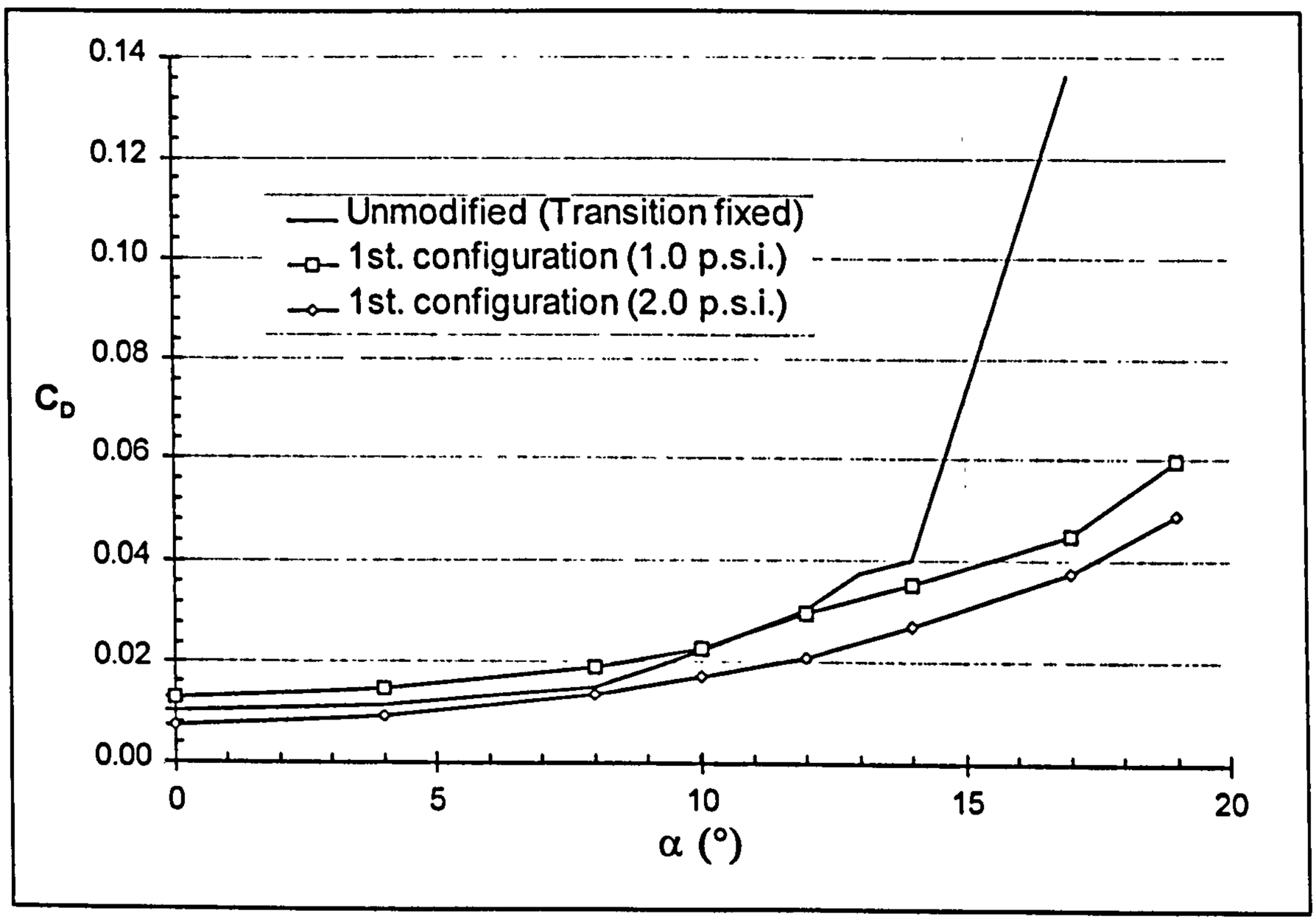

Figure 34 Drag curve modified by air jets (1st. configuration)

The drag reduction stems from the enhanced vortex mixing provided by the higher pressure jet (due to increased jet velocity and hence vortex strength) which further reduces boundary layer growth (trailing edge pressure is higher for the higher pressure jets). There will also be an effective drag reduction due to the fact that more momentum is being imparted to the flow.

The adverse effect on drag is most likely due to the fact that the jet exits are really nothing more than roughness elements on the aerofoil surface. There will also be an increase in skin friction drag due to the vortices reducing the boundary layer thickness.

However, the increase due to skin friction must be small compared to the other effects above because increasing drag is not in the same order as increasing vortex strength.

5.3 Mass flow requirement.

Figure 35 shows how the mass flow requirement per jet varies with aerofoil angle of attack. It will be noted that there is a small but noticeable increase in the mass flow required to maintain a constant blowing pressure in the plenum chamber as the angle of attack increases. This could be due to the fact that at higher angles of attack the suction at the location of the air jets is greater. Although the pressure in the plenum is kept constant, there is effectively a greater pressure differential between the plenum and jet exit. The result of this is to allow a greater jet velocity which requires more mass flow to be supplied.

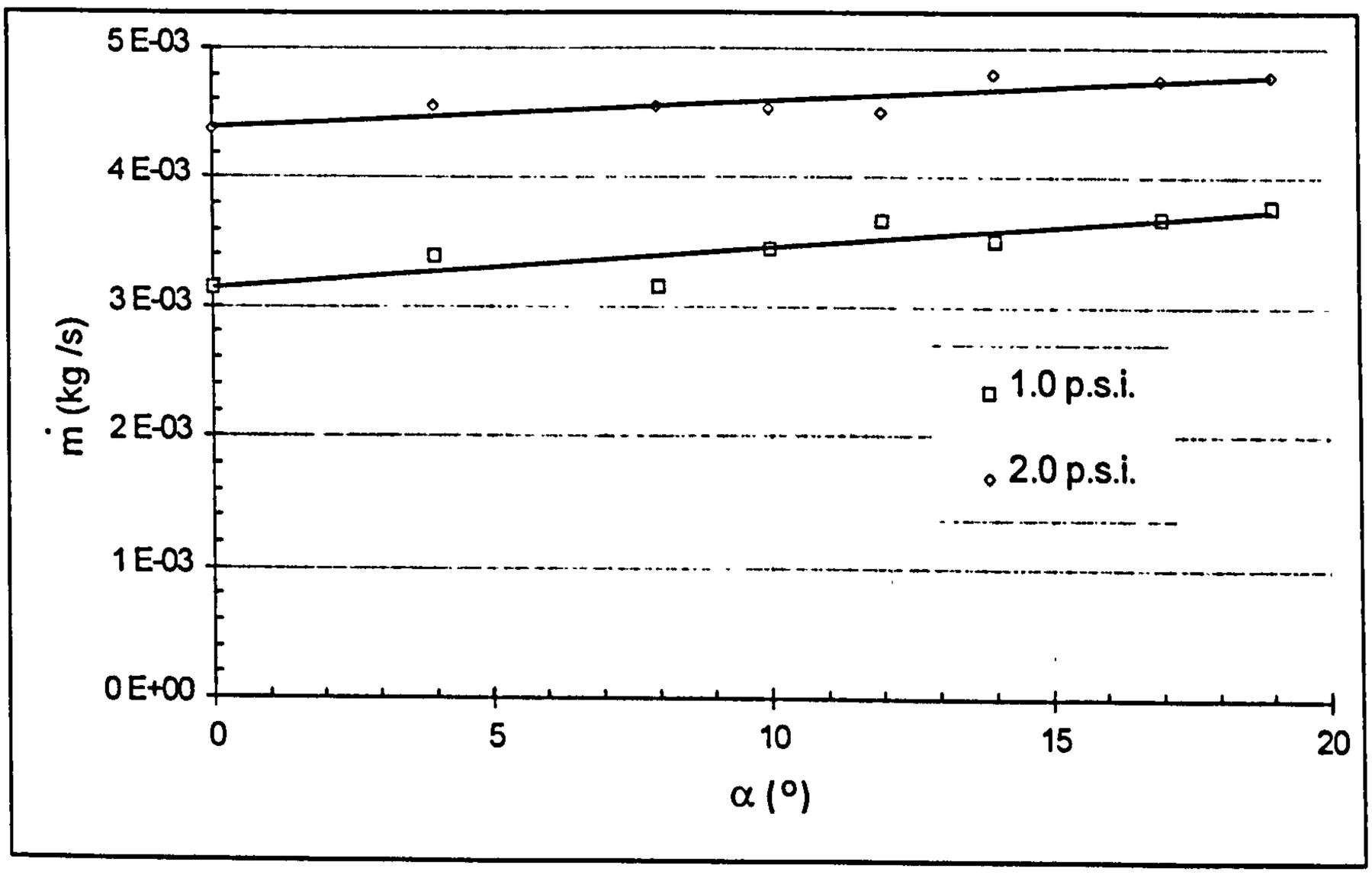

Figure 35 Variation of mass flow (per jet) with angle of attack

5.4 Why the second configuration was needed.

As mentioned previously, a second air jet configuration was tested during the project. The reason for this was that the model chord differed to the blade chord at the location of the jets presenting two options. These were:

1. To scale the air jets by the ratio of blade chord to model chord.
2. To use the same size of jet that was used for the model, i.e. no scaling.

5.4.1 Implication of scale on mass flow requirements

First let us consider the implications of the two options above on mass flow requirements. Figure 36 illustrates the two cases. The small jets are as per wind tunnel model and have been fitted to the blade unchanged. The large jets represent a scale up from wind tunnel model of chord, c, to full scale blade of chord, C. Both sets of jets have the same proportional spacing of 3.75 * L and aspect ratio, L/W[†] of 8, as described in 2.3.

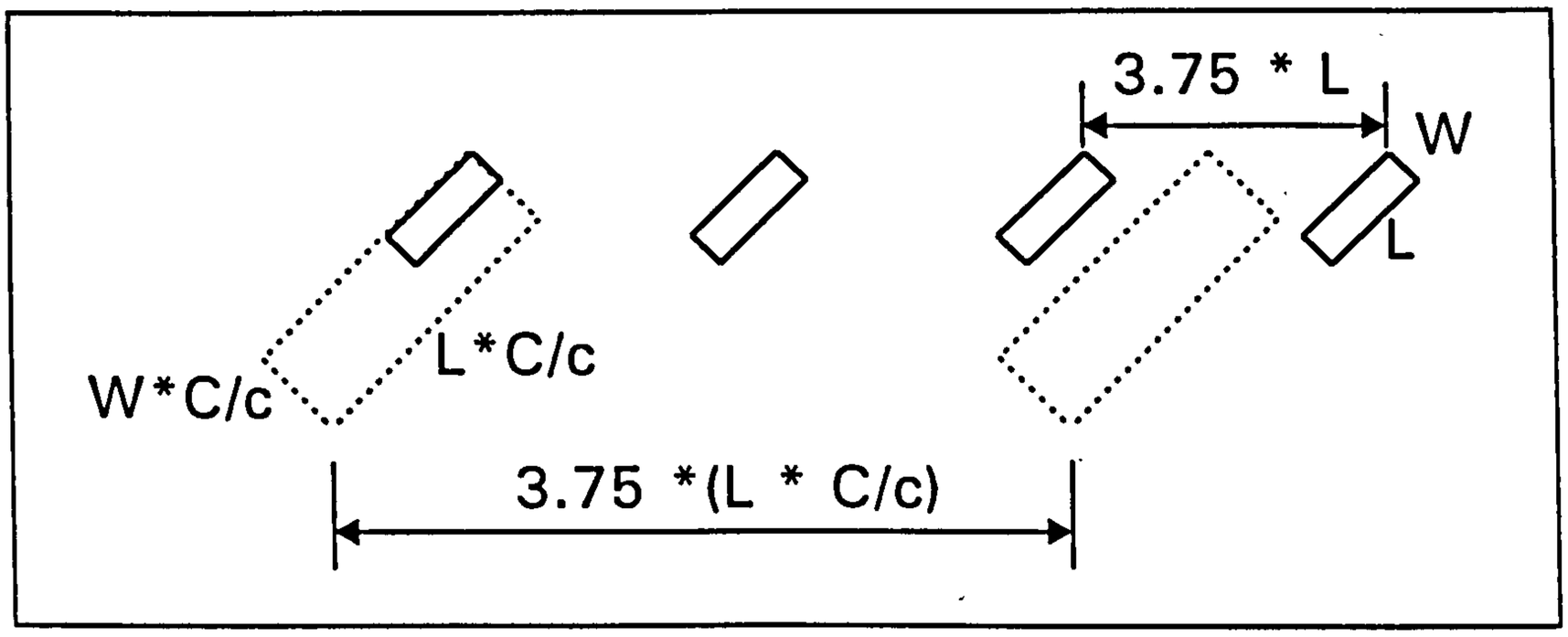

Figure 36 Scaling the air jets to full scale

Now let us assume that we want to maintain a constant jet exit velocity for the two cases. (A reasonable assumption since Compton et al (1991) and Henry et al (1994) showed that the vorticity produced was a strong function of this). It is therefore desirable to choose the option requiring the lowest mass flow per unit array length of ajvg's. The option with the minimum jet exit area per unit length of air jet array should therefore be chosen, since $\dot{m}_{jet} = \rho . A . V_{jet}$.

In terms of mass flow requirement, the second option is clearly the better one. That is to keep the jets the same size as those in the wind tunnel tests and *not* to scale them up. For example, scaling up both the length and width of the jet by a factor of 2, say, (to keep the aspect ratio constant) will result in an area 4 times the original size. However, there will now be half as many air jets per unit length (spacing is related to the air jet length). Hence the total area increase (and hence mass flow requirement) would be doubled for this example. The jet exit velocity, V_{jet} , would remain the same though and the vortex strength would not alter.

[†] The reader is reminded that W is the actual slot width but that for convenience it has been drawn as the projected slot width in the figure.

5.4.2 Implication of scale on lift and drag characteristics

Now let us consider how the lift and drag measurements might vary for the two scaling options.

To supply air to the vortex generators at full scale, in this first application, it was decided to use a fan (Chapter 7). However, it was calculated that the power requirement would be excessive if the blowing pressure of 2.0 p.s.i. was selected (section 7.3). A blowing pressure of 1.0 p.s.i. would reduce the power requirement to within acceptable limits for the demonstration but Figure 34 shows that there would be a drag penalty associated with this choice. (Later, in Chapter 10, it is demonstrated that high blowing pressures are not essential to vortex generation but this was not known at the time of the system design.)

It was considered that the drag penalty of the air jets was probably due to the jet exit on the aerofoil surface acting as a kind of roughness element. If so, the drag penalty would be strongly related to the size of the jet exit (with respect to aerofoil chord). On this basis, option 2 appeared to offer the additional possibility of reducing the drag coefficient measured in the wind tunnel because the jets would now be on the relatively larger chord of the blade. The above discussions are summarised in Figure 37.

However, the risk associated with using smaller and smaller vortex generators is that the vortices may become less enduring in the chord-wise direction. It is hypothesised that an optimum arrangement should exist between the lower mass flows required and lower drag penalty incurred by small jet exit areas (in relation to the aerofoil chord) and the ability of the vortices produced to control separation.

Not wanting to increase the mass flow that would be required in the full scale tests, it was decided that the air jets on the wind turbine should have the same dimensions as those used in the first series of wind tunnel tests (option 2). This meant that the mass flow per jet would be known and given by the first configuration. However, this decision would only be sanctioned if the smaller air jet's proved to be as effective as the first in delaying stall and increasing $C_{Lmax.}$.

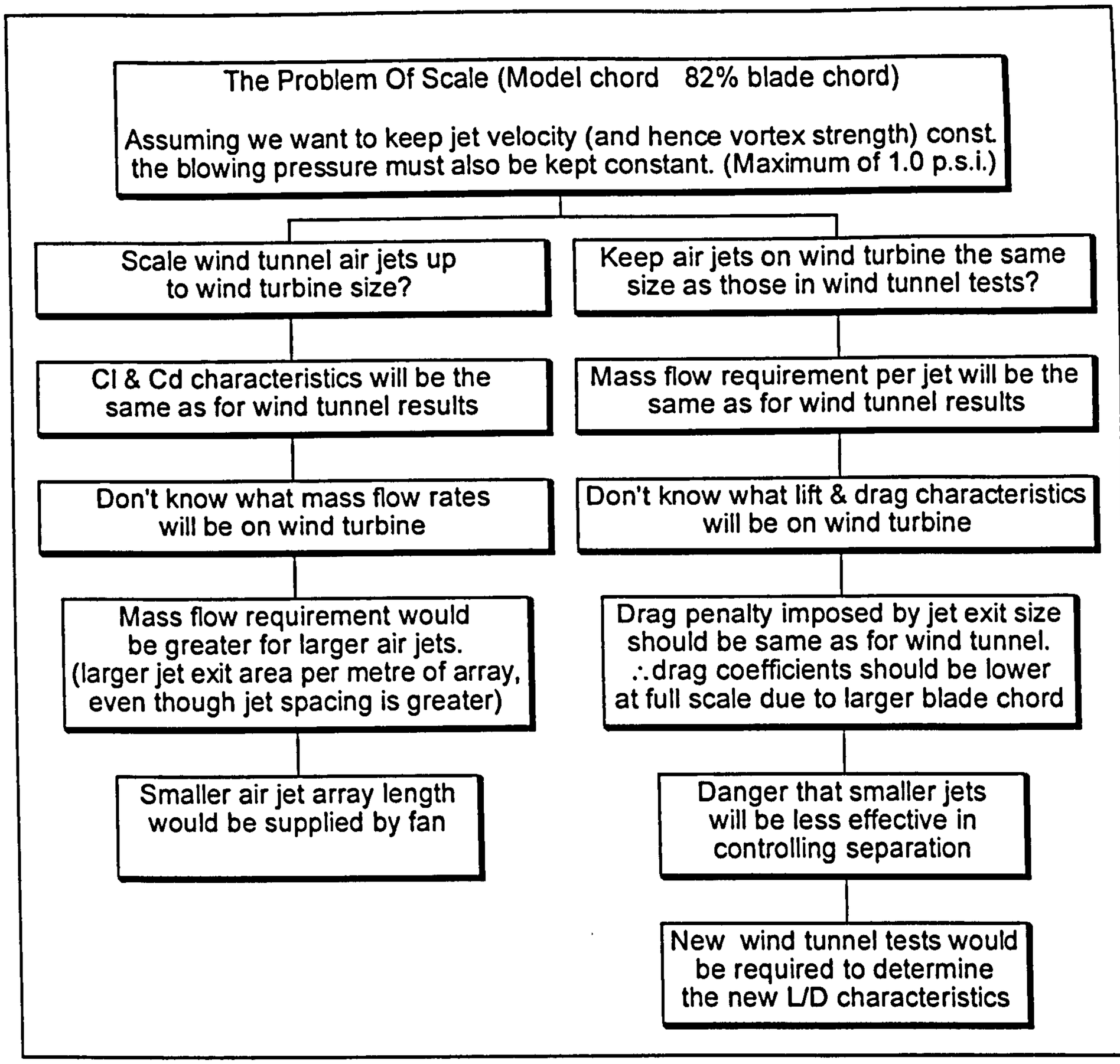

Figure 37 The problem of scaling the air jets to full scale

A second air jet configuration therefore had to be tested to determine what the modified lift and drag characteristics of the full scale blade would be. This second configuration would have to be a scaled down version of the first jet configuration mounted on the full scale blade.

Scaling the original air jets (16mm. x 2mm.) used in the wind tunnel tests by 0.82 (the ratio of model chord to blade chord at blade radius, r/R = 0.806) proved impractical due to available machine tool sizes. They were therefore scaled by 0.75 giving the dimensions of the new jets as 12mm. x 1.5mm.

It was appreciated that in order to reduce full scale production costs only one jet size (one mould) should be used for the whole blade, when ideally the jet size would scale proportionally with blade chord. This means that the model is only strictly representative of one blade radius, $r/R \approx 0.75$, (previously $r/R \approx 0.806$).

However, the point of the new tunnel tests was really to see whether or not the performance was in any way degraded by using relatively smaller air jets.

5.5 Second air jet configuration tested

Details of the second configuration are given alongside the first in Table 2. For a full explanation of these parameters and the selected values, the reader is referred back to section 2.3.

Parameter	First Configuration	Second Configuration
Vortex system	Co-rotating	Co-rotating
Chord-wise location of jets, x/c	0.10	0.10
Blowing pressures, P_b	1.0 p.s.i. & 2.0 p.s.i.	0.5 p.s.i. & 1.0 p.s.i.
Pitch of air jet, ϕ	30°	30°
Skew of air jet, θ	60°	60°
Dimension of jet (L x W)	16mm. x 2mm.	12mm. x 1.5mm.
Aspect ratio of jet (L / W)	8	8
Spacing of air jets	60mm. (3.75 * L)	45mm. (3.75 x L)
Number of jets on model	12	15

Table 2 Details of first and second air jet configurations.

5.5.1 Lift curves: Comparison of first and second configurations.

The lift curves of the two configurations are presented together in Figure 38. The first thing to notice, when comparing the two configurations at the same blowing pressure (1.0 p.s.i.), is that the second performs better in terms of higher maximum lift. The measured lift coefficients at $\alpha = 19°$ being 1.71 and 1.81 for the first and second configurations respectively, a further increase of 9% to 55% over the unmodified aerofoil.

The second interesting feature is that at lower angles of attack in the linear part of the lift curves, the two configurations both marginally increase the slope of the lift curve, $dC_L/d\alpha$. This implies reduced boundary layer growth on the upper surface due to vortex mixing. Plotting of the trailing edge pressure coefficients (Figure 39) would seem to confirm this. It can be seen that the reduction in trailing edge pressure is clearly delayed by the air jets indicating a lower trailing edge velocity and thinner displacement thickness.

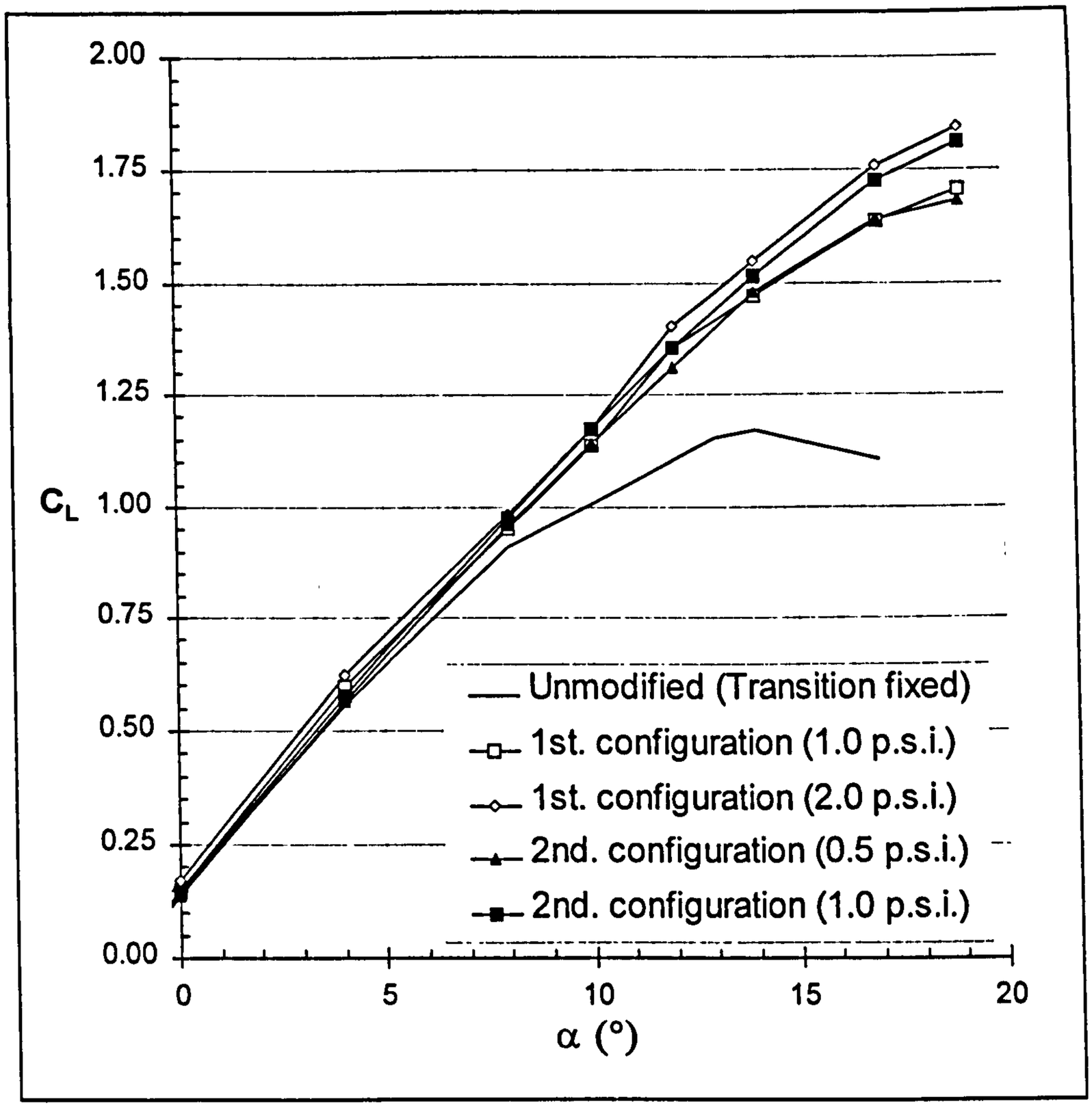

Figure 38 **Lift curves: Comparison of first and second configurations.**

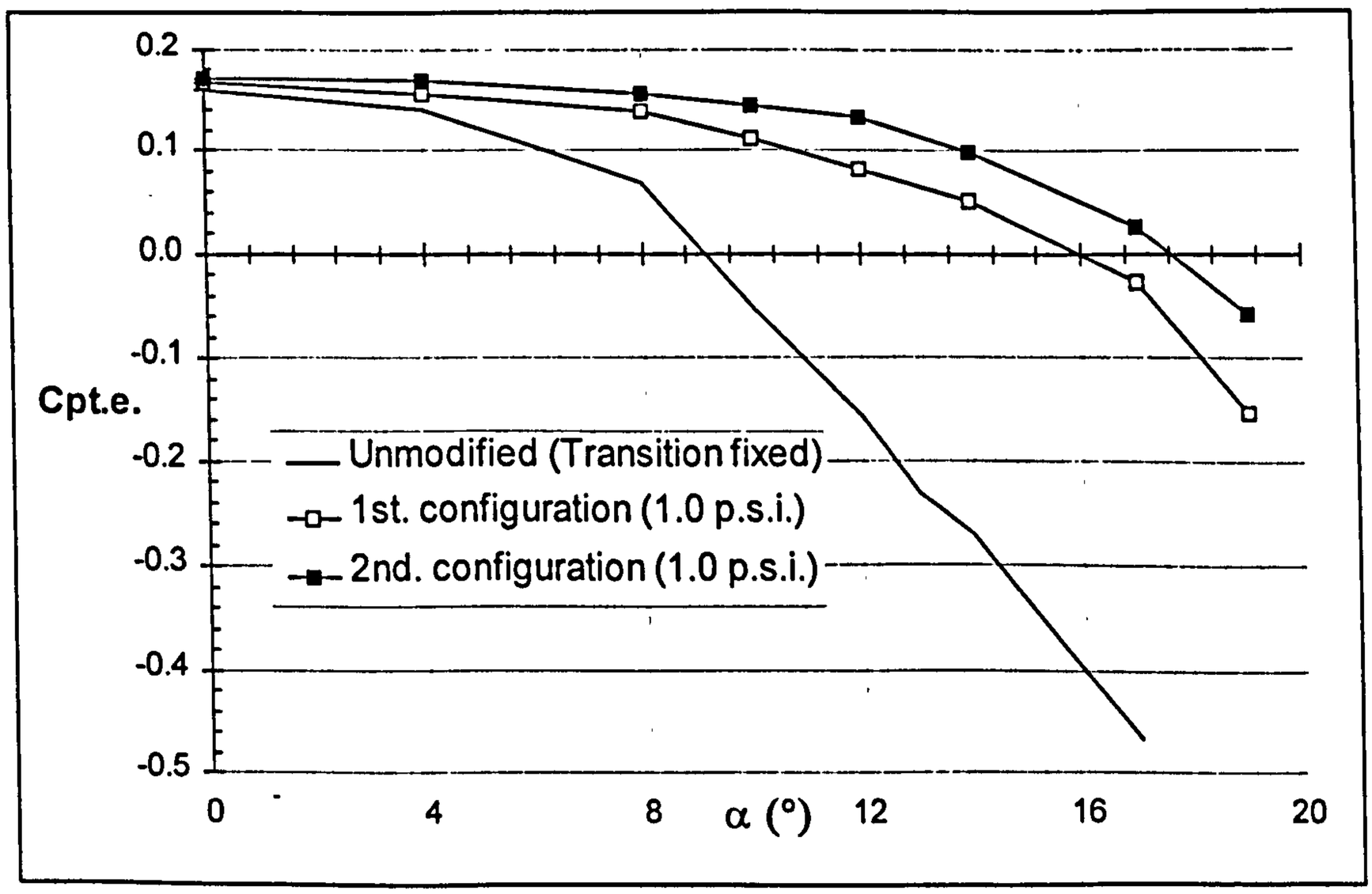

Figure 39 **Variation of trailing edge pressure for the two configurations**

5.5.2 Pressure distributions: Comparison with the unmodified aerofoil

Figure 40 shows the pressure distributions of the aerofoil with air jets (both configurations at 1 p.s.i.) and without air jets for $\alpha = 17°$. It can be clearly seen that whilst the flow remains attached with a full pressure recovery for the air jet cases, separation has occurred at approximately 40% for the unmodified aerofoil.

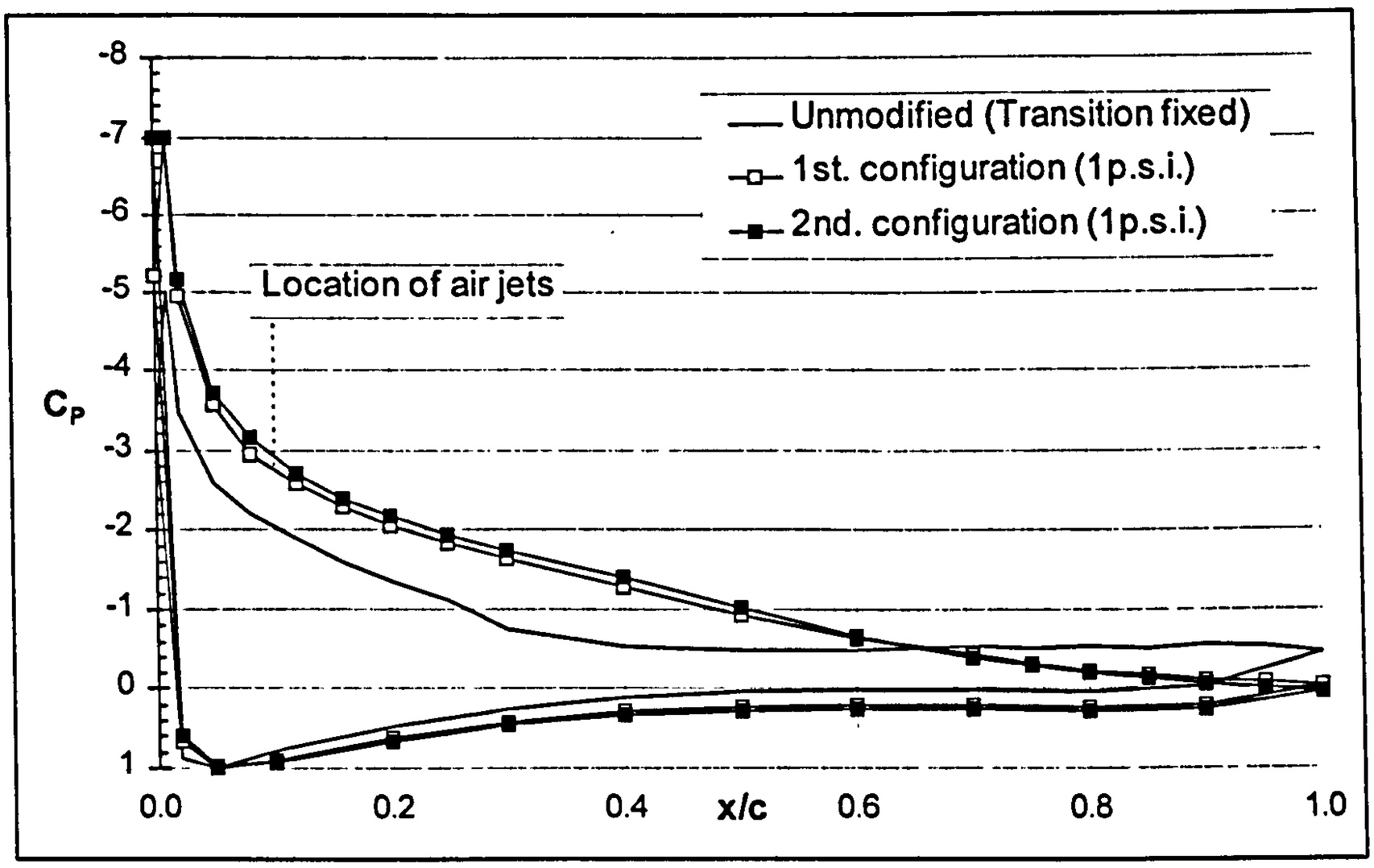

Figure 40 Cp distribution with and without air jets at alpha = 17°

The full pressure recovery has led to a greater 'circulation' and so it is not surprising that the aerofoil has a greater suction before the location of the air jets, (x/c = 0.1). The jets for both configurations have a higher peak suction of Cp_{max} of approximately minus 7 as opposed to minus 5 for the unmodified case.

Comparison of the two air jet configurations shows that the main reason for the higher $C_{Lmax.}$ of the second is a greater suction on the upper surface. The increased velocity on the upper surface implies that the second configuration is producing enhanced vortex mixing in comparison with the first since greater momentum transfer between the shear layers and the boundary layer must be taking place.

5.5.3 Normal force: Estimation of the jets on stall angle.

A few extra tunnel runs were undertaken in order to determine how the aerofoil stalls when the jets are operating and at what angle it occurs. As described in section 5.2.1, the wake rake could not be used at angles of attack greater than about $\alpha = 19°$. For this reason, only normal force coefficient was determined for angles of attack above 19°. The runs were carried out for the second configuration and are shown in Figure 41.

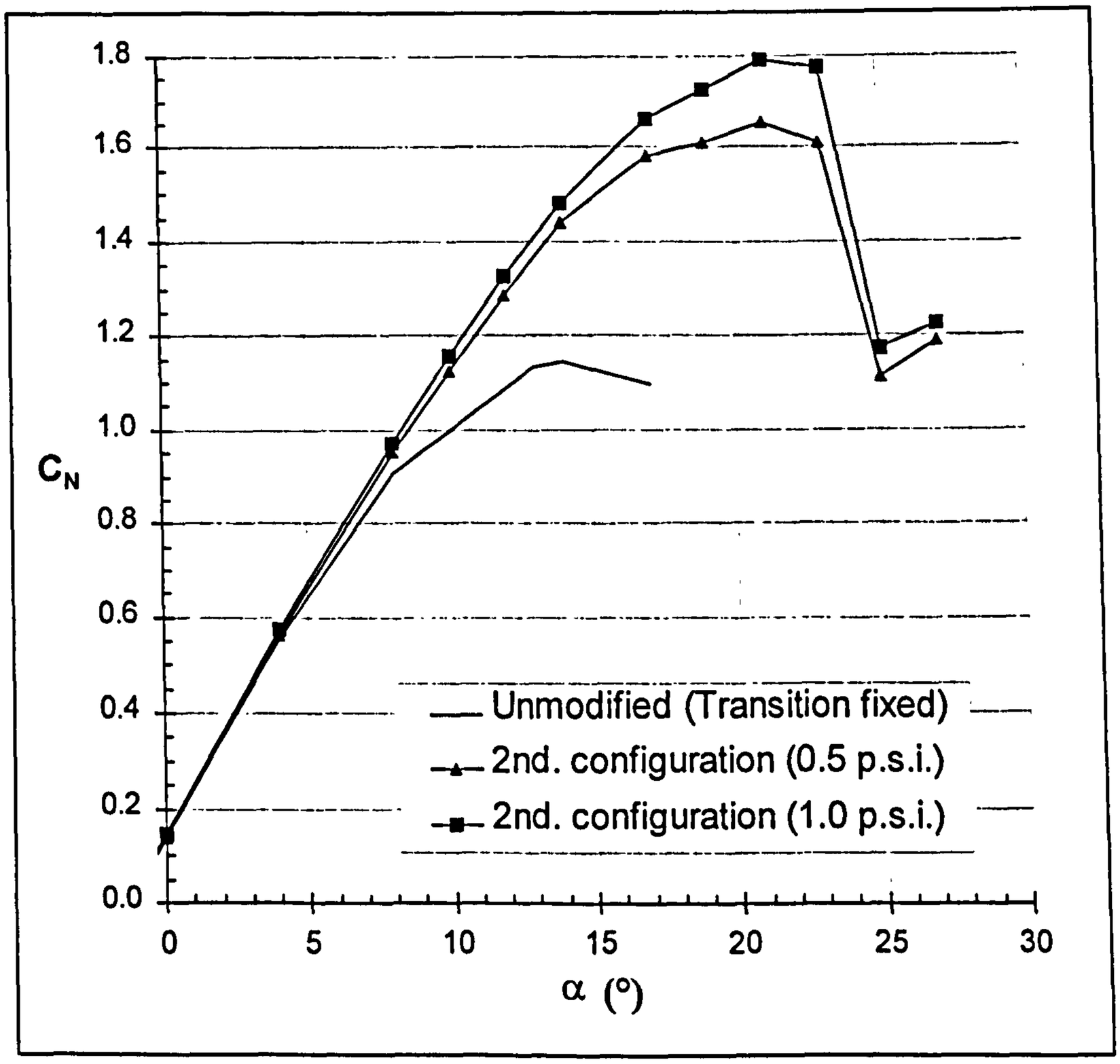

Figure 41 Graph of C_N versus alpha to determine jets on stall angle

The figure shows that the aerofoil does stall quite rapidly (22° - 24°) when the air jets are operating compared to the softer stall when they are not. It was thought that this might create some dynamic stall (6.9) problems and have an adverse effect on power quality.

5.5.4 Drag curves: Comparison of first and second configurations.

In Figure 42 the results of the second configuration have been superimposed on those of the first (Figure 34). Similar results to those of the lift curve are obtained in that, when comparing the two configurations at the same blowing pressure (1.0 p.s.i.), the second performs better than the first.

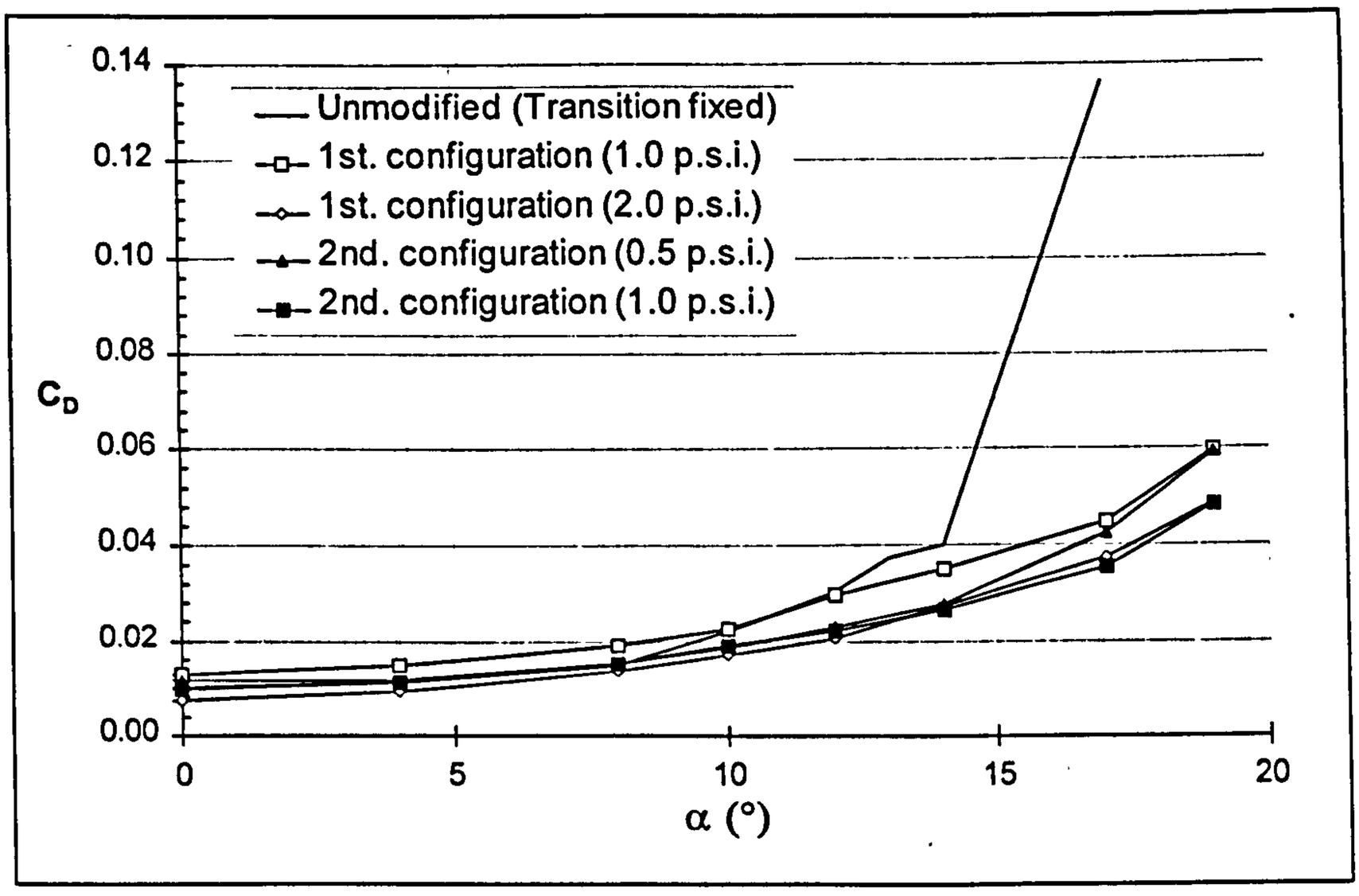

Figure 42 Drag curves: Comparison of 1st. and 2nd. configurations.

Figure 43 shows the region $0° \leq \alpha \leq 10°$ enlarged and the assumption that small jets would incur a smaller drag penalty (section 5.4.2) is found to be true, at least for the two configurations tested (compared at the same blowing pressure of 1.0 p.s.i. (square symbols)).

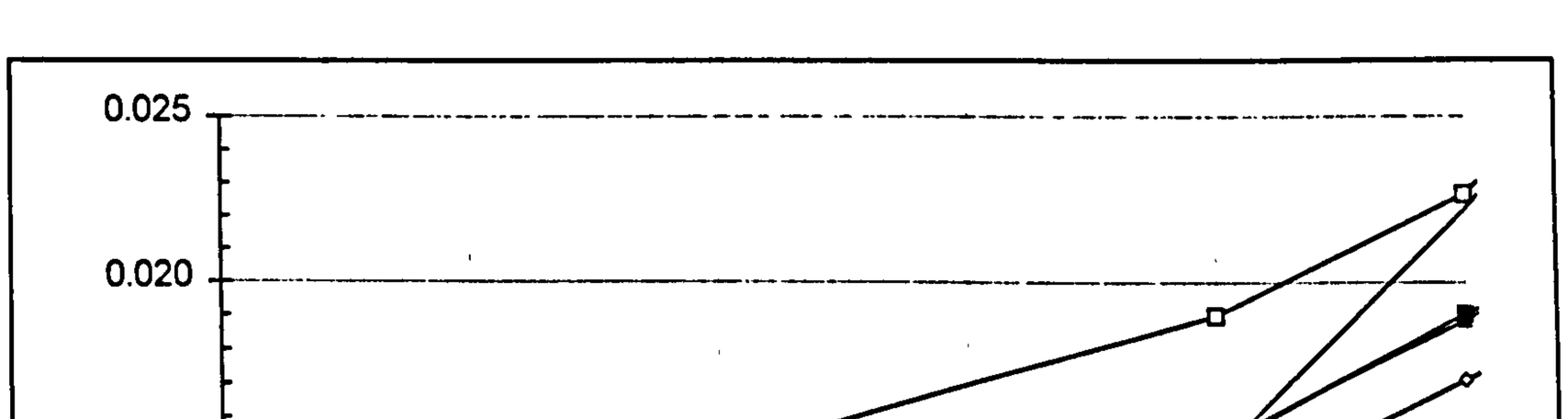

Figure 43 As Figure 42 showing area of detail

Perhaps the most interesting feature though, is that both blowing pressures of the second configuration (0.5 p.s.i. & 1.0 p.s.i. (black symbols)) produce similar results at low incidence and just straddle the unmodified case. This is in marked contrast to the larger jets (1st. configuration (white symbols)) which widely straddle the unmodified case. Various graphs have been plotted to try and determine what causes this effect to occur, but no strong conclusions could be drawn with the available data. Suffice to say that the following mechanisms are occurring and combine to a greater or lesser extent for the two configurations:

1. Drag increase due to the air jets provoking transition at their chordwise location.
2. Drag increase due to an increase in skin friction caused by the vortex.
3. Drag increase due to the air jets acting as a roughness element on the aerofoil surface.
4. Drag reduction due to the momentum that is imparted to the flow by the jet of air.
5. Drag reduction due to vortex mixing and subsequent reduction of trailing edge boundary layer thickness.

The first of the above will be identical for both configurations because in both cases the jets are located at 10% chord. This can therefore be eliminated as a reason for the difference between the two configurations. There are therefore four mechanisms affecting the drag, at low angles of attack, which cannot be readily separated into their component parts with the data available.

At higher angles of attack the influence of the vortex mixing and the subsequent reduction of boundary layer growth in the adverse pressure gradient (point 5.) becomes the most important factor. This is because the effect of the other factors on drag will remain more or less constant with angle of attack. Although the first configuration still performs worse than the second (at 1.0 p.s.i.), it is not as critical in this alpha range because the drag is lower than that of the unmodified aerofoil.

With respect to the short term aims of the project, the above discussions were not considered to be of the utmost importance. The specific question of whether smaller jets would be as effective at a blowing pressure of 1 p.s.i. had been answered. It was clear that at this blowing pressure the smaller jets had not only yielded a reduction in drag but had also increased the maximum lift and, as will be seen in section 5.5.8, had required less mass flow as well.

Nevertheless, it is perhaps important that further work is carried out in this area. Water tunnel visualisation or a boundary layer survey would be helpful as it would reveal whether the vortices created by the larger jets are possibly being generated too far above or close to the aerofoil surface. More testing of the two configurations at the same blowing pressure (other than 1 p.s.i.) would also be useful for determining any trends in the data.

5.5.5 Wake plots: Comparison with the unmodified aerofoil.

Although the wake plots do not reveal a great deal, it is interesting to show one example. Figure 44 then, shows the wake plot for $\alpha = 17°$ behind the model. The horizontal and vertical axes are taken from equation 3.1 and so integration of the bound curve yields $C_D/2$. The horizontal axis has been reversed for the purpose of illustration.

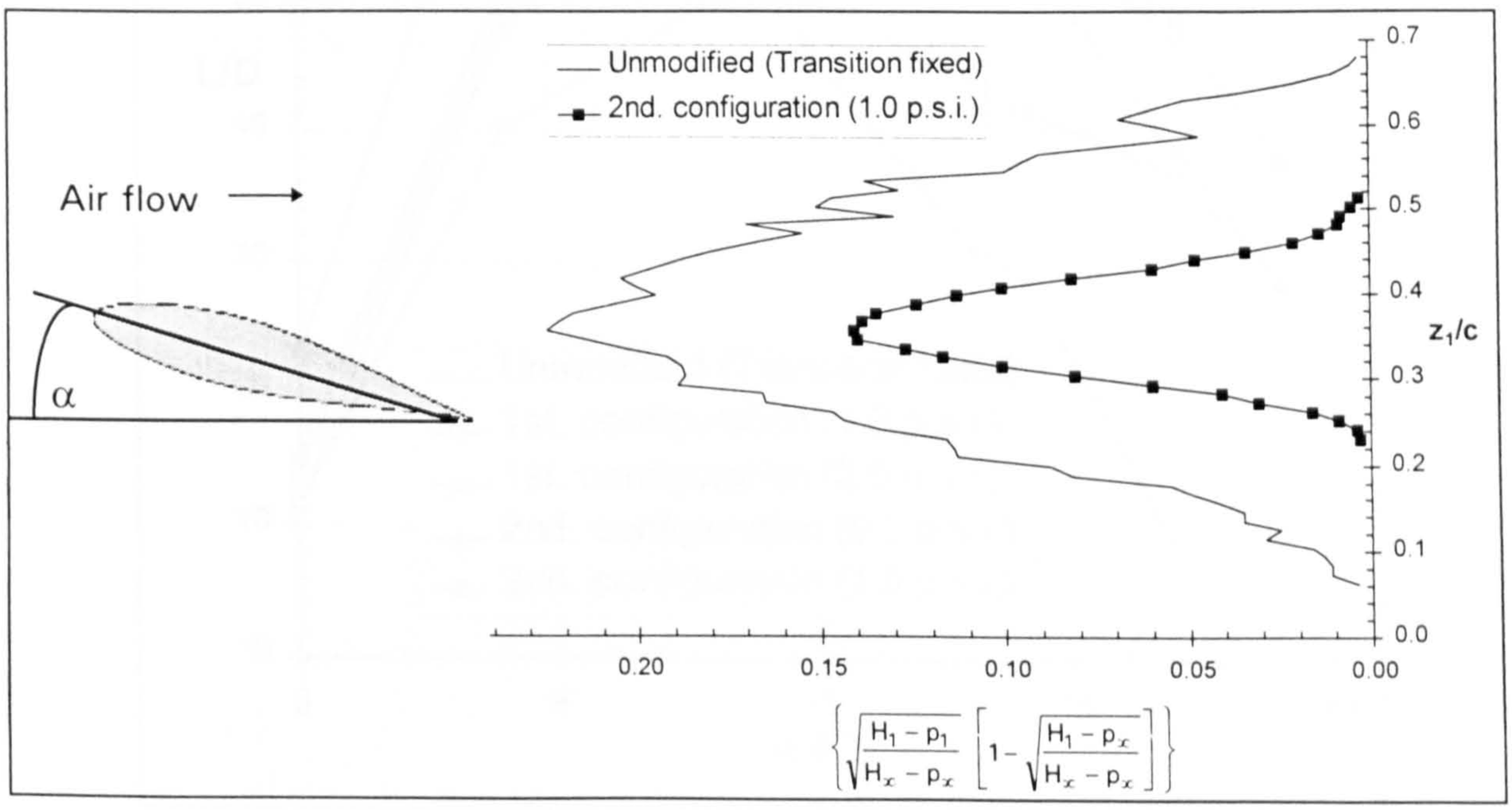

Figure 44 Wake plot with and without air jets operating at $\alpha = 17°$

5.5.6 Lift to drag ratio: Comparison of 1st. and 2nd. configs.

As described in section 1.3, L/D is an important parameter defining the power performance of a wind turbine.

Figure 45 shows the L/D curves corresponding to the graphs already presented in Figure 38 and Figure 42 and so it is only essential to re-iterate the main features. The difference between the two configurations at the 1.0 p.s.i. blowing pressure is now much more apparent, since the second configuration, it will be remembered, had increased lift and reduced drag in comparison with the first.

It is also immediately clear that for the first configuration at low angles of attack, the 1.0 p.s.i. and 2.0 p.s.i. blowing pressures perform worse and better than the unmodified aerofoil (transition fixed), respectively. This is almost entirely due to the reduction of measured drag described in section 5.5.4. The second configuration at low angles of attack, on the other hand, has a similar performance to the unmodified aerofoil.

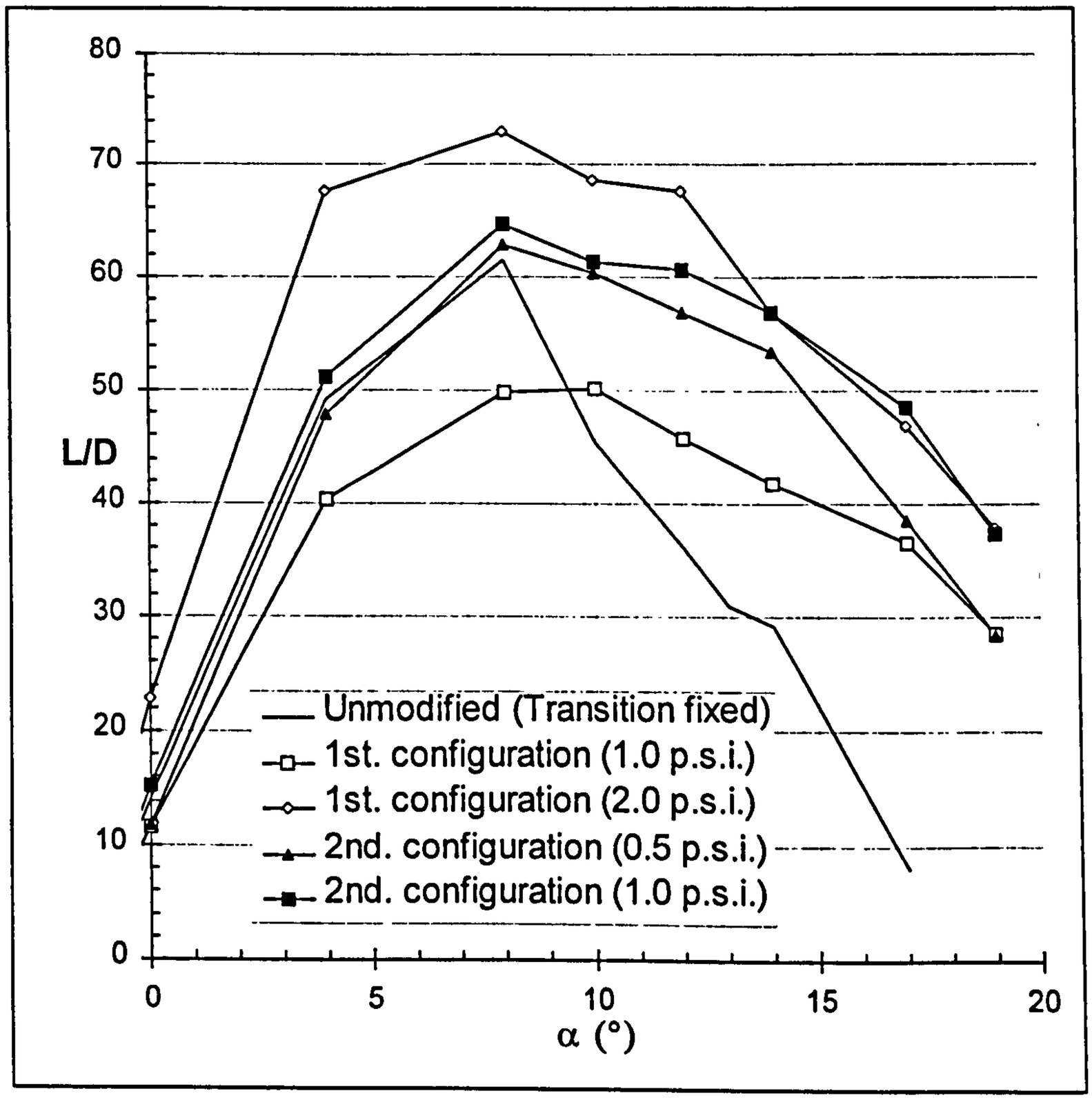

Figure 45 Lift/drag curves: Comparison of first and second configurations

Both configurations have extended the L/D envelope, but at the blowing pressure of 1.0 p.s.i., $L/D_{max.}$ is some 30% higher for the second configuration. The extended range of high L/D (approximately 6° of incidence) is important because it implies that peak power performance of any given blade section can be achieved over a greater range of wind speed.

As well as having a better L/D characteristic, the mass flow required by the second configuration at this blowing pressure was lower, details of which are given in section 5.5.8.

5.5.7 Lift to drag ratio: Air jets and transition fixing.

In terms of chronology the transition study was undertaken after the air jet results so far presented were obtained as it was not an immediate priority. It was thought that the high momentum air being ejected by the jets was forcing transition to occur at the location of the jets (10% chord). It was therefore expected that the performance would not be significantly altered by fitting the transition strip (6.5% chord) to the aerofoil with air jets. Shown in Figure 46 then, are the data for what is referred to as the Design Case from here onwards (2nd config. at 1.0 p.s.i., transition strip fitted). At low angles of attack the two lift and drag curves are virtually identical and this is reflected in the L/D curve. At higher angles of attack, although the lift remains the same, there is a small but noticeable increase in drag with the transition strip fitted, resulting in the reduced L/D ratio. The close comparison between the air jets with and without the transition strip does appear to confirm that they do force transition and that the transition strip selected was therefore a good one.

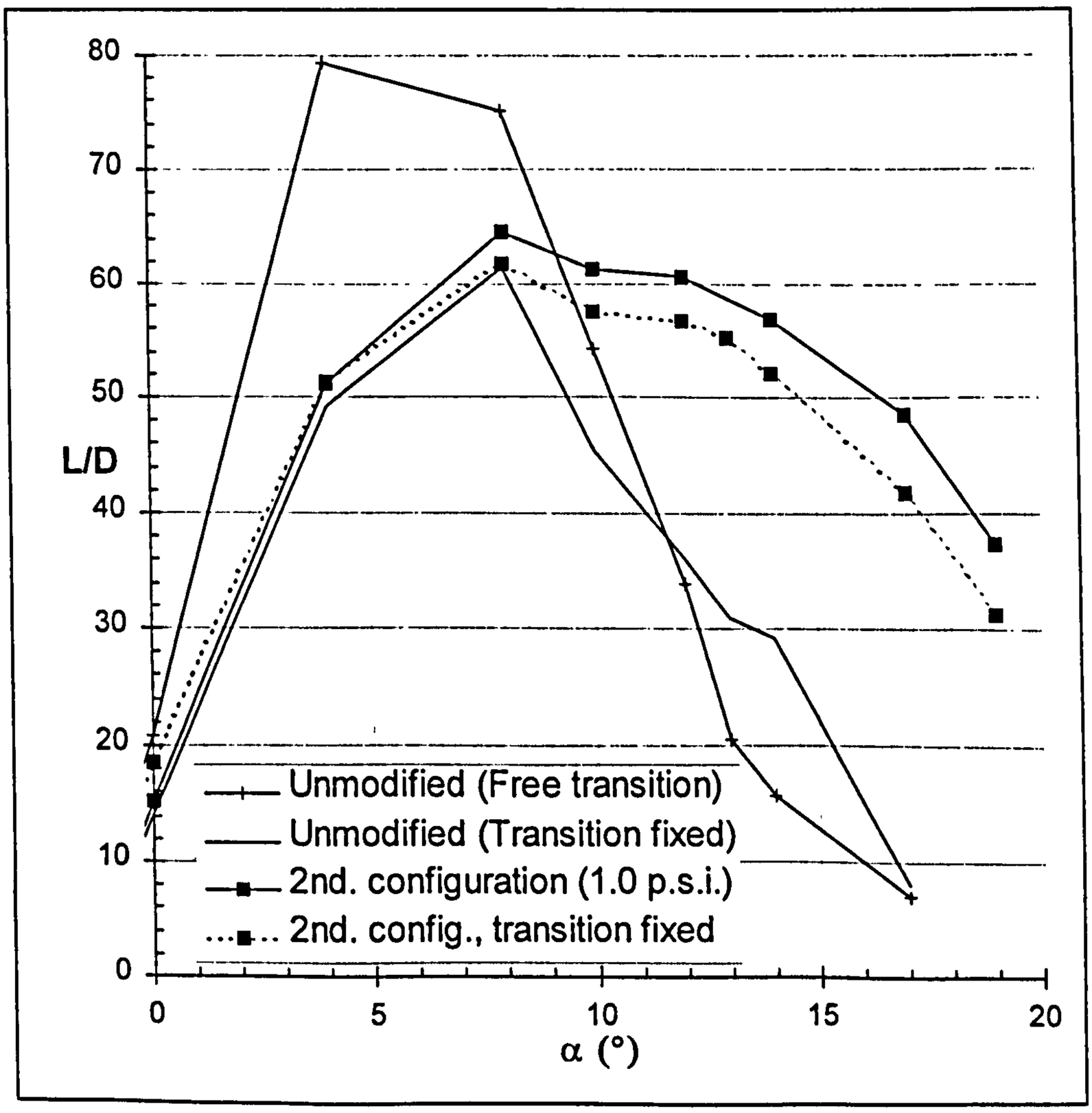

Figure 46 **Lift/drag curves: Comparison of transition free & fixed**

The 'Design Case' wind tunnel data obtained were used to estimate the performance of the air jets in different spanwise locations and with different array lengths (Chapter 7).

Figure 46 also illustrates the free transition case for the unmodified aerofoil. Up to about $\alpha = 9°$ the design case (2nd. config. at 1.0 p.s.i.) compares unfavourably and this is due entirely to higher drag. As previously discussed in section 4.2, free transition is thought to be unlikely to occur on a wind turbine blade due to the build up of dirt and insects. However, the worst case must be considered; what if the blades are clean and the turbine is operating in a smooth uniform wind regime allowing free transition to occur? An unmodified blade will be operating with free transition but one modified with air jets will be forcing transition. It was therefore thought prudent to estimate the effect on the power curve and resulting energy yield of the increased L/D at low angles of attack (section 7.6). The results showed that the effect would be most pronounced at low average wind speeds because the blade then spends more time operating at low angles of attack. Nevertheless, an increase in energy yield was still predicted even for the worst case when free transition occurs over the whole blade and at all wind speeds.

5.5.8 Mass flow: Comparison of 1st and 2nd configs.

Table 3 shows the mass flow requirements of a single jet for both configurations at a blowing pressure of 1.0 p.s.i. and an angle of attack, $\alpha = 10°$. It confirms the supposition (5.4.1) that the relative mass flow requirements of a single air jet at a given pressure is equal to the relative area of the jet exit. This was corroborated over the whole incidence range at a blowing pressure of 1.0 p.s.i. As mass flow measurements are quickly and easily obtained this result was also verified for a blowing pressure of 2.0 p.s.i. (although as discussed previously lift and drag measurements were not recorded at this higher blowing pressure for the second configuration). The relative mass flow of the second configuration to that of the first was always to within $\pm 3\%$ of their relative areas.

Config.	Dimensions of jet (mm.)	Jet area ($mm.^2$)	Jet area (relative)	$\dot{m}$ (kg/s)	$\dot{m}$ (relative)
1st.	16 x 2.0	32 mm^2	100%	3.46 E-3	100%
2nd.	12 x 1.5	18 mm^2	56.3%	1.89 E-3	53.6%

Table 3 **Single jet mass flow requirement for alpha = 10° at 1.0 p.s.i.**

This result is important because it means that we can predict with some confidence how a reduction in jet size will affect the mass flow requirement to produce a given blowing pressure behind it. However, given that smaller jets must be more densely spaced (45mm. as opposed to 60mm.) the reduction of jet exit area is not the true measure of mass flow reduction per unit length of air jet array. The actual relative mass flow of the second to first configuration per unit length of array is:

$$(18mm^2 / 32mm^2) \times (1 / (45\ mm./\ 60mm.)) = 75\%$$

5.5.9 Summary of performance: 1st and 2nd configs.

Summarising the performance of the two configurations at the same blowing pressure (Table 4) we can see that the second achieved a 30% increase in maximum L/D ratio whilst the mass flow required to feed these jets was reduced by some 25% for a unit length of jet array.

Parameter	1st. Config.	2nd. Config.	Change
Blowing pressure	1.0 p.s.i.	1.0 p.s.i.	~
C_{Lmax}	1.707	1.810	+ 6%
C_{Dmin}	0.0129	0.0096	- 26%
L/D_{max} (No transition strip)	50	65	+ 30%
Relative mass flow per unit length of air jet array	100%	75%	- 25%

Table 4 Performance summary of the two configurations

The mass flow reduction per jet was predicted because of the relative areas of the jet exits (5.4.1). The possibility of reducing drag (5.4.2) was also foreseen but the increase in maximum lift was not. These last two factors combined to produce a significantly improved L/D curve at the same blowing pressure (Figure 45).

5.6 Full scale design data

For the full scale trials then, the second configuration was chosen and for the purposes of power prediction it is the lift and drag characteristics of this system that were used. However, it is the mass flow properties of the first configuration that must be used when calculating the power requirement of the air jet supply. This is because the jets used at full scale are the same size as those of the first configuration but that the second configuration represents this at model scale (refer to section 5.4).

The full scale design mass flow requirements were taken as being the maximum recorded values of 0.00377 kg/s (at 1.0 p.s.i.) per jet i.e. those at $\alpha = 19°$ (Figure 35). The lift and drag data of the 'Design Case' are shown in Figure 47.

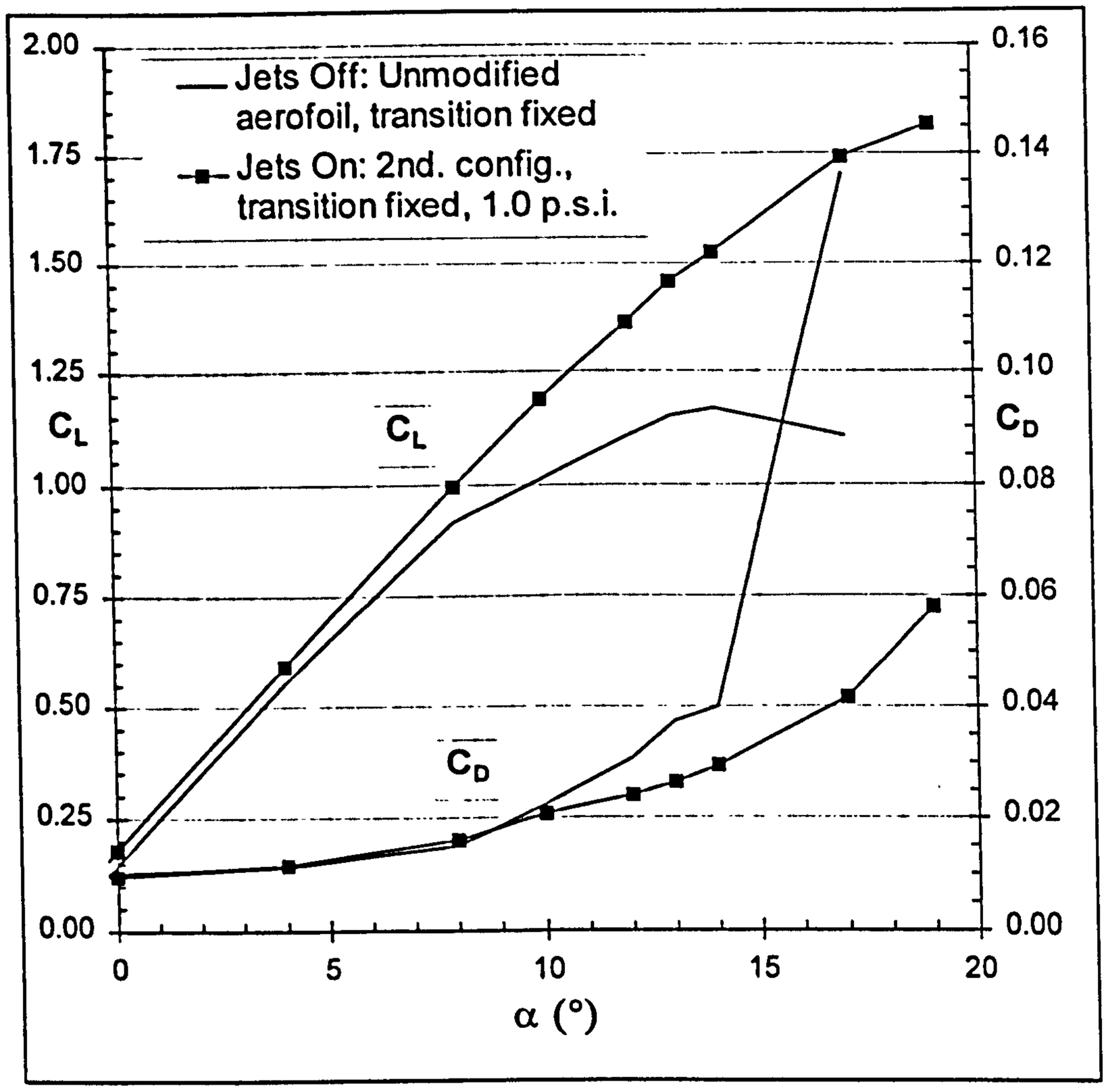

Figure 47 Lift and drag curves used in full scale design

5.7 Flow visualisation: Air jets off and air jets on.

The aerofoil was covered in tufts of silk so that the flow could be visualised. On the left hand side of Figure 48 the aerofoil is shown with the air jets turned 'off' at an angle of attack of $\alpha = 18°$. It can be seen that the aerofoil is fully stalled with a large percentage of the aerofoil experiencing reverse flow. On the right hand side of the same figure the aerofoil is shown at the same incidence with the air jets having been turned on.

Towards the trailing edge of the aerofoil a large amount of crossflow can be observed. This is because the aerofoil is in the early stages of separation, and so the local chordwise velocity is low, but there is still a spanwise velocity component due to the vortex.

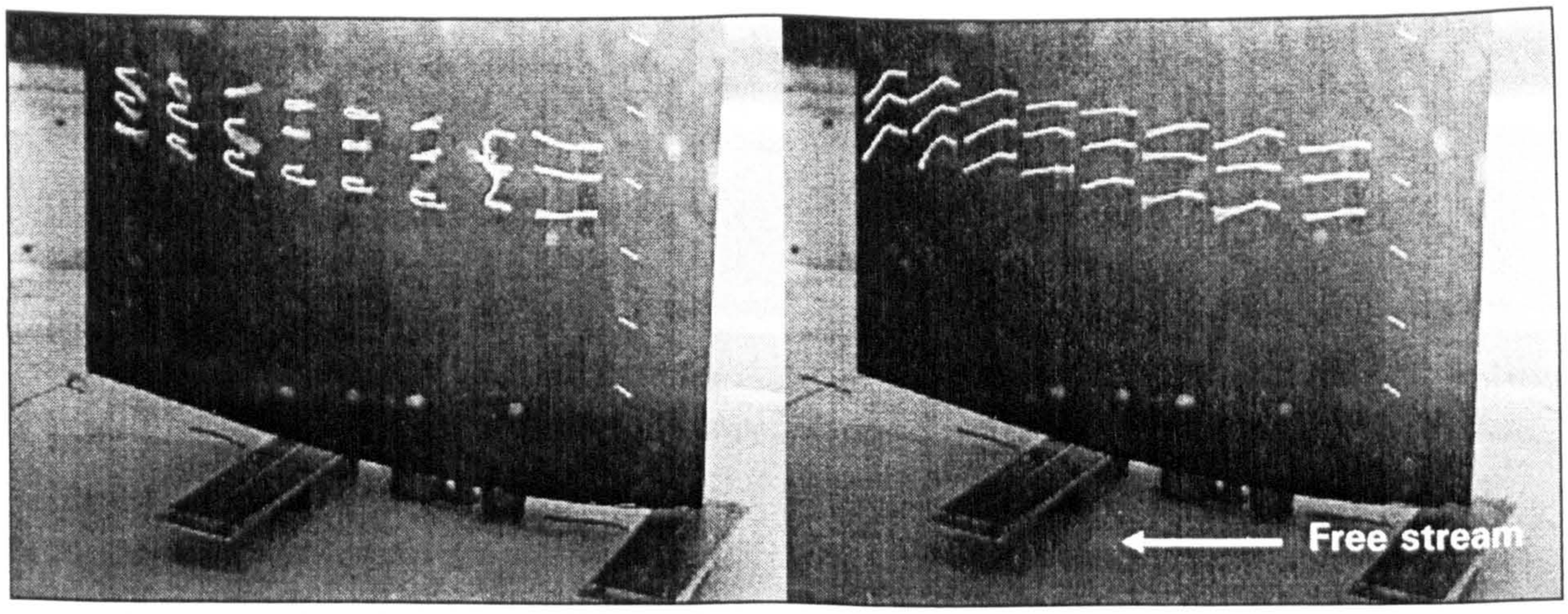

Figure 48 Tufted aerofoil: Air jets 'off' and air jets 'on' at $\alpha = 18°$.

The reattachment of the flow when the air flow valve is opened is instantaneous. The response of the full scale system to a change in wind speed or measured torque is therefore only a function of how quickly the supply of air can be altered.

5.8 Concluding remarks

The work reported in this chapter was carried out as part of a funded project. This placed certain limitations, on the experimental work that could be achieved within the project time frame, i.e. before the final full scale design had to be produced.

In Chapter 10, further experimental investigations are reported on. Specifically air jets blown passively rather than actively.

6. POWER PREDICTION PROGRAM

It was required that the effect of the air jets on the wind turbine's power curve could be predicted. This would allow:

1. The air jets to be located at the optimum spanwise blade radius, i.e. that which would give the best improvement in the power curve, just prior to rated (refer back to Figure 7).
2. An estimate of the expected increase in energy yield to be made.

6.1 Blade element momentum theory

To achieve this objective, a simple blade element, or strip, theory program was written. The method involves splitting each blade of the wind turbine into spanwise sections or 'elements', such that each element forms an annulus when the wind turbine rotates. Each element is analysed in turn and the power, P contributed by that element calculated. The contributions from each element are summated, effectively integrating along the blade, and multiplied by the number of blades to yield the power output for the wind speed in question. In this case, 20 half metre elements were chosen to represent one blade of the rotor.

The program uses the two-dimensional aerofoil data obtained in the wind tunnel tests in order to calculate the torque and hence power contribution of each element. However, it should be noted that using 2D static aerofoil data is not ideal, the reasons for which are discussed in section 6.6. Nevertheless, the method does allow a simple comparison to be made between two blades with different aerodynamic characteristics. With this in mind, a simple modification was made to the original program to allow the effects of air jet's to be calculated.

Upon execution, the program looks to see if the blade element for which it is calculating contains air jet's. If it does, the program will calculate the element's power contribution using the modified aerofoil data, otherwise it will use the standard aerofoil data. The basic operation of the program is given by the flow chart in Figure 49.

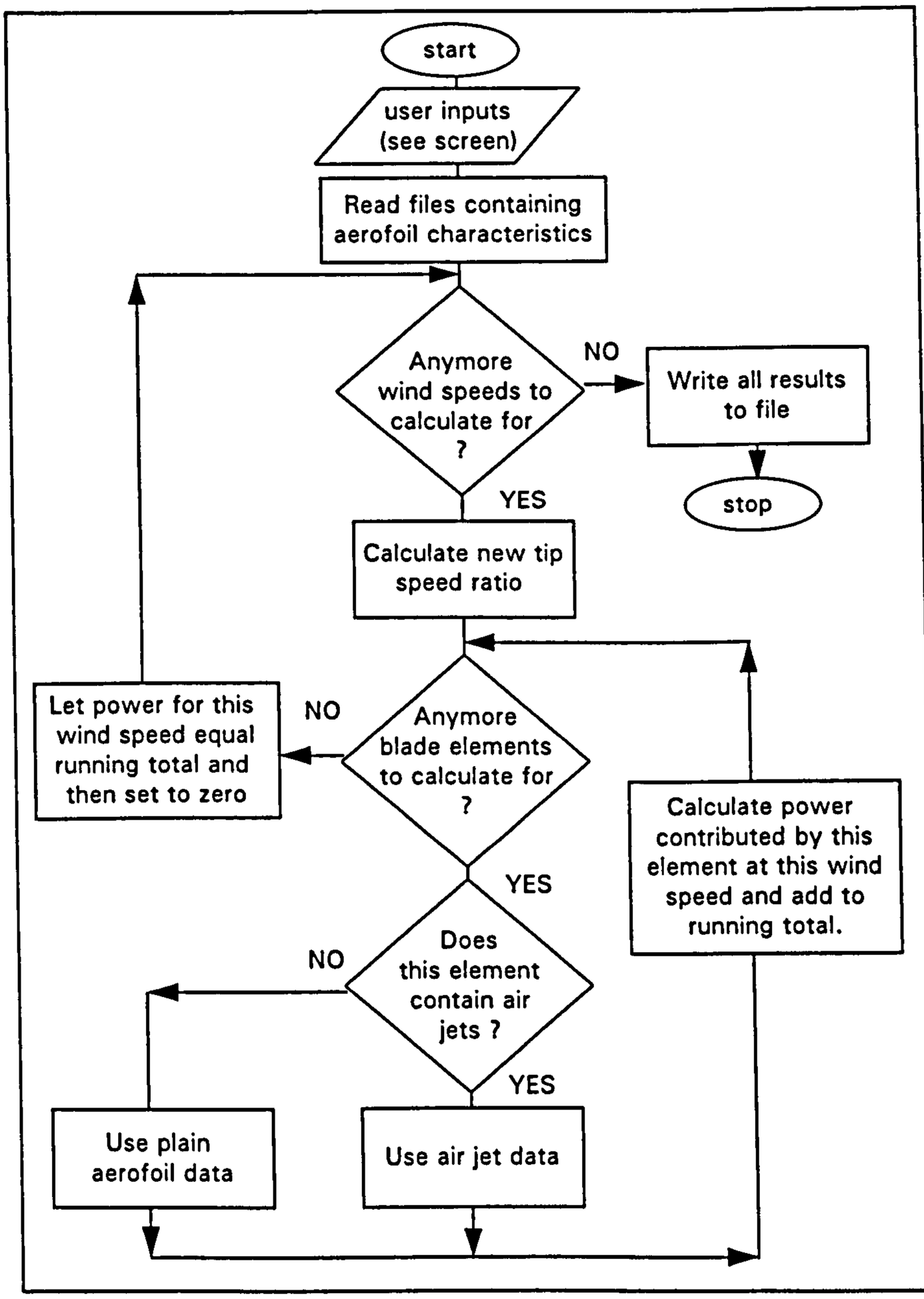

Figure 49 Flow chart showing the basic operation of the program

6.2 Methodology of the program

The equations used by the program are not listed in detail in this thesis, suffice to say that the relevant theories and concepts which are used and / or taken account of by the program are:

- Blade element theory, already described.
- Froude-Rankine theory, which introduces the concept of global axial and tangential flow induction factors a and a' to allow calculation of the changes in axial and tangential momentum across the actuator disc.
- Multiple stream tube theory, which looks at annular stream tubes to determine local values of a and a' for each blade element.

- Breakdown of the momentum theory, which occurs for heavily loaded turbines.
- Tip losses, which are taken account of by Prandtl's equation. Root losses are not taken into account as they are small in comparison.

Initial values of the induction factors, *a* and *a'* are specified in the program and the determination of angle of attack for each blade element is iterative. The iteration is deemed to be complete when the relative flow angle, ϕ, has converged. However, it was found that if ϕ was allowed to converge too quickly the iteration became divergent. To remedy this, the new value of ϕ was set to 80% of the old value plus 20% of the new calculated value. Once ϕ has converged the power and torque for the element in question are calculated. A full listing of the program can be found in Appendix 4.

6.3 Program input

6.3.1 Wind turbine characteristics

All data relating to the wind turbine (Ecotecnia 20/150) i.e. rotational speed, number of blades and radius are stored as variables within the program.

6.3.2 General blade characteristics

Data relating to the blade (LM Glasfiber 9.7m) i.e. twist and solidity as a function of radius are stored in array form as block data. The blade setting angle, β, is specified by the user.

6.3.3 Blade lift and drag characteristics

The program reads in an external file specified by the user. This file must be pre-prepared and should contain, in tabular form, a list of C_L and C_D variation with angle of attack, α. Two constraints are placed on this input file in order to simplify the program. These are:

1. The file should contain only 15 data sets (i.e. α, C_L , C_D) which completely describe the aerodynamic characteristics of the blade profile.
2. That α should be defined only for $-4° < \alpha < 40°$

The same also applies to the file containing air jet lift and drag data, which is asked for should the user specify that the blade is modified with air jets at the first prompt. In practice these two constraints were not found to degrade the performance of the program.

6.4 Program output

Two formats for the output can be specified by the user. 'Full' output will, for each wind speed, list r/R, α, C_L , C_D , Q, and P for each blade element at each wind speed, followed by the power curve. 'Reduced' output will only tabulate the power curve.

6.5 Program validation

In order to validate the program, it was run with aerodynamic data kindly supplied by the blade manufacturer, LM Glasfiber (LM). The output was compared with that of the code that LM use for in-house blade design. Figure 50 then, shows the program output compared to LM's output for the same input blade data. It can be seen that an excellent match is obtained. Assuming that LM's code is itself a good one this result validates the program.

Also shown on the same figure is the electrical power output of the wind turbine obtained from the Ecotecnia 20/150 product brochure. However, the program output should be compared to the rotor 'Shaft power' curve since this is what the program is calculating. As a first approximation the electrical power can be considered to vary linearly with rotor power, where P_{zero} is the zero load loss and η is the generator efficiency:

$$P_{elec} = (P_{shaft} - P_{zero}) * \eta \quad \text{.....(6 - 1)}$$

Values of P_{zero} and η for the Ecotecnia 20/150 are approximately 4.3kW and 93% respectively. Rotor shaft power has therefore been back calculated and plotted in the figure. Although the generator efficiency will actually increase with wind speed, this has not been measured by the turbine manufacturer for the higher wind speeds. This would have the effect of reducing the upper limit of this curve. Nevertheless, the LM prediction using 2D aerofoil data would still fall short of the actual power output recorded and this effect is discussed in the following section.

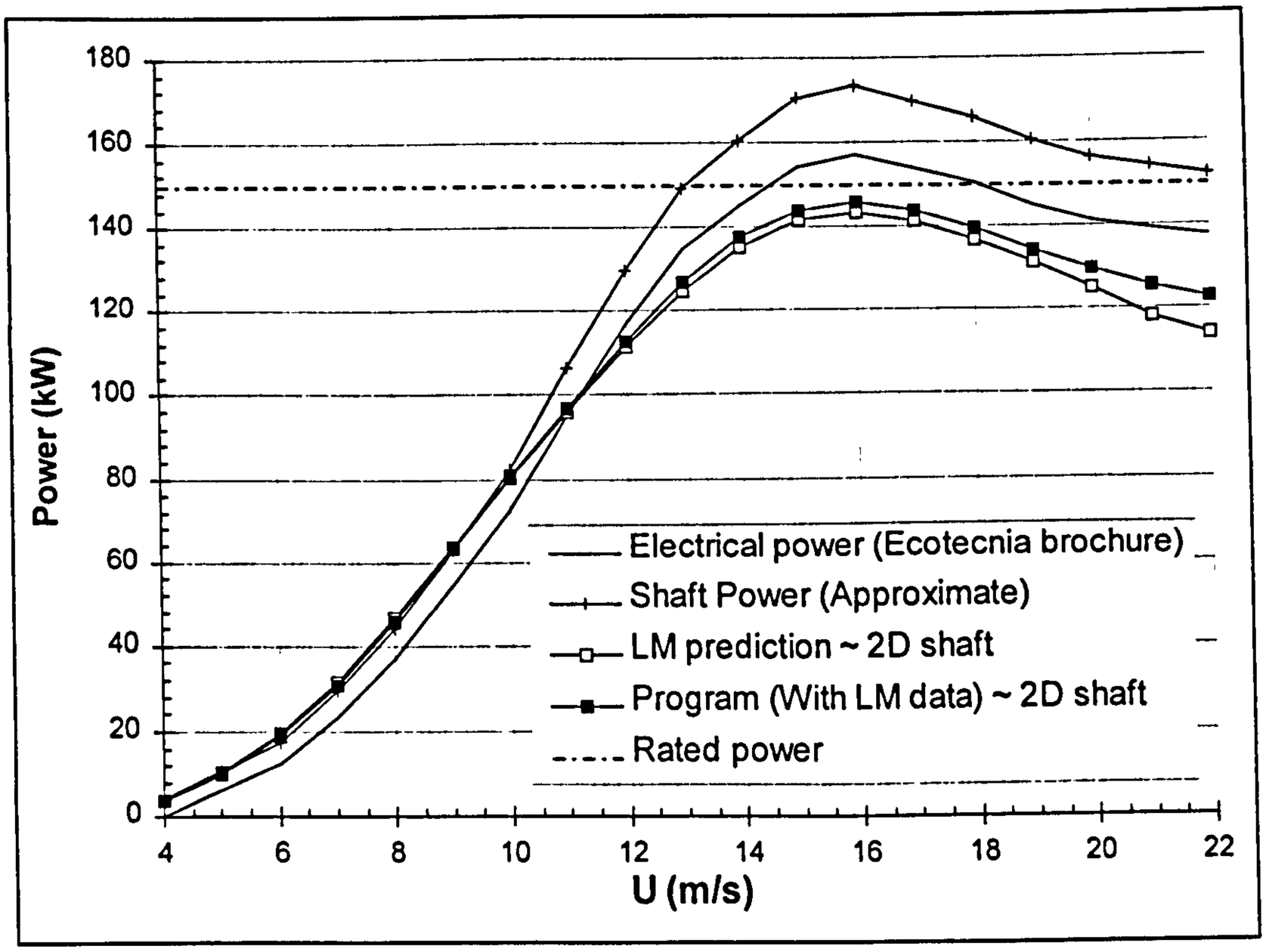

Figure 50 Validation of the program power output

6.6 Three dimensional (Himmelskamp) effect.

The blade element method is generally found to give good agreement at low wind speeds. However, at higher wind speeds where the tip speed ratio is low and angles of attack are high, manufacturers have reported measurements of power that are higher than those that the theory would predict. It can be seen in Figure 50 above that the blade manufacturers prediction using two dimensional aerofoil data differs significantly from the actual shaft power output at higher wind speeds.

The most important effect is the increase in maximum lift near the root of a rotating blade. This effect was first investigated on airscrews by Himmelskamp (1945). He measured lift coefficients over and above the 2D steady values and attributed this to a radial flow from the hub to the tip.

The outflow has subsequently been found to be most pronounced when the blade is operating in stall i.e. near the blade root at higher wind speeds and has been confirmed with flow visualisation techniques, e.g. Milborrow (1985) and by pressure measurements on a rotating wind turbine blade, e.g. Nyland (1987). Two mechanisms have been identified as the main causes of the radial outflow:

1. Centrifugal forces acting on the boundary layer.
2. Spanwise pressure gradient due to the velocity increasing with radius.

The first of the above acts to thin the boundary layer by displacing fluid particles outwards. The second effect of the spanwise pressure gradient on the suction side of the blade results in a Coriolis force acting in the main flow direction. This gives rise to a reduced displacement thickness resulting in less de-cambering of the aerofoil and therefore higher lift coefficients. Further details can be found in the papers by Milborrow (1985), Snel et al (1993) and Bosschers et al (1996) from which the above is abridged.

Snel et al (1993), use an order of magnitude analysis to show that it is the local blade solidity (c/r) which is the dominant parameter affecting lift deviations from the 2D stall behaviour. He and his co-workers suggest a simple formula which they found to be a suitable empirical conversion between results calculated with blade element theory and experimental results for the NACA 44xx section:

$$C_{L\,3D} = C_{L\,2D} + \{3\,(c/r)^2\,.\Delta C_L\} \quad \ldots\ldots\ldots\ldots\ldots\ldots\ldots\ldots \quad (6 - 2)$$

where ΔC_L is given by the difference between the extrapolation of the linear part of the lift curve and the measured 2D data. The parameter $(c/r)^2$ ensures that the effects of three dimensional flow are most significant at the root and diminish towards the tip and so conforms with the observations. Figure 51 shows Snel's formula applied to the unmodified lift curve (no air jets) of our aerofoil.

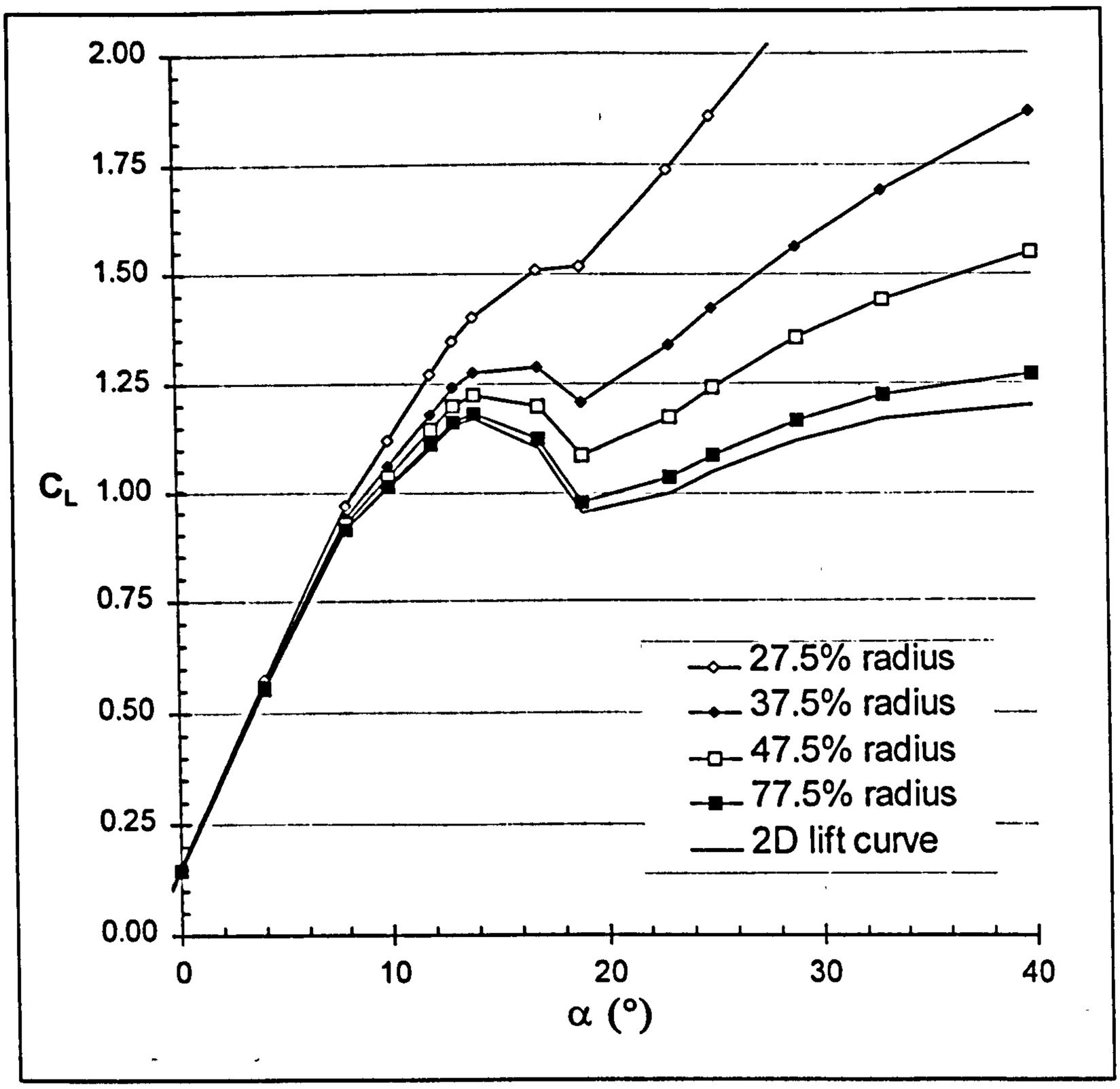

Figure 51 How 3D effects may modify the lift curve (Snel et al, 1993)

The program was altered to include Snel's correction and Figure 52 shows how it modifies the original 2D power curve (LM's aerofoil data). Also shown in Figure 52 is LM's own correction to a 3D power curve. At first sight it looks as though LM's correction is better as it predicts the shape of the actual shaft power curve more precisely at higher wind speeds, when the blade is operating in deep stall. However, it must be remembered that Snel's correction has been applied to LM's 2D data. In reality, the aerofoil lift and drag data for deep stall is usually altered until the power curve with the 3D correction matches the actual power output. It is quite probable therefore that Snel would choose different aerofoil data for deep stall and predict the correct shape at higher wind speeds. This may be very close to guesswork but the fact is that little data is available for aerofoils operating in deep stall. This topic is discussed further in section 6.7.3.

More importantly, the two methods of correcting for 3D effects are complimentary to one another up to and including rated wind speed. At these wind speeds only the inner part of the blade is operating in deep stall and so both methods appear to apply equally well for lower angles of attack.

This result also shows that the factor of 3 in equation 6-2, which Snel et al suggest is aerofoil dependent, applies equally well to our aerofoil.

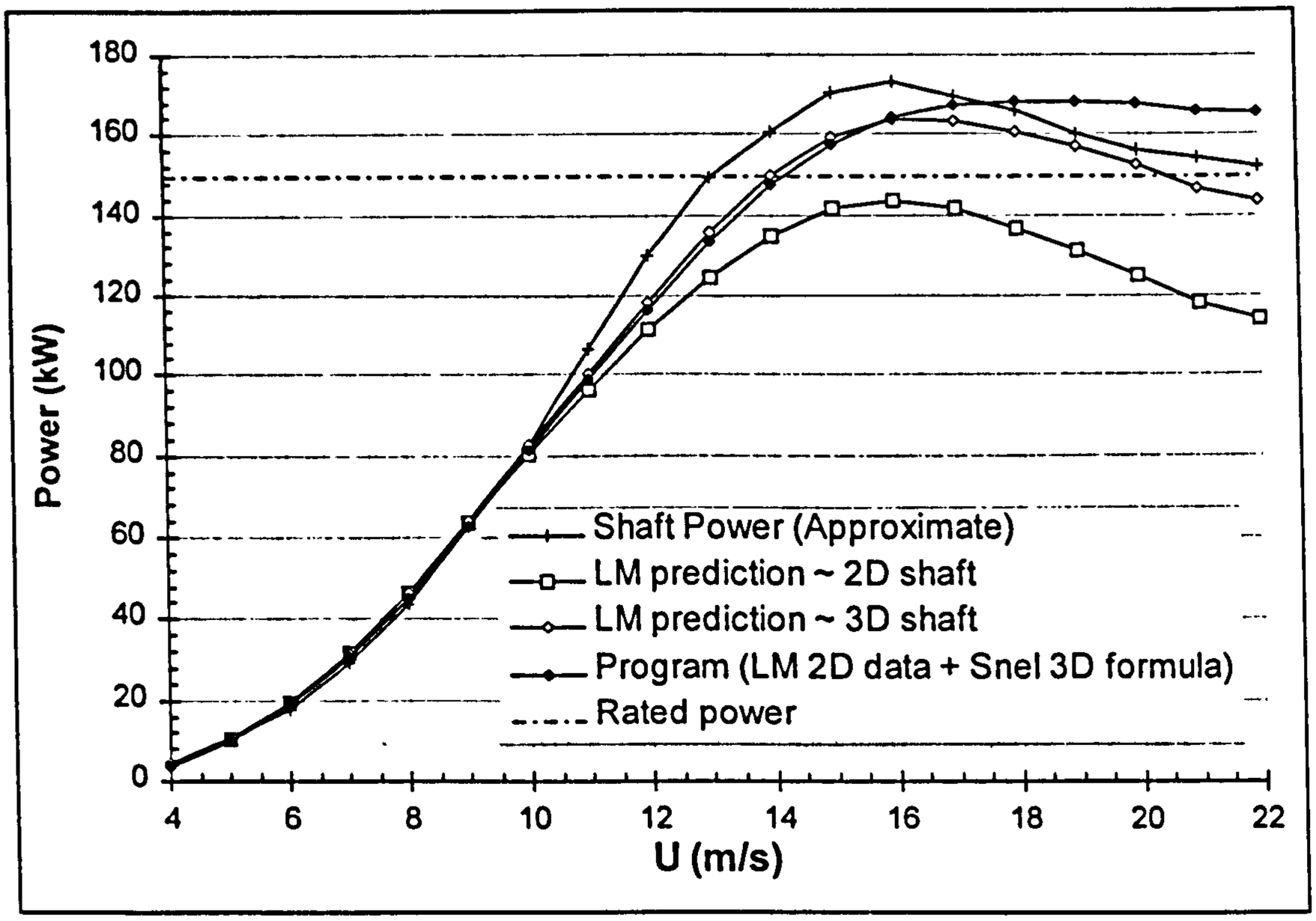

Figure 52 3D correction to predicted power curve

Neither curve matches the shaft power curve but it will be remembered that this is only an approximation based on the electrical power output of the machine. In reality the upper limit of the shaft power curve will be lower due to increased generator efficiency at higher wind speeds (section 6.5).

The program is therefore validated with the blade manufacturers prediction, using the same input data, up to rated wind speed. However, the point of this program is to compare jets 'off' with jets 'on' and also to locate the jets on the blade. To obtain this comparison, the data used must be relative, i.e. that obtained in the wind tunnel. The whole blade therefore had to be modelled with only two sets of wind tunnel data. The implications of this are discussed in the following section.

6.7 Modelling of the blade using the wind tunnel data

Power prediction codes are normally used for blade design and optimisation and incorporate a whole family of lift and drag curves. This is because parameters such as Reynolds number and aerofoil thickness change along the blade length and so alter the aerodynamic characteristics and ultimately the power curve.

To compare the initial power curve with one which has been modified by air jets requires knowledge of how their effectiveness changes with these parameters. This would call for several wind tunnel models and a larger wind tunnel and so this power prediction program must rely on just one set of wind tunnel data, i.e. data measured at one Reynolds number and at one blade thickness. This section investigates the implications of this and also examines the extrapolation of lift and drag curves into deep stall. For simplicity these investigations are carried out without the 3D correction previously described.

6.7.1 Aerofoil thickness / chord ratio

When designing a wind turbine blade a trade off has to be made between thick aerofoils which possess superior strength and thin aerofoils of superior performance. On larger, modern wind turbines, blades are thicker at the root, for structural reasons, and become thinner towards the tip. Sometimes the profile at the blade tip is of a different aerofoil family altogether, in order to limit torque in high winds. Any change in aerofoil camber should also be considered, since increasing camber will effectively 'shift' the lift curve to lower angles of attack.

Although, the LM 9.7m blade fitted to the test machine uses only one aerofoil family whose camber does not vary with blade radius, the effect of thickness is important in terms of the program performance. The variation of thickness-chord ratio with blade radius for the Ecotecnia 20/150 is shown in Figure 53.

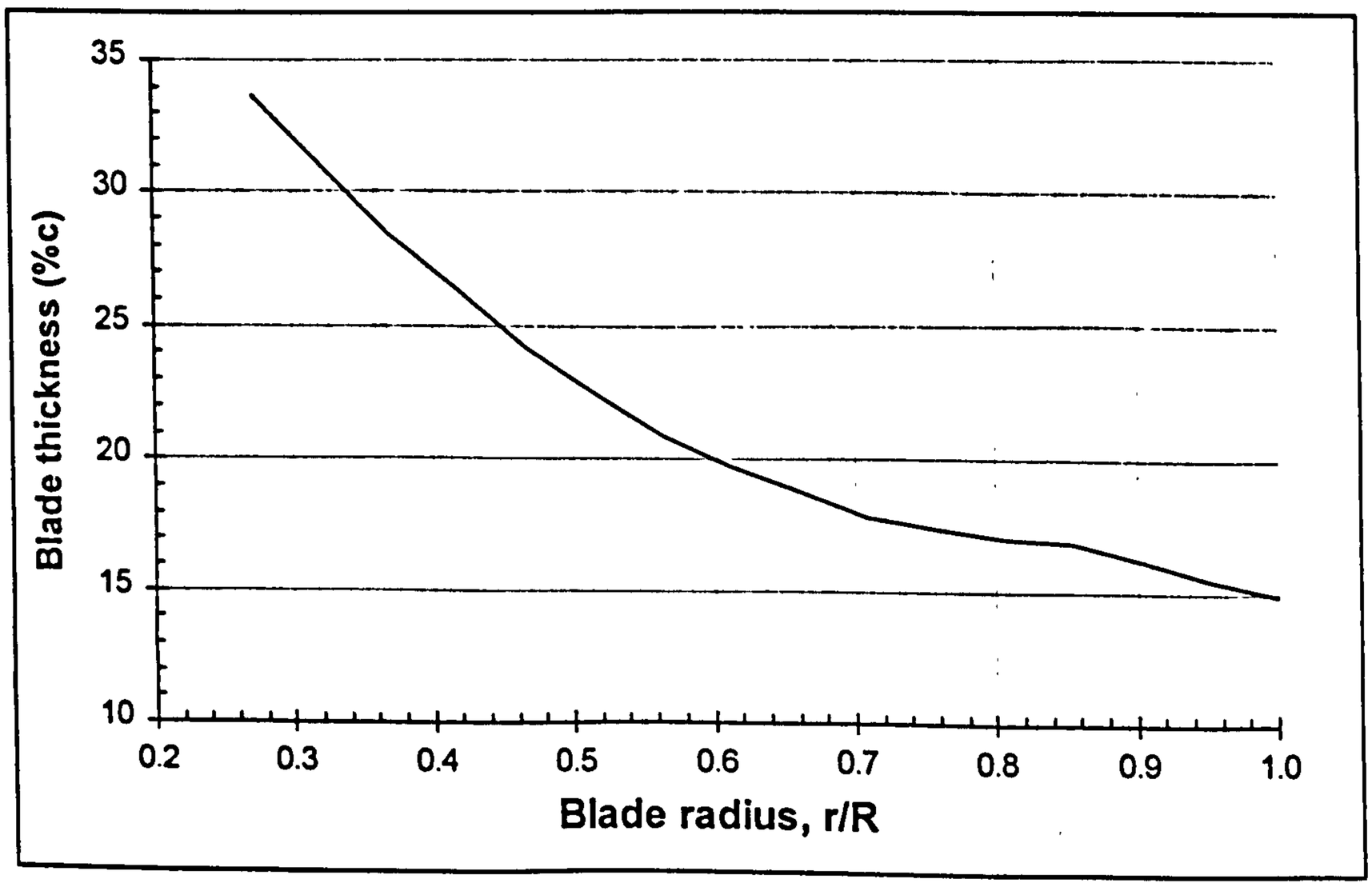

Figure 53 **Variation of aerofoil thickness along the blade.**

LM use data for three aerofoil thicknesses to model this blade; 21%, 18% and 15% which for angles of attack up to about $\alpha = 20°$ is obtained from Abbott et al (1959) and is shown in Figure 54. The Reynolds number is 3.0 million.

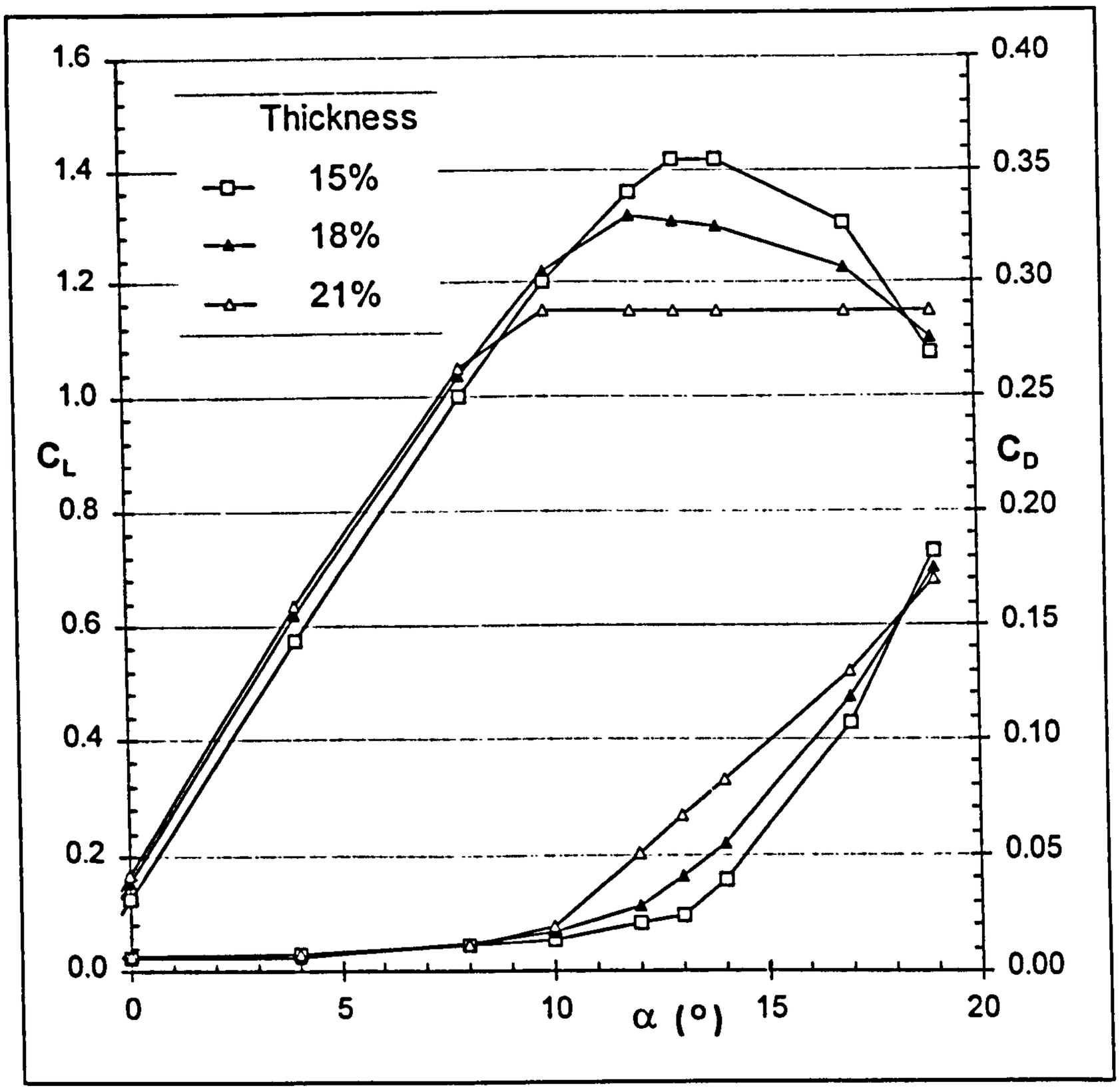

Figure 54 Variation of lift and drag curves with blade thickness

As explained above the author's program relies on data of only one blade thickness and so in order to validate the program with LM's (Figure 50) a rather cumbersome approach was taken. This involved running the program three times with each of the above thicknesses. By selecting 'Full output' it was possible to determine the power contributed by each blade element. Thus to calculate the power output for a given wind speed, contributions were combined from each of these three outputs depending on the thickness of the section at each element.

However, by running the program with just the data for the 18% aerofoil thickness a good approximation to LM's power prediction was still possible (Figure 55). It was on this premise that it was felt permissible to use only the wind tunnel data (obtained for 17.05% thickness) to represent the whole blade.

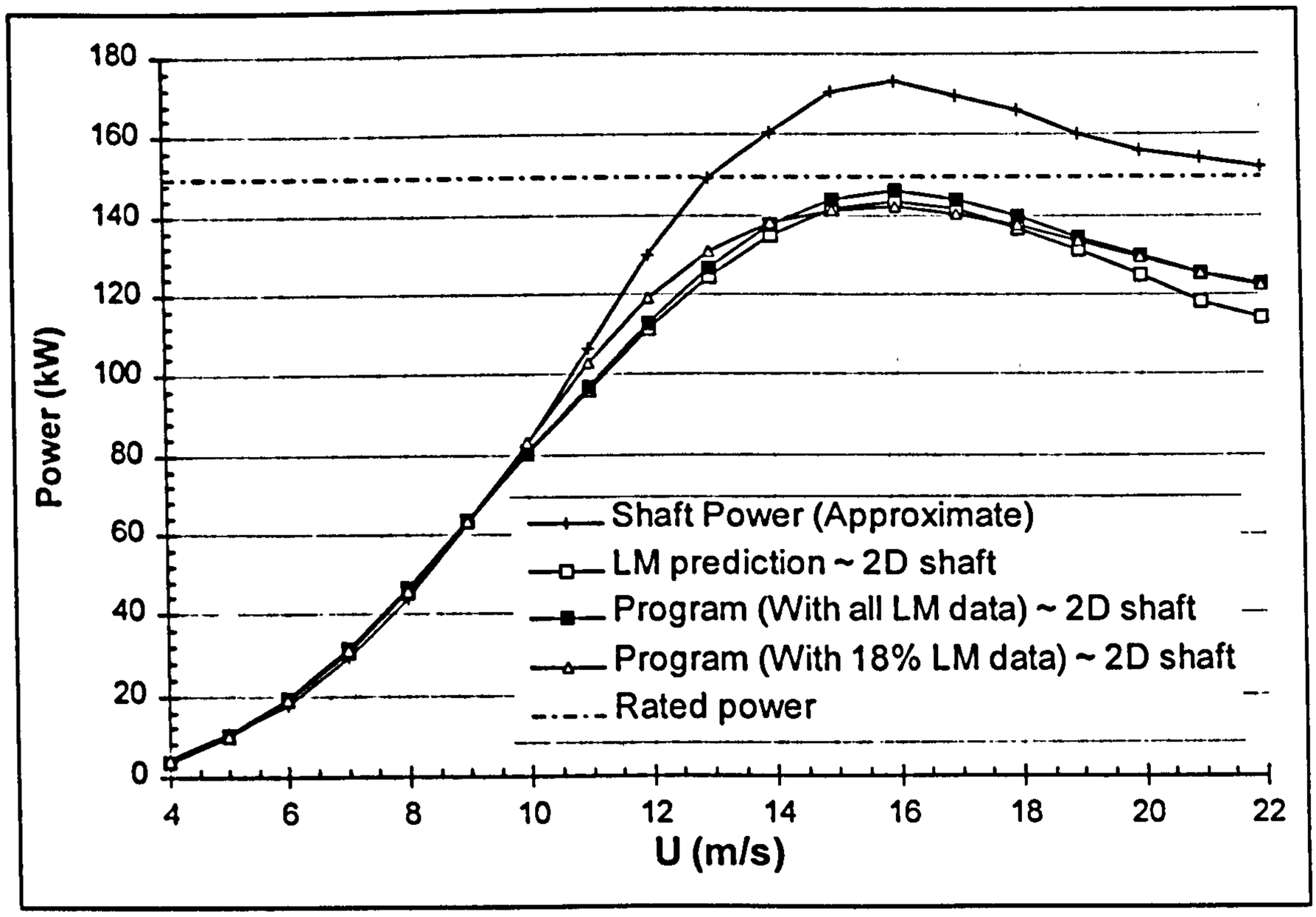

Figure 55 Approximation of the power curve with 18% thick aerofoil

6.7.2 Reynolds number

Reynolds number, Re., varies from root to tip, due to rotational speed, and acts to increase C_{Lmax} and reduce C_{Dmin} as it itself increases. Obviously, Re. also increases with wind speed, particularly towards the root where the rotational speed is lower. Figure 56 shows that, at rated wind speed, where air jets are required to work best and the program must be most accurate the actual Reynolds number varies from 1.5 million to 1.9 million. This is compared to a test Reynolds number of 1.4 million.

Thus the program output will be adversely affected by using the wind tunnel data. However, the effect of Reynolds number is certainly not as important as that of three dimensional flow.

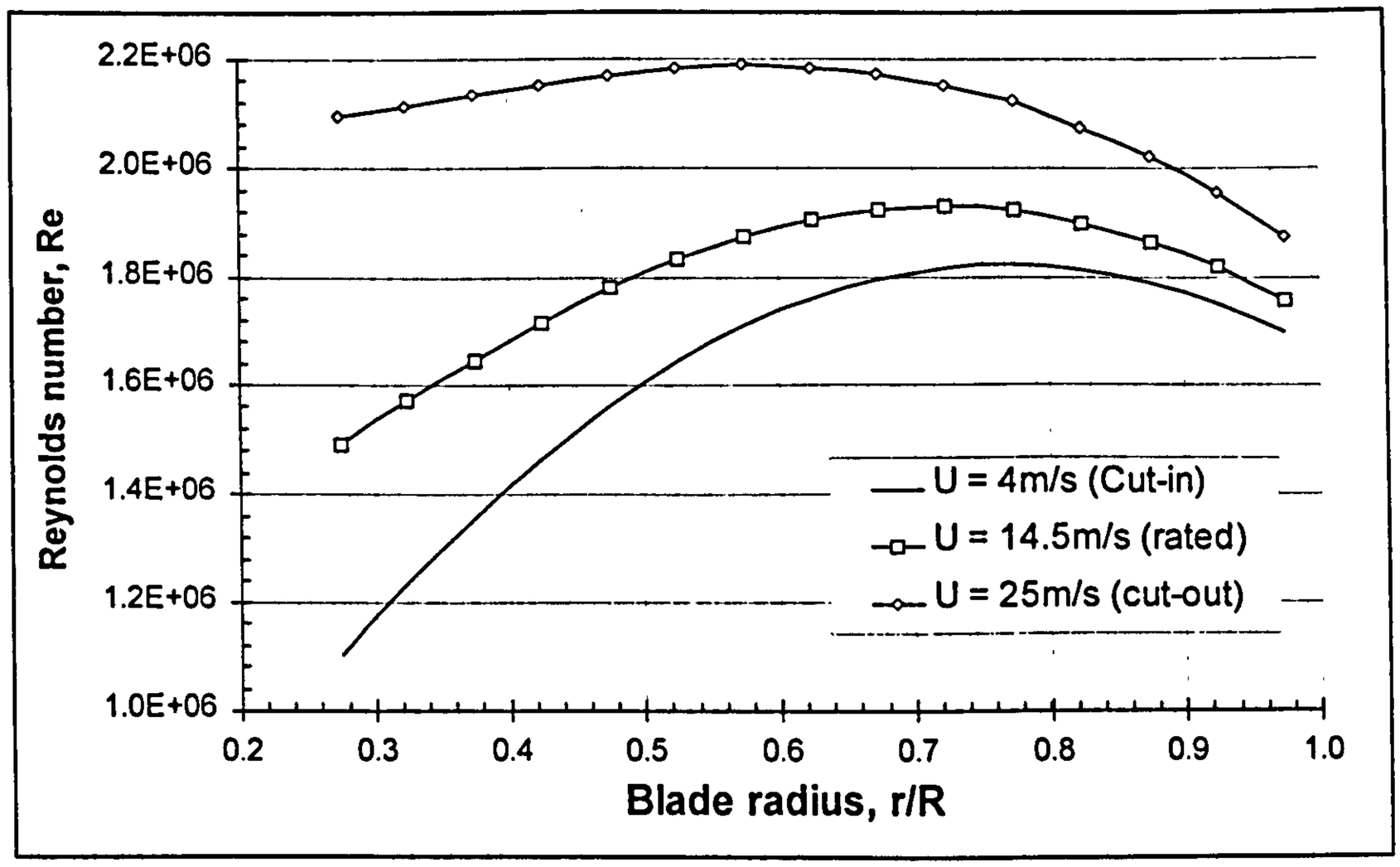

Figure 56 Variation of Reynolds number along the blade

6.7.3 Extrapolation of lift and drag characteristics

The inner region, or root, of a stall regulated wind turbine blade will, at high wind speeds, experience 'deep stall'. Here the blade may be at angles of attack as high as $\alpha = 50°$. Since aircraft designers have little need for aerofoil data above the stall angle and wind turbine engineering is a relatively new technology, little data exists for aerofoils operating in deep stall. As mentioned previously lift and drag was only measured up to $\alpha = 20°$ in the wind tunnel. For this reason the aerofoil data obtained in the wind tunnel had to be extrapolated from $\alpha = 20°$ to $\alpha = 40°$, the upper limit for the input file. Obviously such an extrapolation is extremely subjective, but two references were selected to at least determine the data trend. These were ESDU 70015 (1972), which deals with forces and moments on flat plates, and a paper by Bloy et al (1993) in which 2D lift and drag measurements were made through 360° on the closely related NACA 63_2 -215 aerofoil*. The deep stall data used by LM* was also looked at and lift and drag curves for all three are plotted alongside those from the current wind tunnel tests in Figure 57.

---

* Thanks are due to Dr. A.W. Bloy of Manchester University and Dr. C. Westergaard of LM Glasfiber for supplying this data.

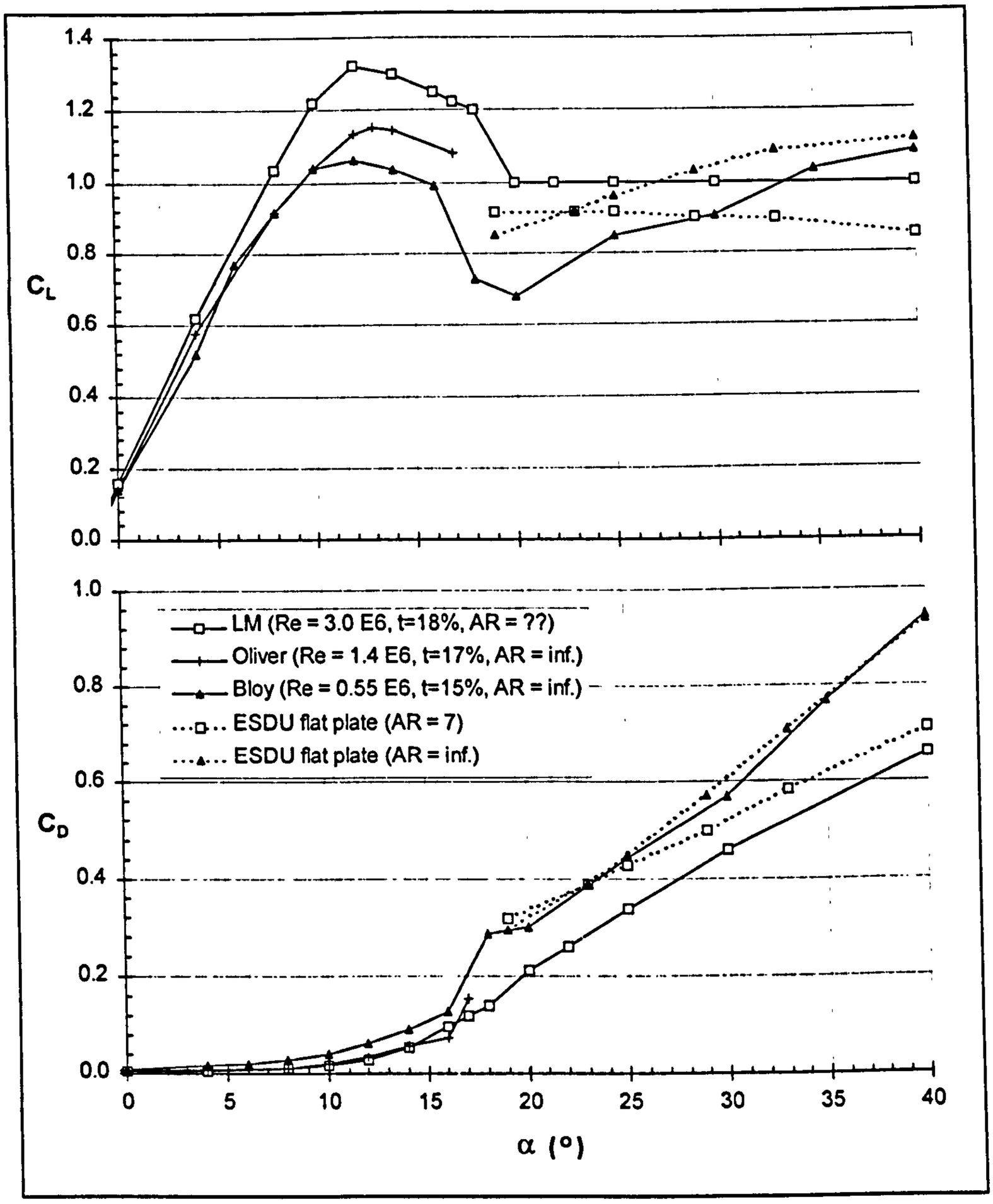

Figure 57 Various references used for the extrapolation of lift and drag

Post-stall, the blade or aerofoil acts like a flat plate and aspect ratio, AR, is the dominant factor. According to ESDU, for a flat plate, C_N does not vary significantly with Reynolds numbers in the range $1.0 * 10^3 < Re. < 3.0 * 10^6$. This is well within the range of Reynolds number for the Ecotecnia 20/150.

The flat plate drag data for Bloy and ESDU are almost identical (both have infinite AR) and thereafter a reducing aspect ratio lowers the drag. The aspect ratio of the blade varies from 7 near the root to 17 at the tip, but the values of drag that LM use would appear to correspond to an aspect ratio much lower than 7.

The lift data at infinite aspect ratio does not show the same consistency between Bloy and ESDU. Lowering the aspect ratio to 7 produces a constant value of lift post stall.

Once again LM's data would appear over optimistic based on the flat plate data. However, when the program is run, their choice of lift and drag seems to be justified in the context of using it with blade element theory. Figure 58 shows output from the program (2D) first with the wind tunnel data extrapolated by the flat plate data, AR = 7 (Case 1). Comparing this with the wind tunnel data extrapolated by LM's data (Case 2) shows that the power output is highly sensitive to lift and, especially drag, at high wind speeds.

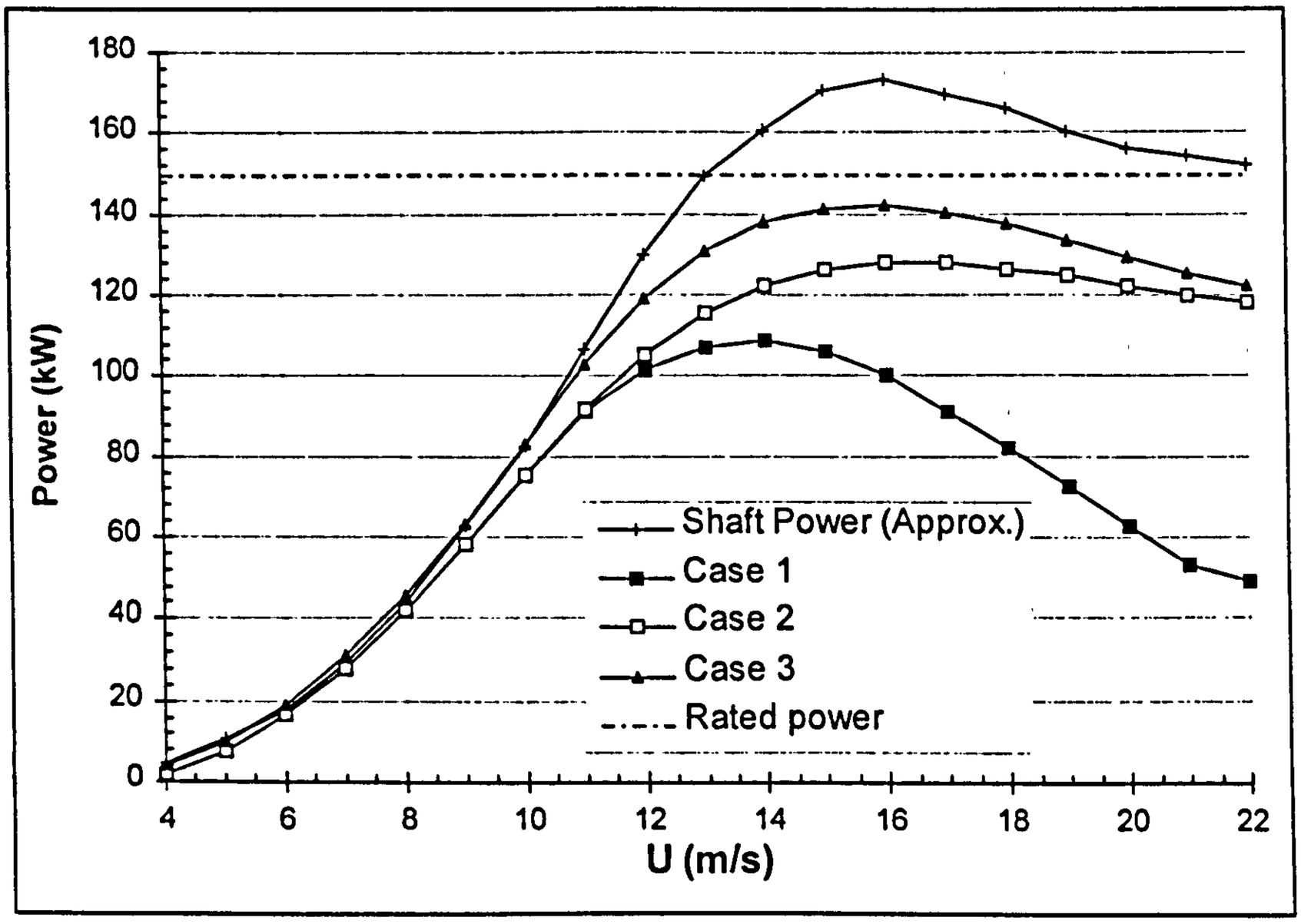

Figure 58 Effects of lift and drag input data on 2D power curve

Pre-stall, Reynolds numbers effects are dominant and this is illustrated by the differing values of C_{Lmax} between Bloy's data (1.06 at 0.55 million), our data (1.19 at 1.4 million) and LM's pre-stall data (1.32 at 3.0 million), taken from Abbott et al, (1959). Although these differences will have been offset slightly by the increasing thickness between these references, as we have already seen.

Case 3 in Figure 58 illustrates how changing the pre-stall characteristics from those obtained in the wind tunnel to those used by LM alters the 2D power output. It illustrates the point that it is C_{Lmax} which dictates peak power. To compare jets 'on' with jets 'off', however, Case 3 cannot be used as the reference power curve because this was not obtained with the unmodified pre-stall lift and drag data.

6.8 Program use in relation to objectives

The power prediction program was written in order that:

1. The air jets could be located at the position of optimum benefit on the blade.
2. An estimate of the expected increase in energy yield could be made.

The program was validated with that used by the blade manufacturer by using their input data and comparing the output. To compare jets 'on' with jets 'off', though, the wind tunnel data must be used. In the previous section it was shown that the program therefore has to rely on:

1. Data obtained at only one blade thickness (17.05%)
2. Data obtained at a Reynolds number lower than full scale (1.4 million as opposed to 1.5 to 1.95 million at rated power where jets must work best)
3. Lower C_{Lmax} due to lower Reynolds number (1.19 as opposed to 1.32)
4. Uncertain post-stall data.

For the program to be of use it must be demonstrated that these factors do not detract from the validity of the results and that the objectives are satisfied.

6.8.1 For the spanwise location of jets

Figure 59 is a plot of blade angle of attack versus blade radius for the critical wind speed range of 10 - 15 m/s (range of wind speed in which jets are required to work best). It shows that the blade angle of attack is virtually independent of whether the input data is LM's (data incorporating all three thicknesses, higher Reynolds number etc.) or the wind tunnel data with the above limitations. In fact the difference between the two is always less than 0.6°. The program can therefore be used with confidence for the spanwise location of the jets as described in section 7.5.

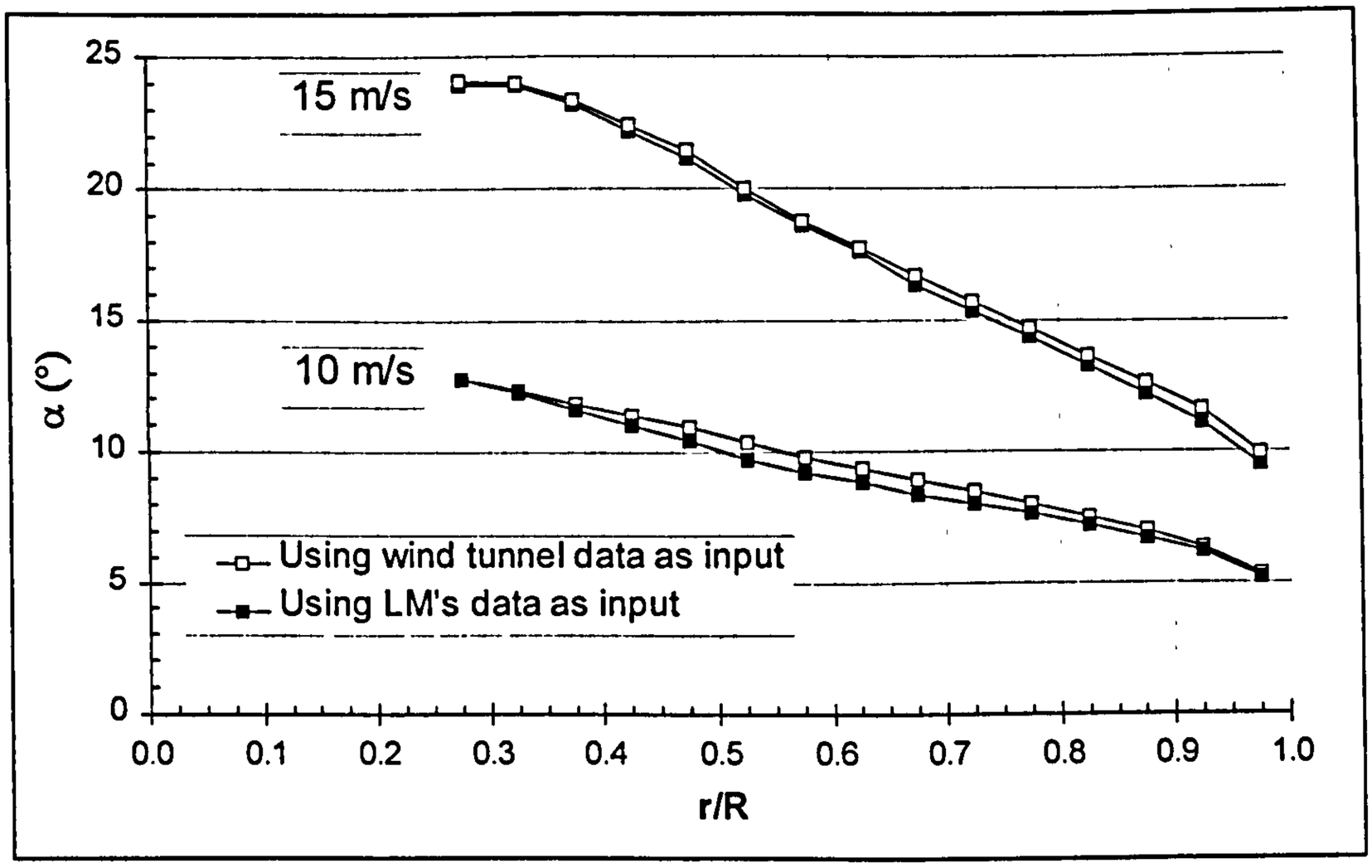

Figure 59 Blade incidence with radius for different input data

6.8.2 For the estimation of increased energy yield

To correctly determine the expected increase in energy yield relies on both the unmodified (no jets) and the modified power curve (with jets) being accurate. As has been shown several factors influence the unmodified curve. Figure 60 shows the 3D prediction obtained by using the wind tunnel data (extrapolated by LM's post stall data) compared with LM's prediction using their input data.

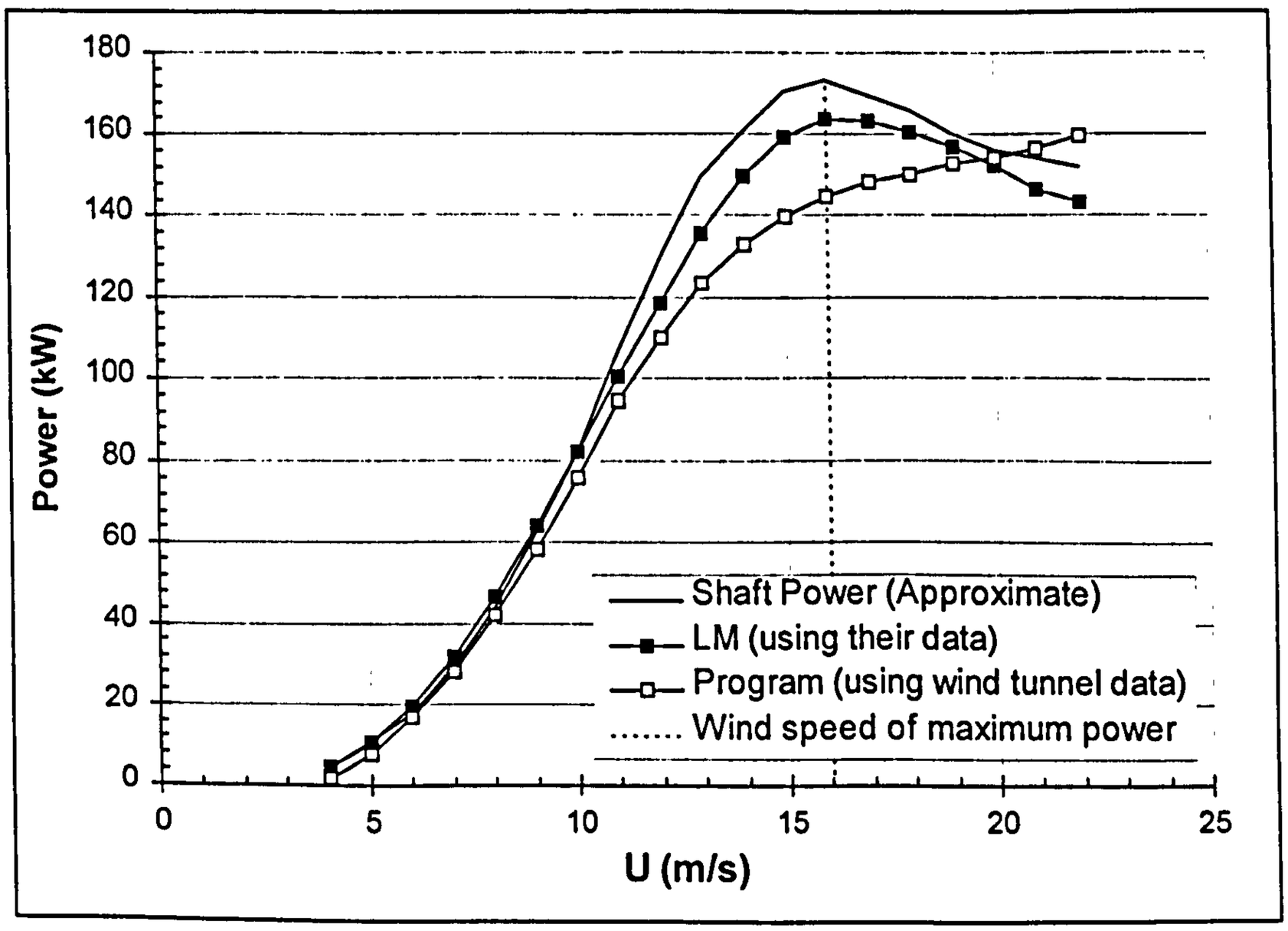

Figure 60 Program 3D prediction using wind tunnel data

The lower peak power of the predicted curve is due to the lower C_{Lmax} of the wind tunnel data. Thus the program cannot be used to determine the expected increase in energy yield because it is not possible to reproduce the unmodified power curve from the measured wind tunnel data.

The high tail of the predicted curve is due to the 3D correction used (section 6.6). It is of less concern because extra energy comes mainly from wind speeds lower than that where maximum power occurs (16m/s). Thus the original and modified power curves could be altered such that they are identical and constant at wind speeds above this. If required the post-stall data could be altered until it was of the correct shape but it is of little point in the context of calculating the increased energy yield due to air jets.

Apart from the inability to reproduce the unmodified power curve it was also considered unrealistic to predict an increase in energy for several other reasons. These being:

1. Unknown how 3D effects would combine with air jets
2. Unknown whether free or fixed transition would be occurring on the unmodified blade and, as we have seen, air jets would cause transition to occur on the modified blade.
3. The estimate would be obtained assuming 'static' power curves when in reality the response of the system (fan) would introduce a time lag.
4. The fan power would have to be taken into account and this would vary according to a table or PID control. (Section 7.9)

Of the above the first point is perhaps the most interesting and important; how do air jets alter the lift curve in three dimensional flow? This question cannot be answered without a full scale trial or perhaps by using CFD techniques. Nevertheless, the best and worst case scenarios can be considered:

1. The 3D correction can be applied direct to the air jet data. That is three dimensional effects enhance further the increased lift due to air jets. However, this is thought unlikely because 3D effects are caused by stall and air jets delay stall. It is modelled by adding an additional line to the program such that the 3D correction is also applied to the air jet data.

2. Delayed stall due to air jets eliminates all benefit due to 3D effects for those blade elements, i.e. the 3D correction is not applied to the blade elements containing air jets. This is modelled by choosing the air jets option in the 3D version of the program.

Summarising, it was thought unwise to try and predict the increase in energy yield due to air jets. However, it seemed to be a good idea to determine the likely range of power curves beforehand and note their characteristics. Then, when the full scale trials had been completed, it would perhaps be possible to at least determine the mechanism by which air jets had combined with 3D effects. This is discussed further in section 7.6.

6.9 Consideration of Dynamic stall

When an aerofoil is pitched rapidly through the angle of attack at which static stall occurs there is a delay in flow separation. The delay is caused by the formation of a vortex which is convected over the upper surface of the aerofoil and the time it takes for the boundary layer to separate under the changing adverse pressure gradient on the upper surface of the aerofoil. The delay in stall increases the lift above the static maximum value. As the vortex is shed, full flow separation occurs. For decreasing angles of attack, flow reattachment is delayed and so a hysteresis effect is set up in the lift curve. The delay in separation and reattachment is dependent on the magnitude of the rate of change of angle of attack. On a wind turbine dynamic stall will therefore occur when both of the following conditions are satisfied:

1. Any part of the blade is operating close to its static stall point. Satisfied at higher wind speeds when angles of attack are large.
2. The wind 'seen' by the blade is of a fluctuating nature. Satisfied by a sudden gust, the blade passing in and out of the tower shadow or yaw mis-alignment.

The overall effect of dynamic stall is to cause fluctuations about rated power on a short time-scale and reduce the fatigue life of the blades. It is still not fully described by current computational methods. However, its effect is not important in the context of comparing 10 minute averages of power, as was done in the full scale trials, because the effect takes place over a much shorter time scale and is therefore 'averaged out'.

7. FULL SCALE DESIGN ISSUES

7.1 Powered or un-powered air jets?

Initially it was thought that the 'centrifugal' pressure gradient inside the rotating blades would be able to supply enough pressure to power the air jets. Calculation of this (Appendix 5) shows that even at the furthest spanwise location this was not nearly enough at only 1360 Pa (0.20 p.s.i.) and so the jets would need to be powered by a fan. The three main options considered were:

1. A small fan mounted in the root of each of the three blades.
2. A single fan mounted in the nacelle supplying air through a pipe in the rotor drive shaft. This would then be connected via a pneumatic slip ring to the rotor whereupon the pipe is split 3 ways to each blade.
3. To have a single fan mounted on, and rotating with, the rotor followed by a three way split to each blade.

The first option was discounted because the available space inside the root of the 9.7m blade was insufficient to house the required fan. However, this option could be considered for larger blades in use on 500 kW machines and above.

The second option looked promising but was eventually dropped because the pipe diameter from the nacelle through the rotor drive shaft would have lead to large head losses. Again this is a possibility for larger machines.

This left the third option, which as a demonstration of the technology was considered acceptable. Clearly this would not be a viable solution for series production but as will be demonstrated in Chapter 10, it does not have to be.

7.2 Fan rated power.

The central objective of the project was to increase the wind turbine's energy yield and so it was essential that the power rating of the fan was low with respect to the wind turbine rated power. However, balancing this was the fact that the project was a demonstration of air jet technology. From the discussion of the wind tunnel results, it is clear that air jets are probably not yet optimised and so it was felt that the rated power of the fan should not be too restrictive.

The wind turbine rated power was 150 kW and the maximum increase in the region of the power curve 'knee' was expected to be about 20 kW. It was felt that a fan power, including frequency inverter, of 5 kW was a sensible target figure for demonstration purposes.

The reader is reminded that in the final application of the technology air jets will only be operating when there is a net power gain. Optimisation of the air jets will lead to a lower required fan power, by reduction of the mass flow and blowing pressure. For example if the air jet spacing could be increased without adversely affecting performance, then the mass flow requirement would be reduced. Indeed ajvg results obtained after the full scale trials show that complete elimination of the fan should be possible by using passive blowing pressures (Chapter10).

7.3 How many air jets can the fan supply?

It will be remembered that the lift and drag characteristics were given by the second configuration because this represented the correct scale. However, it was the first air jet configuration that gave us the correct mass flow because the jets at full scale were to be the same size as this (section 5.4). Pipe friction losses (Appendix 6) and fan power requirement (Appendix 7) were therefore calculated using mass flows of $3.8 * 10^{-3}$ and $4.8 * 10^{-3}$ kg/s/jet for the 1 and 2 p.s.i. blowing pressures respectively.

The reason for calculating fan power was to determine the number of jets, and hence array length, that could be supplied for the target fan power of 5 kW. It was calculated that with a blowing pressure of 2 p.s.i. only a 1 metre array length could be supplied (17 air jets per blade), whereas the 1 p.s.i. blowing pressure could supply 2 metres (34 air jets per blade). Both of these had a power requirement of approximately 4.3 kW.

By using the aerodynamic characteristics of the first configuration in the power prediction program (the second configuration had not then been tested) it was determined that a 2 metre array of the 1 p.s.i. jets would be more effective than a 1 metre array of the 2 p.s.i. jets. It was therefore decided to disregard the 2 p.s.i. air jet option (even though the L/D curve is much better) and this is the reason why the blowing pressures were reduced for the testing of the second configuration.

Other reasons for discarding the higher blowing pressure were that a 1 metre array of jets (10% blade coverage) would not be effective over the same range of wind speed (blade angle of attack) as a 2 metre array (20% blade coverage). Also the radial location of the 1 metre array would be much more critical with respect to improving the power curve in the required wind speed range just prior to rated.

7.3.1 Pipe friction losses with respect to array length supplied.

Air was to be conveyed from the turbine hub to the air jets on the blade through a pipe in the forward cell of the blade (Chapter 8). The internal dimensions of this cell would allow for a maximum pipe diameter of only 58mm. It was not possible to put pipes in any other cells of the blade because its structural integrity would have been compromised.

The pipe losses due to friction were therefore essential to the calculation of the number of air jets that could be supplied. For the chosen design these losses were calculated to be 2.1 kPa or approximately 30% of the blowing pressure required. (Appendix 6).

To put these losses into perspective it was calculated that if the pipe diameter could be increased by 50% from 60mm. to 90mm., then 30% more jets could have been installed for the same power requirement, increasing the blade coverage from 20% to 26%. On a larger wind turbine, friction losses would not be as critical.

7.4 Selection of fan

Correspondence with different fan manufacturers revealed a surprising variety in the dimensions of fans which could supply the required pressure and volume flow, with the largest being almost double the size of the fan selected. The calculated fan requirements (Appendix 7) and those of the selected fan are given in the table below.

It is to be noted here that although the author did gather data and quotes from various fan manufacturers, the final choice was made by Ecotecnia.

Specification	Calculated	Selected
Rated Power	4.3 kW	5.3 kW
Volumetric flow	0.31 m^3/s (based on $\rho = 1.23kg/m^3$)	0.30 m^3/s
Pressure rise across fan	8.5 kPa (Appendix 7)	9.75 kPa
Dimensions	Minimal	0.5m. diameter

Table 5 Fan requirements: Calculated and selected.

Choosing the fan manufacturer's next specification down, rated at 4.0 kW, would have met the pressure criterion at the required volume flow, but only just. Thus the calculated fan power is close considering the fact that an arbitrary efficiency of 65% was used (Appendix 7). As the pressure losses did not include calculation of those due to the three-way split connection, the conservative choice was made.

To enable the air jet performance to be altered it was necessary that the fan delivery pressure and volume flow could be controlled. To do this a frequency inverter was selected which had a nominal power rating of 5.5 kW or 10% more than the original target figure of 5kW. Further details are given in section 7.9

7.5 Determining the location of the 2 metre air jet array

The next logical step was to determine the best spanwise location for this 2 metre array. This was achieved using a technique originally employed by Ecotecnia. However the data used was taken from the power prediction program described in Chapter 6.

From the power prediction program an output of the variation of incidence, α with wind speed could be obtained for each of the 20 elemental spanwise sections of blade. These quantities are plotted in Figure 61. From the lift curve, Figure 38 we can see that the air jets are most effective in the region of $12° < \alpha < 18°$. From the power curve of the Ecotecnia 150 kW wind turbine jets would be most desirable in the wind speed range of $12m/s < U < 15m/s$. These two ranges are highlighted by a grid on the figure. It can be seen that the 2 metre range of radius $0.575 < r/R < 0.725$ runs directly through the centre of this grid. Thus it was decided to locate the air jets between 0.55r/R and 0.75r/R. (The lines in the figure are the mid-spans of the 0.5m. blade elements).

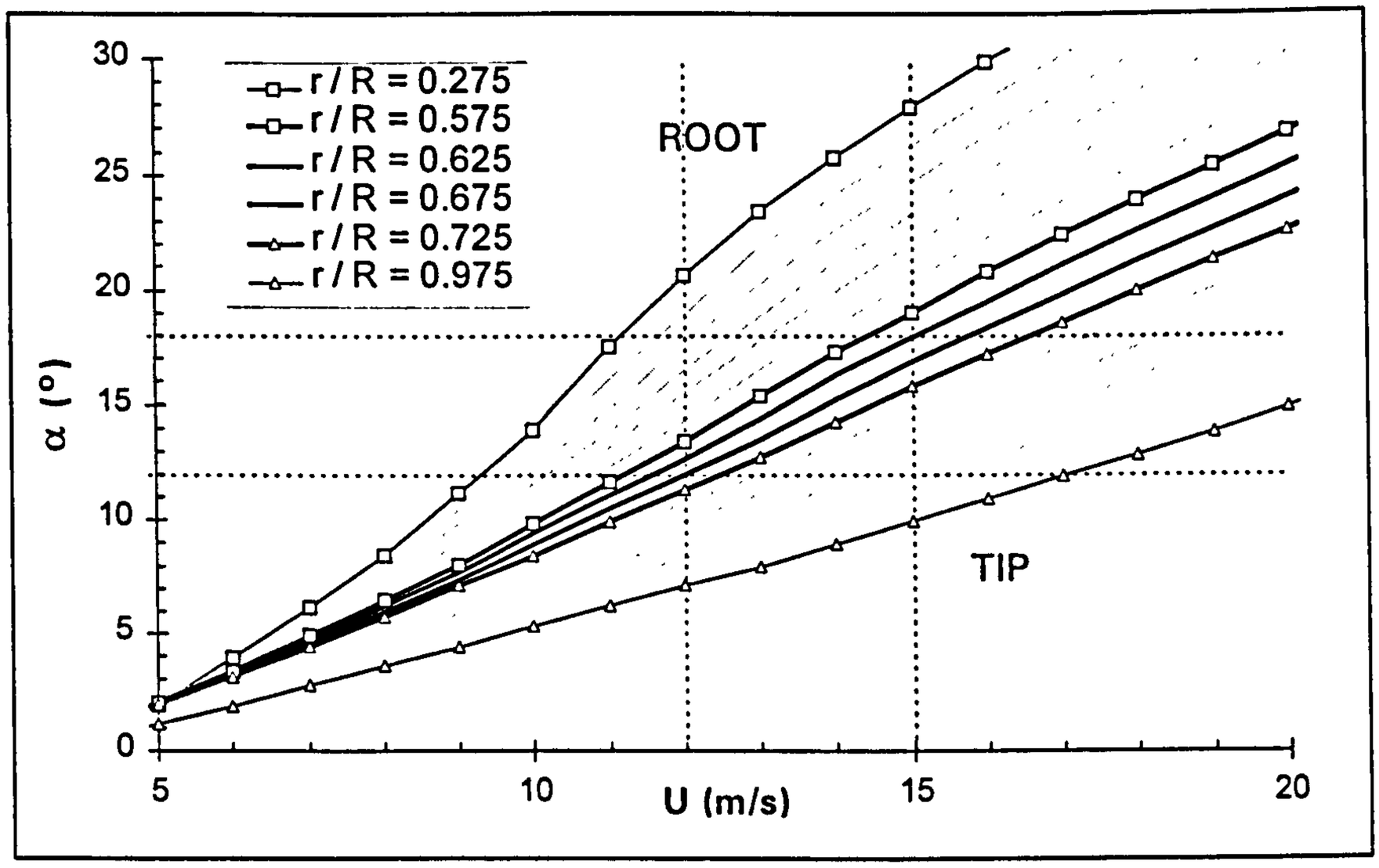

Figure 61 Incidence versus wind speed at different spanwise blade radii.

7.6 Expected power and increase in energy yield.

As described in section 6.8.2 it was considered unwise to try to predict the likely increase in energy yield due to air jets (The energy increase was subjective even after the full scale measurements were to hand as will be seen in section 9.7). However, it was thought appropriate to try and anticipate the likely effect of the air jets on the power curve. After the full scale trials, this would give a clearer picture of how air jets had combined with three dimensional effects.

Reiterating section 6.8.2, two methods were used to combine the air jets with 3D effects. These were expected to represent the extreme cases and were:

1. That the 3D correction could be applied direct to the air jet data, i.e. 3D effects further enhance the increased lift due to air jets.
2. Delayed stall due to air jets eliminates all benefit due to 3D effects for those blade elements.

It can be seen in Figure 62 that if the first option occurs the power curve is predicted to keep rising. It has been stated previously that this was considered unlikely because 3D effects are caused by separated flow and air jets delay stall. However, it is interesting to note that the gradient of the power curves is approximately the same for both options prior to rated power. The energy yield increase would therefore be expected to be similar for both options once regulation is considered.

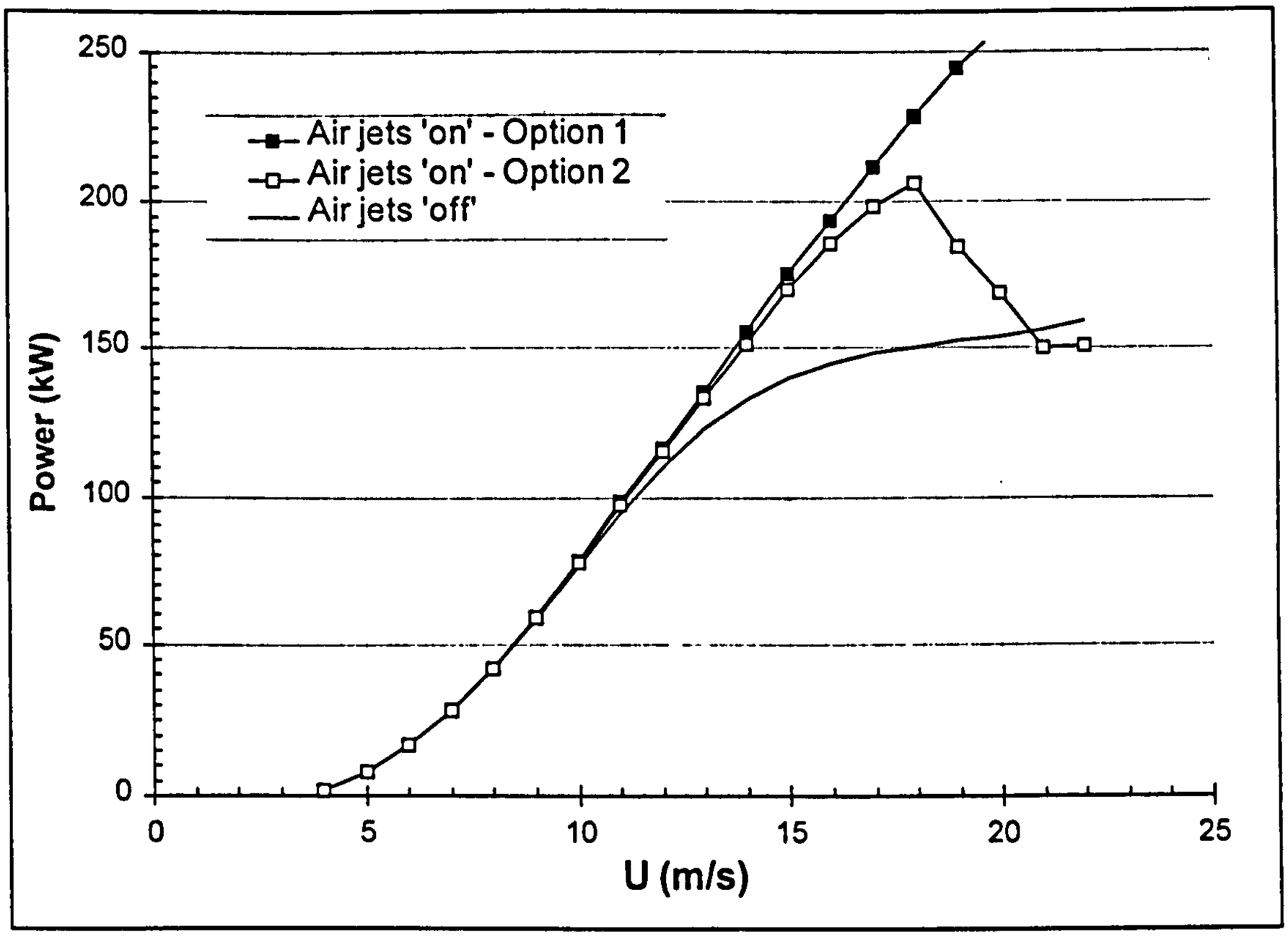

Figure 62 Predicted range of effect of air jets on (shaft) power curve

If the second option occurs then the power curve is expected to reach a maximum at about 18m/s. It is predicted that the jets will no longer have an affect above a wind speed of about 21m/s. The reason for the modified curve then falling below the unmodified one is due to the fact that no 3D correction has been applied to the part of the blade containing air jets (55% to 75%). At this location though, the 3D effects are diminishing. Should jets be placed near the blade root caution may therefore need to be exercised if air jets are found to reduce or eliminate the 3D effect. In such a scenario the jets at a given radius would have to be turned off once the upper wind speed limit for effectiveness has been reached. The question that must be answered is; how do air jets behave in deep stall?

Transition fixing has also been discussed previously (section 4.2). Two extreme cases can be considered for the behaviour of the flow over the unmodified blade:

1. The whole blade operates with free transition at all wind speeds.
2. The whole blade operates with transition fixed at all wind speeds.

Since air jets appear to trigger transition when they are present, the worst case will be the first option above, since the parts of the blade with air jets installed will be experiencing a higher minimum drag. The second option does not present a problem because the drag with jets 'on' is virtually identical to the unmodified aerofoil with transition fixed (Figure 43: 2nd config.,1 p.s.i. - Design case).

The power curve was therefore calculated for the first option above to check that it would not be adversely affected at low wind speeds by the installation of air jets. Figure 63 shows that the effect on the power curve is minimal, with a maximum reduction of less than 0.5kW at U = 7m/s. In practice it would not be possible to measure such a small difference. In any case transition is far more likely to occur because the blades are operating in the earth's boundary layer. The effect of transition is not therefore considered to be particularly relevant to this study. It may become an important feature if jets are to be installed along the whole blade or if a modified turbine is operated in sites of lower average wind speed.

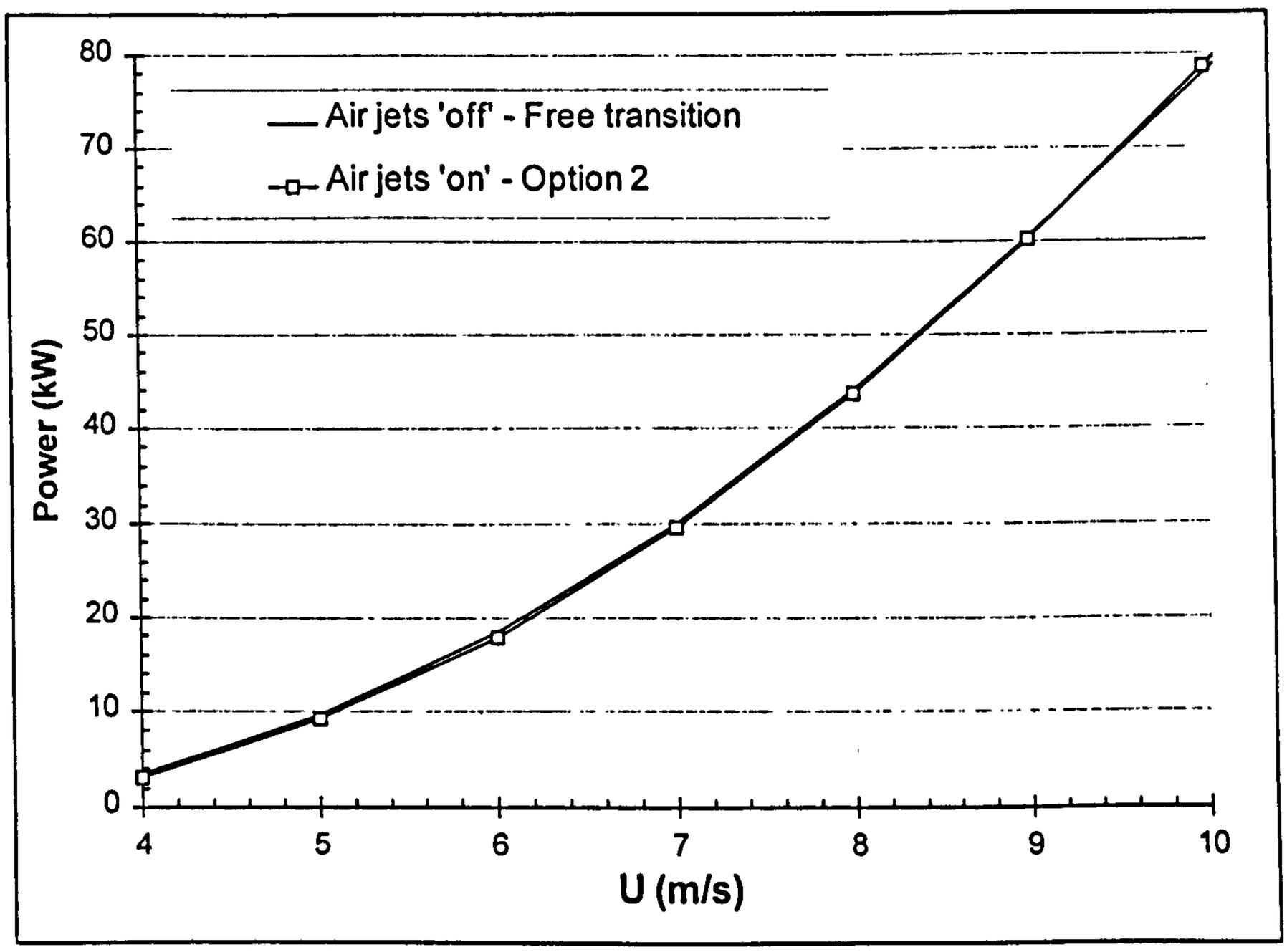

Figure 63 Possible effect on power curve due to transition caused by jets

7.7 Inward or outward facing jets.

It was not known whether the air jets should be skewed towards the root or the tip, or if this particular consideration was irrelevant. In the end it was decided to skew the jets in the direction of the tip as this is the direction of the natural outflow due to three dimensional effects.

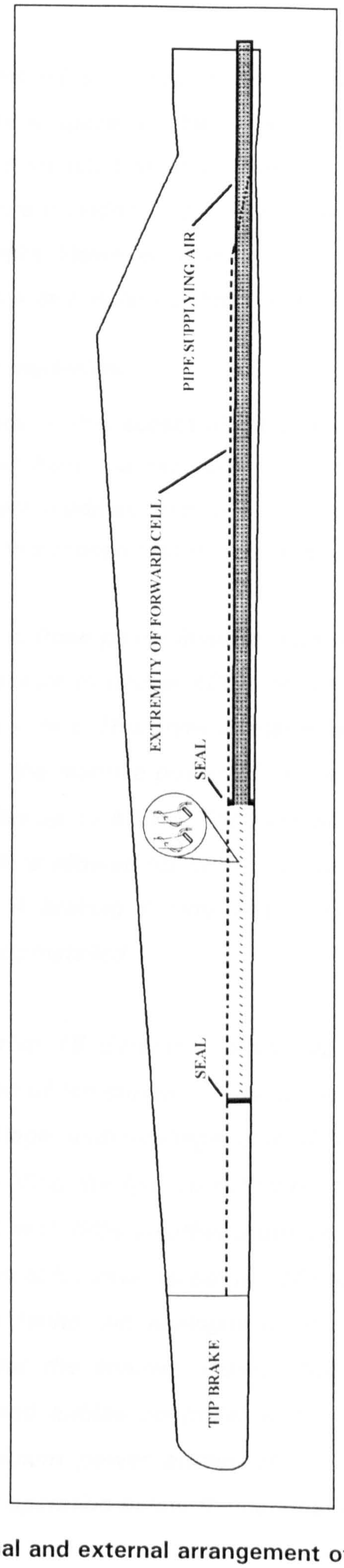

Figure 64 Internal and external arrangement of the modified blade

7.8 Internal blade design

Figure 64 illustrates the internal and external arrangement on the modified blade. Due to lack of internal blade space, no baffle plates were used to disperse the pressure as per wind tunnel model. Two seals, one around the pipe and one at the end of the air jet array were included to prevent air leakage because the internal blade structure is not air-tight. However, a small hole was made at the end of the array nearest the tip to allow any moisture that accumulated to drain.

7.9 Fan control for power regulation.

NB. The author did not work on this aspect of the project but it is included so that the reader may understand how the fan was to control the air jets for power regulation. It is abridged and modified from a section written by Ecotecnia (Prats and Oliver, 1996). It is for this reason that the section has been printed in italics.

In order to control the fan, a three phase inverter with a nominal power of 5.5 kW was selected. Its output is able to deliver 400V between phases and a maximum continuous current of 13.5 A rms. This gives a total inverter capacity of 10.3 kVA, which is enough to supply the reactive power of the fan at its nominal power and extra power to drive the fan up to 55 Hz. The overload capacity of 150% of the rated output current (which is allowed for up to 1 minute), enables start up of the fan in about 2 seconds. A braking facility was provided for by means of an external resistor but was not installed.

The inverter is able to drive 16 different voltage vs. frequency characteristics which enables the reduction of fan current consumption at partial power. Standard thermal, overload, over-voltage, under-voltage, ground fault and fuse protection are included in the inverter, fulfilling the fan protection requirements. The inverter was mounted in a steel cabinet with IP54 weather protection in the base of the tower. Input and output circuitry enables external control of the inverter output frequency and the ability to monitor faults. An analogue communication link between the wind turbine controller and the inverter allowed the output frequency of the inverter to be set. The wind turbine controller was provided with a PID loop in order to control the maximum power output of the wind turbine and a table controller for partial power operation below the nominal wind turbine power.

It was foreseen that the fan would not be activated until the wind turbine power reached a certain level (beginning of the stall). After this point the table controller would set the inverter output directly as function of the wind turbine output. When nominal power is reached power is controlled by means of the PID control loop acting on the fan frequency. When the wind speed reaches an upper limit the fan is turned off again, because of the limitation that the air jets cannot keep the flow attached when the wind speed becomes very high. Figure 65 and Table 6 show how the fan is controlled.

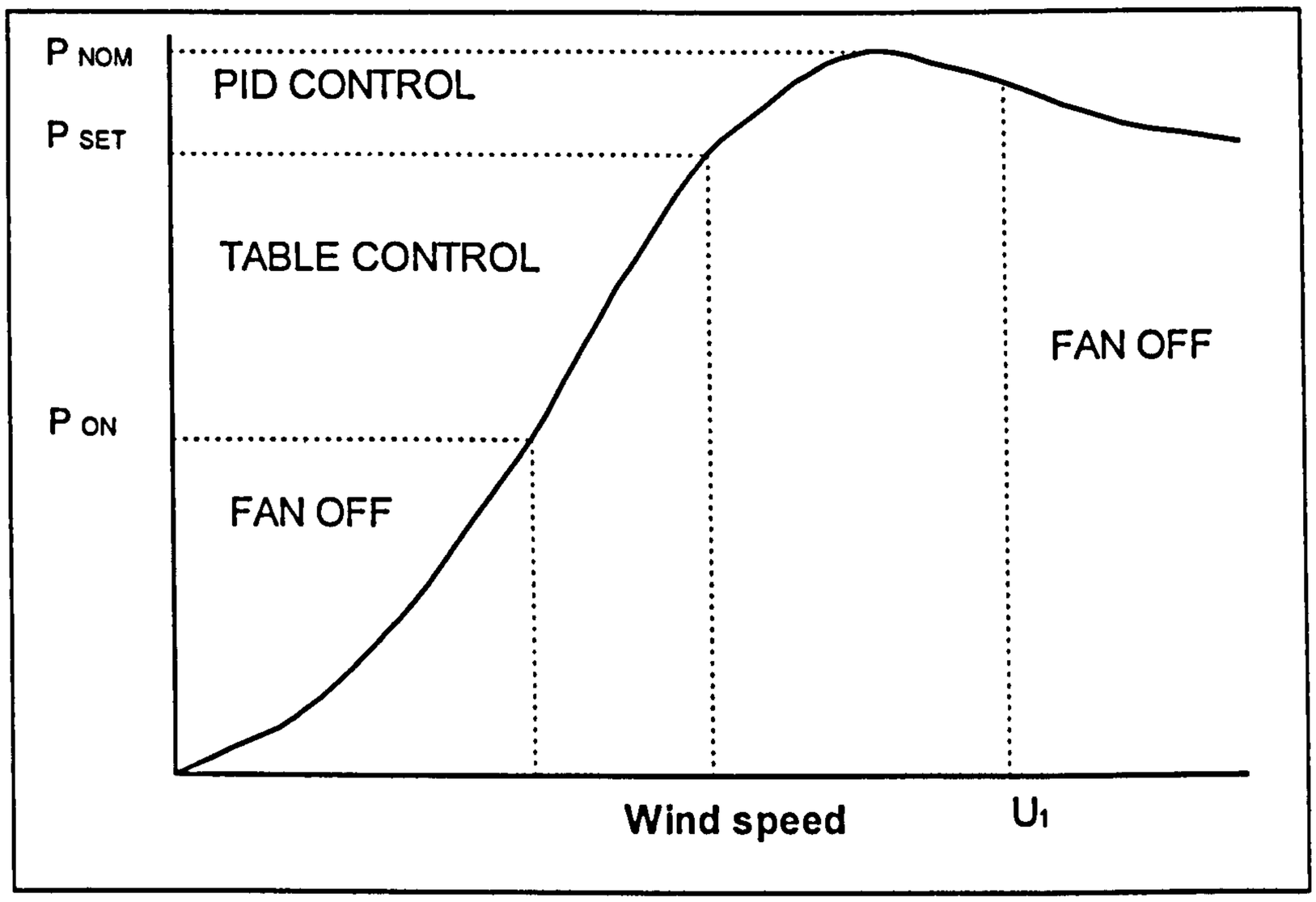

Figure 65 Illustration of the fans control status

Range limits	Mode of operation
Average power smaller than P_{on}	Normal operation, fan is off
Average power bigger than P_{on} and short time average power less than P_{set}	Control of the power by means of a table of frequency output versus short time power average.
Short time average power bigger than P_{set} and short time averaged wind lower than U_1	Dynamic control of the frequency output, PID control of the power close to nominal power, taking into account that higher frequencies produce more power
Short time averaged wind speed greater than U_1	Normal operation, fan is off

Table 6 Control of the fan

8. MODIFICATION OF THE BLADE SET AND FULL SCALE EQUIPMENT

This chapter describes the manufacture and general set up of the experimental equipment used in the field tests. As such the author has had little direct involvement in the material presented in this chapter but the words are his own. The inclusion of this Chapter is to aid the reader in their understanding of that which was tested.

The arrangement is described 'backwards' in a sense that it commences at the jet exits and finishes with the fan and its control.

8.1 Manufacture of air jet inserts.

The air jet array was made up of a series of isolated air jets similar to those used on the wind tunnel model and were designed by the author. A batch of 200 air jet inserts was manufactured using the mould injection method, having first made an original machined aluminium mould. The material used was glass reinforced epoxy resin which does not require an expensive mould and has very good mechanical and bonding properties, although it does take a while for the epoxy polymerisation process to complete.

8.2 Mounting of the air jet inserts on the blade

The inserts were mounted on the blade by Ecotecnia at their facilities near Barcelona. A special tool was manufactured to drill the blade surface. This was made of abrasion resistive material able to machine the glass re-enforced blade skin without wearing.

The inserts differed in design to the wind tunnel inserts (Figure 23) in that they had a rim around them. This allowed the location of all the inserts at precisely the same depth in the blade surface. The moulded inserts were made from a different coloured resin to that of the blade in order to facilitate smoothing and polishing of the blade surface.

As explained previously, the jet exits were pointed in the direction of the tip rather than the root because this is the direction of the natural outflow.

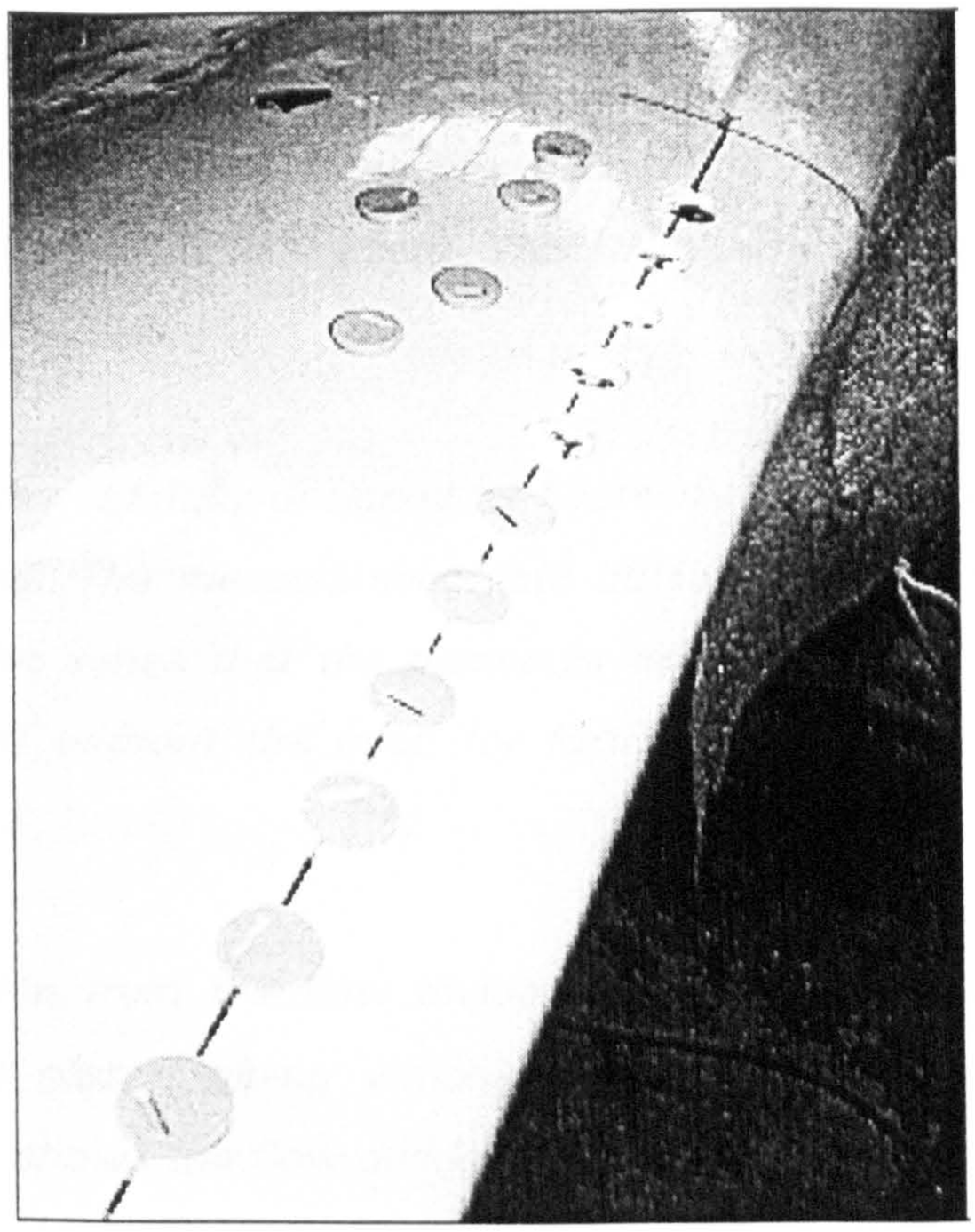

Figure 66 Air jet inserts dropped into the machined holes prior to alignment

8.3 Modification to blade set.

Each blade had one 58mm diameter pipe placed in its forward cell during the manufacturing stage before the two halves were glued together. A hole had to be cut through the conical core of the blade root to enable the pipe to pass into the forward cell (X). LM Glasfiber, the blade manufacturer, were happy that this did not compromise its structural integrity.

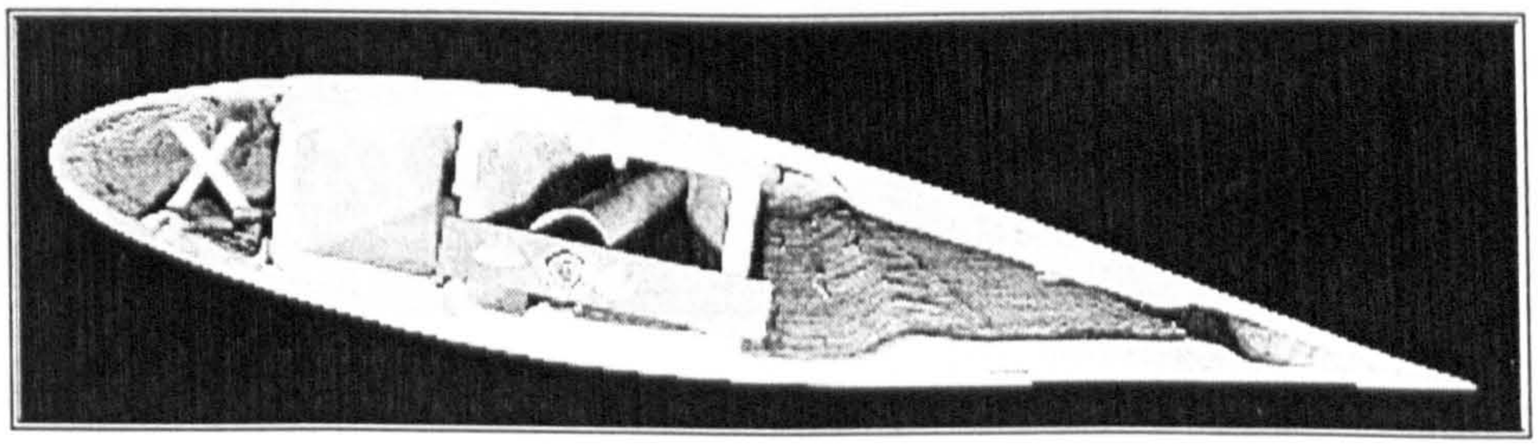

Figure 67 Blade section showing location of pipe marked 'X'

At both ends of the air jet array, seals were put in place to ensure that air could only escape through the jet exits. The reader is referred back to Figure 64, which shows the internal blade construction.

8.4 Piping between the blade pipes and the fan outlet

The pipes extending from the three blade roots are then connected by a flow divider placed in the centre of the hub. This is in turn connected to the fan by a single larger diameter pipe.

The flow divider was carefully designed by Ecotecnia to ensure equal division of air to the three blades. The measurement data obtained during the test phase was very positive in the sense that the pressures achieved in the three blades were very well balanced without the need for further trimming. This is discussed in detail in section 8.8.

The inter-connection from the flow divider to the blades was made from spiral reinforced flexible plastic piping which facilitated the mounting of the whole system. Figure 68 shows the flow divider and the flexible piping to the blades.

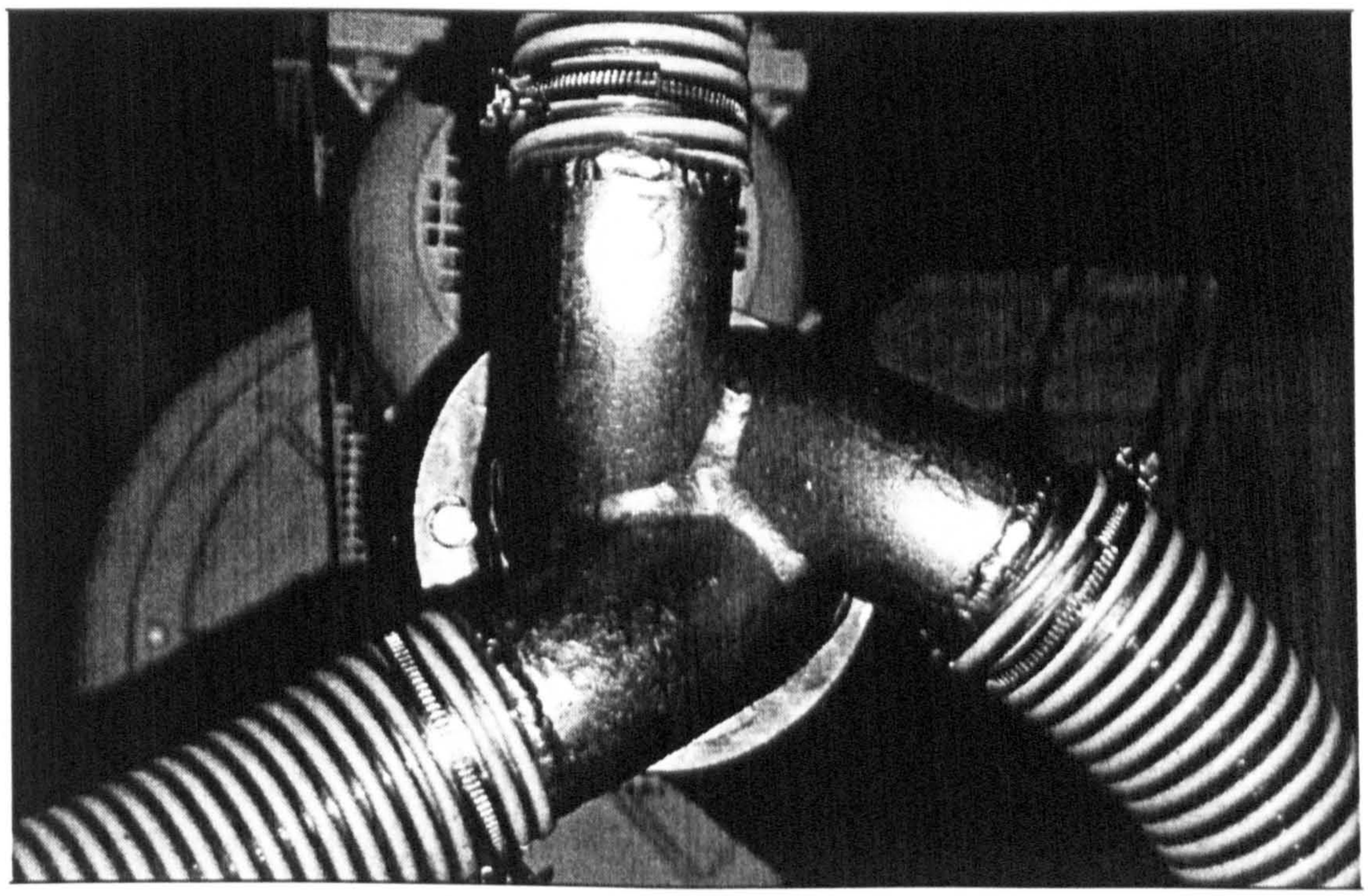

Figure 68 Flow divider and flexible piping to the blades (fan in background)

8.5 Fan mounting

The wind turbine spinner was removed and the fan was mounted in its place at the centre of the hub. After consultation with the fan manufacturer, it was decided to mount the fan rotor concentrically and parallel with the axis of the wind turbine. This was done in order to avoid extreme gyroscopic loading on the fan rotor bearings and was not foreseen in the design stage.

This layout had the drawback of requiring more piping than originally envisaged and two acute angled pipe bends in order for the air supply to reach the centre of the hub. This undoubtedly increased the pressure losses.

The fan was mounted on a specially designed steel frame which was in turn attached to the wind turbine at two points. These were the centre of the hub and to one of the blade flanges. The fans structure was also reinforced in order to survive the permanent cyclic loading due to the wind turbine rotating continuously at 51 rpm. Figure 69 shows the fan-hub arrangement.

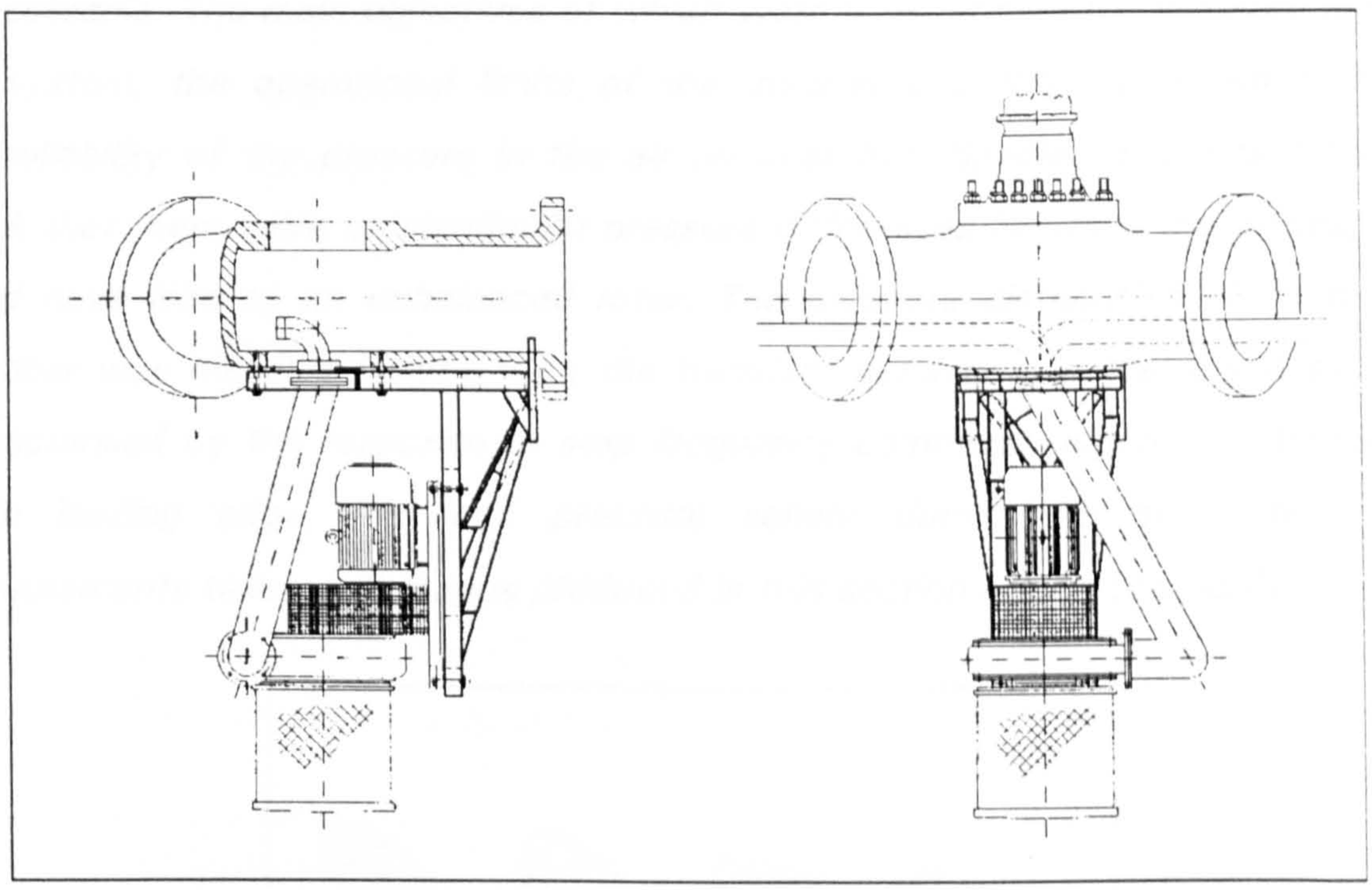

Figure 69 Fan-hub assembly

The fan was delivered with an induction motor and had a filter to avoid dirt contamination of the fan rotor.

8.6 Power supply to the fan

Power to the rotating fan was supplied through a 28mm. bore hole in the main shaft which already existed for the hydraulic supply of the tip brakes (12mm. diameter pipe). Sufficient space remained in the bore hole through which power could be supplied to the fan. The position and size of all the cables was studied by Ecotecnia to enable the fan to be driven at its maximum power. The need for a slip-ring to supply energy to the fan installed on the hub was also foreseen and catered for. The slip-ring system has 4 high current rings and 6 low current rings for possible sensors.

8.7 Power supply to the nacelle

Specific wiring was installed in order to connect the output from the inverter, placed at the tower base, to the slip-ring. This was divided into power and signal wiring in order to avoid electrical interference. The inverter output wiring also had to be distanced from wind turbine control wiring because of interference with rotor speed measurement.

8.8 Static tests

Before mounting of the test equipment, static tests were carried out in a workshop by Ecotecnia. The main objectives of which were to determine the pressure loss of the system, the operational limits of the inverter and fan subsystem and the controllability of the pressure in the air jet chamber. Special care was taken to check that there were no significant pressure differences between the blades, that could have lead to an unbalanced rotor. The pressure distribution along the jet chamber was measured along with the transient behaviour of the whole system, characterised by the response to step frequency command. Figure 70 shows the blade leading edge, jets and pressure sensor during the static tests. All measurements taken and graphs produced in this section are by Ecotecnia.

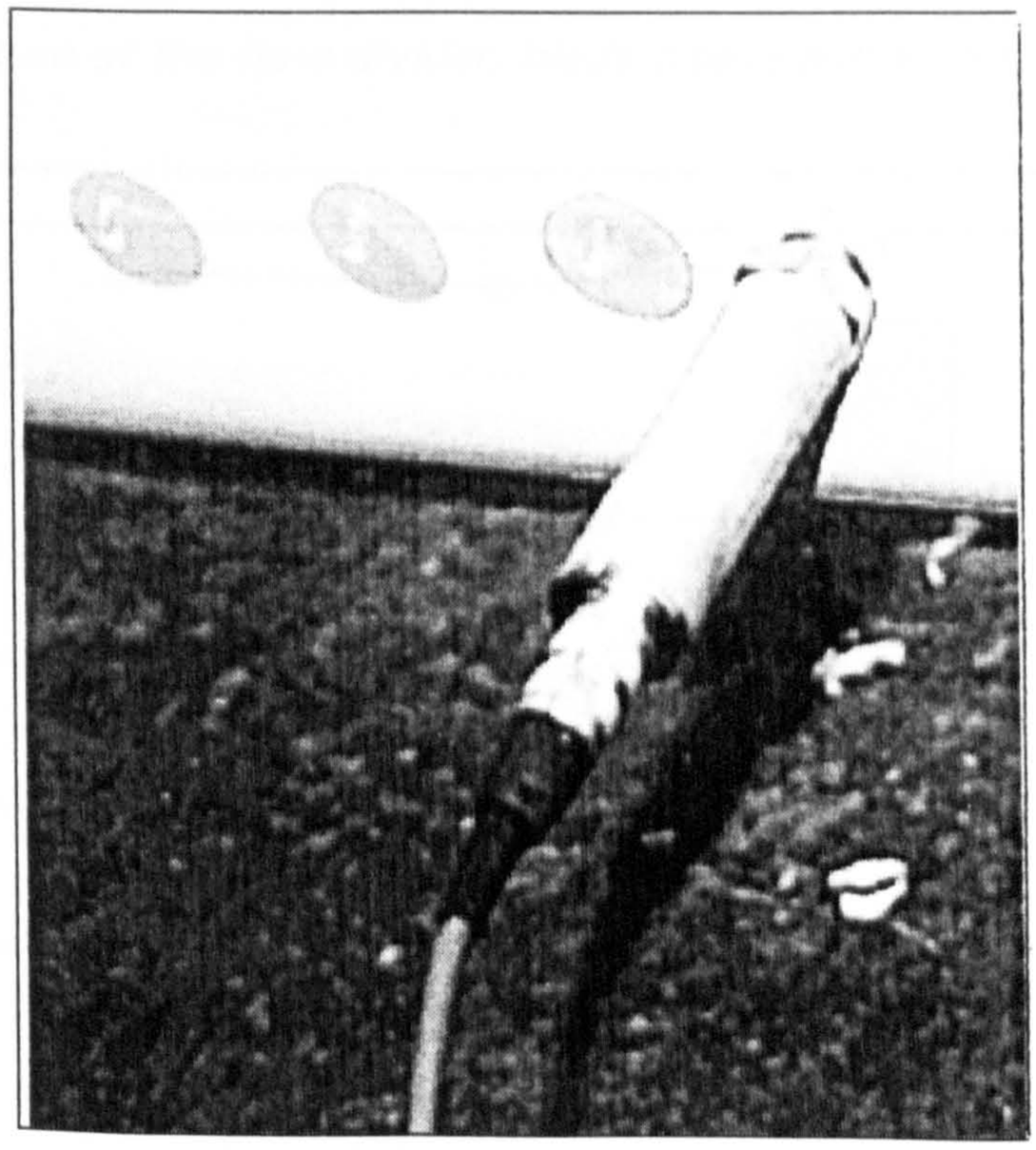

Figure 70 **Blade leading edge, jets and pressure sensor during the tests**

8.8.1 Overall pressure loss in system

The pressure rise across the fan was measured at 9.7 kPa and so from the manufacturers data the available volume flow at 50 Hz should be close to the required 0.3m^3/s (18m^3/min).

The measured pressure drop in the system (fan exit to pressure behind jet) was significantly higher at 3.3 kPa than the calculated value of 2.1kPa. This is due to the introduction of the additional pipe elbows caused by the changes in fan position and the fact that the flow divider was not included in the calculation. However, because a conservative choice of fan was made the actual pressure obtained was only 0.5 kPa lower at 6.4kPa than the design requirement of 6.9 kPa (1.0 p.s.i.). With the blades rotating the increase in pressure due to centrifugal compression is calculated to be 0.54 kPa (Appendix 5) and so the pressure behind the jets in operation should be very nearly exact.

8.8.2 Pressure difference between blades

The maximum pressure difference between the blades was measured in the centre of the array (jet 18 out of 34) and is shown in Figure 71. This was found to be very small, at only 1.2% and will not cause significant differences in aerodynamic performance between blades. This can be attributed to the careful design and accurate manufacture of the flow divider, blade piping and air jet inserts.

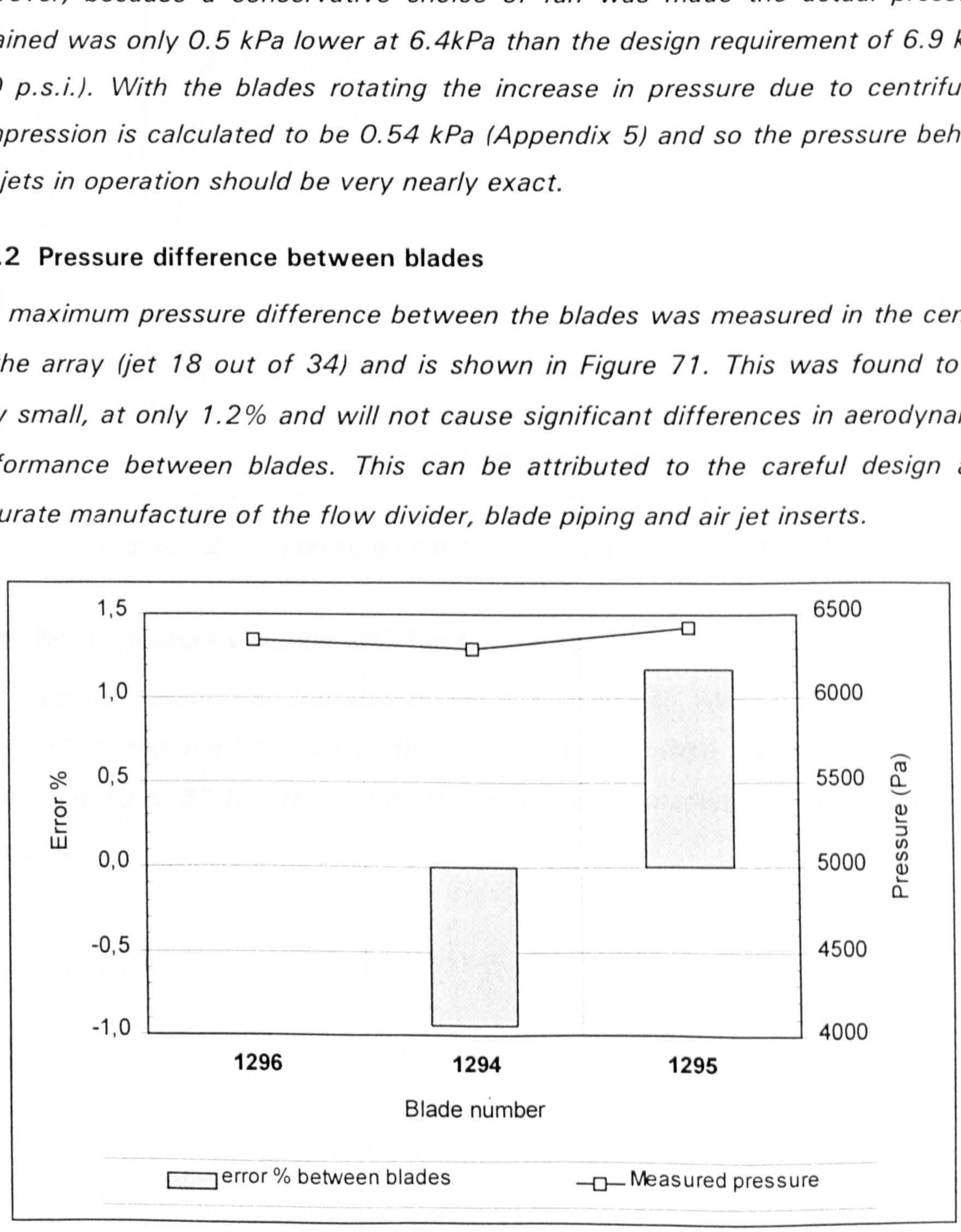

Figure 71 Pressure comparison between blades (jet 18)

8.8.3 Pressure distribution along each blade

Figure 72 shows the pressure distribution along one of the blades and is typical of all three. It is virtually constant, with the exception of the first four jets where the influence of the section change from pipe to the chamber produces a sharp pressure gradient. It can be concluded from this result that it was perhaps over zealous to include a baffle plate in the wind tunnel model.

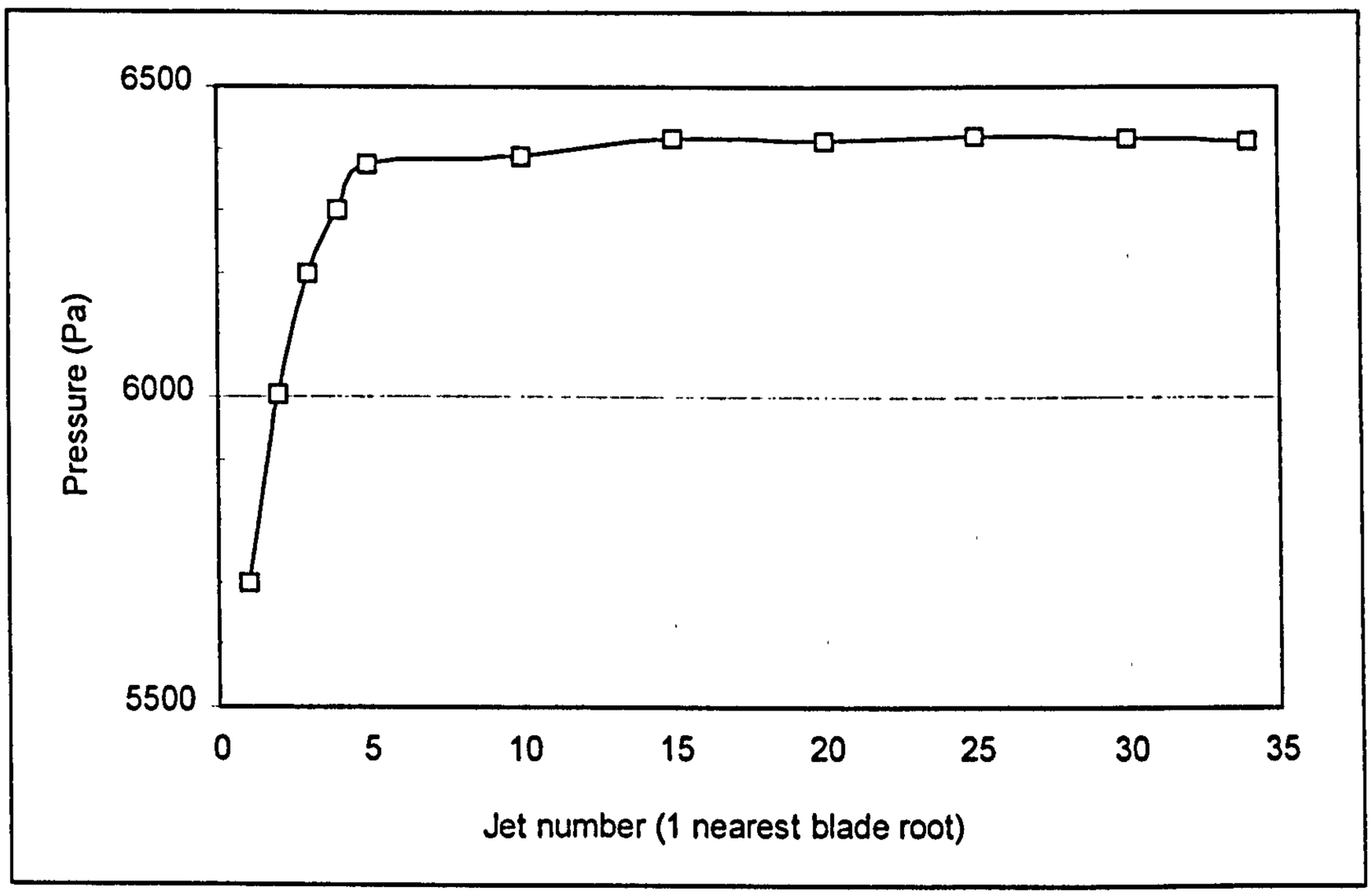

Figure 72 Pressure distribution along the blade at 50Hz

8.8.4 Blade pressure variation with fan frequency

The pressure variation as function of the fan frequency was also measured and Figure 73 shows the pressure at the fan outlet and inside the chamber, for the range from 10 to 50 Hz. The fan motor current consumption is also shown in the same plot.

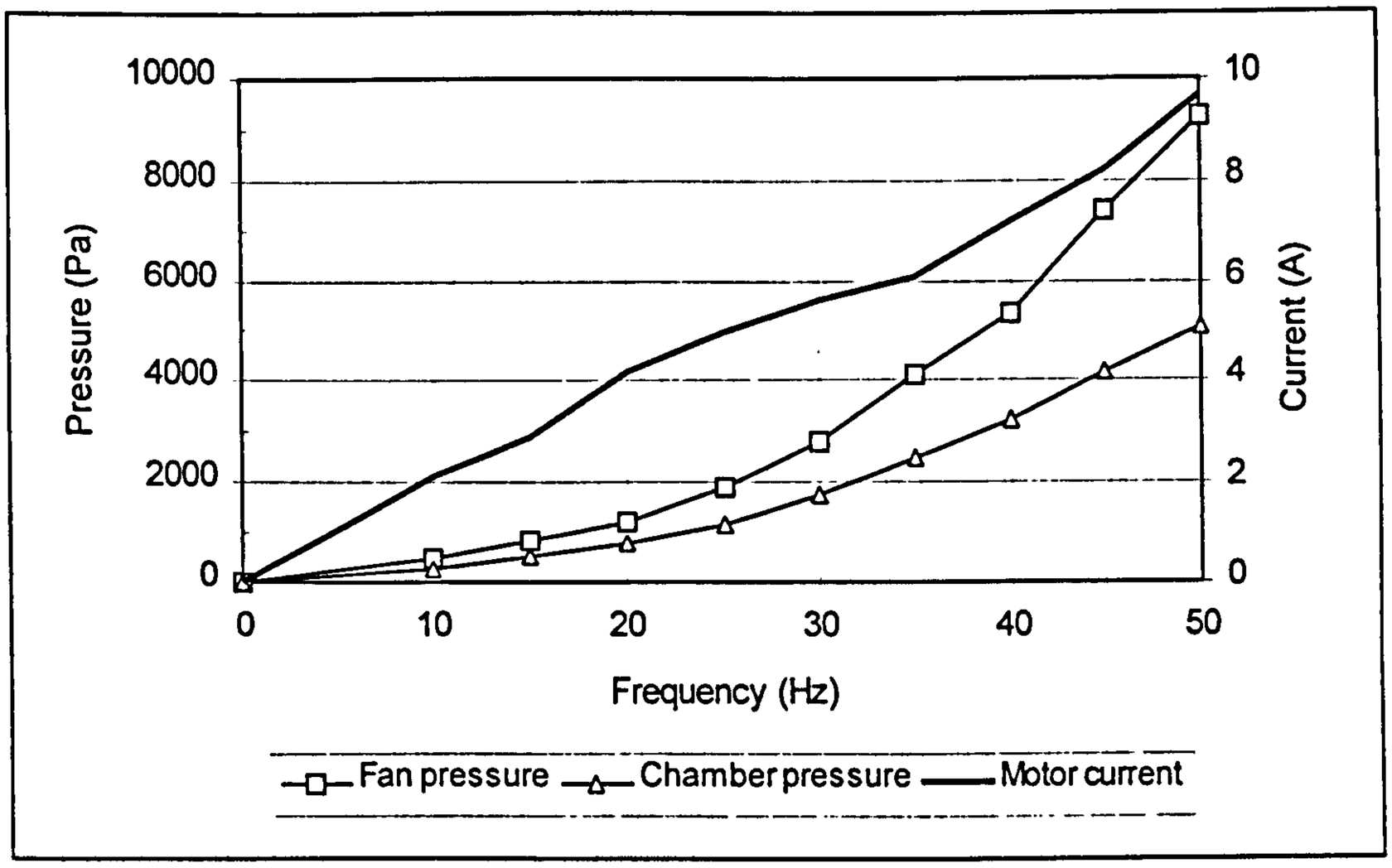

Figure 73 Chamber pressure (jet 1) & motor current versus fan frequency

8.8.5 Time taken for blade to pressurise after step input to fan.

In order to measure the speed of actuation, transient plots were recorded, corresponding to the time taken for the chamber to pressurise. The inverter is able to use a frequency ramp to accelerate the motor. If this ramp is too steep, overload of the inverter may occur. The minimum ramp without overload is shown in Figure 74. It can be seen that the fan is able to pressurise the chamber in approximately 2 seconds.

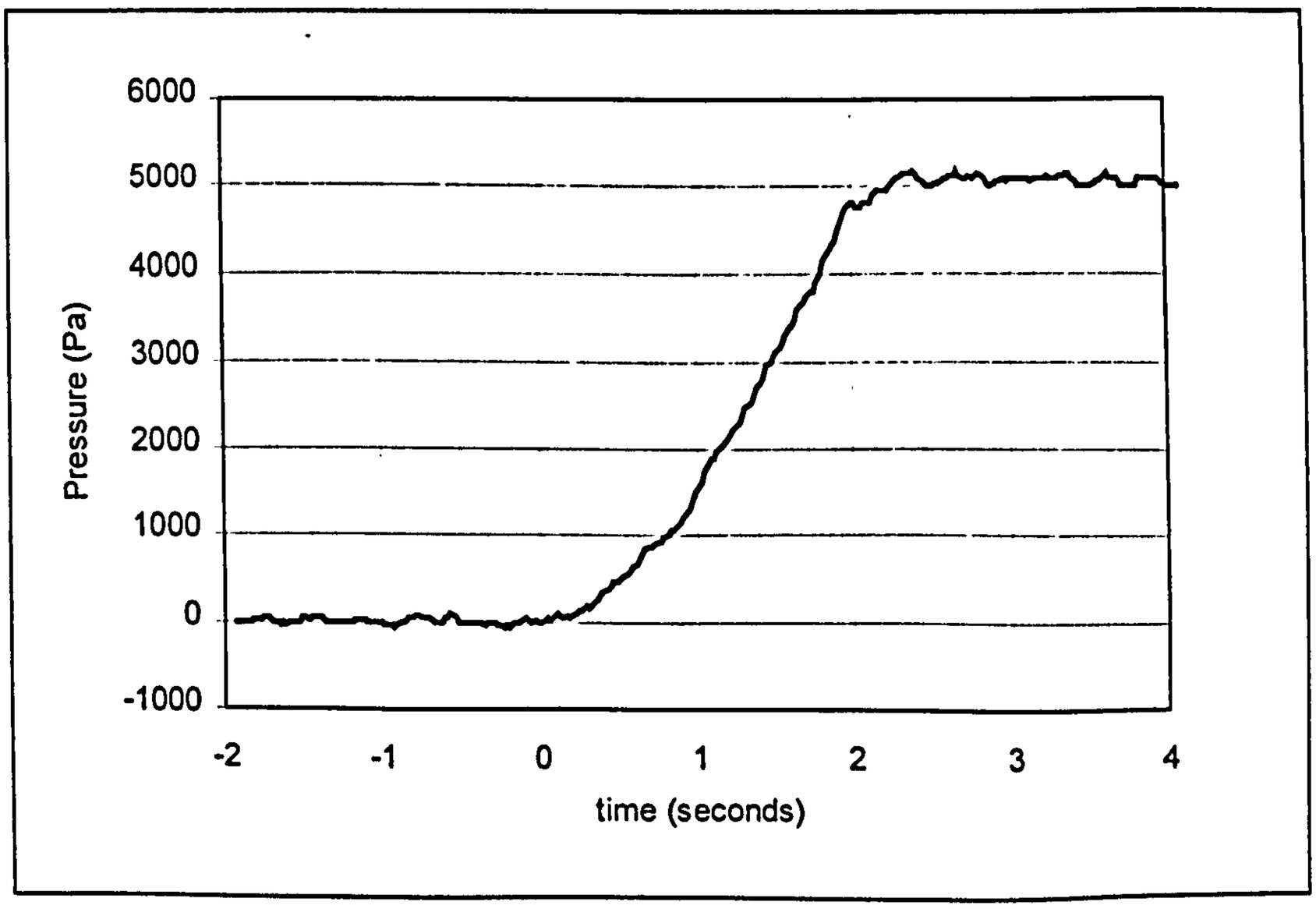

Figure 74 Pressure step response (jet 1), from zero to nominal pressure

8.8.6 Time taken for blade to de-pressurise

The delay in the step down process, from nominal pressure to zero, has a longer transient (4 seconds) because of the lower braking torque that the inverter is able to apply to the fan. Figure 75 shows the plot of the pressure fall transient. This feature could be improved by means of using a complementary braking resistor on the inverter DC output.

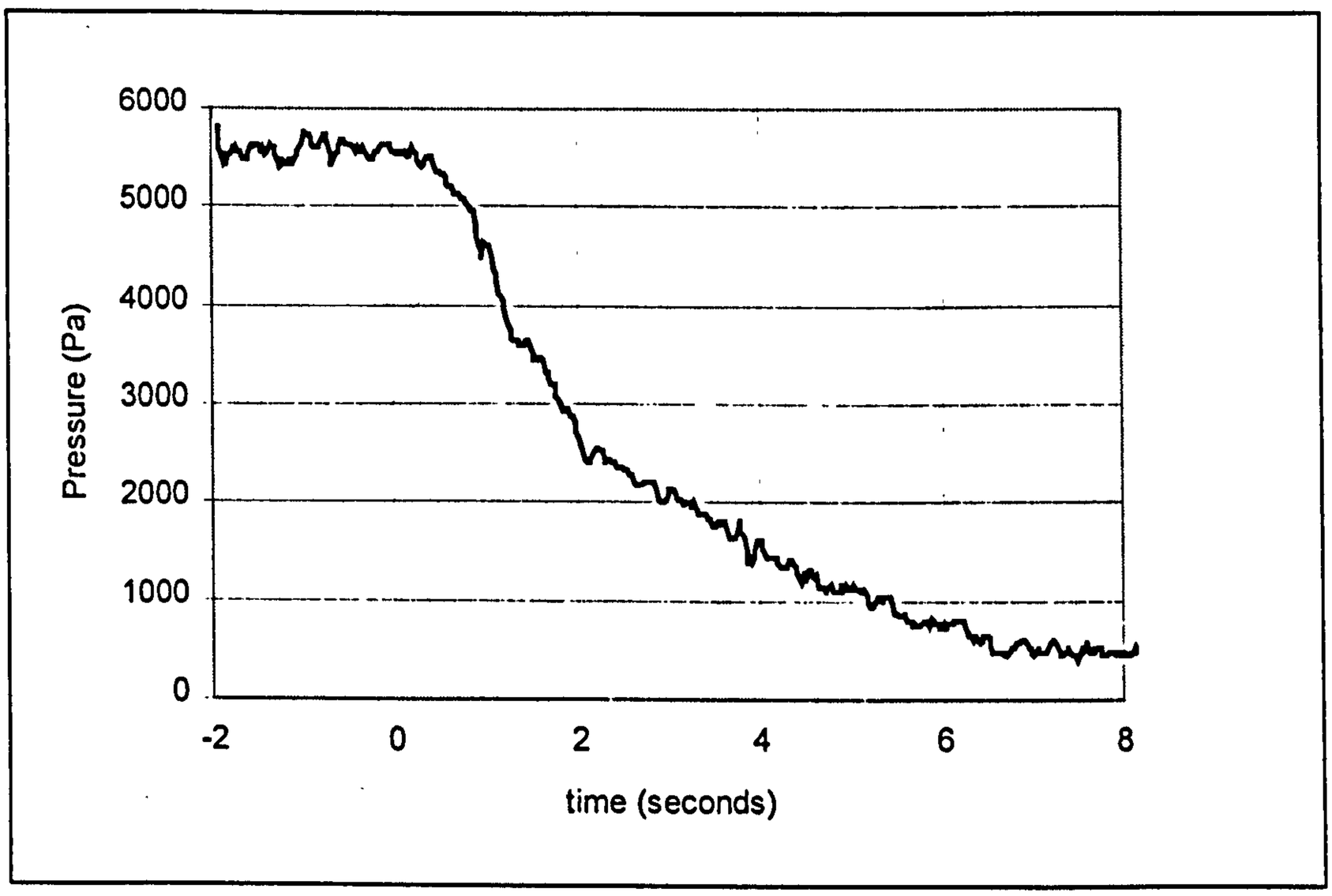

Figure 75 Pressure step response (jet 1), from nominal pressure to zero

8.8.7 Discussion of system response

Assuming that with the braking resistor fitted, the chamber could also be de-pressurised in 2 seconds, control inputs to the test machine's rotor could be provided in under 2 revolutions of the test machine (51 r.p.m.) because as stated previously air jets reattach a separated flow as soon as they are operated. On larger machines which rotate more slowly power regulation could be achieved in 1 revolution of the rotor. This could have significant benefits for electrical power quality.

8.9 Blades and fan mounted on test machine

The following figure shows two selected views of the wind turbine with the blades and fan installed. The first is a view of a blade upper surface (upwind machine) indicating the position of the air jets (55% to 75% blade radius). The second shows the fan occupying the spinner position and one of the sharp pipe bends, the reason for which was explained in section 8.5.

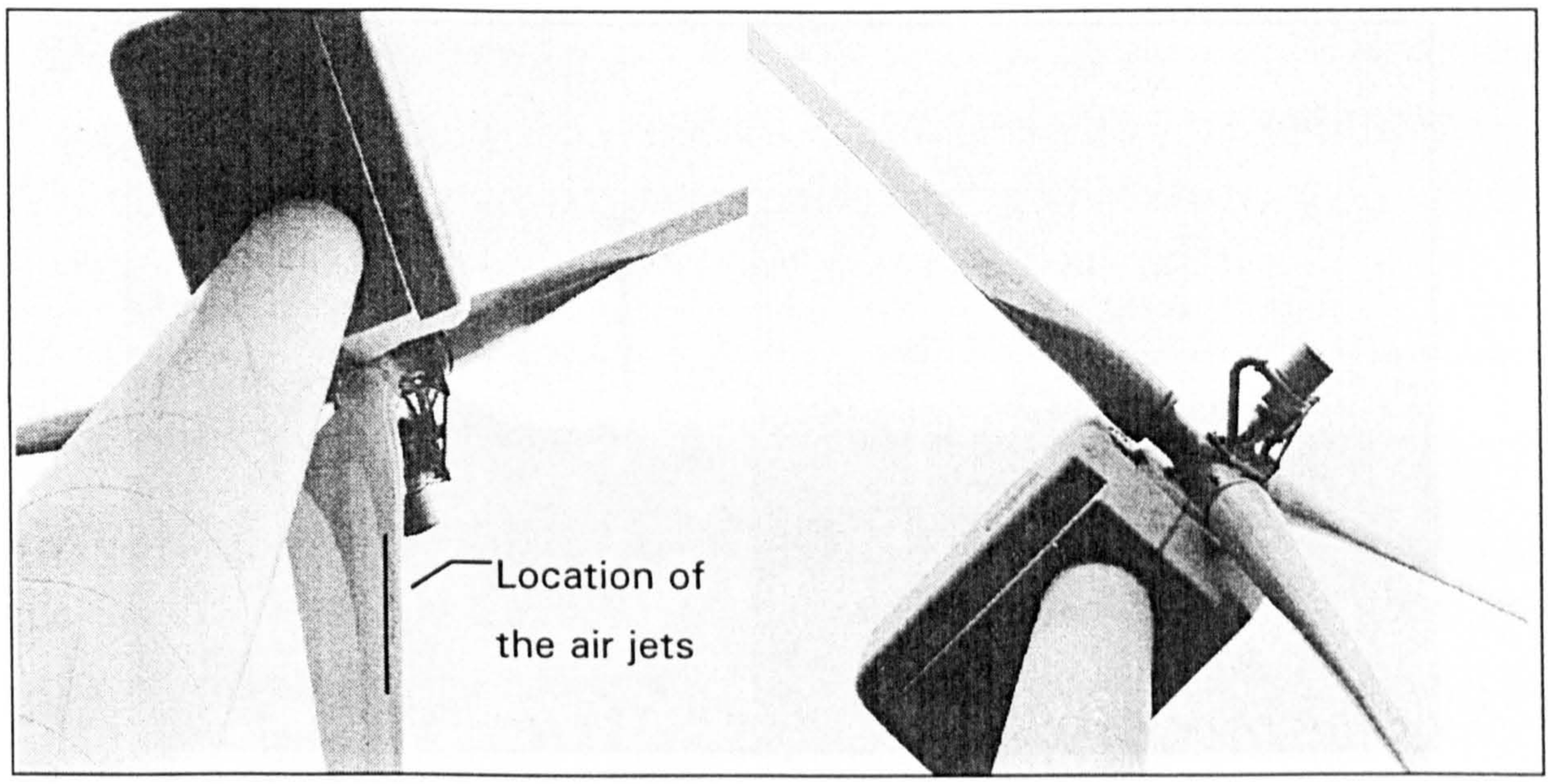

Figure 76 **Selected views of the fan and jets on the test machine.**

9. FULL SCALE TRIALS

9.1 Description of the test site

The full scale tests were carried out at the Parque Eolico de Tarifa, Ecotècnia's test site in Spain. Figure 77 shows the test site, which is characterised by rough terrain and an average wind speed of 8.3 m/s. The leftmost turbine is the test machine.

Figure 77 Ecotecnia's test site in Tarifa.

The exceptional wind conditions are produced by micro-climatic concentration effects due to the confluence of the Atlantic ocean and the Mediterranean sea. This also results in a strongly bi-directional wind. Figure 78 shows the distribution for 1990, which was a typical year (courtesy of Ecotecnia). At the request of Ecotecnia the wind speed distribution is not shown.

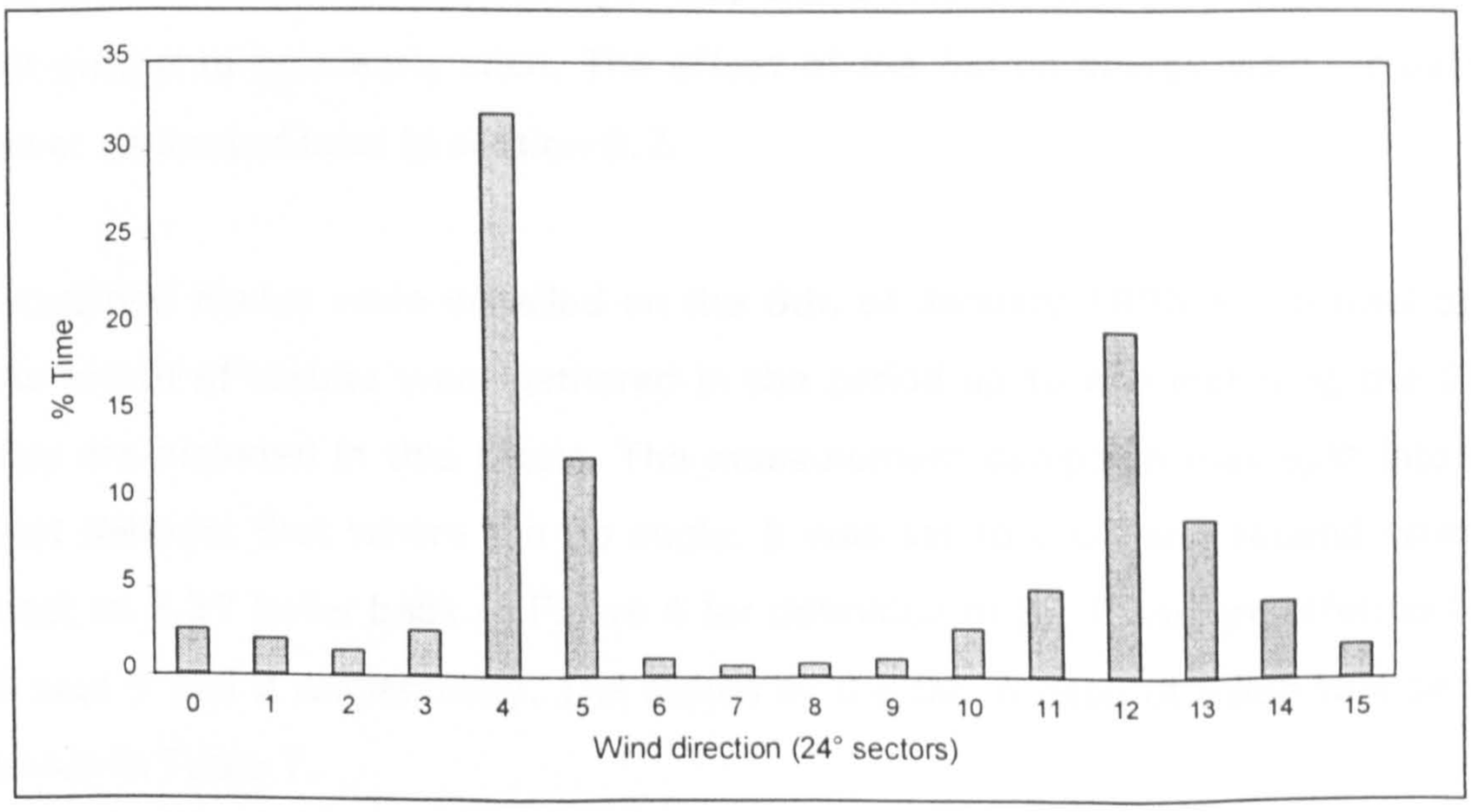

Figure 78 Wind direction at the test site (1990)

The blades equipped with air jets were mounted on the Ecotecnia 20/150 prototype which was installed in 1989 and is situated at one end of the test site. Other wind turbines nearby are the prototypes of Ecotècnia's 225, 500 and 600 kW machines. The hill arrangement (North to South) is perpendicular to the predominant wind directions (East-West) and so no important array effects were foreseen between the turbines.

A monitoring system is provided at the site which continuously logs information on wind speed, power produced and status of each wind turbine averaged over 10 minutes. A 10 metre high meteorological mast fitted with an anemometer and vane is approximately 10 rotor diameters from the test machine and is in line with the machines along the ridge, perpendicular to the predominant wind directions.

9.2 Description of the tests undertaken

The tests concentrated on power curve comparisons with the fan either 'on' or 'off'. This was done in order to get as much data as possible in the high wind speed range, from 13 to 18 m/s and so clearly demonstrate the effect of the air jets on the wind turbine output power.

During the development of the project, it was demonstrated that there is considerable potential for the air jets to be optimised, reducing the mass flow and blowing pressure requirements and thus eliminating the need for a fan. For this reason the power needed to supply the air jets (5.5kW) has not been taken into account in the measurement of the power curves presented. This also allows the air jet control of the boundary layer and the effect of this on the wind turbine power output to be clearly seen. The effect of the fan on energy yield increase is however estimated later in section 9.7.

The modified blades were installed on the 6th. of January 1996 and a total of 18 weeks worth of results were gathered in the period up to and including the 25th. of May are included in this thesis. The measurement campaign was split into two distinct periods; first where the tip angle, β was set to 0.0° and second where it was set to 2.3° (refer back to Figure 4 for definition of β). These are referred to as Data sets 1 and 2 respectively. The status of the fan in each of these test periods is shown in Table 7.

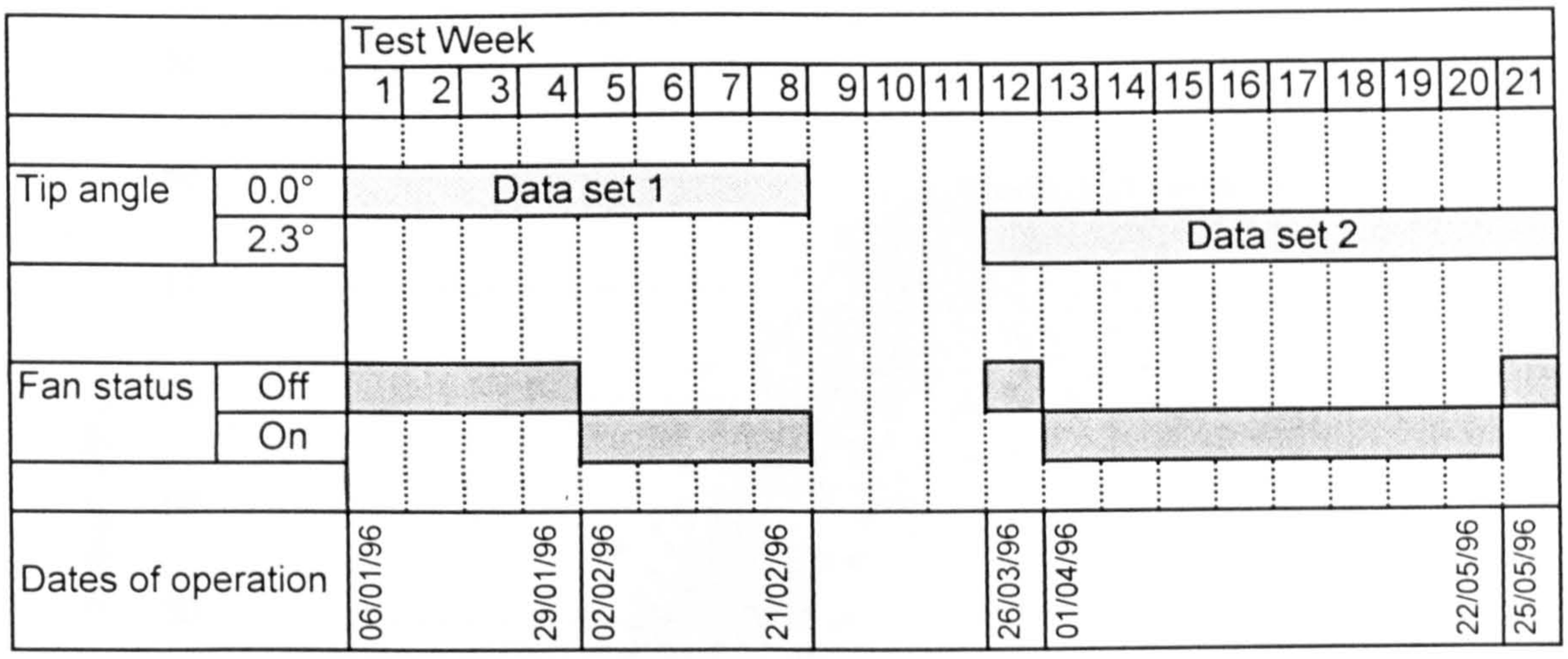

Table 7 Time schedule of the tests performed

9.3 Data measurement and reduction

Power and wind speed measurements were taken every 300 milli-seconds by the turbine controller and then averaged over 10 minutes. Only the latter value was stored. The wind speed was that measured by the turbine anemometer, not the site meteorological mast, and the power measurements with the jets 'on' did not have the fan power automatically deducted. The turbine monitoring system did not record wind direction.

Figure 79 shows a typical power curve for the test machine measured over a period of one month, where each point represents one 10 minute average. It can be seen that there is a wide range of scatter but in order to compare jets 'off' with jets 'on' a single power curve is required. To achieve this the data was processed in the following way:

1. The wind speed measurements were binned by rounding up or down to the nearest integer.
2. Zero values of power measurement were filtered out as this indicates that the machine was not on-line during the 10 minute averaging period.
3. The power data in each bin was then averaged and sample standard deviation was calculated.

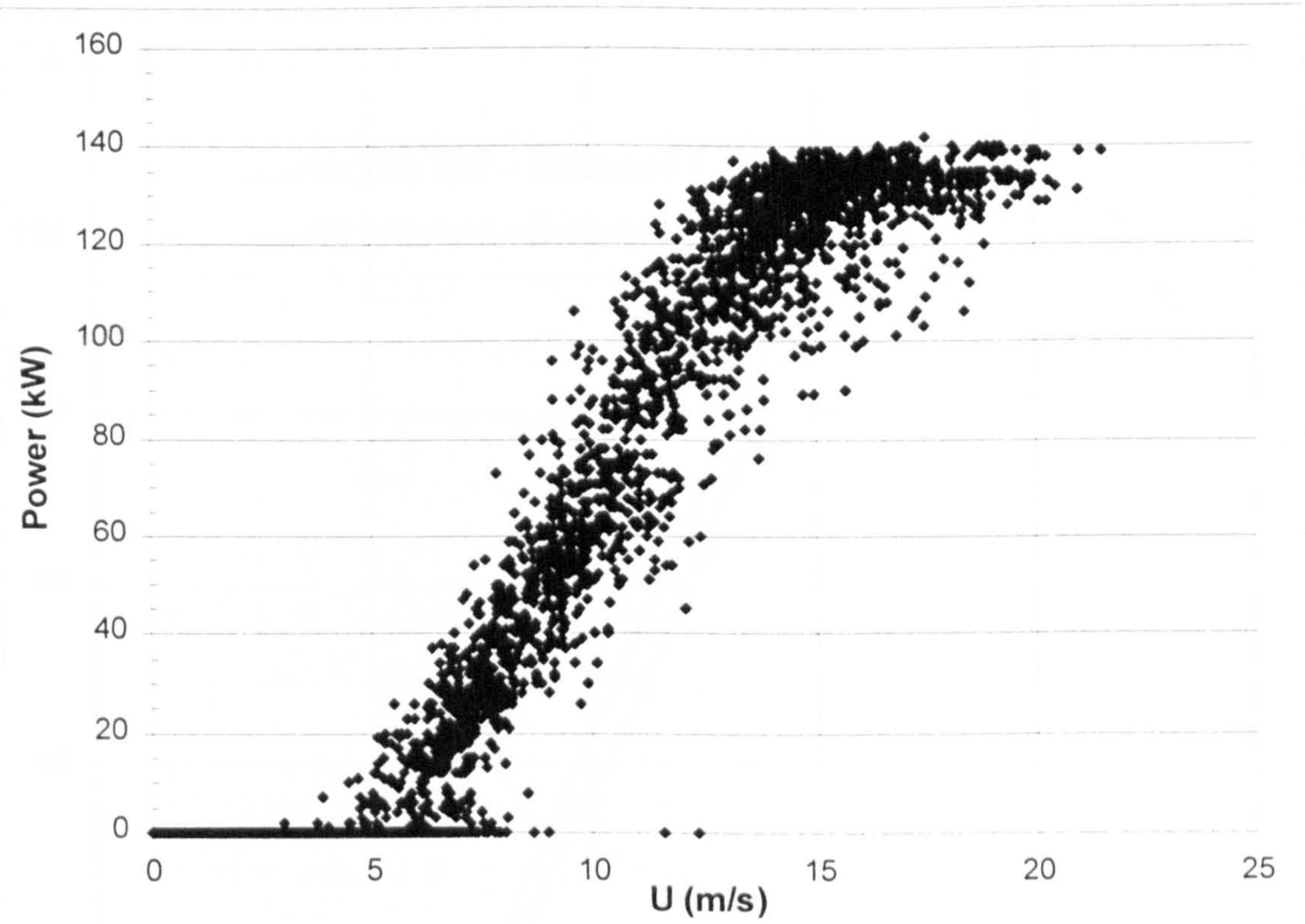

Figure 79 Typical measured power curve

9.4 Tests with reduced blade setting angle - Data set 1.

It will be noted that in Table 7 the first test period (Data set 1) contains all the tests that were carried out with a tip angle of 0°. The nominal tip angle is 2.5° for the basic Ecotecnia machine but this was reduced to 0° in order that the generator would not be overloaded when the air jets were operating in high wind speeds. From the 6th to the 29th. of January the machine was operated with the air jets 'off' and from the 2nd. to the 21st. of February the air jets were continuously on, supplied by the fan at 50 Hz. (full power).

The results from the first period are shown in Figure 80 which is a graph of the average power output for each of the wind speed bins, plotted against the wind speed measured by the nacelle anemometer. The table underneath shows the values plotted, sample deviation and the number of 10 minute averages in the wind speed bin.

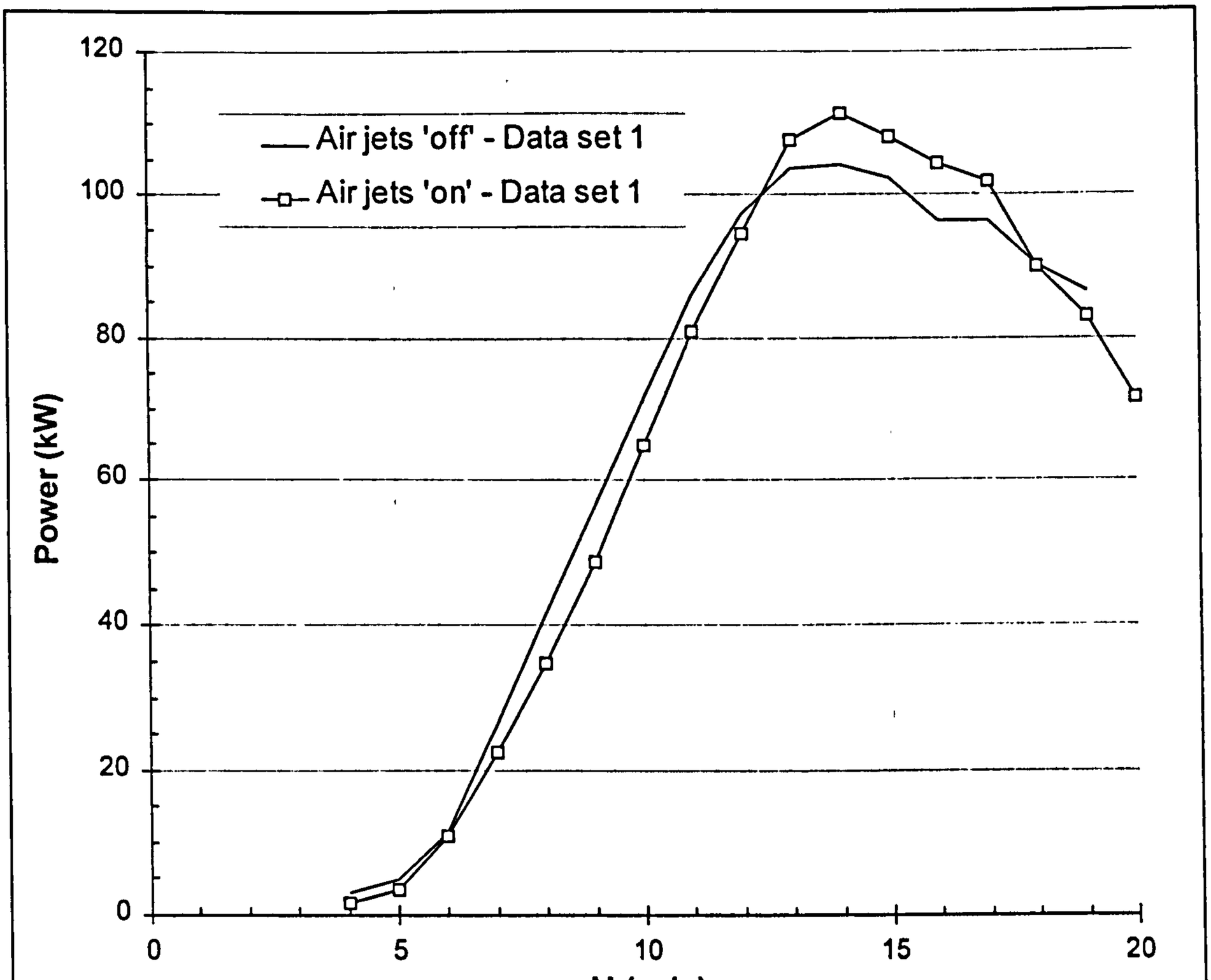

Jets Off:	06/01/96 to 29/01/96																	
U (m/s)	4	5	6	7	8	9	10	11	12	13	14	15	16	17	18	19	20	21
P (kW)	2 9	4 9	11 4	26 4	41 4	56 3	71 5	86 1	97.3	103 8	104 2	102 4	96 3	96 4	90 1	86 5		
σ	1 5	3 3	5 7	8 6	7 6	7 0	6 7	6 1	8 1	6 2	14 1	10 7	21 9	10 3	8 5	13 4		
Readings	15	36	100	206	249	236	262	185	152	107	62	50	19	16	7	2	0	0

Jets On:	02/02/96 to 21/02/96																	
U (m/s)	4	5	6	7	8	9	10	11	12	13	14	15	16	17	18	19	20	21
P (kW)	1 7	3 4	10 9	22 4	34 7	48 7	64 9	80 9	94 6	107 8	111 4	108 1	104 5	101 8	90 0	83 0	71 5	
σ	1 2	2 7	5 8	7 2	8 9	7 6	6 7	7.3	9 9	4 9	9 9	14 5	11 2	12 9	11 7	12 2	23 98	
Readings	3	15	30	110	170	180	143	112	114	113	138	156	147	77	40	30	4	0

Figure 80 Power curves (Data set 1 - All data)

The results for the reduced tip angle were discouraging with a lower jets 'on' peak power than expected and a substantial reduction in power output at wind speeds lower than rated. The lower peak power can be attributed to the fact that, at the reduced tip angle, the 2 metre array of air jets is now in the 'wrong place' on the blade for optimal performance. The lower power output before rated power, however, is harder to account for. In the jets 'off' case the jets were not covered over and so the reduction in power with jets 'on' could not be associated with the irregularity on the aerofoil surface. Also, for such a large power reduction (7.6 kW at 9 m/s) to be caused by air jets covering only 20% of the blade, any increase in drag would need to be very large indeed. (Compare Figure 63 which shows how transition on the section of blade containing air jets affected the predicted curve).

Several reasons were put forward as to what may have caused this strange result but it is best left until the Design Case has first been discussed before any conclusions are drawn. In any case, the air jets would not be operated in this part of the power curve or indeed at this tip angle.

9.5 Tests with near normal tip angle - Data set 2

9.5.1 Measurement of power curve with jets 'on' and 'off'

After the initial tests the tip angle was set to 2.3°. Normally the tip angle for this wind turbine is 2.5° but the re-design of the fan structure, to allow alignment of the fan and turbine axes, meant that this could not be achieved.

Measurements for this tip angle were carried out with the jets 'off' from the 26th. of March to the 1st. of April. The jets were then turned 'on' and operated continuously until the 22nd. of May when they were turned off once more. The final readings included in this thesis were made on the 25th. of May. Sustained high winds throughout enabled the power curve to be measured up to 20m/s.

Figure 81 shows the power curves that are derived from all the data gathered i.e. 26th. of March to the 25th. of May. The first thing to notice is that the rotor does not achieve its nominal power of 150 kW but remains below 140 kW with the air jets 'off'. It was later discovered that other machines whose blades were in the same production batch also suffered from this problem. Additionally, there is the reduced blade setting angle to consider and, as we shall see, dirt on the blade was also an important factor during the measurement campaign.

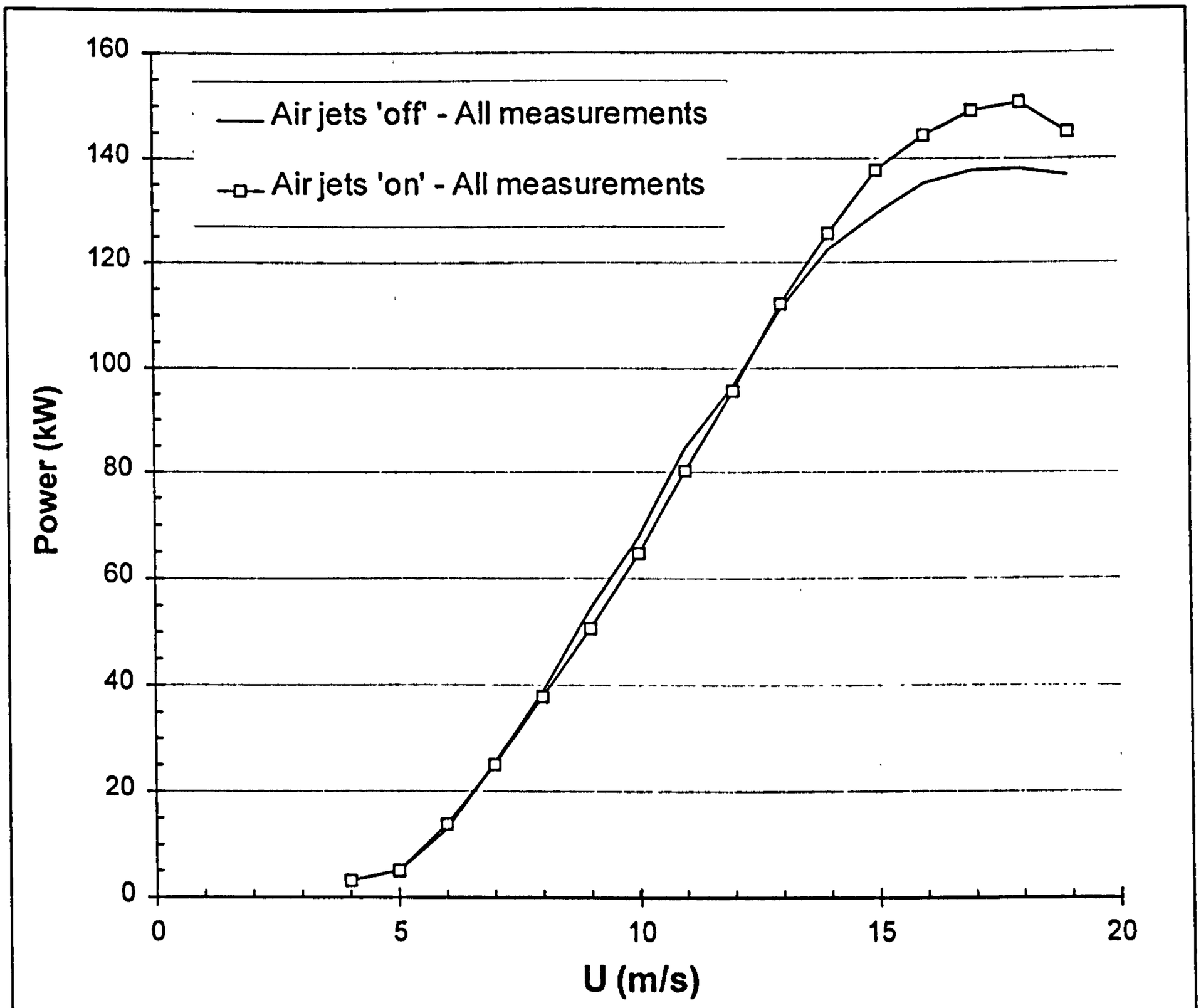

Jets Off:	and	26/03/1996 to 01/04/96 22/05/1996 to 25/05/96																
U (m/s)	4	5	6	7	8	9	10	11	12	13	14	15	16	17	18	19	20	21
P (kW)	3 0	5.1	12 7	25 3	38 8	54 4	67 9	84 5	96 5	111 3	122 5	129 3	135 5	137 7	138 0	137 0		
σ		3 8	5 8	5 2	6 3	5 8	7 0	5 4	5 7	7.7	6 8	4 1	2 1	1 8	1 2	0 9		
Readings	1	11	25	57	59	64	78	73	35	31	34	74	114	115	61	16	0	0

Jets On:	01/04/1996 to 22/05/96																	
U (m/s)	4	5	6	7	8	9	10	11	12	13	14	15	16	17	18	19	20	21
P (kW)	3 1	4 9	13 7	25 0	37 8	50 7	64 8	80 3	95 6	112 1	125 5	137 8	144 2	149 1	150 7	145 1	130 0	
σ	1 5	2.5	5 9	6 6	6 4	6 2	7.4	7 0	7 4	6 9	6 8	5 0	4 3	4 4	4.3	6 1		
Readings	8	64	241	446	532	398	356	393	279	224	182	136	137	116	58	12	1	0

Figure 81 Power curves (Data set 2 - All data)

Leaving the dirt issue aside though, it is clear without doubt, that the air jets have increased the power extracted from the wind prior to the rated wind speed of the unmodified machine. This is the main result of this thesis as the possibility of increasing the energy yield of a stall regulated wind turbine with air jet vortex generators has been demonstrated.

The optimisation is much better than it was for the lower tip angle but inspection of the curves reveals that there is still a small reduction in power output at wind speeds between 8m/s and 12m/s when the air jets are operating. It was suspected that this degradation may have been due to dirt build up on the blades, as the period in question was very dry. If so, the data would in effect be biased.

In order to investigate this supposition further, it was decided to compare the power curves over a shorter period of time. It is possible to do this because the wind speeds were high at the time of each change-over from 'on' to 'off' and from 'off' to 'on' allowing the complete power curves to be produced from just a few days data. Figure 82 shows the 'on' and 'off' power curves in the 96 hours prior to and following the first change-over and Figure 83 shows them in the 72 hours prior to and following the second change-over. (The time taken for complete power curves to be produced to the nearest day.) The effect of dirt has now effectively been removed and no significant difference exists between the 'on' and 'off' curves.

At the end of the measurement campaign (Figure 83) the unmodified power curve suddenly diverges away from the modified curve between a wind speed of 10m/s and 11m/s. However, not too much should be read into this because of the short term measurement of the power curves. The point being made is that dirt build up is a significant factor in the perceived reduction of power at moderate wind speeds with jets 'on' in both Figure 81 and earlier with the reduced blade setting angle (Data set 1, Figure 80).

Unfortunately the significance of the dirt problem was only discovered retrospectively, otherwise the blades would have been cleaned when the blade setting angle was changed and also when the jets were turned 'on' or 'off'.

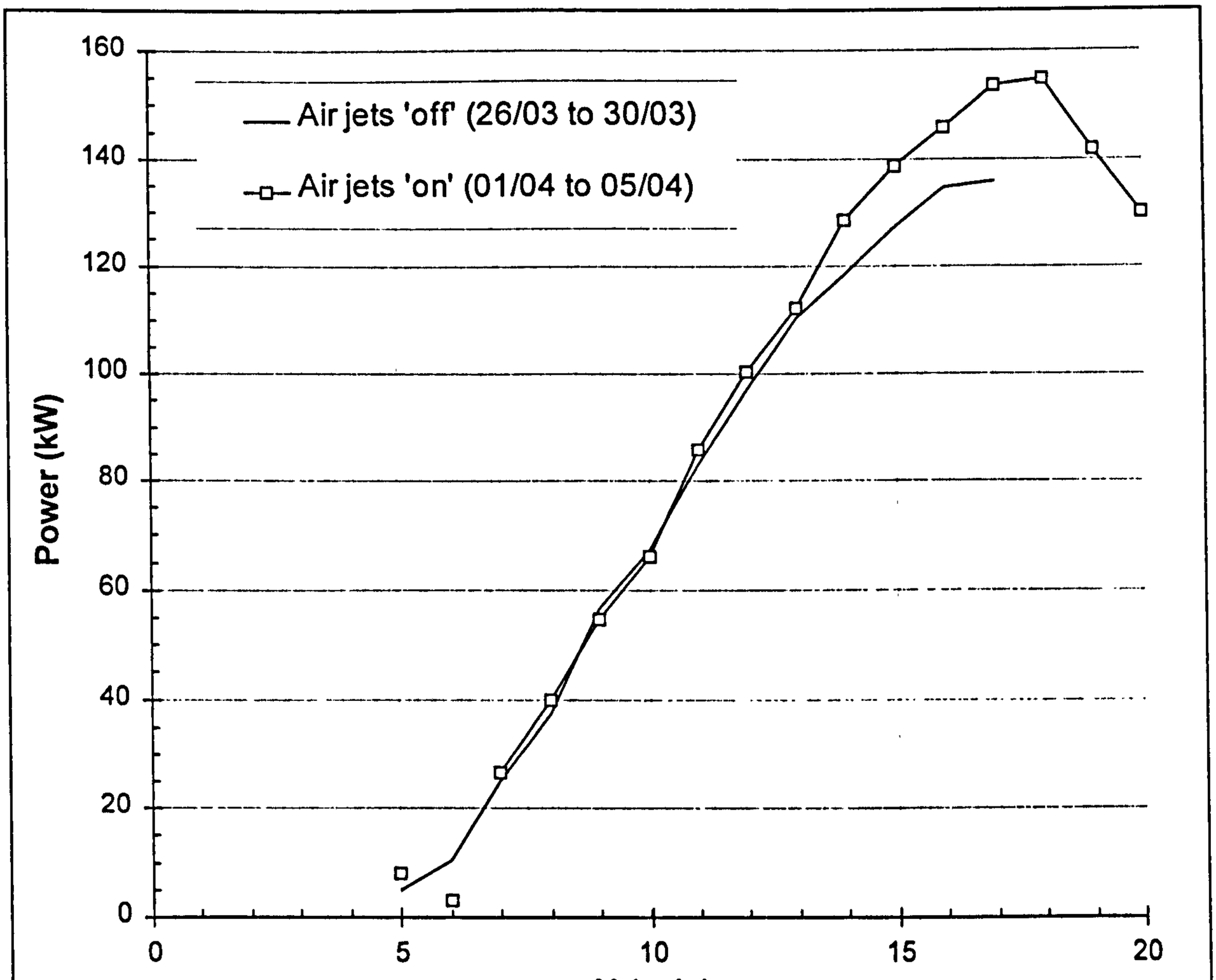

Jets Off:	26/03/96 to 30/03/1996																	
U (m/s)	4	5	6	7	8	9	10	11	12	13	14	15	16	17	18	19	20	21
P (kW)		5 0	10 5	25 0	37 4	56 4	67 5	83 0	97 1	110 2	118 2	127.2	134 7	136 0				
σ		4 2	5 6	5 4	6 3	4 7	6 3	4 6	3 0	7.8	7 6	2 8	2 3					
Readings	0	9	17	41	29	39	42	17	10	9	12	12	3	1	0	0	0	0

Jets On:	01/04/96 to 05/04/96																	
U (m/s)	4	5	6	7	8	9	10	11	12	13	14	15	16	17	18	19	20	21
P (kW)		8 0	3 0	26 7	39 8	54 7	66 1	85 9	100 3	112 2	128 5	138.7	145 9	153 4	154 8	141 8	130 00	
σ		3 0		5 9	5 7	4 3	12 8	6 7	6 6	6 3	5 0	4 9	5 9	7 5	6 0	8 3		
Readings	0	3	1	15	35	23	34	67	54	46	47	45	23	11	12	5	1	0

Figure 82 Power curves (Data set 2 - Start of measurement campaign)

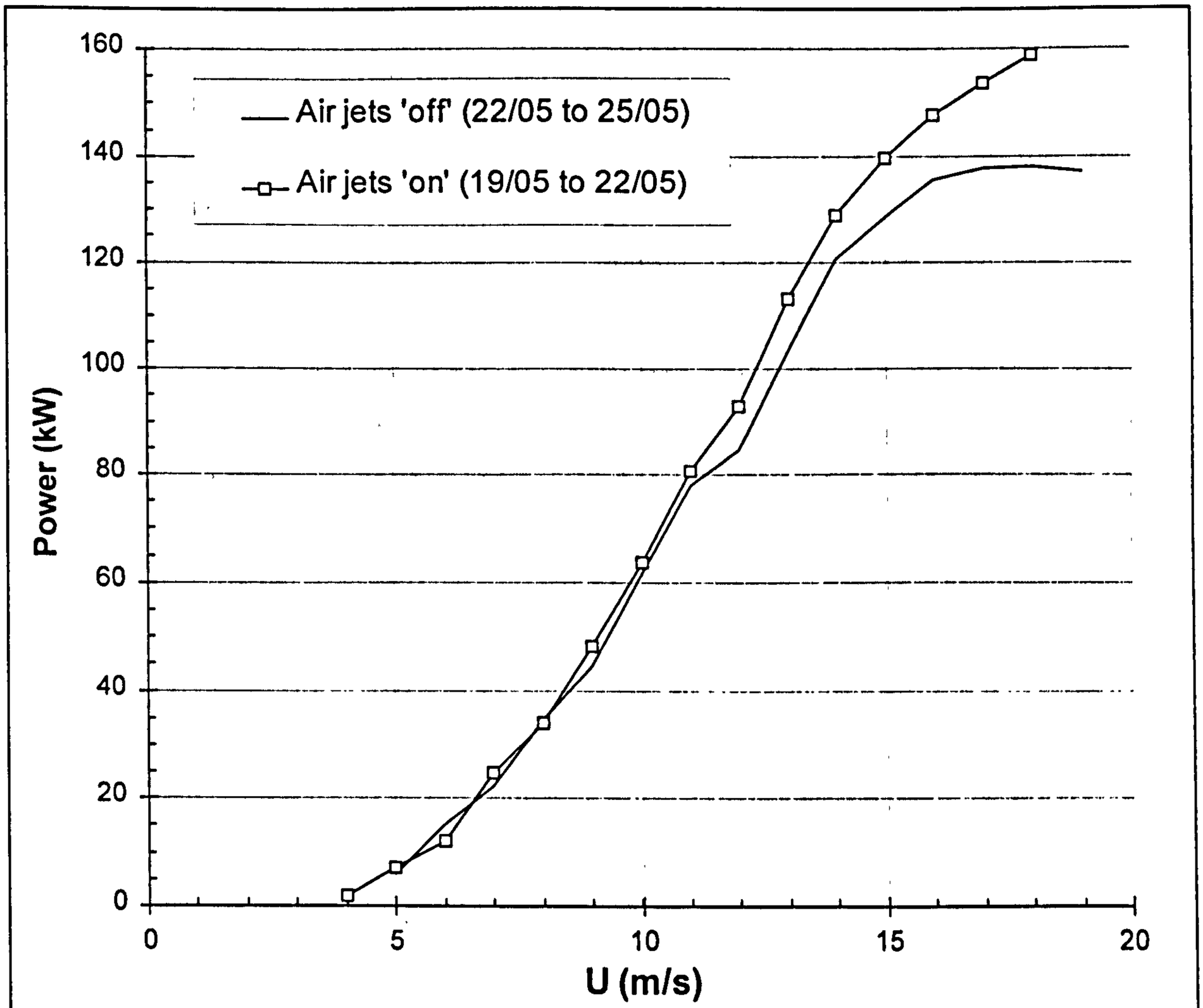

Jets Off:	22/05/1996 to 25/05/96																	
U (m/s)	4	5	6	7	8	9	10	11	12	13	14	15	16	17	18	19	20	21
P (kW)		6 0	15 0	22 3	34 5	44 6	61.7	77 9	84 8	103 5	120 6	128 6	135 5	137.7	138 0	137 0		
σ				2 1	5 2	4 8	4 0	2 3	6 8	5 7	3 1	3 1	2 1	1 8	1 2	0 9		
Readings	0	1	1	3	6	8	3	8	4	8	10	53	111	114	61	16	0	0

Jets On:	19/05/96 to 22/05/1996																	
U (m/s)	4	5	6	7	8	9	10	11	12	13	14	15	16	17	18	19	20	21
P (kW)	2 0	7 0	12 2	24 6	34 1	48 2	63 7	80 6	93 0	113 2	128 7	139 6	147.7	153 6	158 7			
σ		1 4	6 8	5 7	4 7	4 5	7.5	5 6	5 4	5 4	3 4	2 9	3 5	1 8	0 6			
Readings	1	2	10	24	29	32	27	18	12	13	19	22	25	25	3	0	0	0

Figure 83 Power curves (Data set 2 - End of measurement campaign)

It is felt unwise to offer statistics such as reduction in rated wind speed because of the aforementioned blade dirt. What is important is the fact that the jets still perform as a boundary layer control device at high wind speeds when the blade is dirty. This means that besides increasing energy yield, it should be possible to reduce energy yield losses as well. For example, when the blades are clean the air supply must be regulated in order that rated power is not exceeded. In this case a genuine increase in energy yield is registered. However, as the blades become dirty, energy is in effect 'lost'. When the air jets are operating under these circumstances they are really recovering this 'lost' energy. If the blades become very dirty there may be no need to regulate the air supply at all. It is desirable therefore to have an adaptive control mechanism in which the air supply is regulated according to power output rather than wind speed measurements.

When the blade was later inspected it could be seen that the area immediately behind the jet array was cleaner than the adjacent parts of the blade (This has also been observed by the author behind vane vortex generators on aircraft wings). This leads us to the conclusion that the continual vortex action somehow prevents the build up of dirt. It should be remembered that the air jets cover only 20% of the blade. Since the improvement due to air jets was maintained, it is not unrealistic to imagine that if the air jets were powered passively (Chapter 10) and installed on the whole blade, the performance reduction may be less than it currently is due to the blade being kept cleaner.

At lower wind speeds ($U \leq 7m/s$), it is difficult to discern whether or not there is a performance penalty. This is made more difficult because the turbine cuts in and out more often at these wind speeds and in doing so renders that particular 10 minute power average redundant. This is of most importance when there are only a few data points in the wind speed bin being averaged. It is suggested that in future, the data acquisition software should be re-written to filter out data where the turbine has either cut-in or out. The 'on' and 'off' measurement periods should also be reduced significantly. This would help to eliminate other effects such as air density, wind shear and turbulence intensity which are not covered here due to the limited length of the measurement campaign and scope of the data acquisition system. A suggested period would be 1 hour 'on', 1 hour 'off' because this is within the spectral gap of the van der Hoven spectrum and so would be more likely to capture 10 minute averages of similar wind speed.

Plotting graphs of the power coefficient versus tip speed ratio (Cp versus λ) did not reveal any further interpretation of the results and for this reason they are not included.

9.5.2 Standard deviation with jets 'on' and 'off'

The sample standard deviation, σ of the 10 minute averages was calculated for each wind speed bin and is shown in Figure 84 along with the number of readings on which it is based. (The values are shown in the tables under Figure 81). This was done in order to determine if there was any significant difference between jets 'off' and 'on'. The results indicate that there may be an effect due to jets at higher wind speeds where a high sample standard deviation is maintained when the jets are 'on', Although this is most likely to be due to the fact that the power is still increasing with jets 'on' rather than levelling off. Nevertheless, it is important that this is investigated further, as it could indicate that dynamic stall is more serious with air jets 'on', leading to reduced blade fatigue life. This would be of particular concern if air jets are to be fitted to the whole blade.

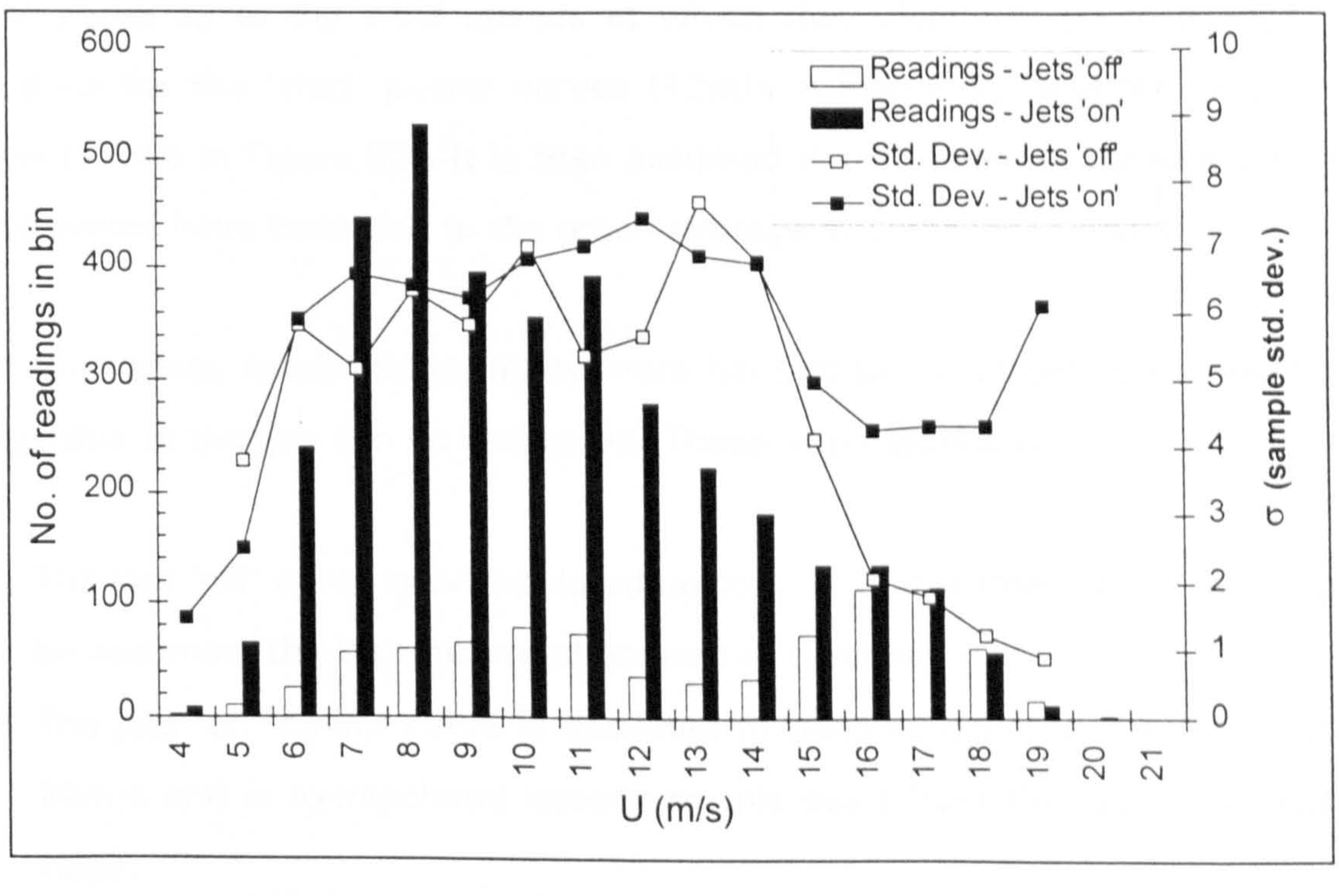

Figure 84 Sample standard deviation at each wind speed

9.6 Power regulation

At the time of writing this thesis, it has not yet been demonstrated that air jets can be used to regulate the power output by controlling the flow of air to the jets. This was due to the fixed term nature of the project. It has, however, been demonstrated in the wind tunnel that the lift and drag of an aerofoil may be altered by controlling the air flow to the jets. This result and power regulation in general is discussed further in Chapter 10.

9.7 Estimation of increased energy yield

The increase in annual energy yield is hard to determine with any real confidence and is extremely subjective. Most of the energy is generated at wind speeds lower than where the air jets influence the power curve and this is where most of the differences were found due to dirt accretion. As the increase being calculated is only a small quantity (< 5%) this influence alone masks the true energy yield gain.

To get around this problem, the air jets 'on' power curve was set equal to the 'off' power curve up to the wind speeds at which they clearly begin to diverge. This was done for the 'start' power curves (12m/s in Figure 82) and the 'end' power curves (11m/s in Figure 83). It is then assumed that the energy capture during the period would have been due to the mean average of these two curves.

Even after these assumptions, many more have to be made before the increase in energy due to the jets can be estimated. These assumptions are:

1. The jets 'off' curve is extrapolated up to U = 25m/s (the cut out wind speed) by assuming the last measured power i.e. constant.
2. The jets 'on' power curve is assumed to become equal to the 'off' curve at 20m/s and is extrapolated linearly to this point from the last measured 'on' value.
3. Above 20m/s the jets 'on' power curve is equal to the jets 'off' power curve.

The result of all these assumptions is shown in Figure 85, where the dotted lines represent an extrapolation.

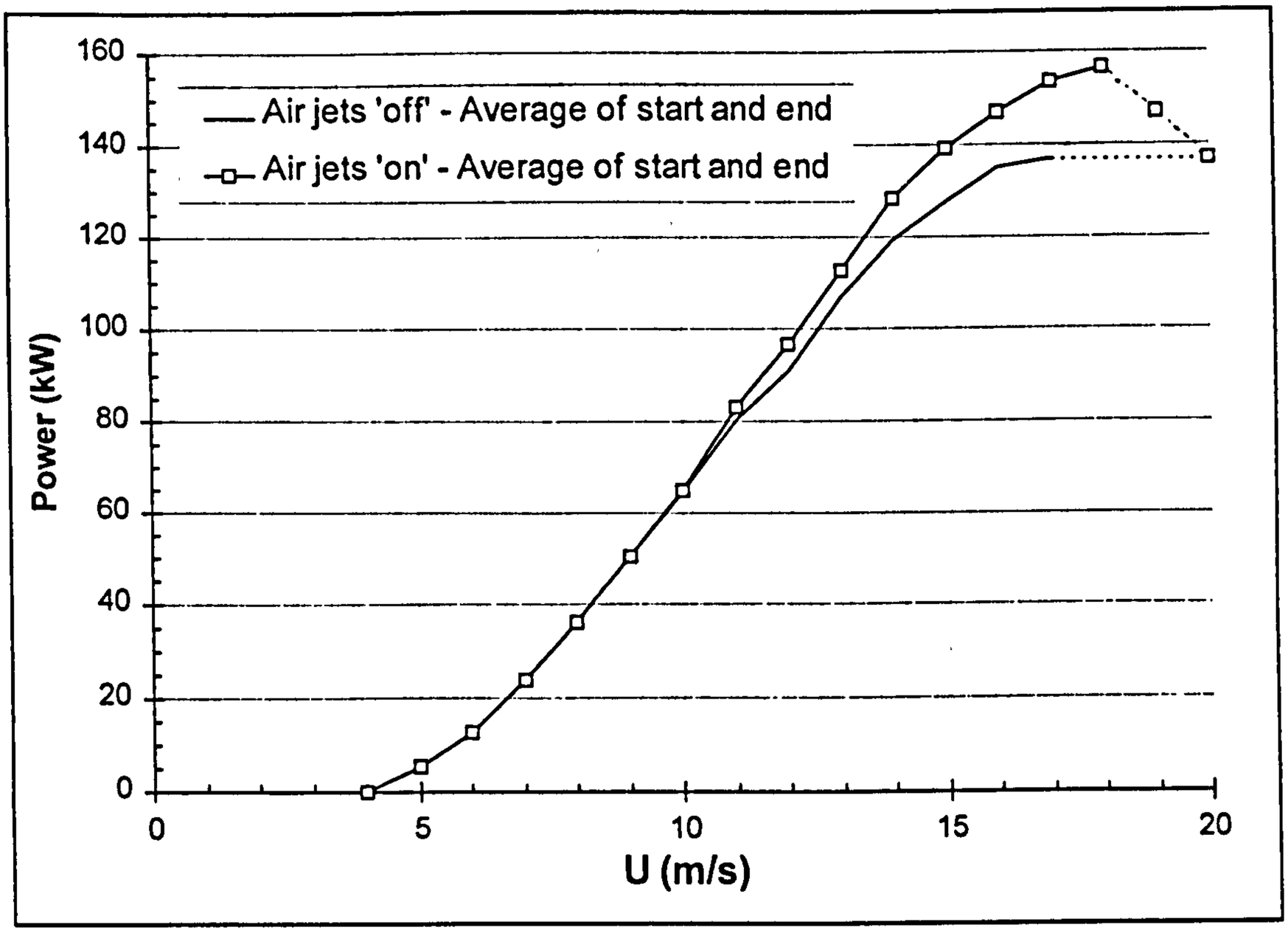

Figure 85 Assumed power curves for calculation of energy increase

The increase in energy yield as a percentage of the unmodified machine's energy yield during the period has then been calculated. This was done for the range of annual average wind speed 6m/s ≤ Uav. ≤ 10m/s (hub height) using the Rayleigh form of the Weibull distribution (k = 2.0). These results are plotted in Figure 86 which shows that the increase in energy would have been approximately 2% to 5% depending on the average wind speed.

Also shown in Figure 86 are the results of the same calculation performed with the power curve obtained at the start of the period (idealised version of Figure 82). This curve is roughly 1% lower at any given average wind speed. This could be due to the strange kink in the jets 'off' power curve (Figure 83) or due to the jets reducing energy yield losses by keeping part of each blade cleaner (both of which effectively increase the percentage energy gained when considering the 'average' power curves). Either way a range of energy difference (increase + reduced losses?) between jets 'on' and 'off' is arrived at. It is emphasised that this is an extremely subjective approach and therefore not a result, but only an indication of the energy gain that could be expected.

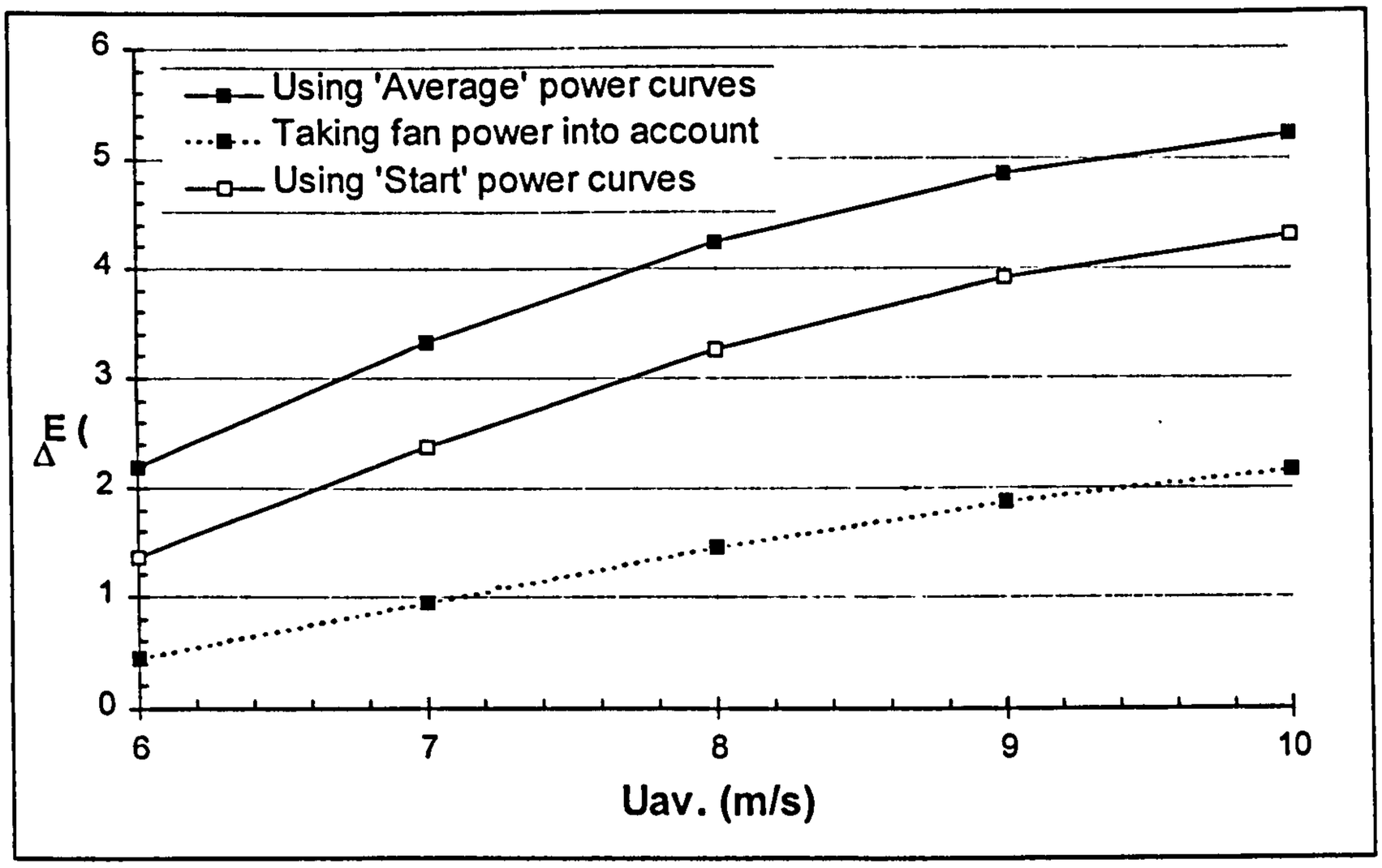

Figure 86 Range of likely energy gain due to air jets

To end this particular discussion it is interesting to report that an energy yield increase is calculated even if the fan power requirement (Figure 86) is taken into account (with respect to the 'Average' power curves). It was calculated by subtracting the fan power consumption of 5.5kW from the jets 'on' curve (Figure 85) and then assuming the jets were 'on' when the turbine output still exceeded the 'off' output. Otherwise the fan was assumed to be 'off'. Again this approach is highly idealised but is probably unnecessary anyway since wind tunnel results in Chapter 10 suggest that a fan is not required.

9.8 Comparison of predicted and actual effect of air jets

In section 7.6 two methods were used to predict the effect air jets would have on the power curve. These were:

1. That the 3D correction could be applied direct to the air jet data, i.e. 3D effects further enhance the increased lift due to air jets.
2. Delayed stall due to air jets eliminates all benefit due to 3D effects for those blade elements.

Figure 87 shows the same predictions as Figure 62 in section 7.6 but adjusted for the slightly lower blade setting angle of 2.3° as opposed to 2.5° and having taken into account the loss conversion factor used by the turbine manufacturer to convert shaft power to electrical power (equation 6 -1 in section 6.5).

Also shown in Figure 87 are the measured power curves, at the start of the measurement campaign (Data set 2) when the blades would have been cleanest.

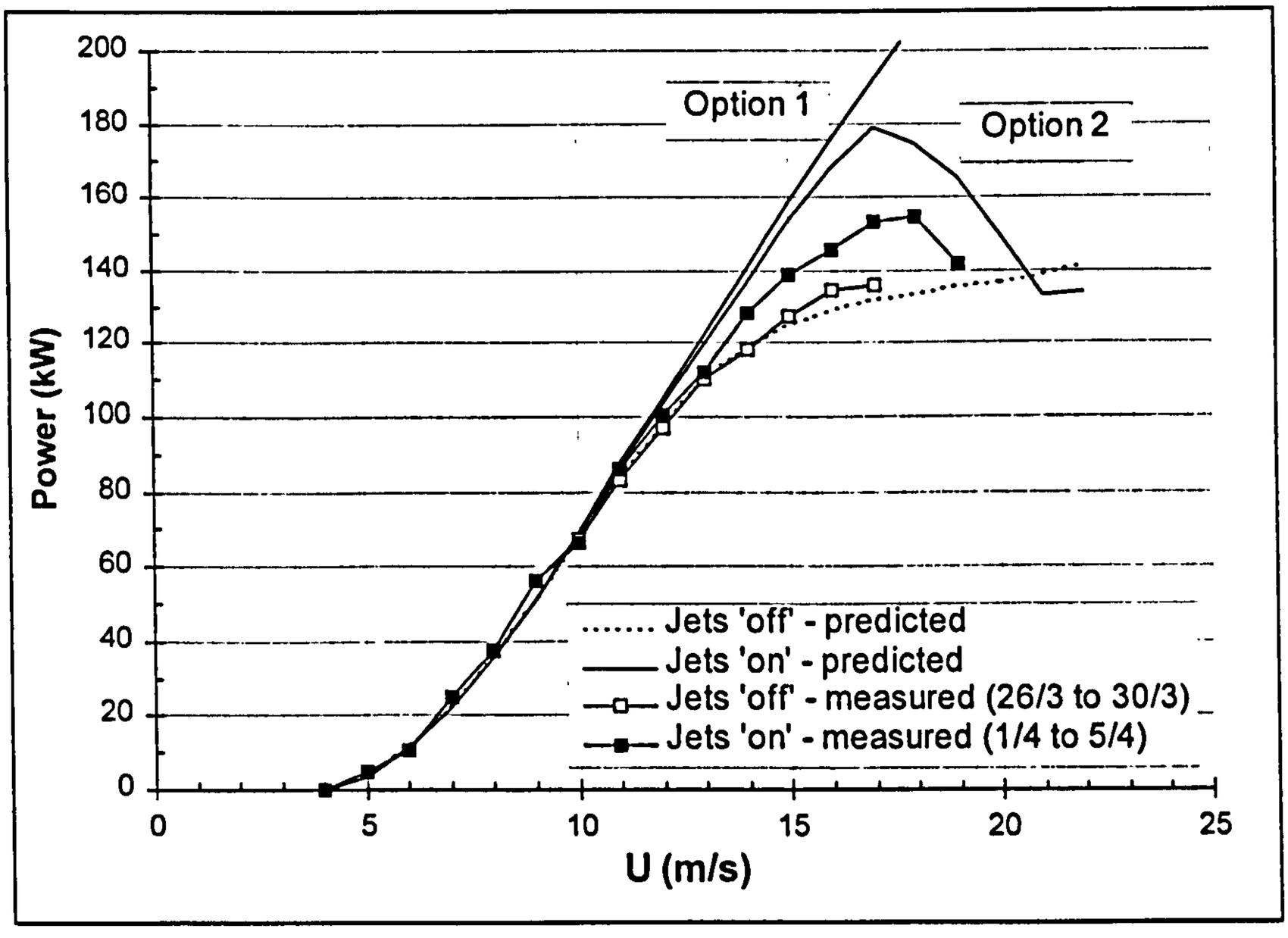

Figure 87 Comparison of predicted and measured power curves

It can be seen that the prediction of the unmodified blade correlates well with the measurements made. This result may in part explain the difficulty in producing the power curve specified in the product brochure (Chapter 6).

Option 1 above, which was thought unlikely, can be ruled out completely. Option 2, however was expected to be the lower limit of improvement due to the air jets. The peak of the prediction is at roughly the correct wind speed but is much higher than the full scale measurements. This indicates that the maximum lift coefficient ($C_{Lmax.}$) with air jets on the blade is not as high as measured in the wind tunnel on all or part of the array. Or to be more precise the relative C_{Lmax} of the modified and unmodified blade are much closer (since we cannot be certain that the unmodified blade has the same C_{Lmax} as that recorded in the wind tunnel).

The fact that the upper wind speed at which jets are effective is lower than predicted is of less concern. This is because it is related to the way in which the lift and drag curves have been extrapolated from the wind tunnel data.

Many theories can be put forward as to the reason why the power increase due to jets was not as great as predicted. Some of these theories are presented below in what the author considers to be descending order of importance:

1. Blade element theory is not suited to this type of problem because it interprets only 2D static aerofoil data and applies it to a rotating case. Specifically it cannot be used to combine 3D effects with those of air jets.
2. It is not known if array end effects were occurring on the blade.
3. The jets may be starting to lose effectiveness on the inner part of the array due to the effect of chord. The jets on the blade were 16mm. in length on a chord of 810mm. (1:51) at 55% radius. The jets on the model were 12mm. on 500mm. (1:42). The model was only representative at the tip end of the jet array.
4. It is not known what happens to the blade lift and drag as air jets remain 'on' in deep stall. The effect could be adverse.
5. Dirt ingestion in the fan filter was observed after the tests had been completed.
6. All of the jets were slightly under-powered (6.5kPa as opposed to 6.9kPa) due to the additional pipe bends caused by the change in fan position.
7. The first four jets on each blade were under-powered. (see Figure 72).

The above does not detract from the main result which is that air jets can increase the power production of a stall regulated wind turbine prior to the rated wind speed of the unmodified machine.

MISSING

PAGE

NOT

AVAILABLE

Instead of a costly redesign of the model it was decided that a first approach to modelling 'Ram-jets' should be to keep the lower surface intact and blow a pressure equal to stagnation pressure into the plenum chamber. Of course this is slightly higher than one might expect in reality because the stagnation point moves backwards as angle of attack is increased and there would be pressure losses through the jets. Also, any drag increment that might exist due to the lower surface holes would not be measured. Nonetheless, it was still felt to be a worthwhile exercise as the experiment was really to determine whether any potential existed for 'Ram-jets'. Additionally, the earlier experiments indicate that the air jets are not yet optimised and a further reduction in jet exit area would lead to smaller exits on the lower surface and possibly improved lift/drag ratios.

The problem that existed now was what absolute value of stagnation pressure to use because both wind speed and blade radius (rotational velocity) have an affect on its dynamic pressure component. This is discussed in more detail in 10.4.2, but initially it was decided to keep the same tunnel speed of 43m/s as for all the previous tests. This also allowed direct comparison with the previous results from this configuration at the same Reynolds number (Chapter 5).

In order to match the plenum pressure to stagnation pressure additional apparatus was set up. This consisted simply of a pitot-static probe mounted in the tunnel of which the pitot tube was connected to a manometer bank, referenced to atmosphere (1). The adjacent manometer tube was connected to a pressure line from the model plenum chamber and was also referenced to atmosphere (2). By operating the air jet flow rate valve the fluid height (2) could be controlled to the level of the tunnel dynamic pressure (1).

This set-up is only valid if the tunnel static pressure, P_∞ is equal to atmospheric pressure, P_a. We can then write:

$$H_\infty = p_a + \tfrac{1}{2}.\rho.U_\infty^2 \quad \text{.....(10-1)}$$

By balancing the pressure in the plenum chamber of the model with the tunnel stagnation pressure which are both referenced to atmosphere, stagnation pressure in the plenum chamber is achieved.

The assumption that static pressure is equal to atmospheric pressure is valid because the tunnel working section is vented to atmosphere at the rear. This was confirmed by taking a static pressure line from the probe to the manometer.

Finally, the dynamic pressure was checked to make sure the procedure was sufficiently accurate. Since both of the balanced manometer tubes were referenced to atmosphere:

$$\rho_{man}.g.\Delta h_{plenum} \equiv \rho_{man}.g.\Delta h_{tunnel} = \tfrac{1}{2}.\rho.U_{\infty}^{2} \quad \text{.....(10-2)}$$

Where ρ_{man} is the manometer fluid density (885kg/m^3) and Δh_{plenum} given by the height of displaced fluid (0.140m.), the left hand side of the expression is calculated to be 1215 Pa (0.18 p.s.i.). This should be equivalent to the tunnel dynamic pressure, the right hand side of the expression. Using the velocity calculated by the Data Acquisition System for this run of 44.2m/s we find this to be equal to 1201 Pa. Thus the pressure in the plenum chamber could be fairly accurately controlled to simulate stagnation pressure which itself is closely analogous to a 'Ram-jet'.

10.1.2 'Ram-jet' lift and drag curves.

Figure 89 shows the results obtained by blowing air at the tunnel stagnation pressure into the plenum chamber of the model fitted with the second configuration of air jets. For comparison the results obtained with the blowing pressure at 1.0 p.s.i. ('Active-jet') and the unmodified aerofoil are also shown. In all three cases the transition strip has been fitted.

The results obtained were startling. The blowing pressure has been reduced by over 80% from the 1 p.s.i. case and yet the improvement in lift (33% increase on C_{Lmax}.) and drag reduction at high angles of attack mean that the vortices are still being generated and boundary layer mixing is still occurring. There is a small increase in drag in the low incidence drag range however which is shown more clearly by Figure 91 later.

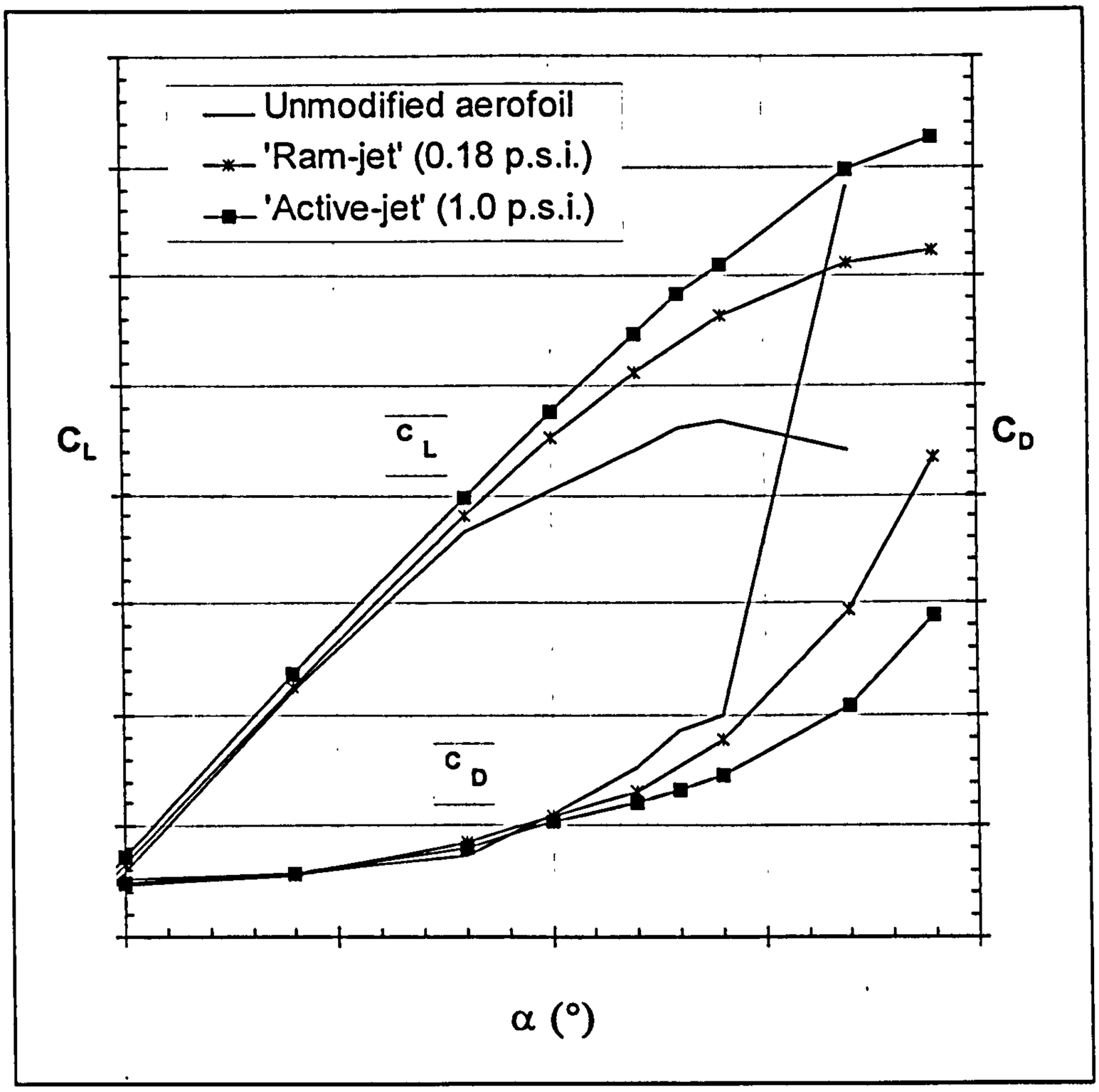

Figure 89 'Ram-jet' lift and drag curves

10.2 'Ambi-jets'

With promising results obtained with the 'Ram-jets' operating at a very low blowing pressure an additional set of tests was performed to see what would happen if the plenum chamber was open to ambient atmospheric pressure.

It was hoped that the pressure difference between atmospheric pressure and the upper surface suction would be sufficient to create air jets capable of inducing vortices to form around them.

'Ambi-jets', as they will be referred to, were easier to model than 'Ram-jets' because the two pipes supplying air to the plenum chamber were simply disconnected. The open ends of the pipes (Figure 20) were outside the wind tunnel working section and thus open to atmospheric pressure.

If 'Ambi-jets' worked, the blade manufacturing process would be simpler than for 'Ram-jets' because only the upper surface would need to be modified. For example, the air supply could be piped internally from the root as with the powered tests. Instead of having a fan at the hub though, there could just be an 'air collector'. There would also be no risk of incurring any extra drag penalty due to inlet holes on the lower surface of the blade, which is likely to be the case with 'Ram-jets'.

10.2.1 'Ambi-jet' lift and drag curves

Figure 90 shows that even with no blowing air jet vortex generators are still able to delay stall. It appears that the suction on the upper surface is sufficiently strong to pull enough air through the air jets to generate vortices. This has resulted in an increase in maximum lift coefficient of some 22% from 1.17 to 1.43. However, a large increase in low incidence drag coefficient is now evident with C_{Dmin} increasing by approximately 11% from 0.0103 to 0.0114.

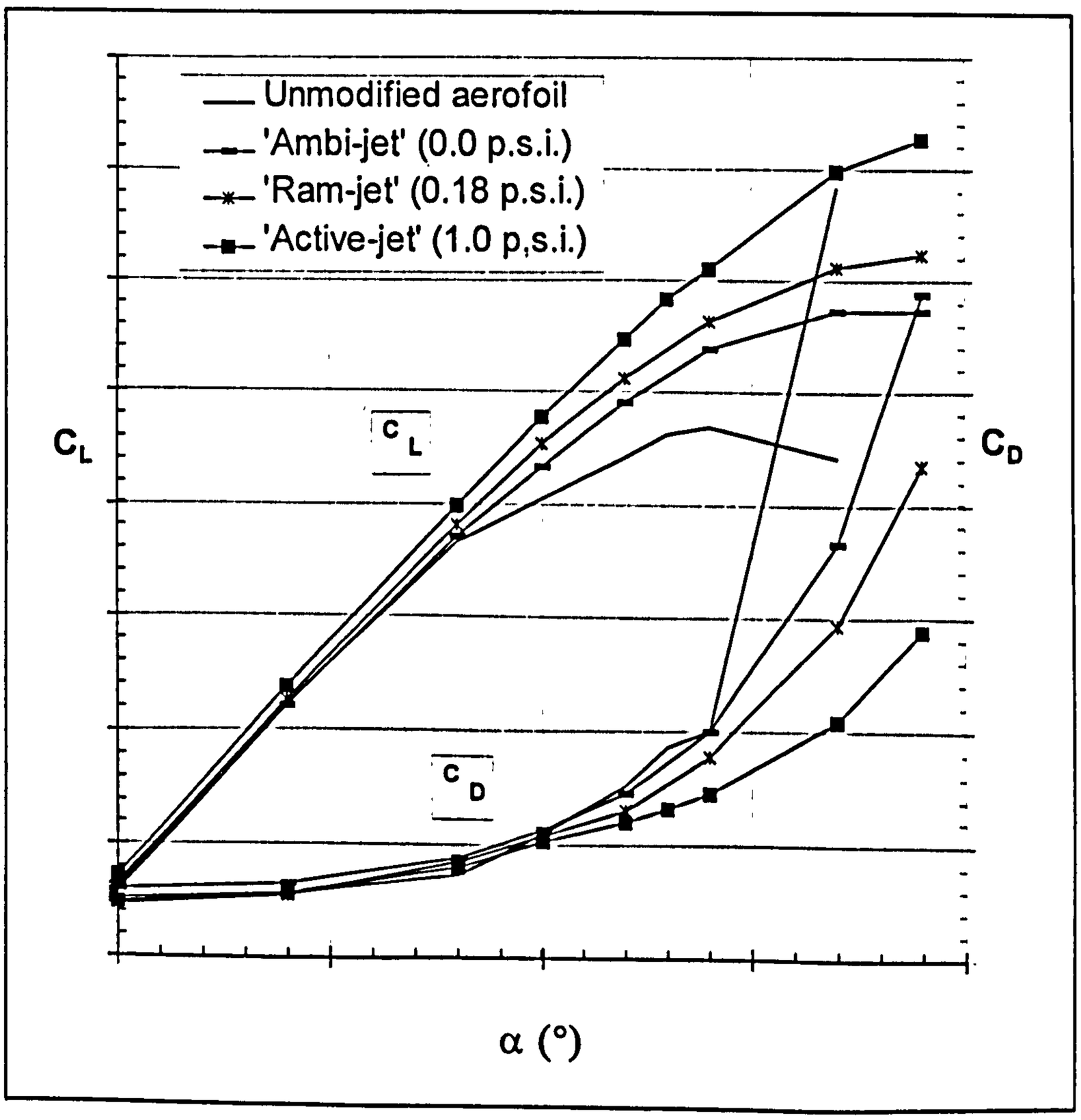

Figure 90 'Ambi-jet' lift and drag curves

10.2.2 Lift / Drag curves: Active, passive and unmodified.

The increase in low incidence drag for the 'Ambi-jet' is revealed more clearly in the lift/drag curve, Figure 91. At angles of attack lower than about $\alpha = 9.5°$ the unmodified aerofoil possesses a superior lift/drag ratio to the modified one when the jets are passively driven by ambient air pressure. For comparison the lift/drag curves of the 'Ram-jet' and 'Active-jet' at 1.0 p.s.i. are also shown.

To confirm that air really was being drawn through the pipes by the 'Ambi-jets' and that the stall delay was not due to some other phenomenon, the pipes were first sealed and then partially sealed by sticky tape.

Although lift and drag were only measured for one angle of attack ($\alpha = 17°$), the point is illustrated that the jets really must draw their own air supply (Figure 91). The result for the partially closed pipe indicates that it should be possible to exert control with a valve rather than by changing the pressure supplied.

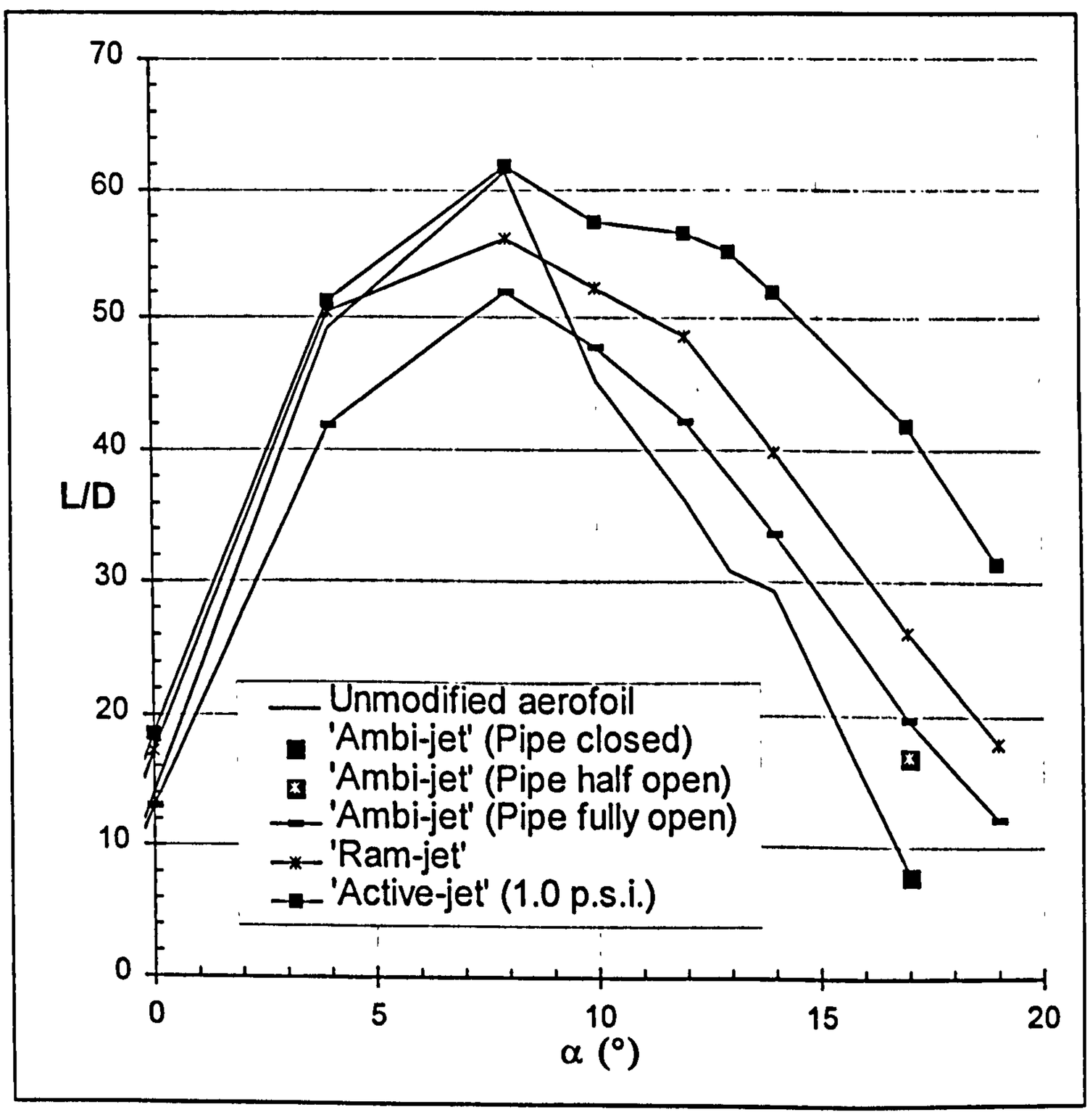

Figure 91 **Lift/drag curves for the passive and active blowing methods**

10.3 Further dissemination of the air jet results

10.3.1 Increase in lift coefficient due to pressure across the jet.

With the second configuration having now been tested at four different blowing pressures, the effect of this quantity on aerofoil performance could now be investigated further. It was considered that one way of quantifying air jet performance would be in terms of improved lift coefficient. This was defined as being the change in C_L (i.e. ΔC_L) due to air jets, with respect to the unmodified aerofoil at any given angle of attack, α , as shown on the left hand side of Figure 92.

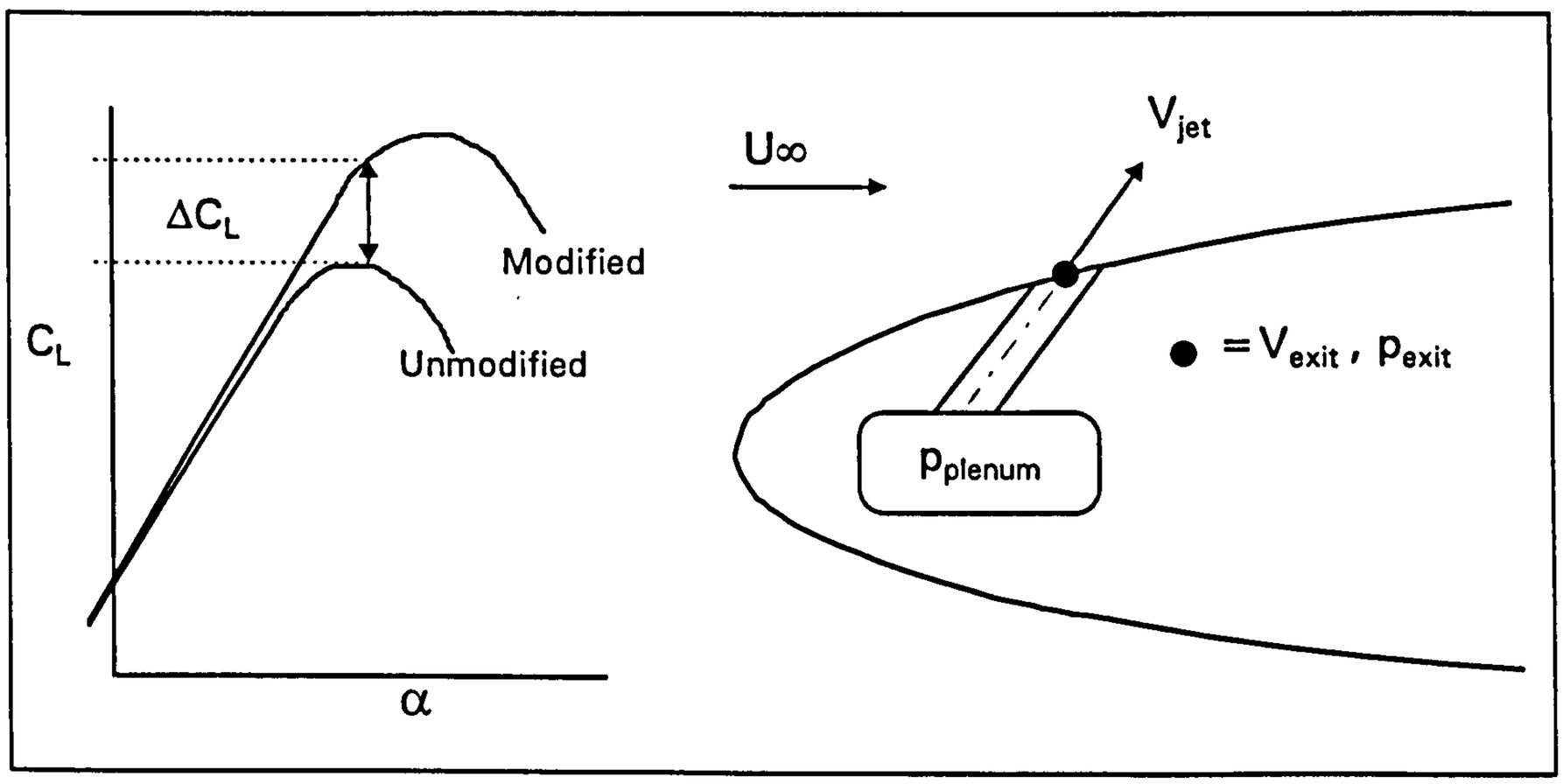

Figure 92 Sketch showing air jet performance parameters

Initially the relationship between ΔC_L and the blowing pressure across the jet, Δp_{jet} was examined, i.e. $p_{plenum} - p_{exit}$, where the absolute pressure p_{plenum} is given by $p_b + p_a$ the gauge blowing pressure plus atmospheric pressure. The pressure at the jet exit, p_{exit} is assumed to be the value given by the aerofoil pressure distribution at this point due to the local velocity , V_{exit}. (As the jets were located at 10% chord and the nearest static holes were at 8% and 12% chord, a straight-line interpolation was performed to obtain Cp_{exit}). Hence:

$$\Delta p_{jet} = p_{plenum} - p_{exit} = (p_b + p_a) - (p_\infty + \tfrac{1}{2}.\rho.U_\infty^2.Cp_{exit}) \quad .....(10\text{-}3)$$

As the tunnel static pressure, p_∞ is approximately equal to atmospheric pressure, p_a, the pressure difference Δp_{jet} can now be written as:

$$\Delta p_{jet} = p_b - (\tfrac{1}{2}.\rho.U_\infty^2.Cp_{exit}) \quad .....(10\text{-}4)$$

Figure 93 shows how the change in C_L varies with this change in pressure across the jet for four different angles of attack.

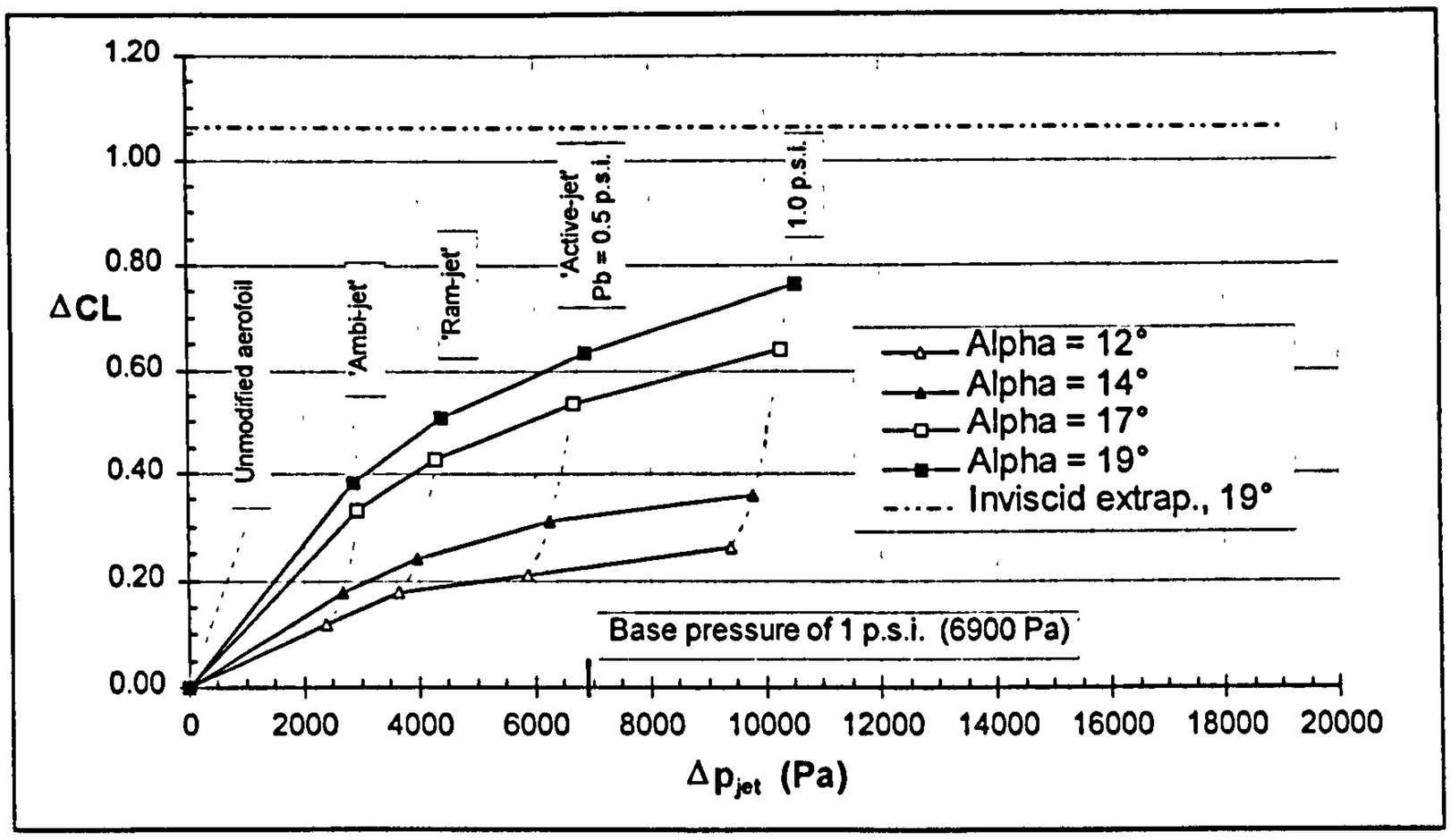

Figure 93 Change in C_L plotted against pressure across the jet

The lift curve has been extrapolated linearly for the angle of attack $\alpha = 19°$ and differenced with respect to the unmodified aerofoil, and is shown as 'Inviscid extrapolation, 19°' on the graph. It is the maximum value of ΔC_L that could be attained at $\alpha = 19°$. Just over one third of this is achieved by the 'Ambi-jet' and about half by the 'Ram-jet'. The gradient of these curves, $d\Delta C_L / d\Delta p_{jet}$ is decreasing with increasing pressure across the jet and so the law of diminishing returns applies to ajvg's.

One feature of the figure that must be pointed out is that the pressure across the jet increases with angle of attack, α, due to the reducing pressure at the location of the jet exit. This is illustrated by the dotted lines which join the points of constant blowing pressure.

Additionally, separate from an increase in blowing pressure, p_{plenum} directly increasing Δp_{jet}, a secondary, marginal increase in Δp_{jet} is also caused by the improved circulation reducing the surface pressure, p_{exit}.

10.3.2 Increase in lift coefficient due to jet velocity

Taking the idea of using ΔC_L as a performance parameter one step further, it was decided to see how this varied with the Velocity Ratio VR, the ratio of jet exit velocity, V_{jet} to the local velocity at the jet exit, V_{exit} . Compton et al (1991) and Henry et al (1994), showed that the vortex strength is a strong positive function of this ratio.

$$VR = V_{jet} / V_{exit} \quad \text{.....(10-5)}$$

The jet velocity, V_{jet} , is hard to calculate accurately, since there are a number of unknowns. Principally these are the pressure losses through the jet due to friction, the displacement thickness on the walls of the jet which causes the hydraulic area of the jet to diminish and the effect of compressibility on the air density. If the plenum is considered to be a reservoir a first approximation to the jet exit velocity is achieved by using Bernoulli's equation:

$$\Delta p_{jet} = p_{plenum} - p_{exit} = \tfrac{1}{2}.\rho_{jet}.V_{jet}^2. \quad \text{.....(10-6)}$$

Assuming incompressible flow ($\rho_{jet} = \rho_\infty$) and that the other aforementioned effects are minimal and substituting equation 10-4 we can rewrite this as:

$$V_{jet} = \sqrt{\{(p_b - \tfrac{1}{2}.\rho_\infty.U_\infty^2.Cp_{exit}).2/\rho_\infty\}} \quad \text{.....(10-7)}$$

It seems sensible to rewrite the absolute plenum pressure p_{plenum} , in terms of a pressure coefficient, Cp_b using the tunnel dynamic pressure as the denominator, in the same way that surface pressure coefficients are defined.

$$Cp_b = (p_{plenum} - p_\infty) / \tfrac{1}{2}.\rho_\infty.U_\infty^2 \quad \text{.....(10-8)}$$

Since we have an atmospherically vented wind tunnel we can write:

$$p_b = p_{plenum} - p_a \approx p_{plenum} - p_\infty = \tfrac{1}{2}.\rho_\infty.U_\infty^2\, Cp_b \quad \text{.....(10-9)}$$

substituting in equation 10-7 yields V_{jet} as being:

$$V_{jet} = U_\infty . \sqrt{\{Cp_b - Cp_{exit}\}} \quad \text{.....(10-10)}$$

The local velocity into which the jet is issuing, V_{exit} is given by Bernoulli as being:

$$V_{exit} = U_\infty \sqrt{\{ 1 - Cp_{exit} \}} \quad \text{.....(10-11)}$$

Hence

$$VR = \sqrt{\frac{Cp_b - Cp_{exit}}{1 - Cp_{exit}}} \quad \text{.....(10-12)}$$

Plotting the lift increment against this approximated jet velocity ratio (equation 10-12) shows that the former is a very strong positive function of the latter (Figure 94). This is indicated by the near unity values for Pearson's correlation coefficient, R^2 . At angles of attack greater than $\alpha = 19°$ as the modified aerofoil begins to stall it is to be expected that the gradient $d\Delta C_L$ / dVR will reduce and eventually fall to zero.

The usefulness of this finding is that, if found to hold for other air jet configurations, it could be used to quickly produce all air jet 'on' lift curves from the results gained at only one blowing pressure and the unmodified aerofoil. This would inevitably speed up the design of the full scale power control strategy.

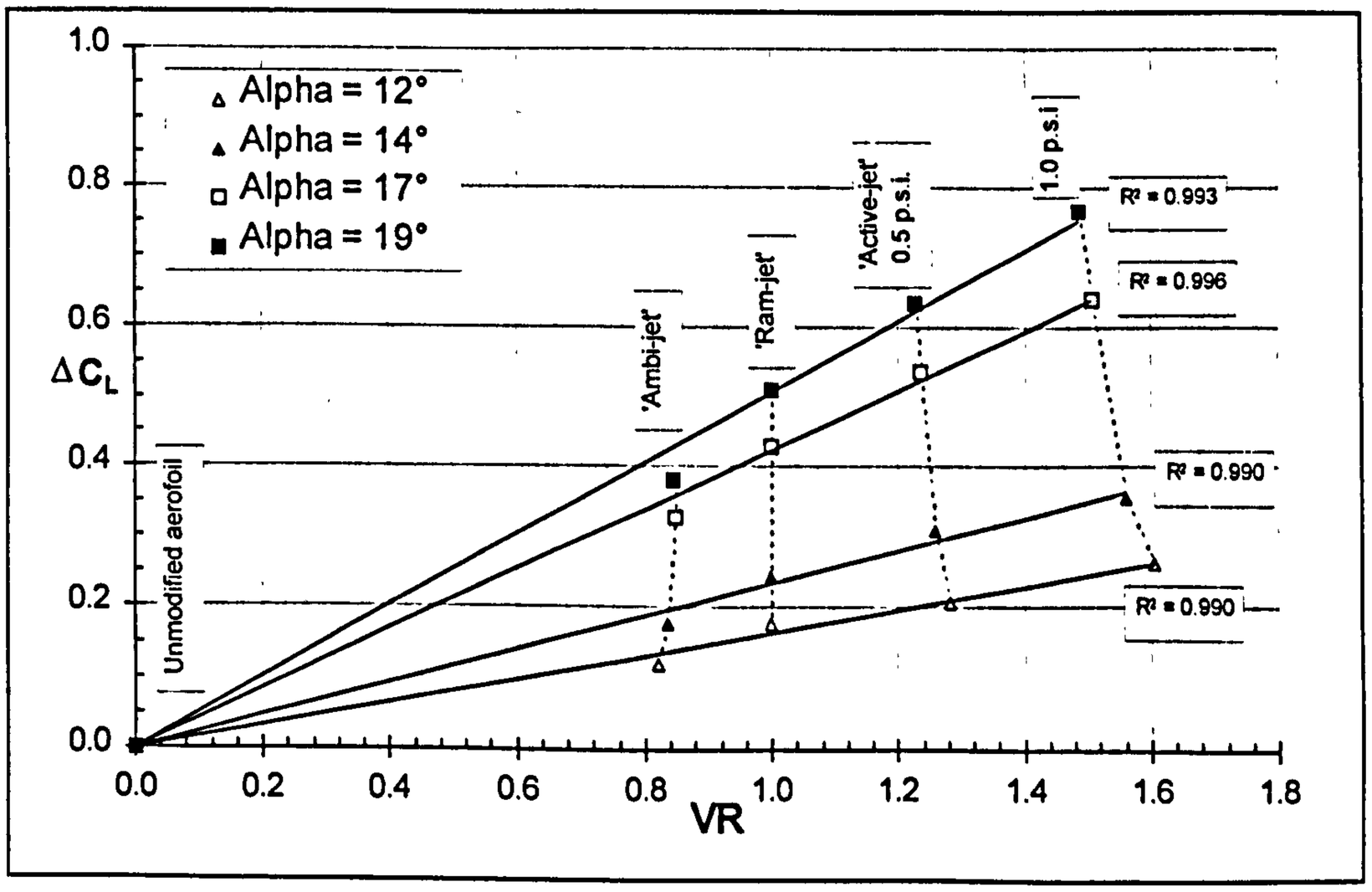

Figure 94 Change in C_L plotted against Velocity Ratio (determined by Bernoulli)

One of the critical issues for the success of air jet vortex generators for wind turbines will be how passive air jets perform at the lower velocities that are encountered near the hub (rotational speed).

Henry and Pearcey (1994) showed that the mass flow rate (jet velocity) is directly related to the location of the generated vortex above the aerofoil surface. It is therefore conceivable that performance will deteriorate if the vortices are centred too low or too high (due to jet velocity), in relation to the boundary layer height, for optimum mixing to occur. This could explain why all of the 'Ambi-jet' data (low air jet velocity) falls below the least-squares fitted straight line in Figure 94 above. It is an indication that air jet performance is not only dependent on the Velocity Ratio, VR, but also on the velocity of the air jet, V_{jet} or its mass flow rate, $\dot{m}$. If this is the case it is to be expected that the air jets will not operate as effectively at lower wind speeds (inboard sections of the blade), since the pressure across the jet, Δp_{jet} and implicitly, the air jet velocity, V_{jet} will be lower. Any future work should include tests at a lower free-stream velocity, U_∞ in order to determine the independent variable(s).

10.3.3 Ideal upper surface location of ajvg's

Here it is demonstrated that, in terms of the Velocity Ratio only, there will be an ideal upper surface jet location depending on whether the jets are driven by ambient air pressure ('Ambi-jets') or are driven by an active air supply.

If we install 'Ambi-jets', then from equation 10-9, $Cp_b = 0$ and so it is desirable to site them in the region of highest suction to obtain the maximum Velocity Ratio (equation 10-12). Interestingly, it appears that 'Ram-jets' ($Cp_b = 1$) need not be located in a region of high suction and may be located anywhere on the upper surface as the Velocity Ratio will remain constant. This could be of some use if the jets are tripping the boundary layer early. Finally, it would seem that powered jets should be located in a region of low suction (trailing edge) to obtain the highest Velocity Ratios because Cp_b now exceeds unity ($Cp_b = 3.03$ and 6.06 for blowing pressures of 0.5 p.s.i. and 1.0 p.s.i. respectively at $U_\infty = 43$m/s). Figure 95 shows how VR varies as a function of chordwise location and blowing pressure for an angle of attack of $\alpha = 17°$.

Figure 95 is only a simplification because it was constructed using the pressure distributions measured with the jets at 10% chord. In reality, siting the jets at a different chordwise location would produce slightly different pressure distributions and therefore different Velocity Ratios. However, the general trend of the graph can be relied upon.

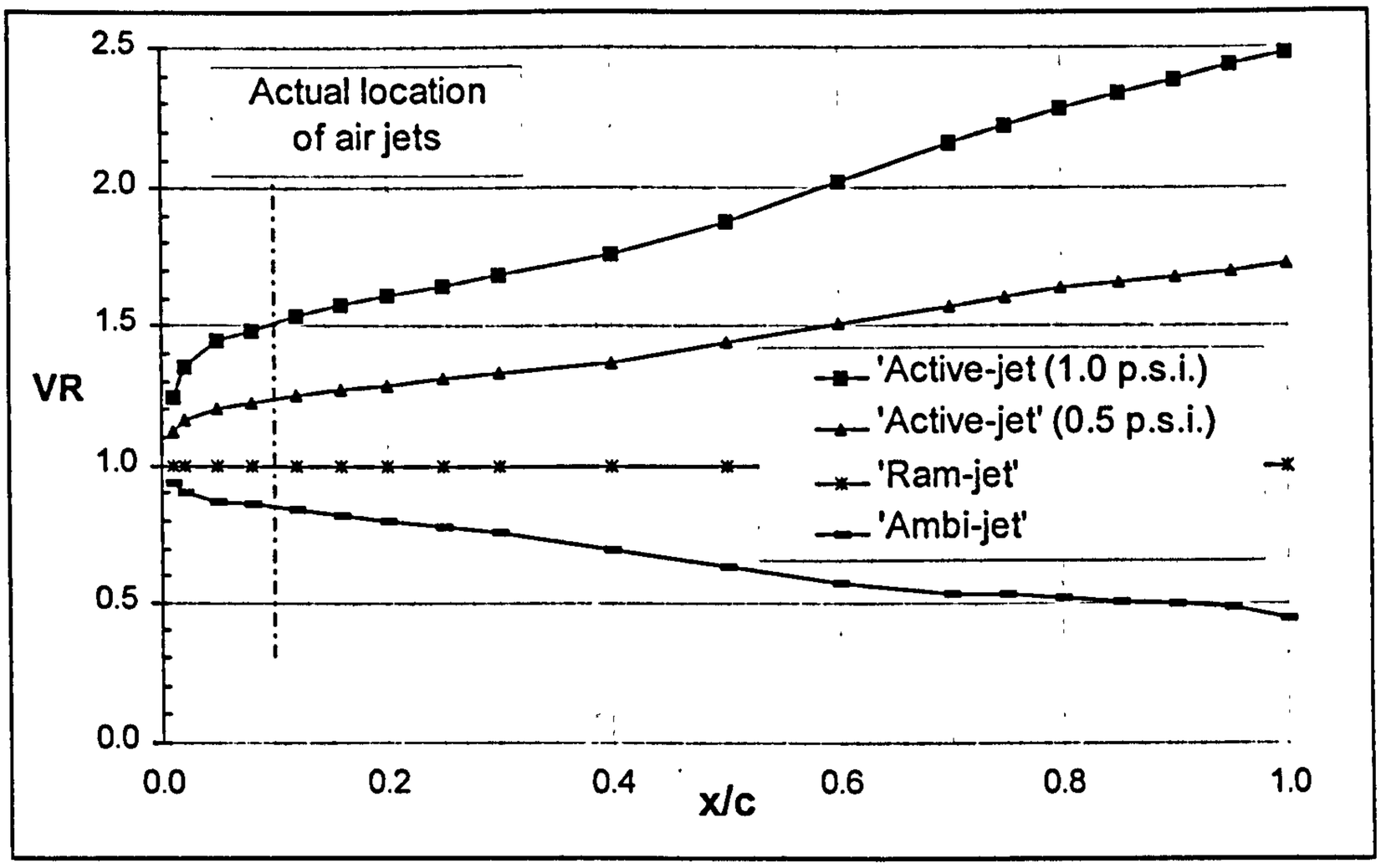

Figure 95 Velocity Ratio as a function of x/c and p_b at $\alpha = 17°$

This result indicates that for the NACA 63_2-2xx aerofoil, the 'Ambi-jets' are located at approximately the right location to generate vortices of maximum strength. For 'Active-jets' such as those used in the full scale trials however, quite the opposite is true and the Velocity Ratio can be significantly improved if the jets are located more towards the trailing edge.

These results should not be taken in isolation when determining the chord-wise location of air jets, though. The prime factor in effecting stall delay is more likely to be where the vortices are generated and not how strong the initial vortices are. For example, it is likely that the best place to generate vortices is somewhere near the leading edge because boundary layer mixing then occurs over most of the chord. This is inconsistent with 'Active-jets' which generate the strongest vortices at the trailing edge.

Although, the finding is probably not of utmost importance then, it could have its uses. For example if the jets are actively powered then it is possible that a greater degree of control could be attained at a more aft chordwise location because the Velocity Ratio changes more rapidly with blowing pressure. Also, a trade-off could be made between 'Ambi-jets' tripping the boundary layer early at a forward chordwise location, producing more drag and the reduced performance by moving them further back.

10.3.4 Effect of angle of attack on velocity ratio, VR

Another interesting feature is the way in which the Velocity Ratio changes with angle of attack for a given blowing pressure, due to the changing pressure distribution. Figure 96 shows that, generally, the Velocity Ratio increases and decreases for 'Ambi-jets' and 'Active-jets' respectively, with increasing angle of attack.

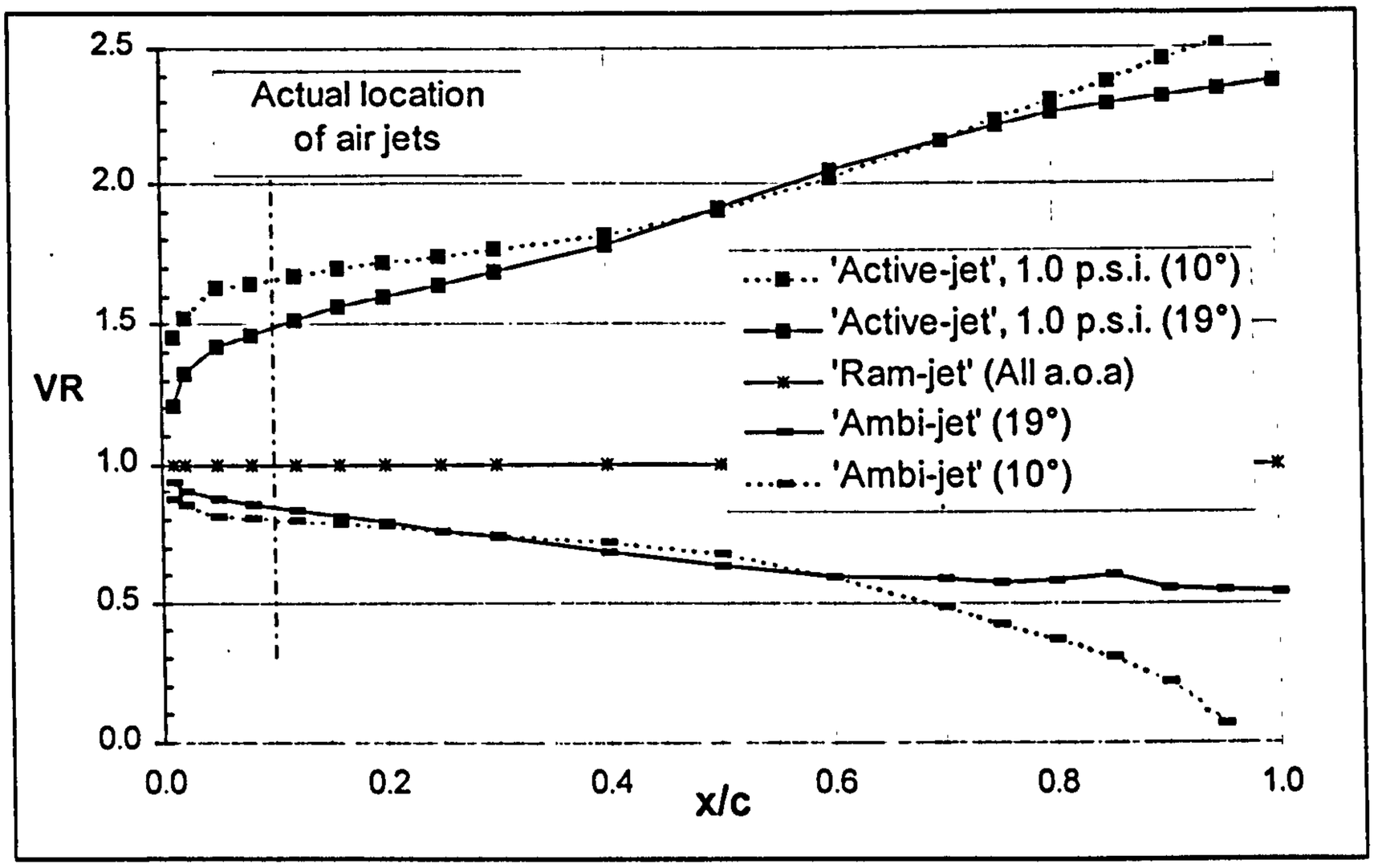

Figure 96 Velocity ratio as a function of x/c, p_b and α

It appears that there is a small detrimental effect on Velocity Ratio for 'Active-jets' at their current location since the Velocity Ratio is reducing with increasing boundary layer thickness (angle of attack).

Ambiguities such as those described are further complicated by the type of aerofoil on which air jets are to be installed. For example, how does leading or trailing edge separation affect the jet location? Also, what sorts of pressure distribution are most amenable to air jet installation? Obviously some aerofoils will be better suited to air jets than others and so these 'ideal' conditions need to be established. It is suggested that this sort of study is more suited to Computational Fluid Dynamics (CFD) than the wind tunnel, where solutions may be arrived at more quickly. It certainly seems to be a pre-requisite, however, that the type of blowing system (passive or active) should be decided before any such optimisation is undertaken.

10.4 Discussion of 'passive' air jets in relation to a wind turbine

As already described, the fitting of 'passively' supplied air jets would have two key advantages over 'actively' supplied jets. These are first and foremost that no external powering is required, except for perhaps a control mechanism. The second advantage is implicitly linked to the first in that because they do not require an external air supply they could, in theory, be mounted on the whole blade length.

The main disadvantage is that the low incidence drag penalty caused by the presence of the air jets is not counteracted by the drag reduction due to vortex mixing at 'passive' blowing pressures. However, the drag penalty is small and it has already been shown that the parasitic drag penalty may be lessened by reducing the jet exit size in relation to the aerofoil chord. It is not therefore unreasonable to expect that a further reduction in jet exit size may bring the jets 'on' drag in line with that of the unmodified aerofoil.

Apart from these 'advantages' and 'disadvantages', there are still three 'unknowns' which may or may not preclude a 'passive' system from being successful. These are:

1. Over how much of the blade could 'passive' ajvg's be installed in reality?
2. How may 'passive' ajvg's be controlled?
3. How quickly can they respond to a change in wind speed?

In addition to these factors, the effect of relative wind speed, V_r must be considered. For example, near the root the rotational speed is very low. The dynamic pressure available to drive 'Ram-jets' may therefore obviate their usefulness and it may be better to have a hybrid system of 'Ambi-jets' near the root and 'Ram-jets' further out along the blade.

In the following sections it is described how 'Ambi-jets' and 'Ram-jets' may be installed on a wind turbine and an attempt is made at answering these questions.

10.4.1 'Ambi-jets'

We might think that both 'Ambi-jets' and 'Ram-jets' could be located over the whole length of the blade. For both types of passive jet though, it is not practical to install jets on the movable tip of the blade because control would be difficult. In any case it is desirable to maintain a lower C_{Lmax} at the tip for the control of peak power in high winds. For the Ecotecnia machine both types of passive air jet would therefore be limited to between 2.5 metres and 8.8 metres blade radius (25 to 88%), where the blade and tip-brake begin respectively.

As for the supply and control of 'Ambi-jets', it is envisaged that an air 'collector' could be formed in the spinner at the hub. The air would then be split three ways in a similar manner to that employed in the field tests (Figure 97). This would not affect the velocity ratio (equation 10-12) because free stream static, $p\infty = pa$ does not change with blade radius and so Cpb (equation 10-9) is always zero.

To allow maintenance (i.e. the spinner should be hinged at its base to allow a mechanic to stand in it) the large initial pipe must be easily disconnected prior to the three way split. This is easily accomplished by using flexible piping fastened with nothing more than a Jubilee clip at either end.

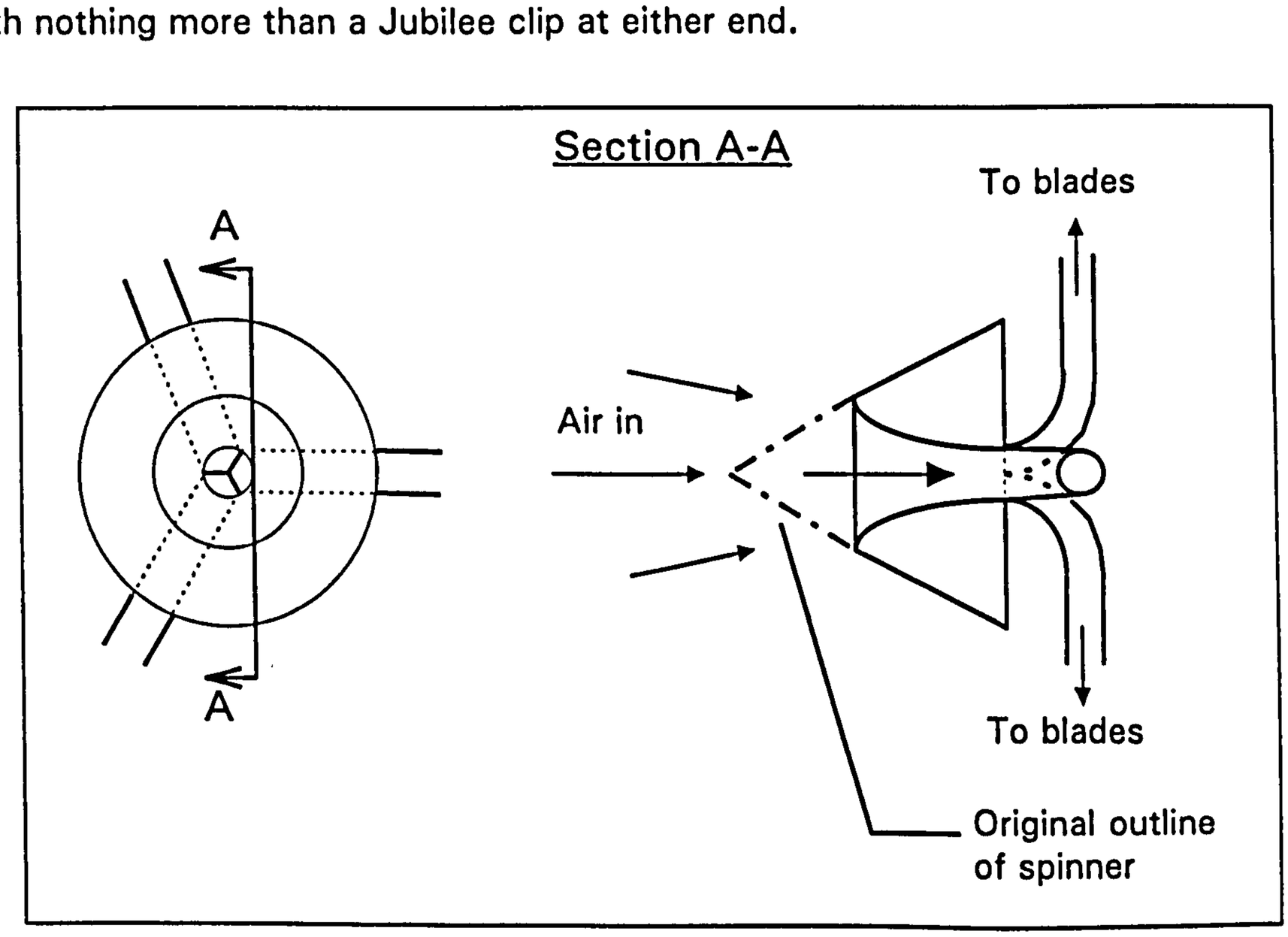

Figure 97 Possible modification to spinner

To control the power output, two different methods are visualised. In both methods all the 'Ambi-jets' would be 'on' up to rated power. Thereafter the first and simplest method of control would be to have a valve just prior to the three way split to control the mass flow rate. The second, and technically more complex, method would be to increasingly shut off more sections of blade allowing these parts to stall. This could be accomplished by further sub-division of the pipe following the three way split. Each additional pipe would now supply air jets to a fraction of the blade and would be controlled with a gate valve. However, the number of individual sections into which the blade could be practically split is limited. This method is not therefore conducive to a rated power which is constant with increasing wind speed.

Obviously the first method above is preferable to the second but the problem lies in predicting how much to close the valve in order to achieve the desired power level and it is likely that in this case a 'suck it and see' approach will be required. An adaptive system would be most desirable, whereby as the blades get dirtier, less and less regulation of the air supply is made. This is because, when the blades are clean, the air supply must be regulated otherwise the rated power is exceeded. However, when the blades become dirty more air must be supplied to the jets before rated power is reached. Such a system would allow the energy savings that were discussed in the previous chapter to be made.

If such a system were developed, the flow of air at high winds could perhaps be based on recent averages of the power curve when the jets were 'off'.

If a simpler system is required, a particularly novel way of controlling the air supply, other than using an electrically operated valve, would be to use a furling mechanism located in the air collector. This could be designed to start automatically restricting the flow of air at rated wind speed and completely shut off the air supply to the blades in high winds.

Let us now consider how an array of 'Ambi-jets' may affect the power curve of the test machine. The prediction program uses 5% radius for the element size and it has already been stated that jets could be located between 25% and 88% blade radius. It is therefore assumed in this example that they are located between 25% and 85% of the blade. Figure 98 shows how 'Ambi-jets' would compare to the prediction for the 'Active-jets' at 1.0 p.s.i. which were fitted to the test machine between 55% and 75% blade radius. It appears that the two cases would be virtually equivalent prior to rated wind speed. Once the power required to supply an array of 'Active-jets' is considered then it is clear that 'Ambi-jets' would be chosen.

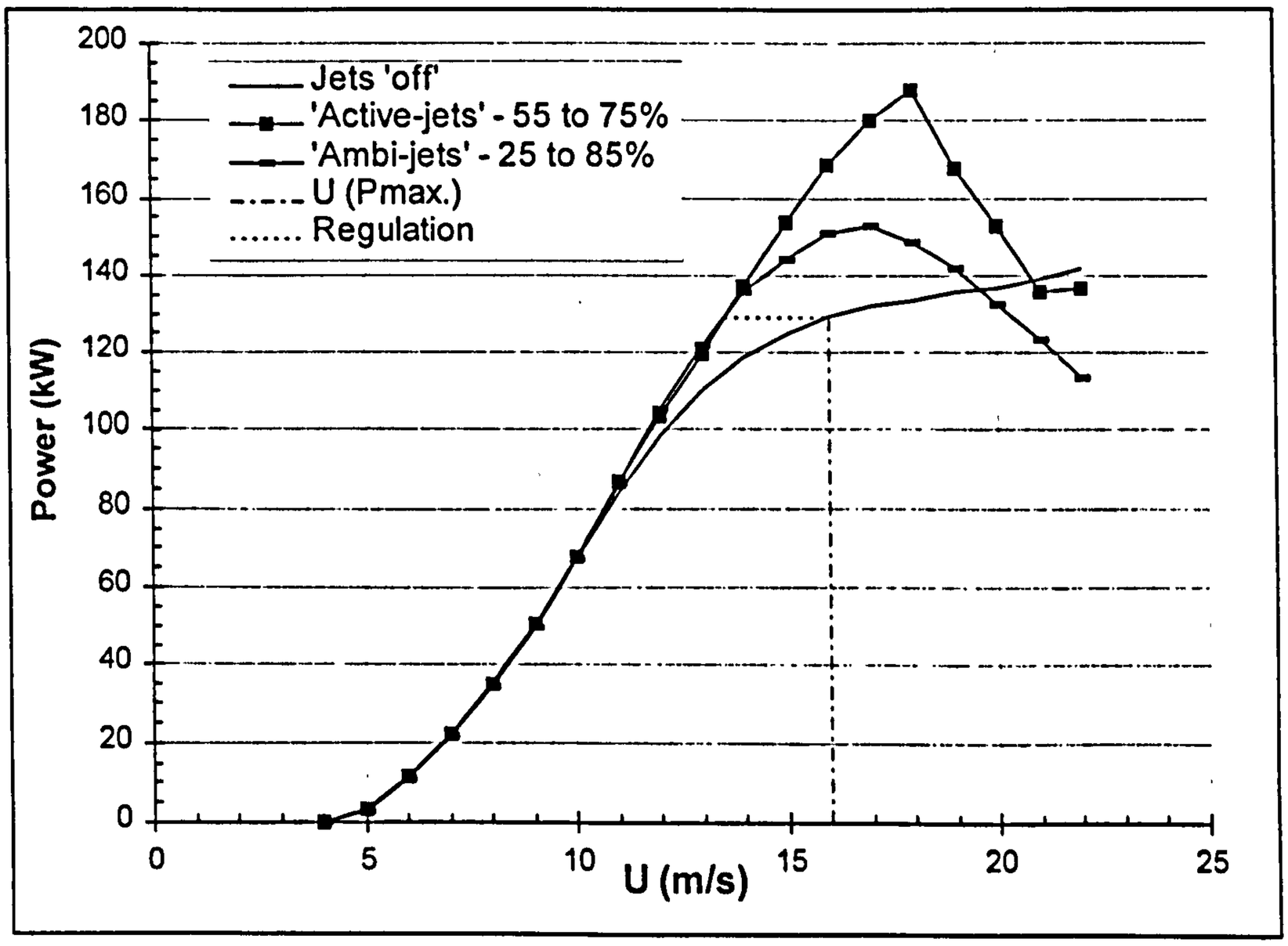

Figure 98 Predicted modification to power curve by 'Ambi-' and 'Active-jets'

The above cannot be concluded firmly though. Firstly, the actual improvement obtained in the field tests was lower than predicted. In the above example, 'Ambi-jets' cover more of the blade and so the improvement might not be as great as with 'Active-jets' because the two cases are not relative. Secondly we do not know how the performance of air jets changes with blade properties such as thickness, Reynolds number and wind velocity etc. The result is promising, nevertheless. (NB. The tail of the power curve drops below the unmodified value at high wind speeds because the elements containing air jets have not been modified by the 3D correction; refer to 'Option 2', section 7.6).

10.4.2 'Ram-jets' for wind turbines

'Ram-jets' are different from 'Ambi-jets' and 'Active-jets' in that the pressure behind the jets, or what would be the equivalent plenum pressure, is a function of wind speed and rotational velocity. The dynamic pressure, q, available to drive the jets is given by the wind speed and the rotation of the blade.

$$q = \tfrac{1}{2}.\rho.(U_\infty^2 + V_r^2) \quad \text{..... (10 -13)}$$

Figure 99 shows how dynamic pressure, q, varies with blade radius and wind speed for the Ecotecnia machine (rotational speed = 51 r.p.m.). The pressure available to the jets would be slightly less than this because any losses, that would be incurred as the air passed through the blade from lower to upper surface, would need to be taken into account.

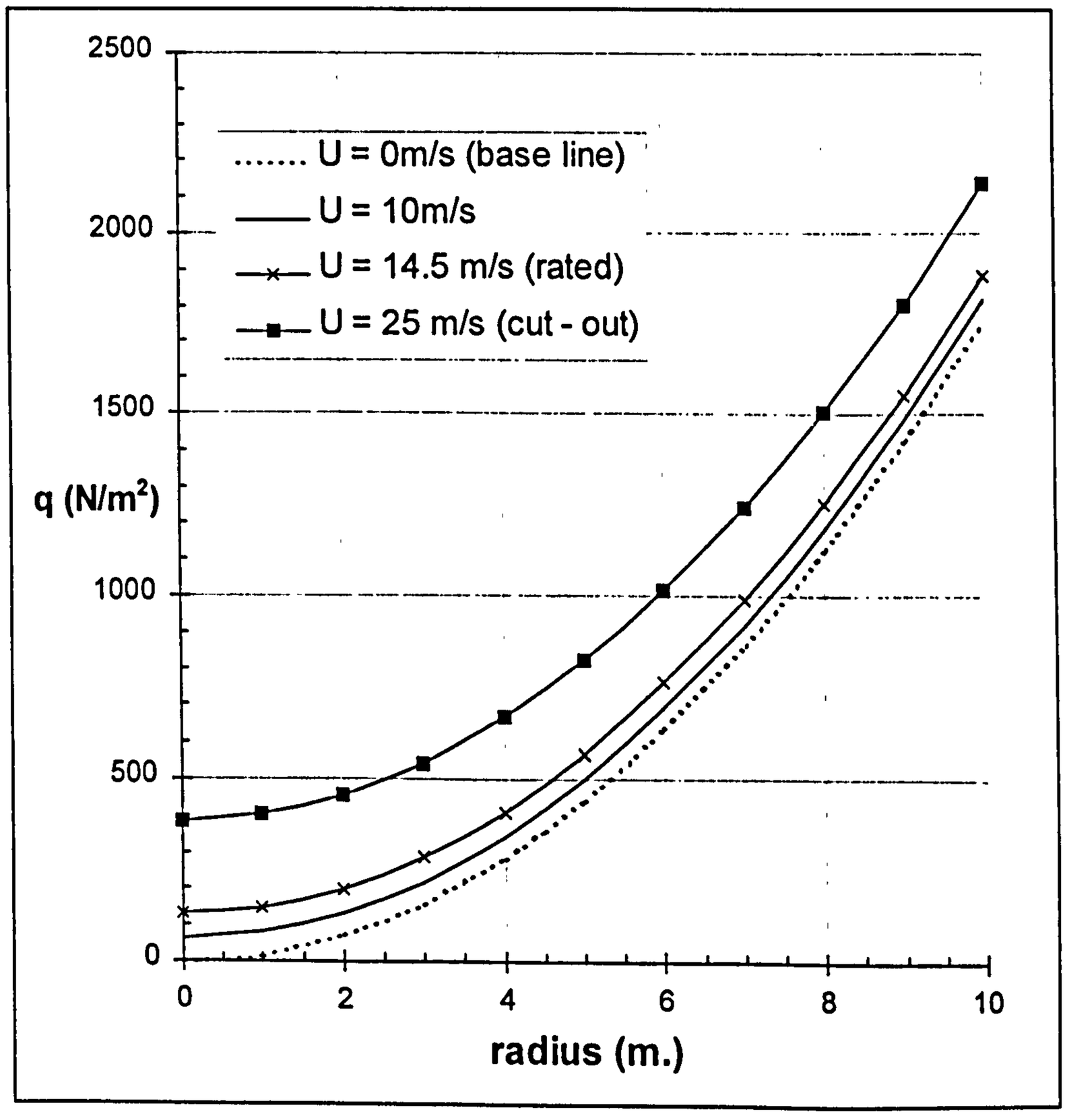

Figure 99 Dynamic pressure variation with blade radius and wind speed

Below wind speeds of 14.5m/s (rated wind speed) where air jets are required to work it can be seen that wind speed has little bearing on the dynamic pressure and rotational velocity is dominant. Even at 50% blade radius (5 m.) though, the dynamic pressure available is only about 500 Pa for this machine. Once losses through the jets and drag due to holes on the blade lower surface are considered it is unlikely that 'Ram-jets' would yield better performance than 'Ambi-jets' where, as discussed, the air would come from the hub in a larger pipe and no lower surface holes would be required.

It therefore appears that it would probably not be worthwhile installing 'Ram-jets' on the inner part of the blade. Studies would need to be made to determine an appropriate blade radius where it becomes more beneficial to use 'Ram-jets' rather than 'Ambi-jets'. This will be machine and blade specific.

In fact, a hybrid system of 'Ambi-jets' on the inboard sections of the blade and 'Ram-jets' on the outboard sections would seem to be the ideal combination. The 'Ambi-jets' would be used principally for increased energy capture by obtaining rated power at a lower wind speed. However, they would be of little use for power regulation because the lower torque supplied by the root would mean slow regulation of power. Parts of the blade nearest the root would be stalled by rated wind speed anyway, even with air jets installed.

The power regulation could be provided by 'Ram-jets', located nearer the tip. These would provide rapid changes in torque because of their spanwise location and therefore fast regulation of power. 'Ram-jets' have the advantage over 'Ambi-jets' for power regulation in that the air does not have to travel very far before it is coming out of the jet and over the aerofoil surface (through the blade). Thus control of the blade torque would be achieved as soon as air supply to the jets was limited. A greater range of torque variation is also possible due to the improved lift curve of 'Ram-jets' compared with 'Ambi-jets'.

The most difficult aspect would be the control of air through the jets. Again two systems could be envisaged. The first would be controlled by the turbine processor (power or torque dependent) operating a mechanism which partially or fully obstructs the flow of air through the blade. The second would be to use the power of the wind to close, or partially close, the jets during a gust (possibly a small furling mechanism). This may be preferable because it would eliminate or reduce

the response of the blade to a gust occurring and thus attenuate the torque loading on the drive train. If the system is very fast it may be possible to reduce the effect of tower shadow. By 'very fast' the system would have to respond in say 18° of arc on a machine rotating at say 30 r.p.m., which equates to 0.1 seconds.

However, the question that must then be answered is; how complicated do we allow the system to become? It must be borne in mind that if mechanisms are put inside the blade, they must be easily accessed for maintenance, probably at least once in the blade's life-time.

10.4.3 'Active-jets' for wind turbines and other applications.

For a given blowing pressure, the coefficient Cp_b (equation 10 - 9) will reduce with wind speed. This means that unlike 'Ambi-jets' and 'Ram-jets', the velocity ratio (equation 10 - 12) and hence vortex strength will reduce with blade radius. Even at the beginning of the tip brake though, the use of 'Active-jets' as opposed to 'Ram-jets' can still be warranted because the coefficient of blowing pressure is significantly greater than 1.0 for a blowing pressure of 1 p.s.i. ($Cp_b = 5.1$).

For high operating speeds such as those experienced by an aircraft this is not the case, since, for a blowing pressure of 1 p.s.i., Cp_b becomes unity at a speed of approximately 106 m/s and so 'Ram-jets' could be used instead. Of course this is very much dependent on the blowing pressure of any 'Active' system and whether the air jets would be required for the whole flight or during take off and landing only when the speed is much lower and a higher Cp_b could be obtained.

11. SUMMARY AND CONCLUSIONS

11.1 Air jet vortex generators.

A NACA 63- series blade section was tested in 2D and modified with two configurations of air jet vortex generators at a Reynolds number of 1.4 million. The Williams aerofoil analysis code was used to check the unmodified aerofoil characteristics (transition free) and then to aid the choice of a suitable transition strip.

The first configuration of ajvg's increased C_{Lmax} from 1.17 to 1.71 at the blowing pressure of 1.0 p.s.i. (6900Pa) but also produced an associated increase in C_{Dmin} . The jets were able to reattach a separated flow, which is not the case with vane vortex generators, and this reattachment was instantaneous.

Since the wind tunnel model was a scale model of the blade, the air jets should have been scaled up in size for their full scale installation. However, it was considered that the mass flow requirement could be reduced if the jets were reduced in both length and width whilst still maintaining a spacing based on their length. It was also considered that the low incidence drag may be reduced because the size of the jets, which are in effect roughness elements, would be reduced relative to the chord length.

The second configuration tested was at the same chordwise location, had the same skew and pitch, was of the same aspect ratio and had the same spacing based on jet length as the first. Only the length and width of the jets changed and these were both scaled by 75%.

The second configuration increased C_{Lmax} further to 1.81, an increase of 55% over the unmodified aerofoil at a blowing pressure of 1.0 p.s.i. Most importantly though, the minimum drag, C_{Dmin} was reduced to that of the unmodified aerofoil at the same blowing pressure. It was also found that the reduction in mass flow per jet corresponded to the reduction in jet exit area (43.7% ± 3%). Though the actual total reduction per unit length of jet array is only 25% because of the spacing being reduced.

These two results are considered to be extremely important for the further optimisation of air jets since an improvement in aerodynamic performance was achieved with a reduction in the equivalent system power requirement. For such a large improvement in performance for a relatively minor change to the configuration, it is not unrealistic to expect that further optimisation of air jet vortex generators can be achieved.

After the full scale testing, further wind tunnel tests were carried out to determine a minimum successful blowing pressure. First 'Ram-jets' were modelled by blowing a pressure equivalent to the tunnel dynamic into the plenum chamber of the model. In practice 'Ram-jets' could be achieved by allowing air to flow through the blade from its lower surface, near the stagnation point, to air jets on the upper surface. Following these tests, the pipes supplying air to the plenum chamber were completely disconnected and left open to atmospheric pressure. These were referred to as 'Ambi-jets' and in practice could be achieved by allowing air to flow from a collector at the hub through pipes inside the blade to jets on the blade surface.

Both these configurations increased C_{Lmax} over and above that of the unmodified aerofoil (33% and 22% for the 'Ram-jets' and 'Ambi-jets' respectively). Although reducing the blowing pressure was at the expense of increasing C_{Dmin} .

In the case of the 'Ambi-jets' air is actually being pulled through by the suction on the upper surface of the aerofoil to generate vortices. Depending on the application these may be preferable to 'Ram-jets' because they do not require holes on the lower surface which would increase minimum drag. Also it has been demonstrated that the dynamic pressure available is less than 500Pa on the inner half of this blade (or any blade with roughly the same tip speed of 53 m/s). Once losses through the 'Ram-jets' are considered, it is doubtful that they would be more effective than 'Ambi-jets' on the inner part of the blade.

It was suggested that an optimum combination may be to have 'Ambi-jets' on the inner part of the blade and 'Ram-jets' on the outer part. The 'Ambi-jets' would lead to a reduction of the rated wind speed, thereby increasing energy capture whilst the 'Ram-jets' on the outer part would provide power regulation.

The results also indicated that the increase in C_{Lmax} over the unmodified aerofoil was proportional to the velocity ratio (jet exit velocity divided by local velocity into which jet is issuing). Although this was calculated using Bernoulli's equation and did not take into account losses, this relationship could provide a good starting point when determining a control strategy from measurements of the lift curve at only one or two blowing pressures.

11.2 Full scale testing

A blade element theory power prediction program was written in order to locate the air jets on the blade (55 to 75% blade radius) and determine the expected effect on the power curve. The air jet system was designed and the power required of a fan to supply air to the jets was calculated. The electrical system was designed by the turbine manufacturers.

A blade set was then modified with air jets and the control equipment manufactured for the Ecotecnia 20/150 stall regulated wind turbine. The jets used were roughly equivalent to the second configuration in scale (aerodynamic characteristics) but were the same size as those of the first configuration (mass flow requirement).

The full scale trials were carried out in Tarifa, southern Spain. First the jets were tested at a reduced blade setting angle (0.0°) in order that the rated power of the machine was not exceeded. However, it was realised that the jets were now in the wrong place on the blade and effectively too far out to influence the power curve before rated power.

The blades were then restored to almost their original blade setting angle (2.3°) and the power curve measured again. It was clearly demonstrated that the air jets had increased power production before rated wind speed. This is the most important result because it means that air jets have the potential to increase the energy capture of a stall regulated wind turbine.

It was also shown that the air jets were able to operate even though the blade had become dirty. It is suggested that to take advantage of this, the control strategy should be adaptive, i.e. the blowing strength is only reduced once maximum power is reached and not fixed beforehand. Such a system would also allow factors which may adversely affect power output, such as air density and wind direction (turbulence intensity) to be taken into account. Rather than simply take account of any extra energy produced then, we should also consider the energy which would not be lost by installing a system of air jets. In other words, the difference in annual energy yield between a turbine with air jets and one without would be greater than that calculated by just considering the 'clean blade' power curves. The ability of jets to overcome blade dirt would be of most benefit in climates such as Spain and Greece, where rainfall, which helps with blade cleaning, is rarer.

This work originates from a demonstration project of limited time-scale. As such, a number of compromises were made in the design of equipment for the 150 kW test machine, which would not need to be made on the larger more recent commercial sizes of wind turbine. For example restricted internal blade space which lead to large pressure head losses. For these reasons and the fact that the air jets are not yet optimised, the fan's power requirement of 5.5 kW should be noted but not taken as an absolute measure of that which is required. Indeed, the wind tunnel results show that it should be possible to eliminate the fan altogether by using the aforementioned 'Ambi-jets' or 'Ram-jets'.

It was also demonstrated in the wind tunnel that air jets can be controlled so that a family of lift and drag characteristics can be achieved. Furthermore, the air jets reattached separated flow instantaneously. Applying these two findings to a wind turbine it should be possible to achieve a degree of power regulation in high winds. Although the control system to do this was built and installed, lack of project time meant that this aspect was not demonstrated at full scale.

11.3 Future Work

The issue that is central to whether or not air jets have a role to play in the performance and control of wind turbines is their supply requirements. If they can be optimised such that the drag penalty with passive blowing can be reduced or eliminated or they can be operated by a fan with a fraction of the current power consumption, then the answer is that they do.

In the short term existing blades could be modified to incorporate air jets for improved energy yield. In the longer term, the impact of air jets being used to completely redesign the blade should be envisaged. For example, it is possible that blades could be designed with smaller chords, saving structural costs due to reduced maximum park loads. Thus, to fully exploit air jet technology commercially it needs to be flexible enough that:

1. Existing blade designs can be easily upgraded at the point of manufacture in an optimised configuration.
2. The potential exists to design new blades which use the benefits of air jets as wind turbines inevitably become larger.

Both of the above require a highly adaptable, fast and efficient design tool, namely the computer. It is therefore proposed that a CFD study of the problem be undertaken which, combined with further experimental and full scale testing, will help to bring this innovative concept to market quickly. The problem may be tackled in any number of ways. One such method is given in the flow chart Figure 100 and is described in this section.

11.3.1 Phase 1: Optimisation of the air jets

The first stage would be to model the existing wind tunnel results numerically in two dimensions. With these results validated, the model can then be used to optimise the design of air jets. By building a wind tunnel model of a different aerofoil family a second validation of the numerical model for the non-rotating case can be obtained.

Prior to this though, the question of whether circular or rectangular jets produce the strongest vortices has to be answered. As described in section 2.3.6, doubt exists in this area. This question could be answered with the current wind tunnel model and would preclude the need to construct two different grids in the

computational work. Wind tunnel tests at different wind velocities should also be carried out to provide additional information for the CFD model.

Although this phase has been referred to as an optimisation it is really an evaluation and validation process because certain variables such as chordwise location will probably alter according to the radial location and type of blowing used (passive or active). It is more important to determine which variables are the key ones with respect to aerodynamic performance for a given mass flow. For example how small can the air jets be made in relation to the aerofoil chord whilst still retaining their effectiveness? Spacing of the jets is another important factor because of the desire to place them as far apart as possible without degrading performance.

The most difficult part of the proposed work will be to transfer the numerical model to the rotating case and model the existing full scale results. However, it should be possible to do this with the following tools (Voutsinas, 1996):

1. A 3D unsteady model which predicts the flow over the whole rotor.
2. A 3D solver of the Navier-Stokes turbulent equations.
3. A mapping model which will determine the vortex intensities of the air-jets based on a numerically generated database.

The first two of the above already exist and the third is the numerical model used above. Additionally, complementary results could be obtained from the pilot machine to aid this process. For example every other jet could be sealed so that the CFD tool has an extra set of data regarding jet spacing. Different lengths of the array, say the outer 50%, could also be sealed in order to gain more information about how control may be achieved.

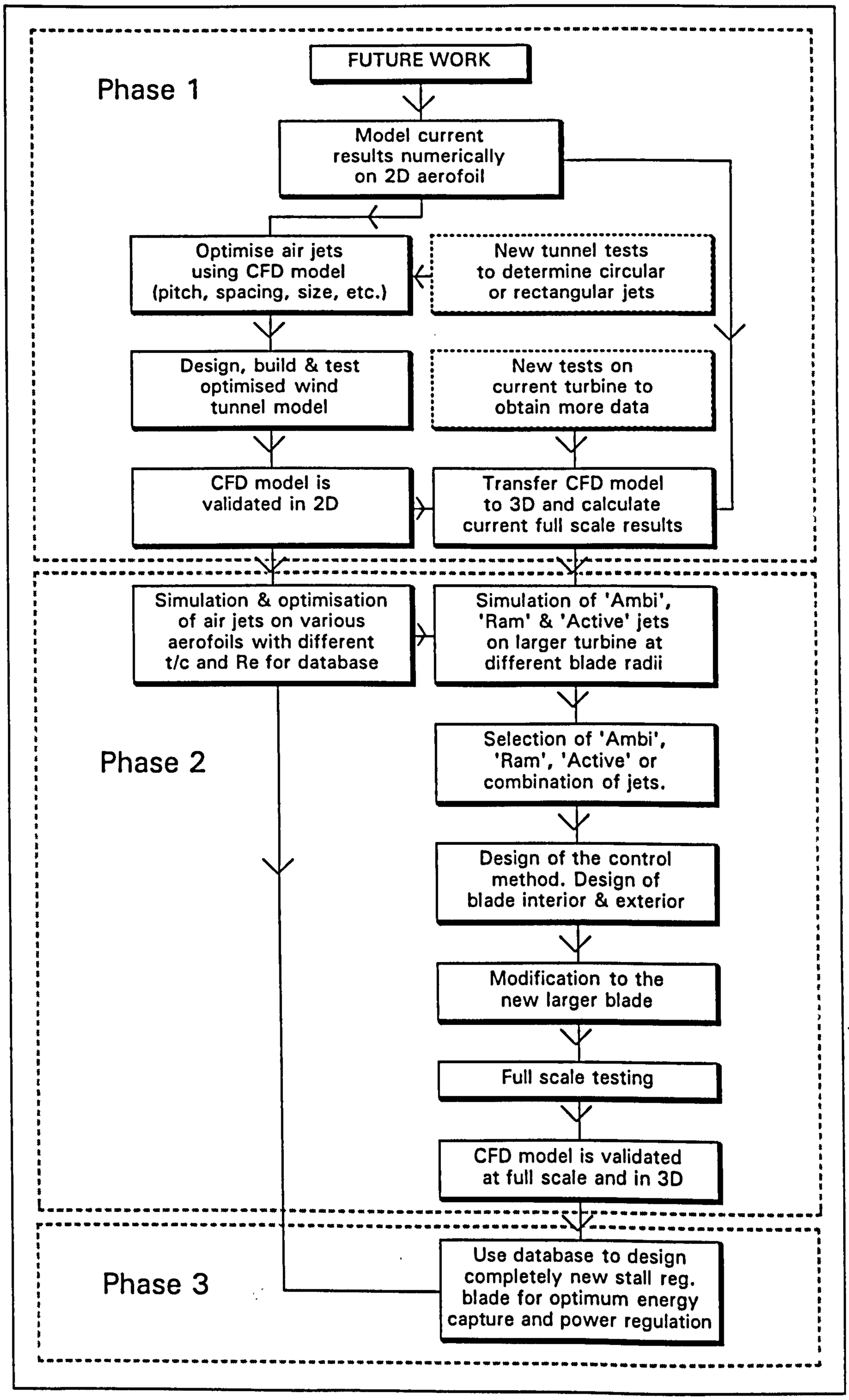

Figure 100 Flow chart for proposed future work

11.3.2 Phase 2: Second full scale validation of 3D model

The second phase would be to build and test a modified blade set and its control equipment. This validates the CFD model for the rotational case.

It is recommended that the test wind turbine should be of a more modern commercial size i.e. 500 to 750kW rated power. There are two main reasons for this. The first is that the results will be immediately applicable to the most popular class of wind turbine. The second is that the later machines are more efficient and so a truer picture of benefit will be obtained. Another advantage would be the larger space inside the blades for possible control equipment and for reduced pressure losses due to friction.

At this juncture the flow of air through the aerofoil from lower to upper surface needs to be modelled to see if 'Ram-jet's' are a viable proposition. The jet exit should also be modelled and the losses minimised for all types of air jet. Due regard should be paid to the varying blade shell thickness as it varies along the blade.

Many simulations must then be undertaken with the numerical model to build up a database of how performance changes with aerofoil thickness, Reynolds number (rotational velocity) and with different aerofoil families. The blade can then be optimised for the cases of 'Ambi', 'Ram' or 'Active' jets. In the case of passively blown jets it may be beneficial to have jets at two chordwise locations and this should also be investigated.

A number of possibilities for the control system may be entertained. Among them are the following:

1. Air jets arrays at different radial blade stations could be shut off in different combinations, say 10% blade lengths.
2. All air jets are kept 'open' but the flow is reduced. For 'Ambi-jets' this could involve closing an air collector at the hub. For 'Ram-jets' a simple push-pull slide mechanism could be considered to obscure the intakes.

Once the control method is selected, the design, construction and testing of the blades can be undertaken. It is possible that the blades could be more carefully designed internally so that jets may be placed in a variety of locations. The jets not

under test could be sealed and opened at a later time if more test results are required. This was not done in the pilot project because the blade manufacturer was not directly involved.

The power curve should be measured according to the pre-determined control strategy. This should be compared to the numerical predictions and the control system software should then be 'tuned' as required. A database of different rotating cases, such as different blade setting angles and different control strategies should be built up so that the numerical model can be verified.

Noise measurements should be undertaken as this will have a big influence on the application of air jets in sensitive areas. Such a study was not undertaken in the pilot project chiefly because the fan was not housed, which it would be in any commercial application (if required). At the end of this phase, a fully validated numerical model will exist for the optimisation of air jets in a wind turbine application.

11.3.3 Phase 3: Design of a new blade.

In this final phase the CFD model should be used to design a completely new blade as opposed to using ajvg's to modify an existing blade.

Particular emphasis should be placed on investigating how to use ajvg's in designing blades that have smaller chords and are therefore of a relatively thicker section. This will lead to lighter blades and lower extreme loads. It is likely that ajvg's can change the characteristics of some aerofoil profiles more drastically than others, so the benefits of pairing air jets with aerofoils currently used for wind turbine blades such as the NACA and SERI families should be examined and optimised. For example, one design criteria is that outboard sections of blade should have a limited C_{Lmax} so that peak power may be controlled in high winds. This inevitably degrades performance at lower wind speeds but by using an air jet system it is possible to have high a C_{Lmax} in low wind speeds and a low C_{Lmax} in high wind speeds. Other aims of this phase would be to determine the limits of air jet use, to produce guidelines for using the CFD tool and package it for industry use.

As this brief analysis shows, this thesis has probably asked more questions than it has answered. However, it is hoped that this work will, at the very least, act as a guide in the application of *Air Jet Vortex Generators For Wind Turbines*.

REFERENCES

Abbott, I.H. & von Doenhoff, A.E (1959)
'Theory Of Wing Sections'
Dover Publications, New York.

Afjeh, A.A., Keith, T.G. and Ardeshir, F. (1990)
'Predicted aerodynamic performance of a horizontal axis wind turbine equipped with vortex generators'
Journal of Wind Engineering and Industrial Aerodynamics, Vol. 33, pp. 515 -529

Antoniou,I.,Petersen, S., Øye, S.,Westergaard, C.,Raben, N. and Jensen, F. (1996)
'The Elkraft 1MW wind turbine: Results from the test program'
Proc. European Wind Energy Conference., Gothenburg, Sweden, 1996.

Bloy, A.W. and Roberts, D.G. (1993)
'Aerodynamic characteristics of the NACA 63_2-215 aerofoil for use in wind turbines'
Wind Engineering, Vol. 17, No. 2, pp 67-75

Boeing, (1982)
'Mod-2 Wind turbine system development final report, Vol. II Detailed report'
NASACR-168007, DOE/NASA/0002-82/2

Bosschers, J., Montgomerie, B., Brand, A.J., and van Rooy, R.P.J.O.M. (1996)
'Influence of blade rotation on the sectional aerodynamics of rotating blades'
Proc. 22nd. European rotorcraft forum, Vol. 1.,Brighton, England.

Compton, D.A. and Johnston, J.P. (1991)
'Streamwise vortex production by pitched and skewed jets in a turbulent boundary layer'
AIAA paper 91-0038

Corrigan, R.D. and Savino, J.M. (1985)
'Vortex generators as a means for increasing rotor performance'
Proc. 20th. Inter-soc. Energy Conversion Engineering Conf., Vol.3, pp.3.663-3.668, Miami, USA.

Eggleston, D.M. and Stoddard, F.S. (1987)
'Wind turbine engineering design'
Van Nostrand Reinhold, New York

Engineering Sciences Data Item No. 70015 (1972)
'Fluid forces and moments on flat plates'
ESDU International, London.

Freestone, M.M., (1985)
'Preliminary tests at low speed on the vorticity produced by air jet vortex generators'
RM 85/1, Dept. of Aeronautics, City University, London.

Freris, L.L. (1990)
'Wind energy conversion systems'
Prentice Hall International (UK) Ltd., Herts., England.

Garrad, A.D. (1985)
'The use of vortex generators to improve wind turbine performance'
Report 135/R/1, Garrad Hassan and Partners, Bristol, England.

Gyatt, G.W. (1986)
'Development and testing of vortex generators for small horizontal axis wind turbines'
DOE/NASA/0367-1, NASA CR-179514, AV-FR-86/822

Henry, F.S. and Pearcey, H.H. (1994)
'Numerical model of boundary layer control using air jet generated vortices'
AIAA journal, Vol. 32, no. 12, pp 2415 -2425

Hill, D.C. and Garrad, A.D. (1989)
'Aerofoils for pitch controlled horizontal axis wind turbines'
Department of Energy, RN 160/R/7

Himmelskamp, H. (1945)
'Profile investigations on a rotating airscrew'
PhD. thesis, Gottingen, Germany

Houghton, E.L. and Carruthers, N.B. (1982)
'Aerodynamics for engineering students'
Third edition, Edward Arnold, London. pp 353 - 354

Innes, F (1995)
'An experimental investigation into the use of vortex generators to enhance the performance of a high lift system'
PhD. thesis, City University, London.

Innes, F., Pearcey, H.H. and Sykes, D.M. (1995)
'Improvements in the performance of a high lift system by the application of air jet vortex generators'
RAeS Aeronautical Journal, August/September 1995.

Johnston, J.P. and Nishi, M. (1990)
'Vortex generator jets - Means for flow separation control'
AIAA journal Vol. 28, no. 6, pp. 989 -994.

Milborrow, D.J. (1978)
'Performance prediction methods for horizontal axis wind turbines'
Wind Engineering, Vol. 2, No.3, pp. 165- 175.

Milborrow, D.J. (1985)
'Changes in aerofoil characteristics due to radial flow on rotating blades'
Proc. 7th BWEA Annual workshop, Oxford.

Milborrow, D.J. (1994-1996)
Personal Communications
City University, London.

Nyland, T.W. (1987)
'Surface pressure measurements on the blade of an operating Mod-2 wind turbine with and without vortex generators'
DOE/NASA/20320-59, NASA TM-83680.

Oliver, A.G. (1994)
'Use of air jet vortex generators to improve the L/D ratio of the NACA 63-2xx section, leading to improved power capture of the Ecotecnia 20/150 machine'
8th. IEA symposium on the aerodynamics of wind turbines, Lyngby, Denmark.

Oliver, A.G., Wootton, L.R.W. and Prats, J. (1996)
'Use of air jet vortex generators leading to improved energy capture and power regulation of a stall regulated wind turbine'
Proc. 18th. BWEA wind energy conference, Exeter, England, pp 61 -68

Øye, S. (1995)
'The effect of vortex generators on the performance of the Elkraft 1000kW turbine'
Proc. 9th. IEA symposium on the aerodynamics of wind turbines, Stockholm, 1995

Pankhurst, R.C. and Holder, D.W. (1952)
'Wind Tunnel Technique'
Sir Isaac Pitman & Sons Ltd., London.

Pearcey, H.H (1961)
'Shock induced separation & its prevention by design & boundary layer control'
Boundary layer and flow separation control, Pergammon Press, pp1166-1344.

Pearcey, H.H., Rao, K. and Sykes, D.M. (1993)
'Inclined air-jets used as vortex generators to suppress shock induced separation'
AGARD conference proceedings 534, paper 40.

Prats, J. and Oliver, A.G. (1996)
'Optimising the performance and control of wind turbines'
Final report, European Union project number JOU2-CT93-0411.

Rao, M.K (1988)
'An experimental investigation of the use of air jet vortex generators to control shock induced boundary layer separation'
PhD. thesis, City University, London.

Schmidt, F.W., Henderson, R.E. and Wolgemuth, C.H. (1984)
'Introduction to thermal sciences'
John Wiley and Sons Ltd., New York.

Selby, G.V., Lin, J.C. and Howard, F.G. (1992)
'Control of low-speed turbulent separated flow using jet vortex generators'
Experiments in Fluids Vol. 12, pp. 394 - 400

Snel,H., Houwink,R., Bosschers,J., Piers, W., van Bussel, G. & Bruining, A. (1993)
'Sectional prediction of 3D effects for stalled flow on rotating blades and comparison with measurements'
Proc. ECWEC, Lubeck-Travemunde, Germany.

Spera, D.A. (1994)
'Wind turbine technology'
ASME press, New York.

Sullivan, T.S. (1984)
'Effect of vortex generators on the power conversion performance and structural dynamic loads of the Mod-2 wind turbine'
DOE/NASA/20320-59, NASA TM-83680

Timmer, W.A. & van Rooy, R.P.J.O.M. (1994)
'The effect of stall strips, Gurney flaps and vortex generators on the performance of a stall controlled wind turbine'
Proc. 5th. European Wind Energy Association Conference, Thessaloniki, Greece

Voutsinas, S. (1997)
Personal Communication
City University, London.

Wallis, R.A. (1952)
'The use of air jets for boundary layer control'
A.R.L (Australia), Aero note 110.

Wallis, R.A. (1956)
'A preliminary note on a modified type of air jet for boundary layer control'
A.R.C., CP 513., London.

Wetzel, K.K. and Farokhi, S. (1995)
'Performance of advanced wind turbine airfoils with vortex generators'
Proc. 25th. AWEA Conf., Washington D.C.

Williams, B.R (1984)
'The Prediction Of Separated Flow Using A Viscous-Inviscid Interaction Method'
AIAA journal 1984, pp 308 - 320.

Zhang, X. (1993)
'Interaction between a turbulent boundary layer and elliptic and rectangular jets'
2nd. International Symposium on Engineering Turbulence Modeling & Measurements, Florence, Italy.

APPENDICES

NOTATION FOR THE APPENDICES

a	Acceleration of the blade (m/s^2)
A	Swept area of rotor (m^2)
A_{pipe}	Area of pipe cross section (m^2)
Cp	Constant pressure specific heat (J/kg.K)
d	Diameter of pipe (m)
f	Friction factor
F	Force (N)
g	Acceleration due to gravity (m/s^2)
h_f	Head loss due to friction (m)
L	Length of pipe (m)
m	Mass (kg)
$\dot{m}$	Mass flow (kg/s)
M	Free stream Mach number
p	Pressure (N/m^2)
p_a	Atmospheric pressure (N/m^2)
p_b	Blowing pressure (N/m^2)
p_{centri}	Pressure rise due to centrifugal compression (N/m^2)
p_f	Pressure loss due to pipe friction (N/m^2)
P	Power (kW)
r	Arbitrary radial distance along blade (m)
R	Gas constant (J/kg.K)
R_d	Reynolds number based on pipe diameter
T	Temperature (K)
T_0	Stagnation temperature (K)
V	Velocity (m/s)
x	Distance along the chord measured from leading edge (m)
X	Non-dimensional aerofoil abscissa
Y	Non-dimensional aerofoil ordinate

Greek

γ	Ratio of specific heats
η	Assumed efficiency of fan powering air jets
Θ	Gradient of aerofoil camber line
μ	Absolute viscosity (kg/m.s)
ρ	Density (kg/m^3)
Ω	Angular velocity of wind turbine rotor (rad/s)

Subscripts

c	Of camber line
l	Of lower surface
t	Of thickness distribution
u	Of upper surface

APPENDIX 1. - CONTRACT MANAGEMENT

General

The author was responsible for the management and technical leadership of the contract upon which this thesis is based. The project was entitled 'Optimising the Performance and Control of Wind Turbines' (European Union contract number JOU2-CT93-0411) and was for a fixed term of 2 years which commenced on 01/01/94.

The project was unusual in that it was really two mini-projects that had been put together for administration purposes by the European Commission. As well as the work on Air Jet Vortex Generators, the contract included a Flap Control Study which the author had to keep abreast of. The partners in the project were:

Co-ordinator:	City University (GB)	Air Jet Study
Partner:	Ecotecnia SCC (ES)	Air Jet Study
Partner:	D.E.W.I (D)	Flap Control Study
Partner:	Tech. Uni. Braunschweig (D)	Flap Control Study

The management of the contract included Task Scheduling, Reporting, Meetings, Financial Budgeting and Dissemination. Each of these is briefly described below.

Task scheduling

The author was responsible for making sure that the project kept to schedule and was completed on time. The first year of the project was completed on schedule but during year two significant delays occurred as shown in Table 8. All of the delays were related to the fan and were unforeseen. They included:

- Procurement of a fan capable of producing the required mass flow rate and pressure.
- Redesign of the fan housing due to fan re-alignment (section 8.5).
- Delay in fan delivery from the manufacturer.

When it became clear that the full scale testing would not be carried out before the planned start date the author applied for an extension to the contract which was duly granted by the European Commission.

T	DESCRIPTION	1994												1995												1996				
		J	F	M	A	M	J	J	A	S	O	N	D	J	F	M	A	M	J	J	A	S	O	N	D	J	F	M	A	M
1	Design/manufact. wind tunnel model																													
2	Wind tunnel testing																													
3	Design of modified blade																													
4	Design of jet supply and control system																													
5	Modification to blade set																													
6	Construction of jet supply system																													
7	Static testing of full scale equipment																													
8	Transport and mounting of equip.																													
9	Full scale testing of Air Jets																													
10	Reporting																													

Time Scheduled For Task Time Actually Spent On Task

Table 8 **Tasks undertaken and completed during the project**

Reporting

Reports had to be sent to the European Commission every 6 months and be received by the following dates:

Progress Report:	31/07/94
Progress Report:	31/01/95
Progress Report:	31/07/95
Progress Report:	31/01/96
Final Report:	31/05/96

As well as writing City University's contribution, the author was responsible for securing, compiling and editing the contributions from the other partners.

Meetings

The author was responsible for arranging meetings between the partners at regular intervals, setting of agenda and taking minutes.

Financial Budgeting

The total budget for the project was 250 kECU, of which City University's allocation was 68 kECU (≈ £52k). The author was responsible for the monitoring of City University's account and allocation of expenditure such that all the tasks were completed within the allowable budget.

Financial cost statements had to be sent to the European Commission by the following dates:

End of year cost statement:	31/01/95
End of year cost statement:	31/01/96
Final cost statement:	31/05/96

Although the author did not prepare these statements he was responsible for securing them from the other partners and liaison with the Commission on their behalf.

Dissemination

The author presented the work of the four partners at the JOULE contractors meeting in East Kilbride (8-10 Feb 1995) and presented the work on Air Jets at BWEA 18 (Oliver et al, 1996) and EWEC '97 (To be published).

APPENDIX 2. - A BRIEF GUIDE TO USING THE WILLIAMS V.I.I. CODE

This is a brief guide to using the B.R. Williams' Viscous Inviscid Interaction code which can be run on any IBM compatible computer.

The main program is SIVPDOS.FOR which must be compiled using a FORTRAN compiler. When the program is run two user files are read. These are INCOR and INP which are described below.

INCOR

This file contains the aerofoil geometry. The first line should contain the number of co-ordinates minus 1. The author of the code suggests 60 co-ordinates as a minimum and the aerofoil should be especially well defined at the leading and trailing edges.

The rest of this file should list the co-ordinates defined from the lower trailing edge, to the leading edge, to the upper trailing edge. The co-ordinates should be entered in terms of x/c, where is x is the chordwise distance along the aerofoil and c is the chord. The co-ordinate (0.000 , 0.000) should be input only once and the abscissa of the trailing edge must be 1.000.

INP

This file describes the flow conditions. The way that the file should be constructed is set out in Table 9 below. A key for the file variables is given in Table 10.

Line number	File variables
1	Title
2	Number of iterations, Output type
3	M, Re, T_0
4	α (start), α (finish), α (step), 0.0005, θ (step), 4
5	1, 1, 1
6	Transition type
7	l/s trans. point, u/s trans. point

Table 9 Construction of 'INP' file.

Item	Description
Number of iterations	Number of iterations performed before output. The program author suggests 200 - 300.
Output type	0 will list output in reduced form and 1 will list a full output
M	Mach number
Re	Reynolds number
T_0	Stagnation temperature (must be entered in °K)
α (start, finish and step)	Starting incidence, finishing incidence and step in incidence for which lift and drag are to be calculated.
0.0005	Number giving the required accuracy in the integration of the turbulent boundary layer. Williams suggests 0.0005.
θ (step)	Step increase in momentum thickness at transition. Used for simulating roughness.
4	Number used in the iteration. Fastest results are achieved with this number set to 4.
1, 1, 1	Numbers used in calculating second order effects
Transition type	0 will simulate free transition whilst 1 simulates fixed transition
l/s trans. point, u/s trans. point	This line is only used if line 6 is set to '1'. The required transition points for l/s (lower surface) and u/s (upper surface) are entered in terms of x/c. i.e. 0.0 is the leading edge and 1.0 is the trailing edge.

Table 10 Key for 'INP' file variables

When the program is executed, several output files are generated. The essential information is stored in the file OUT12.DAT. From this file, pressure distributions are obtained along with lift, drag and pitching moment predictions.

APPENDIX 3. - DERIVATION OF THE AEROFOIL CO-ORDINATES

The model tested in the wind tunnel was the NACA 63_2 -217.05 , α = 1.0. The meanings of these numbers are as follows (Abbott et al, 1959):

6	The series designation.
3	The chordwise position of minimum pressure in tenths of the chord behind the leading edge for the basic symmetrical section at zero lift.
2	The range of lift coefficient in tenths above and below the design lift coefficient in which favourable pressure gradients exist on both surfaces.
2	The design lift coefficient in tenths.
17.05	The thickness of the aerofoil section as a percentage of the chord.
$\alpha = 1.0$	The mean line type.

NACA cambered aerofoil sections in this family (6-series) are defined in terms of the shape of the mean or camber line, Y_c and a thickness distribution Y_t ,which is measured along the lines normal to the local camber line. The formulae are:

$$Xu = X - Yt.\sin\Theta \qquad Yu = Yc + Yt.\cos\Theta$$
$$Xl = X + Yt.\sin\Theta \qquad Yl = Yc - Yt.\cos\Theta$$

The thickness distribution Y_t is found by taking ordinates for the symmetrical profile NACA 63-018 and multiplying by 17.05 / 18, the ratio of the thickness/chord ratios.

The mean line ordinates Y_c for the $\alpha = 1.0$ mean line are tabulated by Abbott et al. These are for an ideal lift coefficient of C_{Li} = 1.0 and must be scaled by the ideal lift coefficient required which is 0.2 in this case.

The final variable , Θ, is equal to the arctangent of dY_c/dX and is the gradient of the mean line. It must also scaled by a factor of 0.2 and is again tabulated in Abbott et al.

APPENDIX 4. - POWER PREDICTION CODE LISTING

```
c  Wind turbine performance prediction code tailored for the Ecotecnia machine
c  Written by Andy Oliver

      integer g,speed,lid,full,x
      real L
      dimension aazz(15),clzz(15),cdzz(15), torquezz(15),rzz(15), powzz(15),
      dimension tpow(19),alpha(15),clalpha(15),cdalpha(15)
      dimension ajalpha(15),ajcl(15),ajcd(15),dcl(150),cltd(150)
      common/angle/set(15)
      common/solid/s(15)
      common/bin/wind(19)
      character*12 filename
      character*12 filenam2

c  All variables followed by the subscript 'zz(g)' are the values
c  of that variable calculated for element 'g'

c  aa          is the angle of attack of the blade to the local wind
c  adash       is the tangential induction factor
c  anew        (& aold) are axial induction factors
c  beta        is the total local blade setting angle
c  bset        is the machine blade setting angle
c  c           is the local chord
c  cl          is the Cl returned by the sub-routine 'interp'
c  cd          is the Cd returned by the sub-routine 'interp'
c  dr          is the width of one blade element (0.5m in this case)
c  f(& fold)   is the tip loss correction factor
c  fbracket    is just an intermediary equation involving Cos & Sin
c  fstar       is a force coefficient used in determining anew
c  g           is a counter and the blade element number
c  i           is a loop variable used in the sub-routine 'interp'
c  int         is a counter
c  j           lets the code to switch from Cl to Cd calculation
c  L           is the tip speed ratio that the code is calculating for
c  lid         determines which model is under test (clean foil or air jets)
c  n           is the number of blades that the turbine has
c  omega       is the angular velocity of the blade
c  phi         is the relative flow angle at the blade
c  pow         is the power on one element * n blades
c  qbracket    is just an intermediary equation involving Cos & Sin
c  r           is the local radius that data is being calculated at
c  rad         is the radius of the turbine
c  rpm         is the revolutions per minute of the turbine
c  s(g)        is the local solidity of the annulus
c  set(g)      is the local twist of the element
c  tip         counter allowing calculate for a range of tip speed ratios
c  torque      is the torque on one element * n blades
c  tpow        is the total power produced by the machine
c  v           is the relative velocity
c  w           is the value returned by the sub-routine 'interp' (Cl or Cd)
c  y           is the number of angles that you have Cl's and Cd's for
```

```
c  ***********************************************************
c                          Main program
c  ***********************************************************
c  input the blade setting angle
      write(6,'(/1x,'' WIND TURBINE PERFORMANCE PREDICTION CODE'')')
      write(6,'(1x,'' FOR THE ECOTECNIA 20/150 MACHINE'')')

      write(6,'(/1x,'' Please read the file "use.doc" if you '')')
      write(6,'(1x,'' are unfamiliar with this program.'')')

1     write(6,'(/1x,''Do you require:  '')')
      write(6,'(/1x,''1) Unmodified blade, with either transition''')')
      write(6,'(1x,''   fixed or transition free?'')')
      write(6,'(/1x,''2) Blade modified with air jets?'')')

      read(5,*) lid
      if (lid.lt.1.or.lid.gt.2) then
       goto1
      endif
      write(6,'(/1x,''Which file contains the ORIGINAL blade data? '')')
      write(6,'(1x,''(Either fixed or free transition)'')')
      read (5,'(a12)') filename
      open (1,file=filename,status = 'old')
      read (1,*) (alpha(x),clalpha(x),cdalpha(x),x=1,15)

      if (lid.eq.2) then
       write(6,'(/1x,''Which file contains the AIR JET data?'')')
       read(5,'(a12)') filenam2
       open (2,file=filenam2,status = 'old')
       read (2,*) (ajalpha(x),ajcl(x),ajcd(x),x=1,15)
      endif

      write(6,'(/1x,''What is the blade setting angle (degrees)?'')')
      read(5,*) bset

      write(6,'(/1x,''Full output (1) or Reduced output (2) ?'')')
      read(5,*) full

c  open a file to write the output to
      write(6,'(/1x,''Plese enter a filename for the output'')')
      read (5,'(a12)') filename
      open (7,file=filename,status = 'unknown')
      write(7,'(/1x,''BLADE SETTING ANGLE = '',f5.2)') bset
      write(6,'(/1x,''Data being written to file.....'')')

c  set known variables of the Ecotecnia machine
      rpm = 51.1
      rad = 10.0
      rho = 1.225
      n   = 3
      dr  = 0.5
      pi  = 4*ATAN(1.0)
      omega=2.0*pi*rpm/60.0
```

```
c  this loop enables calculation for a whole range of wind speeds
     do 100 speed=1,19

c  find (tip speed / wind speed) ratio for current wind speed
     L= omega*rad/wind(speed)

c  This loop enables the code to calculate for all radial stations. There are 20
c  elements but the first 5 are assumed to be non-contributing, hence 15 in total
     do 200 g=1,15

c  relates the non-dimensional local radius, r at the centre of each
c  element to the element number, g.
     r=(g/20.)+.225

c  makes r the local radius (metres)
     r=r*rad

c  calculates the local chord
     c=2.0*pi*r*s(g)/n

c  Converts all non air jet lift coefficients to 3D lift coefficients
     do 250 x=1,15
     dcl(x)=(2.0*pi*pi*(alpha(x)+1.5)/180.0)-clalpha(x)
     cltd(x)=clalpha(x)+(3*dcl(x)*(c/r)**2)
250   continue

c  find the local blade setting angle ( B.S.A + twist)
     beta = bset + set(g)

c  sets initial 'guestimates' for some variables
     anew=0.3
     adash=0.03
     fold=1.0
     phi=0.0
     int=1

c  find the relative velocity
2      v=((wind(speed)*(1-anew))**2+(omega*r*(1+adash))**2)**0.5

c  sets the old value of phi to that in the last iteration
     phiold=phi

c  calculate phi the relative flow angle which will later converge
     phi=180/pi*ATAN(wind(speed)*(1-anew)/(r*omega*(1+adash)))

c  check to see if phi has converged (new values are calculated first
c  so that if it has converged the most recent values are used.)
     check=ABS(phi-phiold)
     if (check.lt.0.01) then
       goto 3
     endif
```

```
c  Prevents phi diverging too quickly after the first iteration
c  which causes an unstable iteration
     if (int.gt.1) then
       phi=0.8*phiold  +  0.2*phi
     endif
     int=int+1

c  calculates the angle of attack
     aa=phi-beta

c  if guess is out of data range then sets initial value for aa
       if (aa.lt.-4) then
         aa=-4.0
       endif

       if (aa.gt.40.) then
         aa=40.0
       endif

c  Finds the Cl for the above angle of attack. The first line checks
c  to see if the element contains air jets, which are positioned between
c  element 7 (5.5m) and element 10 (7.5m) on the blade.
     if(lid.eq.2.and.g.gt.6.and.g.lt.11) then
       call intajcl(ajalpha,ajcl,cl,aa)
     else
       call interpcl(alpha,cltd,cl,aa)
     endif

c  Finds the corresponding Cd for the iterated angle of attack
c  the first line checks to see if the element contains air jets
     if(lid.eq.2.and.g.gt.6.and.g.lt.11) then
       call intajcd(ajalpha,ajcd,cd,aa)
     else
       call interpcd(alpha,cdalpha,cd,aa)
     endif

c  calculates the fstar coefficient and cf
     fbracket=cl*COS(phi*pi/180)+cd*SIN(phi*pi/180)
     fstar=s(g)*v**2*fbracket/(4*wind(speed)**2)
     cf=4.0*fstar

c  sets variables for the case when cf is high i.e. not equal to 4a(1-a)
     at=0.326
     cfone=1.816
     cft=4.0*at*(1-at)

c  sets the old value of f and a to those just used
     aold=anew
     fold=fnew

c  tip loss correction factor (new)
     fnew=2/pi * ACOS( EXP( (r/rad-1)*n / (2*SIN(phi*pi/180)) ) )
```

```
c  checking axial force to see if it follows 4a(1-a) law
     if (cf.lt.cft) then
       anew=cf/(4.0*fnew*(1-aold*fold))
     else
       anew=(1-((cfone-cf)/(4*(cfone**0.5-1))))/fnew
     endif

c  calculates the qstar coefficient
     qbracket=cl*SIN(phi*pi/180)-cd*COS(phi*pi/180)
     qstar=s(g)*rad*v**2*qbracket/(4*L*r*wind(speed)**2)

c  calculates the new adash
     adash=qstar/((1-anew*fnew)*fnew)

c  returns for next iteration
     goto 2

3     aazz(g)=aa
     clzz(g)=cl
     cdzz(g)=cd
     rzz(g)=r

c  calculates the elemental torque
     qbracket=cl*SIN(phi*pi/180)-cd*COS(phi*pi/180)
     torquezz(g)=s(g)*pi*r**2*rho*v**2*qbracket*dr

c  find the elemental power in kW
     powzz(g) = torquezz(g)*omega/1000

c  Add this elemental power to the machine power
     tpow(speed) = tpow(speed) + powzz(g)

c  returns to calculate for the next element
200   continue


c  writing data to file
     if (full.eq.2) then
       goto 100
     endif

     write(7,'(/1x,''U       '',f4.1)') wind(speed)
     write(7,'(1x,''Vtip/U  '',f5.2)') L

     write(7,'(/1x,''r/R    Alpha  CL      CD      Q       POW(kW)'')')
     write(7,'(1x,(f5.3,2x,f6.3,2x,f5.3,2x,f6.4,1x,f7.2,2x,f7.3))')
    & (rzz(g),aazz(g),clzz(g),cdzz(g),torquezz(g),powzz(g),g=1,15)

c  returns to calculate for the next wind speed
100   continue

     write(7,'(/1x,''U (M/S)    POWER (kW) '')')
     write(7,'(/1x,(f5.2,3x,3x,f8.3))')
    & (wind(speed),tpow(speed),speed=1,19)
```

```
c  closes the input/output files
      close(1,status='keep')
      close(2,status='keep')
      close(7,status='keep')

      stop
      end

c ***********************************************************************
c                              Subroutines
c ***********************************************************************
c  interpolates for Cl (no air jets on these elements)
      subroutine interpcl(alpha,cltd,cl,aa)
      real alpha(15),cltd(15),aa,cl
      i=1
5     if(alpha(i).lt.aa) then
       i=i+1
       goto 5
      else
       cl=cltd(i-1)+(aa-alpha(i-1))*(cltd(i)-cltd(i-1))/(alpha(i)-alpha(i-1))
      endif
      return
      end

c  interpolates for Cl (when the element has air jets on it)
      subroutine intajcl(ajalpha,ajcl,cl,aa)
      real ajalpha(15),ajcl(15),aa,cl
      i=1
15    if(ajalpha(i).lt.aa) then
       i=i+1
       goto 15
      else
       cl=ajcl(i-1)+(aa-ajalpha(i-1))*(ajcl(i)-ajcl(i-1))/(ajalpha(i)-ajalpha(i-1))
      endif
      return
      end

c  interpolates for Cd (no air jets on these elements)
      subroutine interpcd(alpha,cdalpha,cd,aa)
      real alpha(15),cdalpha(15),aa,cd
      i=1
25    if(alpha(i).lt.aa) then
       i=i+1
       goto 25
      else
      cd=cdalpha(i-1)+(aa-alpha(i-1))*(cdalpha(i)-cdalpha(i-1))/(alpha(i)-alpha(i-1))
      endif
      return
      end
```

```
c  interpolates for Cd (when the element has air jets on it)
      subroutine intajcd(ajalpha,ajcd,cd,aa)
      real ajalpha(15),ajcd(15),aa,cd
      i=1
35     if(ajalpha(i).lt.aa) then
       i=i+1
       goto 35
      else
       cd=ajcd(i-1)+(aa-ajalpha(i-1))*(ajcd(i)-ajcd(i-1))/(ajalpha(i)-ajalpha(i-1))
      endif
      return
      end

c ***********************************************************************
c                              Block data
c ***********************************************************************

      block data
      common/angle/set(15)
      common/solid/s(15)
      common/bin/wind(19)

c  this block contains the variance of twist along the blade
      data set/10.9,8.2,6.1,4.4,3.0,2.2,1.5,.9,.5,.2,0.,0.,0.,0.,0./

c  this block contains the variance of solidity along the blade
      data s/.18196,.14794,.12287,.10381,.08876,.07658,.06651,
     + .05798,.05079,.04459,.03918,.03438,.03018,.02643,.02307/

c  this block contains the wind speeds that power will be calculated for
      data wind/4.0,5.0,6.0,7.0,8.0,9.0,10.0,11.0,12.0,13.0,14.0,15.0,
     +16.0,17.0,18.0,19.0,20.0,21.0,22.0/

      end
```

APPENDIX 5. - PRESSURE RISE IN BLADE DUE TO CENTRIFUGAL COMPRESSION

It was considered that air jets could be powered by the pressure rise in the blade due to 'centrifugal' compression.

A first approximation is to assume that the system is closed at both ends as shown in Figure 101.

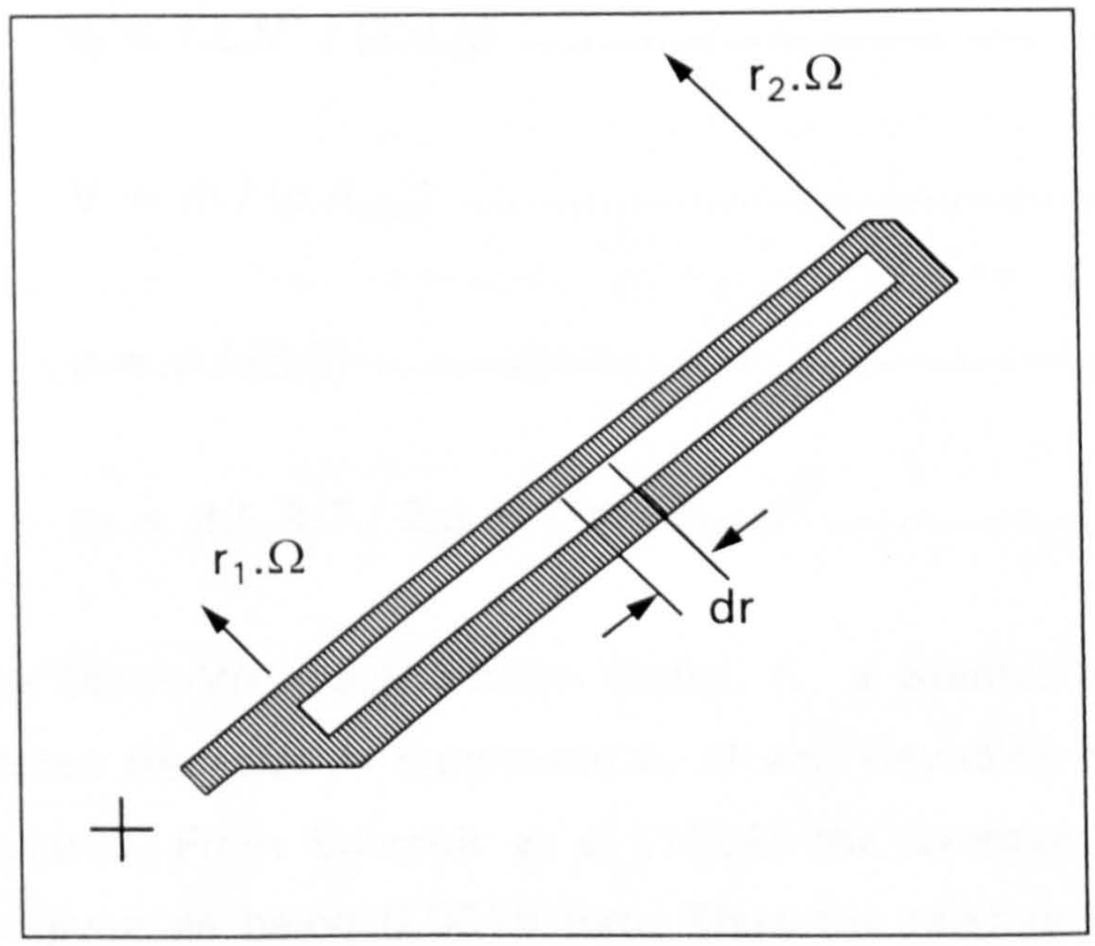

Figure 101 Sketch of the blade

Now $$p_{centri} = \int_{r1}^{r2} dp \quad \text{..... [1]}$$

$$F = m.a \quad \text{..... [2]}$$

$$dF = \rho.A.dr \ * \ r.\Omega^2 \quad \text{..... [3]}$$

$$dp = dF/A = \rho.\Omega^2 \int_{r1}^{r2} r.dr \quad \text{..... [4]}$$

$$p_{centri} = \tfrac{1}{2}.\rho.\Omega^2.(r_2^{\,2} - r_1^{\,2}) \quad \text{..... [5]}$$

Assuming, that the air jets could only be installed up to 88% blade radius (8.8m.) because of the tip brake and assuming that r_1 is the blade root, then the maximum pressure rise available due to centrifugal compression is calculated to be 1360Pa.

APPENDIX 6. - CALCULATION OF PRESSURE LOSS IN PIPE DUE TO FRICTION

Before calculation of the fan power requirement, the losses due to friction in the pipe had to be calculated. The form of the head loss equation is that used by Schmidt et al, (1984). The calculation is performed for the chosen design.

$$p_f = \rho.g.h_f \quad \text{..... [1]}$$

and

$$h_f = f.L.V^2 / (2.d.g) \quad \text{..... [2]}$$

and

$$V = \dot{m} / (\rho.A_{pipe}) \quad \text{..... [3]}$$

and

$$\rho = p / (R.T) \quad \text{..... [4]}$$

gives

$$p_f = (f.L.R.T / 2.p.d) . (\dot{m} / A_{pipe})^2 \quad \text{..... [5]}$$

To determine the Darcy-Weisbach friction factor, f, a Stanton / Moody chart is used which requires the relative roughness h_r /d and Reynolds number R_d of the pipe to be calculated. From Schmidt et al (1984) the average roughness, h_r of drawn tubing is given as being 0.0015 mm. Thus the relative roughness of the 58 mm. diameter pipe is $0.25 * 10^{-3}$. For simplicity it is assumed that the air in the pipe is at standard atmospheric conditions in the calculation of R_d as this does not affect the accuracy to which f can be determined.

$$R_d = \rho.V.d / \mu = \dot{m}.d / (A_{pipe}. \mu) \quad \text{..... [6]}$$

The mass flow is given by the wind tunnel tests as being 0.00377 kg/s/jet and there are 34 jets per blade. Thus the mass flow per blade is 0.128 kg/s. With the diameter of the pipe 58mm. and an absolute viscosity of $1.783 * 10^{-5}$ kg/m/s the pipe Reynolds number is calculated as being $1.6 * 10^5$. From the Stanton / Moody chart the pipe friction factor is found to be approximately, f = 0.018.

The length of pipe, L is assumed to be up to and including the last air jet and is 7.54m. The total temperature is assumed to be standard atmospheric and the pressure in the pipe is assumed to be atmosphere plus 1 p.s.i. behind the jets or 108.2 kPa. Substituting these values into equation [5] the pressure lost to friction in the pipe is calculated to be $p_f \approx 2100$ Pa.

APPENDIX 7. - CALCULATION OF THE REQUIRED FAN POWER

The fan power had to be calculated in order to determine the maximum length of air jet array that could be installed.

Assuming an adiabatic compression and an ideal gas with constant specific heats and neglecting changes in potential energy, we can calculate the power, P, required to drive the fan from:

$$P = \dot{m} \{ C_p (T_2 - T_1) + \tfrac{1}{2} (V_2^2 - V_1^2) \quad \text{.....[1]}$$

where C_p is the constant-pressure specific heat and approximately equal to 1006 J/kg.K at standard atmospheric temperature.

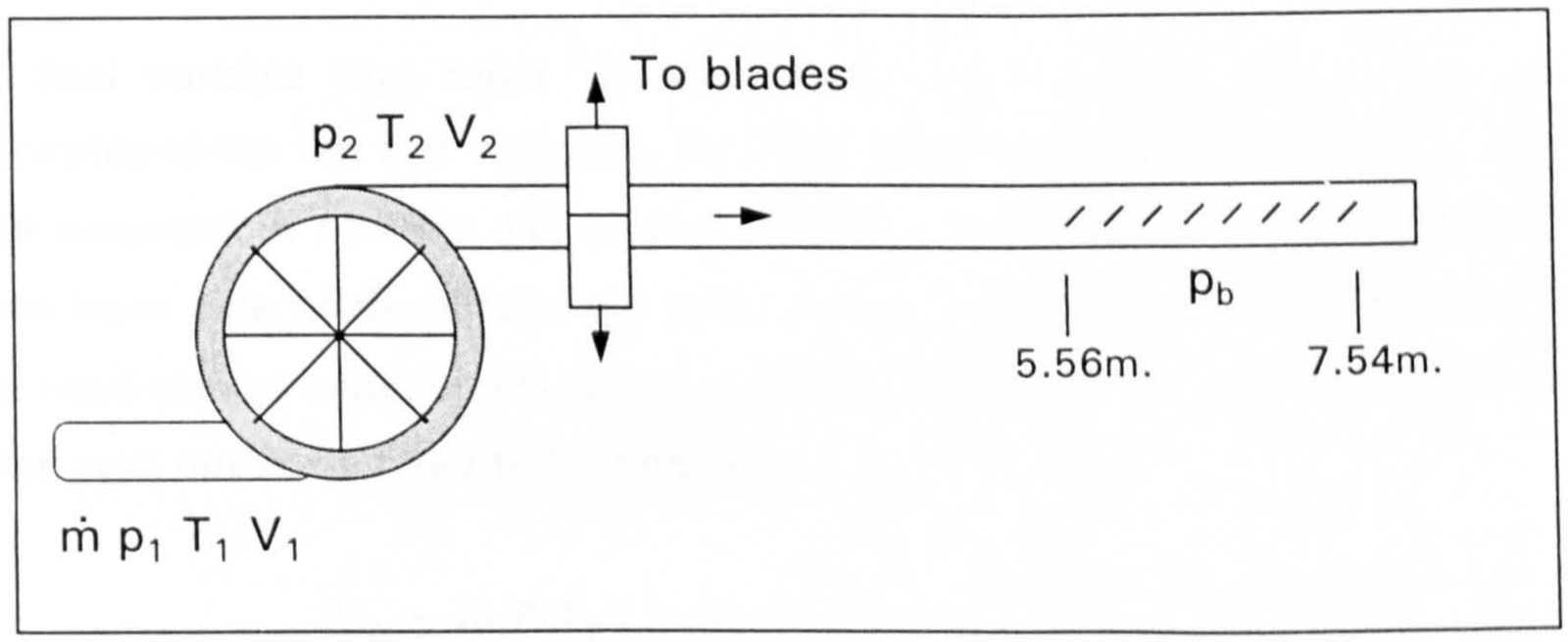

Figure 102 Relevant variables for calculation of fan power

The fan had to supply a mass flow of $\dot{m}$ = 0.00377kg/s/jet * 34 jets/blade * 3 blades = 0.385kg/s. and produce a pressure rise of $p_2 - p_1$. The fan inlet was open to atmosphere (p_1 = 101,325 Pa). p_2 is given in the following equation, where p_b is the blowing pressure, p_f is the pipe loss due to friction (Appendix 5) and p_{centri} is the pressure rise due to centrifugal compression (Appendix 4):

$$p_2 = p_a + p_b + p_f - p_{centri} \quad \text{.....[2]}$$

The pipe loss due to friction and the pressure rise due to centrifugal compression are assumed to be worst case, i.e. calculated at the end (7.54m.) and beginning of the air jet array respectively (5.56m.).

$$p_2 = (101{,}325 + 6900 + 2100 - 540)\ \text{Pa}$$

$$p_2 = 109{,}785\ \text{Pa}$$

The pressure rise required of $p_2 - p_1$ is therefore approximately 8.5 kPa.

Calculating T_2', the temperature if the fan operates with 100% efficiency:

$$T_2' = T_1 (P_2/P_1)^{(\gamma-1)/\gamma} \quad \text{..... [3]}$$

$$T_2' = 288 * (109{,}785 / 101{,}325)^{0.4/1.4}$$

$$T_2' = 294.7 \text{ K}$$

To determine T_2, an efficiency, η for the fan / compressor must be assumed. This was taken to be 65%.

$$(T_2' - T_1) / (T_2 - T_1) = \eta \quad \text{..... [4]}$$

$$T_2 = (294.7 - 288) / 0.65 + 288$$

$$T_2 = 298.3 \text{ K}$$

The final variable that must be calculated before power requirement can be determined is the fan exit velocity., V_2 . The diameter of the fan exit, A_2 , also has to be assumed. A nominal diameter of 100mm. was selected which corresponded to the input side of the three-way split. As we shall see, the velocity term in the right hand side of equation [1] is not as significant as the enthalpy term and so this choice was not considered to be critical.

$$V_2 = \dot{m}.R.T_2 / p_2.A_2 \quad \text{..... [5]}$$

V_2 is therefore calculated to be 38.2 m/s. Substituting the appropriate values in equation [1] yields:

$$P = 0.385 \{ 1006 (298.3 - 288) + \tfrac{1}{2} (38.2^2 - 0^2)$$

$$P = 0.385 * \{10{,}360 + 730\} \text{ W}$$

$$P = 4.3 \text{ kW}$$